Aeroelastic modal dynamics of wind turbines including anisotropic effects

Skjoldan, Peter Fisker

Publication date:
2011

Document Version
Publisher's PDF, also known as Version of record

SIEMENS

DTU

Aeroelastic modal dynamics of wind turbines including anisotropic effects

Risø-PhD-Report

Peter Fisker Skjoldan
Risø-PhD-66(EN)
March 2011

Risø DTU
National Laboratory for Sustainable Energy

Author: Peter Fisker Skjoldan
Title: Aeroelastic modal dynamics of wind turbines including anisotropic effects
Division: Wind Energy

The present thesis is submitted in partial fulfilment of the requirements for the degree of PhD at The Technical University of Denmark.

Abstract (max. 2000 char.):
Several methods for aeroelastic modal analysis of a rotating wind turbine are developed and used to analyse the modal dynamics of two simplified models and a complex model in isotropic and anisotropic conditions.
The Coleman transformation is used to enable extraction of the modal frequencies, damping, and periodic mode shapes of a rotating wind turbine by describing the rotor degrees of freedom in the inertial frame. This approach is valid only for an isotropic system. Anisotropic systems, e.g., with an unbalanced rotor or operating in wind shear, are treated with the general approaches of Floquet analysis or Hill's method which do not provide a unique reference frame for observing the modal frequency, to which any multiple of the rotor speed can be added. This indeterminacy is resolved by requiring that the periodic mode shape be as constant as possible in the inertial frame. The modal frequency is thus identified as the dominant frequency in the response of a pure excitation of the mode observed in the inertial frame.
A modal analysis tool based directly on the complex aeroelastic wind turbine code BHawC is presented. It uses the Coleman approach in isotropic conditions and the computationally efficient implicit Floquet analysis in anisotropic conditions. The tool is validated against system identifications with the partial Floquet method on the nonlinear BHawC model of a 2.3 MW wind turbine. System identification results show that nonlinear effects on the 2.3 MW turbine in most cases are small, but indicate that the controller creates nonlinear damping. In isotropic conditions the periodic mode shape contains up to three harmonic components, but in anisotropic conditions it can contain an infinite number of harmonic components with frequencies that are multiples of the rotor speed. These harmonics appear in calculated frequency responses of the turbine. Extreme wind shear changes the modal damping when the flow is separated due to an interaction between the periodic mode shape and the local aerodynamic damping influenced by a periodic variation in angle of attack.

Risø-PhD-66(EN)
March 2011

ISBN 978-87-550-3848-6

Contract no.:
07-023357

Group's own reg. no.:
1191024-01

Sponsorship:
Siemens Wind Power A/S
Danish Agency for Science Technology and Innovation, Industrial PhD programme

Cover :
Siemens 3.0 MW prototype direct drive wind turbine with 101 m rotor.

Pages: 158
Tables: 1
References: 55

Information Service Department
Risø National Laboratory for Sustainable Energy
Technical University of Denmark
P.O.Box 49
DK-4000 Roskilde
Denmark
Telephone +45 46774005
bibl@risoe.dtu.dk
Fax +45 46774013
www.risoe.dtu.dk

Aeroelastic modal dynamics of wind turbines including anisotropic effects

Peter Fisker Skjoldan

Contents

Preface

The present thesis is submitted in partial fulfilment of the requirements for the degree of PhD at The Technical University of Denmark. The thesis is structured as a summary of and additions to the work of five publications which are appended. The work results from a collaboration between Siemens Wind Power A/S and the Wind Energy Department at Risø DTU. The project has been sponsored jointly by Siemens and the Danish Ministry of Science, Technology, and Innovation through the Industrial PhD programme.

The work has been carried out between August 2007 and October 2010 under guidance of senior scientist Morten Hartvig Hansen from Risø as main advisor and Rune Rubak (until July 2010 where he left Siemens) and Kenneth Thomsen as advisors at Siemens.

I would like to thank the following persons for helping me reach the end of this project. Kenneth Thomsen was the initial driving force for realising the project at Siemens and has followed it with a helicopter overview since. Jørgen Thirstrup Petersen at Siemens has been helpful guiding me through the mazes of BHawC. Rune Rubak was always full of good ideas and showed an admirable ability to delve right into the details at project meetings distant in time. Jesper Winther Stærdahl at Siemens has given many valuable tips on how to handle the aerodynamics. Olivier A. Bauchau, professor at Georgia Tech, received me for a rewarding stay in Atlanta and widened my horizons. Last, but not least, Morten Hartvig Hansen has guided me through these three years with a stream of ideas, abundant experience, fruitful discussions, and encouragement both in moments of crisis and success.

Copenhagen, 3rd March 2011

Peter Fisker Skjoldan

Abstract

Several methods for aeroelastic modal analysis of a rotating wind turbine are developed and used to analyse the modal dynamics of two simplified models and a complex model in isotropic and anisotropic conditions.

The Coleman transformation is used to enable extraction of the modal frequencies, damping, and periodic mode shapes of a rotating wind turbine by describing the rotor degrees of freedom in the inertial frame. This approach is valid only for an isotropic system. Anisotropic systems, e.g., with an unbalanced rotor or operating in wind shear, are treated with the general approaches of Floquet analysis or Hill's method which do not provide a unique reference frame for observing the modal frequency, to which any multiple of the rotor speed can be added. This indeterminacy is resolved by requiring that the periodic mode shape be as constant as possible in the inertial frame. The modal frequency is thus identified as the dominant frequency in the response of a pure excitation of the mode observed in the inertial frame.

A modal analysis tool based directly on the complex aeroelastic wind turbine code BHawC is presented. It uses the Coleman approach in isotropic conditions and the computationally efficient implicit Floquet analysis in anisotropic conditions. The tool is validated against system identifications with the partial Floquet method on the nonlinear BHawC model of a 2.3 MW wind turbine.

System identification results show that nonlinear effects on the 2.3 MW turbine in most cases are small, but indicate that the controller creates nonlinear damping. In isotropic conditions the periodic mode shape contains up to three harmonic components, but in anisotropic conditions it can contain an infinite number of harmonic components with frequencies that are multiples of the rotor speed. These harmonics appear in calculated frequency responses of the turbine. Extreme wind shear changes the modal damping when the flow is separated due to an interaction between the periodic mode shape and the local aerodynamic damping influenced by a periodic variation in angle of attack.

Resumé

Denne afhandling har udviklet flere metoder til aeroelastisk modalanalyse af en roterende vindmølle og har brugt dem til at analysere modaldynamikken for to forsimplede modeller og en avanceret model under isotropiske og anisotropiske betingelser.

Coleman-transformationen bruges til at bestemme modale frekvenser, dæmpninger og periodiske modalformer for en roterende vindmølle ved at beskrive rotorens frihedsgrader i inertialsystemet. Denne fremgangsmåde gælder kun for isotropiske systemer. For anisotropiske systemer, der fx har en ubalanceret rotor eller er påvirket af en vindgradient, bruges en generel metode som Floquet-analyse eller Hill's metode, som ikke definerer en unik referenceramme hvori modalfrekvensen bestemmes. Der kan derimod lægges et vilkårligt multiplum af rotorhastigheden til frekvensen. Denne ubestemthed afklares ved at sørge for at den periodiske modalform er så konstant som muligt i inertialsystemet. Modalfrekvensen bliver dermed den dominerende frekvens i responset for den rent anslåede modalform observeret i inertialsystemet.

Et værktøj til modalanalyse baseret direkte på det avancerede aeroelastiske vindmølle-beregningsværktøj BHawC præsenteres i afhandlingen. Det bruger Colemanfremgangsmåden under isotropiske betingelser og implicit Floquet-analyse, som er en beregningsmæssigt effektiv metode, under anisotropiske betingelser. Værktøjet er blevet efterprøvet ved sammenligning med en systemidentifikation med den partielle Floquet-metode anvendt på en ikke-lineær BHawC-model af en vindmølle på 2.3 MW.

Resulter af systemidentifikationen viser at de ikke-lineære effekter for denne vindmølle i de fleste tilfælde er små, men de viser til gengæld at møllestyringen kan skabe en ikke-lineær dæmpning. Under isotropiske betingelser har den periodiske modalform op til tre harmoniske komponenter, mens den under anisotropiske betingelser kan have et uendeligt antal harmoniske komponenter med frekvenser, som er et multiplum af rotorhastigheden. Disse harmoniske komponenter indgår i møllens beregnede frekvensrespons. En ekstrem vindgradient ændrer modaldæmpningen når strømningen er separeret som følge af et samspil mellem den periodiske modalform og den lokale aerodynamiske dæmpning, som er påvirket af en periodisk variation af angrebsvinklen.

Publications

The following five papers constituting the majority of the work for this thesis are appended.

[P1] P.F. Skjoldan, M.H. Hansen. On the similarity of the Coleman and Lyapunov-Floquet transformations for modal analysis of bladed rotor structures. *Journal of Sound and Vibration*, 327:424–439, 2009.

[P2] P.F. Skjoldan. Modal Dynamics of wind turbines with anisotropic rotors. In *Proceedings of 47th AIAA Aerospace Sciences Meeting*, Orlando FL, USA, 2009.

[P3] P.F. Skjoldan, M.H. Hansen. Implicit Floquet analysis of wind turbines using tangent matrices of a nonlinear aeroelastic code. *Wind Energy*. Accepted for publication, delivered to production 15th February 2011.

[P4] P.F. Skjoldan, M.H. Hansen. Effects of extreme wind shear on aeroelastic modal damping of wind turbines. *Wind Energy*. Accepted for publication, submitted in revised form 28th February 2011.

[P5] P.F. Skjoldan, O.A. Bauchau. Determination of modal parameters in complex nonlinear systems. *Journal of Nonlinear and Computational Dynamics*, 6(3):031017, 2011.

Nomenclature

Symbols are presented in the text. only the most common notation is listed here.

Notation

x	scalar
$\mathbf{x}$	vector (lowercase)
$\mathbf{X}$	matrix (uppercase)
$\mathbf{X}^{\mathrm{T}}$	transpose
$\dot{x}$	time derivative
$\tilde{x}$	approximate quantity

Symbols

$\mathbf{a}$	aerodynamic state vector
$\mathbf{A}$	state matrix
$\mathbf{A}_{\mathrm{L}}$	Lyapunov-Floquet transformed state matrix
$\mathbf{C}$	damping/gyroscopic matrix
i	imaginary unit, $\sqrt{-1}$
j_k	integer identifying the modal frequency
$\mathbf{K}$	stiffness matrix
$\mathbf{L}$	Lyapunov-Floquet (L-F) transformation
$\mathbf{M}$	mass matrix
N	number of state variables
$\mathbf{p}$	nodal positions
$\mathbf{q}$	nodal quaternions
t	time
T	rotor period
$\mathbf{u}$	vector of degrees of freedom
$\mathbf{u}_k$	periodic mode shape
$\mathbf{V}$	eigenvector matrix
$\mathbf{x}$	perturbation to aerodynamic state vector
$\mathbf{y}$	perturbation to degrees of freedom or state vector
$\mathbf{\Lambda}$	eigenvalue (characteristic exponent) diagonal matrix
φ	fundamental solution
ψ	azimuth angle
ω_k	frequency of mode k
Ω	rotor speed
φ	fundamental solution
σ_k	damping rate of mode k

Mode names

Index	*Component*		*Direction*	
1	T	tower	LO	longitudinal
2	E	rotor edgewise	LA	lateral
	F	rotor flapwise	Y	yaw
⋮	DRV	drivetrain	T	tilt
			V	vertical
			H	horizontal
			S	symmetric
			BW	backward whirling
			FW	forward whirling

Chapter 1

Introduction

Wind turbines are a proven and mature technology for generation of electricity from renewable sources. But the ongoing effort of lowering the cost of energy compared to traditional sources depends on the continuous optimisation of the turbines. This optimisation consists of increasing the efficiency of the turbine through better aerodynamics of the rotor, smaller loss in the drivetrain and energy conversion, and more intelligent control. On the other hand it also consists of making the turbines cheaper by minimising the material needed for the structure to withstand the aerodynamic and inertial loads or by minimising the load itself. Both the assessment of the loads and the design of control algorithms require a thorough understanding of the dynamics of the turbines. A decomposition of the turbine dynamic response into modal contributions, which is the subject of this thesis, is indeed an effective way to gain this understanding of the dynamics and the factors contributing to the loads.

This chapter introduces the basic concepts related to modal analysis of a rotating wind turbine, gives a summary of the state of the art on this subject, and details the motivation for and structuring of this thesis.

1.1 Concepts

A wind turbine in operation is subjected to loads from a variety of sources. The wind deflects the blades and the tower, and the rotation produces strong centrifugal forces in the blade. The wind is, however, not constant: it varies with the height due to wind shear and in general due to turbulence. These factors generate a very dynamic loading scenario. In the design process this scenario is determined by a standard suite of time simulations of the response to the varying loading. The time simulations yield detailed, important design loads, but they disclose little of the underlying phenomena causing the loads. A modal analysis divides a small-amplitude free response to perturbations about a steady state into modal contributions. Each contribution is characterised by a modal frequency, modal damping, and a mode shape. These results, which are in the frequency domain, directly show if the steady state equilibrium is stable and can be used to explain frequency spectra determined from time simulations.

Figure 1.1: Siemens 3.0 MW prototype direct drive wind turbine with 101 m rotor.

In this section the fundamental concepts used in this thesis are defined. The terminology might be slightly different from that used in the publications appended to this thesis, illustrating that this has been a progressive work.

Modal analysis of numerical models consists of three steps:

1. Location of a **steady state** operating condition;
2. **Linearisation** of the equations of motion about the steady state;
3. **Modal decomposition** of the linearised system providing modal frequencies, modal damping, and mode shapes.

The nature of the steady state depends on the characteristics of the rotor and the external, or environment, conditions. *Isotropic external conditions* are defined as a uniform wind field constant in time and aligned in tilt and yaw to be perpendicular to the rotor plane and no gravity present, or the academic special case of the rotor rotating in vacuum. An *isotropic rotor* is defined as being polarly symmetric and balanced. The presence of these two conditions of isotropy result in a *stationary steady state* with constant deflections of the turbine members. In the general case of *anisotropic external conditions*, an *anisotropic rotor*, or simply *anisotropic conditions* in case either is present, the resulting steady state is periodic. In a *periodic steady state* the deflections of the turbine members are periodic with the rotor period, and the rotor speed varies periodically with the mean rotor speed determined by the rotor period. Non-periodic effects like turbulence are not included in the steady state, but rather considered a source of excitation of different modes under the assumption that the turbulence does not change the mean rotor speed significantly. Larger non-periodic variations in the rotor speed must be modelled by different steady states.

The linearisation of the equations of motion about the steady state is necessary to make the linear concept of modal decomposition possible. It can either be done analytically or approximately by considering small perturbations to the steady state calculated with a nonlinear model.

The equations of motion for a wind turbine in steady state operation have periodic coefficients caused by the rotor rotation. Therefore, a coordinate transformation that yields an equivalent set of equations of motion with constant coefficients, must be performed before the *modal properties*, consisting of a modal frequency, modal damping, and a mode shape for each mode, can be extracted by eigenvalue analysis. In *isotropic conditions*, defined by isotropic external conditions and an isotropic rotor, such a transformation is known a priori as the Coleman transformation, which describes the blade degrees of freedom in the *inertial frame*, or ground-fixed frame. The resulting mode shapes are constant for degrees of freedom on the supporting structure. For degrees of freedom on the blade the mode shapes are periodic, containing as many harmonic components as the number of blades, which can result in whirling motion of the blades. In anisotropic conditions, the coordinate transformation is included implicitly in a general method such as Floquet analysis or Hill's method. The resulting periodic mode shapes can contain an infinite number of harmonics both on the supporting structure and on the blades, allowing for more complex motion.

Modal analysis predicts the stability of the steady state equilibrium determined by the lowest modal damping. Stability analysis is often used to denote a modal analysis including aerodynamics, because the aerodynamic forces are the most common cause of instabilities. In other cases stability analysis refers to the search for stability boundaries under variation of some parameter. In this thesis the term is avoided, and modal analysis is used about any structural or aeroelastic system.

On three-bladed wind turbines the anisotropy mainly stems from wind shear and a possible yaw error, making the effect modest. Two-bladed turbines, on the other hand, have inherently anisotropic rotors, resulting in a significantly different dynamic behaviour. This thesis, however, focuses on three-bladed horizontal-axis wind turbines because they are the most commercially viable type.

1.2 State of the art

The methods for modal analysis of wind turbines, build to a large extent on methods developed in other fields, which include general rotating systems and in particular helicopters. This section presents selected literature from these fields to give an idea of the chronology and span of the approaches.

1.2.1 Theoretical foundations

The theory for solution of differential equations with periodic coefficients has been known for over a century. Floquet (1883) is the first to show that the solution to a system of homogeneous linear ordinary differential equations with periodic coefficients consists of a product of a purely periodic term and a time-dependent exponential term, determined from a set of fundamental solutions to the system. His achievement has since become known as *Floquet theory*, allowing modal analysis of periodic equations. While calculating the motion of the lunar perigee, Hill (1886) solves an equation with periodic coefficients by setting up a determinant of infinite

size containing the terms of a series expansion of the coefficients. He shows that the eigenvalues calculated from the determinant converge when the determinant is truncated, an idea that subsequently has developed into *Hill's method*. Lyapunov (1896) is the first to specifically mention a coordinate transformation as a way to form the solution derived by Floquet, and it has been aptly named the *Lyapunov-Floquet transformation*.

These theories are now standard material in text books on mathematical analysis and on dynamics, see, e.g., Whittaker and Watson (1927), Coddington and Levinson (1955), Meirovitch (1970), Yakubovich and Starzhinskii (1975), and Nayfeh and Balachandran (1995).

Coleman (1943) derives the first example of a Lyapunov-Floquet transformation for bladed rotors. The *Coleman transformation* introduces multi-blade coordinates describing the rotor motion in the inertial frame of reference, thereby eliminating the periodic coefficients in the equations of motion for systems with isotropic rotors.

1.2.2 Analytical modelling approaches

The earliest modal analyses on bladed rotor systems are carried out for simplified, analytical models of helicopters. Coleman and Feingold (1947) apply Hill's method to determine the stability of an anisotropic two-bladed rotor on an anisotropic support, where the equations of motion still have periodic coefficients after introduction of the Coleman transformation. Hill's method is basically a harmonic balance method, which is described by, e.g., Krylov and Bogolyubov (1947) or Nayfeh and Mook (1979).

The advent of the digital computer in the second half of the 20$^{\text{th}}$ century allows performing modal analyses of more complex models. Early Floquet analyses are performed by Lowis (1963) who determines the stability of a helicopter rotor system by numerical integration of the equations of motion to find the *transition matrix*, which maps the fundamental solution from one point in time to another. Peters and Hohenemser (1971) study the stability properties of a helicopter rotor where they obtain the transition matrix using a predictor-corrector integration scheme. In this thesis a distinction is made between the terms Floquet *theory* and Floquet *analysis*: the theory states the form of the solution, and the analysis is a practical application of the theory, which typically means that the fundamental solution is obtained numerically. Hill's method also sees advantage of the computer, applied by Crimi (1969) to the problem of stability of a rotor blade which is in forward flight, thus introducing anisotropy.

Floquet analysis is applied to calculate the aeroelastic modal parameters of a wind turbine by Kirchgässner (1984) who uses mode shape expansion of tower and blades separately to obtain a model with a small number of generalised degrees of freedom.

The computational effort in performing Floquet analysis on these models is still substantial, and to allow the treatment of models with more degrees of freedom, improvements to the numerical schemes are suggested by several researchers. Peters (1994) introduces Fast Floquet Theory where it is only necessary to compute the transition matrix over $1/B$ of a rotor period, where B is the number of blades on the isotropic rotor. Sinha and Pandiyan (1994) approximate the transition matrix based on an expansion of the equations of motion in Chebyshev polynomials, thereby converting the differential equations into a small set of algebraic equations. Bauchau and Nikishkov (2001) develop the *implicit Floquet analysis*, which approximates the

lowest damped modes from a partially calculated fundamental solution, and they apply it to a large finite element model where the transition matrix is furthermore calculated using a nonlinear model, avoiding the task of linearising the equations of motion.

Another approach to handling small periodic terms in the equations of motion, caused by anisotropic effects, is taken by Johnson (1972) who solves the problem of helicopter rotor flapping stability using the perturbation method of multiple scales. The equations of motion are described in the rotating frame with the anisotropy caused by forward flight, and the advance ratio (the ratio of the helicopter forward speed to the rotor tip speed; equivalent to yaw error for a wind turbine) is used as the small parameter in the perturbation analysis.

1.2.3 System identification

An alternative to the analytical modelling of the rotor systems is enabled by advances in experimental modal analysis made by, e.g., Hammond and Doggett (1975) who determine the damping of helicopter rotor systems by analysis of the time responses to a random excitation of the system. Similar methods are used by Carne and Nord (1983) in NExT (Natural Excitation Technique) to identify the modal properties of a vertical axis wind turbine with the advantage that the excitation is provided by the turbulence in the wind and that it is not necessary to measure the excitation force. This technique is subsequently refined as *operational modal analysis* and applied by, e.g., Hansen et al. (2006) who determine the damping of edgewise modes using measured response signals from an operating wind turbine and compare it to results from an analytical model.

These *system identification* approaches suffer from being based on theoretical models that do not take effects of anisotropy into account. Liu (1997) derives a methodology for system identification of linear time-varying systems, and in particular periodically varying systems, which, however, requires the measurement of both input and output. It is not always straightforward to obtain a linear version of a complex analytical model, which leads Wang and Peters (1998) and Fuehne (2000) to introduce *generalised Floquet theory*. They use elements of experimental signal analysis to eliminate noise from modelled nonlinearities or measurements and approximate the modal parameters from the free response to an excitation. The method is subsequently refined by Bauchau and Wang (2008) in the *partial Floquet analysis*. The assumption of a free response causes some difficulties in the application of these methods to measurements from wind turbines in operation because of turbulence acting as a source of excitation.

A system identification method that successfully combines time-variance, admits input from natural excitations, and only requires measurement of the system response has, to the author's knowledge, yet to be derived.

1.2.4 Benchmark tools

There already exists a number of tools able to calculate the modal parameters of a rotating wind turbine, which the work in this thesis must be held up against. These methods are best compared by considering them using the following framework. The starting point of a *bottom-up approach* is the solution procedure, which limits the complexity of the model to allow for an exact solution. In this way the results are based on sound physical and mathematical principles and are easy to interpret, but

more complex effects cannot be modelled. An example of a bottom-up approach is an isotropic model solved using the Coleman transformation. On the other hand, a *top-down approach* starts off with a given model (or experiment) with all its complexities and obtains an approximate solution based on a practical solution procedure. This approach can deal with complex effects, but it can be more difficult to tell whether the results are physically based or are artefacts of the method, because the model and solution procedure are inconsistent. An extreme case of a top-down approach would be a black-box system identification where no knowledge of the physical system is assumed. Most existing tools are based on a compromise between a bottom-up and a top-down approach.

All current wind turbine modal analysis tools considered here are based on the Coleman transformation. The most bottom-up approach is HAWCStab (Hansen, 2004), which models a wind turbine with an isotropic rotor using linear finite beam elements where three identical elements on each blade are formulated directly in the inertial frame by the Coleman transformation. Unsteady aerodynamic forces are derived from a blade element momentum (BEM) method providing for isotropic external conditions. TURBU (van Engelen and Braam, 2004) is based on a nonlinear structural model with spring- and damper-connected rigid bodies and a BEM aerodynamic model, performing modal analysis for an isotropic system. Bir and Jonkman (2007) use the mode shape-based structural model FAST coupled to the aerodynamic code AeroDyn and obtain the modal properties after application of the Coleman transformation (MBC). The periodicity remaining in the Coleman transformed system equations due to anisotropy from external conditions or the rotor is averaged over a rotor rotation to allow an approximate modal analysis of an anisotropic system from a standard eigenvalue problem. Riziotis et al. (2004) base their stability tool on the GAST nonlinear aeroelastic code, which features aeroelastic finite beam elements with both structural and aerodynamic degrees of freedom. The periodic steady state due to a general inflow is found by time simulation, and an eigenvalue problem is set up after averaging over a rotor rotation. In case of an instability the steady state is obtained as the periodic part of the response.

The tools mentioned above and the tool presented in this thesis together with some of the approaches mentioned in the previous sections are inserted approximately on a 'bottom-up/top-down' scale in Figure 1.2.

1.3 Motivation

The motivation behind the work contained in this thesis is two-fold, relating to its status as an Industrial PhD project: on the practical side, Siemens Wind Power has wished to gain the ability to apply aeroelastic modal analysis on operating turbines; on the scientific side, the goal has been to develop methodologies for modal analysis of complex models of rotating wind turbines and through these models to gain additional insight into the dynamics of wind turbines influenced by anisotropic effects.

Aeroelastic modal analysis of an operating wind turbine has not yet seen much use in the industry. This situation has arisen because the modal analysis tools are most often based on simplified models obtained separately from the complex aeroelastic codes used for time simulation, necessitating a fitting of the models used for modal analysis and causing a possible discrepancy between results from modal analysis and time simulation. Also, there is a lack of experience with the practical

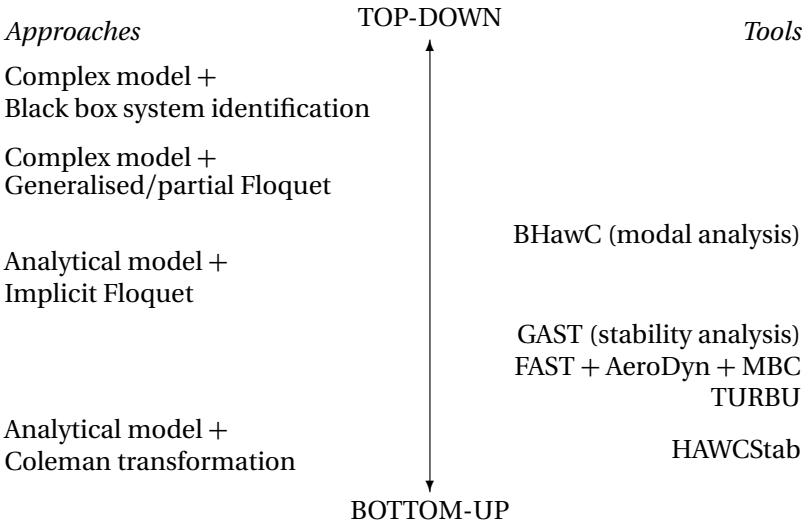

Figure 1.2: Selected approaches and tools inserted approximately on a 'bottom-up/top-down' scale characterising the modelling and solution procedure.

use of aeroelastic modal analysis in the industry, where the focus has been mostly on time simulations mandated by the certification standards.

Even though modal analysis of rotating systems has been researched for more than half a century, the focus has been mostly on the question of stability and not so much on the physical understanding of the motion causing the behaviour. The effects of anisotropy are more apparent in the periodic mode shape, determining the local motion, than in the modal damping, dictating increase or decrease of motion amplitude over a period. There is still a need for a more thorough understanding of what is the importance of the periodic mode shape, and whether anisotropic effects need be investigated at all.

The work on which this thesis is based has sought to provide a state of the art aeroelastic modal analysis tool based directly on the aeroelastic code BHawC used at Siemens Wind Power. In this process, analysis methods novel in the wind turbine community, have been used to obtain a tool that is able to correctly handle anisotropic effects. This tool is placed higher on the bottom-up/top-down scale in Figure 1.2 than existing tools for wind turbines, because it is built on a complex model not designed for modal analysis and because approximate solution methods are used. As a side-effect this frequency-domain tool can provide a means of validation and insight into the BHawC code. The tool is used for modal analysis of operating wind turbines and for examining the effects of anisotropy on the modal parameters.

The methods presented in this thesis can be applied to examine instability phenomena like stall-induced edgewise vibrations and flutter described by, e.g., Hansen (2007). This thesis does not, however, contain an investigation into these phenomena because the focus has been on the implementation of methods for modal analysis of anisotropic systems and the effects on the dynamics that the anisotropy has.

1.4 Structure

The goal of this thesis is to provide a coherent overview of the material contained in the papers [P1–P5] and also to present material that did not make it into these

papers. Writing this thesis has been an exercise in logically dividing three years' work. The outcome is a separation of modal analysis methods and their performance, which are covered in Chapters 2 to 4, and the modal dynamics of wind turbines, which is covered in Chapters 5 and Chapter 6.

Chapter 2 describes the three models used to illustrate the modal analysis methods: a simple model of flapwise vibrations, a simple model of edgewise vibrations, and the BHawC model. Chapter 3 defines modal analysis on a periodic system and describes the methods of Floquet analysis, Hill's method, the Coleman transformation approach, and partial Floquet analysis for a generic model. In Chapter 4 the implementation of the main analysis tool based on the linearised BHawC model and the approaches of Coleman transformation and implicit Floquet analysis is described in more detail. Chapter 5 describes the modal dynamics of wind turbines in isotropic conditions. In Chapter 6 the effects of an anisotropy on the rotor or the external conditions are assessed. Chapter 7 contains the conclusions and sums up suggestions for future work.

The original contributions of this thesis are:

1. a rigourous application of periodic modal analysis to an existing complex aeroelastic wind turbine code, which is the subject of Chapters 2 to 4, and

2. a survey of the modal dynamics in anisotropic conditions, which is the subject of Chapter 6.

Chapter 2

Wind turbine models

This chapter presents the three different models of a wind turbine that are used in this thesis. A simple model with flapwise vibrations is used as a testbed for the modal analysis methods. Another simple model with edgewise vibrations is used to simulate the lowly damped edgewise modes that are most easily identifiable on a realistic model. Finally, the aeroelastic BHawC model including a linearised version is presented.

2.1 Simple model of flapwise vibrations

A simple model that still represents some of the essential dynamics of a wind turbine is very useful for obtaining an understanding of the dynamics and for testing different solution methods with a minimum of implementation effort and computation time. Figure 2.1 shows such a model containing flapwise blade motion and a coupling between the blades through tilt and yaw of the nacelle for a total of five degrees of freedom. The nacelle and blades are modelled as rigid bodies connected by rotational springs and dampers. The model is purely structural.

The equations of motion are derived using Lagrange's equation, then linearised analytically around the steady state of zero deflections and written as

$$\mathbf{M}(t)\ddot{\mathbf{u}} + \mathbf{C}(t)\dot{\mathbf{u}} + \mathbf{K}(t)\mathbf{u} = \mathbf{0} \tag{2.1}$$

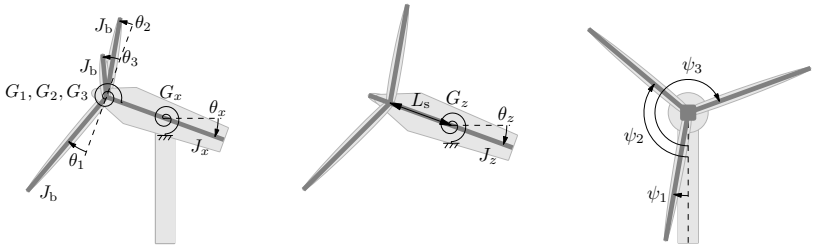

Figure 2.1: Simple model of wind turbine with five rotational degrees of freedom: flapwise blade deflections θ_1, θ_2, and θ_3, and nacelle tilt θ_x and yaw θ_z. From [P1, Fig. 1]

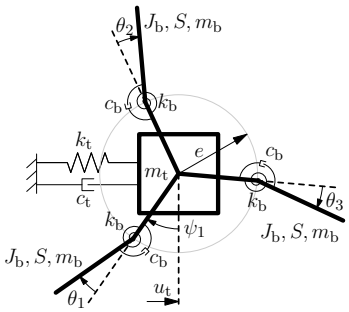

Figure 2.2: Simple model of wind turbine with four degrees of freedom: edgewise blade deflections θ_1, θ_2, θ_3, and tower top lateral displacement u_t. From [P5, Fig. 2].

where **M**, **C**, and **K** are the mass, damping/gyroscopic, and stiffness matrices, respectively, given in [P1, App. A.2], **u** is the vector of degrees of freedom, and $\dot{()} = \mathrm{d}/\mathrm{d}t$ denotes a time derivative. To simplify the notation in Equation 2.1 and onwards the time-dependence of the degrees of freedom or state variables is not explicitly stated.

This model is used in [P1], and in [P2] it is formulated in multi-blade coordinates. The parameters of the model are fitted to represent the dynamics of a generic multi-MW wind turbine [P1, Tab. 1].

2.2 Simple model of edgewise vibrations

A model derived similarly to that presented in the previous section but with edgewise blade deflections is used in [P5] for modelling the edgewise rotor modes and lateral tower mode that are lowly damped and thus easily identifiable on a real turbine. Figure 2.2 shows the purely structural model consisting of three blades modelled as rigid bodies connected with rotational springs and dampers to a tower top mass which can move laterally, for a total of four degrees of freedom. The linearised equations of motion are of the form given in Equation (2.1) with the matrices given in [P5, Sec. 3.1.1] in non-dimensional form.

This model is used in [P5] in a linearised version and also with cubic damping and stiffness terms to examine the effects of nonlinearities. The non-dimensional parameters of the model are chosen to represent the dynamics of a generic wind turbine [P5, Sec. 3.2].

2.3 The aeroelastic code BHawC

The nonlinear aeroelastic code BHawC has been developed in-house at Siemens Wind Power over the last eight years. It is used for design and certification of wind turbines, and it is continuously being validated against measured data. BHawC is a complex entity; this section serves to provide an overview of the underlying theory and the features most relevant for the modal analysis tool.

The main purpose of BHawC is to simulate the dynamic response of and calculate the loads on three-bladed wind turbines. The model consists of substructures for foundation, tower, nacelle, drivetrain, shaft, hub, and blades as shown in Figure 2.3. The structure is modelled primarily with finite beam elements and the aero-

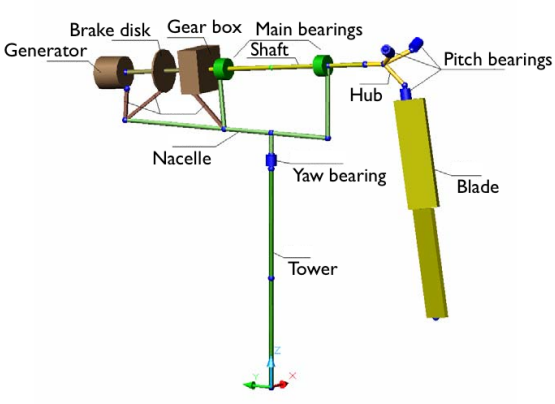

Figure 2.3: Sketch of BHawC model substructures. From [P3, Fig. 1].

dynamics is modelled using blade element momentum theory. The code is coupled to a controller identical to that on the real turbine.

2.3.1 Structural formulation

The finite beam element model in BHawC uses a co-rotational formulation where each element has its own coordinate system that rotates with the element. BHawC uses linear two-node Timoshenko beam elements derived by Petersen (1990) with 12 degrees of freedom: three positions and three rotations in each node. Special elements are introduced where bearings are present, and the drivetrain consists of purely torsional elements.

The substructures are connected through a predefined, direct kinematic coupling. The structural degrees of freedom for all elements are given relative to a coordinate system fixed at the turbine base (tower or foundation bottom), i.e., the coordinates are absolute and global. The configuration of the turbine is given by the nodal positions $\mathbf{p}$ and nodal orientations $\mathbf{q}$, and their velocities and accelerations. In a model valid for arbitrarily large rotations of the elements, special care must be taken of the representation of the orientations. In BHawC the orientations of the nodes are expressed as quaternions, a four-parameter equivalent to a rotation matrix (Krenk, 2009, Nikravesh, 1988), as a practical way of handling the non-commutativity of finite rotations. The derivatives of the orientations are expressed as angular velocities and accelerations about the three axes represented by the respective quaternions. Velocities and accelerations of the positions and orientations are collected in the vectors $\dot{\mathbf{u}}$ and $\ddot{\mathbf{u}}$, respectively.

The equilibrium equation is stated in global coordinates as

$$\mathbf{f}_{\text{iner}}(\mathbf{p},\mathbf{q},\dot{\mathbf{u}},\ddot{\mathbf{u}})+\mathbf{f}_{\text{damp}}(\mathbf{q},\dot{\mathbf{u}})+\mathbf{f}_{\text{int}}(\mathbf{p},\mathbf{q})=\mathbf{f}_{\text{ext}}(\mathbf{p},\mathbf{q},\dot{\mathbf{u}},\ddot{\mathbf{u}}) \tag{2.2}$$

where $\mathbf{f}_{\text{iner}}$ is the inertial force vector, $\mathbf{f}_{\text{damp}}$ is the structural viscous damping force vector, $\mathbf{f}_{\text{int}}$ is the internal force vector corresponding to elastic deformation, and $\mathbf{f}_{\text{ext}}$ is the external force vector. The inertial force vector is written as

$$\mathbf{f}_{\text{iner}}(\mathbf{p},\mathbf{q},\dot{\mathbf{u}},\ddot{\mathbf{u}})=\bar{\mathbf{M}}(\mathbf{q})\ddot{\mathbf{u}}+\bar{\mathbf{C}}(\mathbf{q},\dot{\mathbf{u}})\dot{\mathbf{u}}+\mathbf{f}_{\text{iner,stiff}}(\mathbf{p},\mathbf{q},\dot{\mathbf{u}},\ddot{\mathbf{u}}) \tag{2.3}$$

where $\bar{\mathbf{M}}$ and $\bar{\mathbf{C}}$ are mass and gyroscopic matrices, respectively, and $\mathbf{f}_{\text{iner,stiff}}$ is the inertial stiffness force. In element coordinates $\bar{\mathbf{M}}$ is constant, $\bar{\mathbf{C}}$ depends on the angular

velocities of the elements, and $\mathbf{f}_{\text{iner,stiff}}$ is due to elastic deformation and depending on the angular velocities and accelerations. All three terms are transformed into global coordinates using rotation matrices represented by the nodal quaternions $\mathbf{q}$. Because the formulation is in global coordinates $\bar{\mathbf{M}}$ provides the majority of the inertial forces, and the two last terms in Equation (2.3) are in fact negligible. The damping force is obtained as $\mathbf{f}_{\text{damp}}(\mathbf{q},\dot{\mathbf{u}}) = \mathbf{C}_{\text{damp}}(\mathbf{q})\dot{\mathbf{u}}$, where $\mathbf{C}_{\text{damp}}$ is a combined mass and stiffness proportional damping matrix transformed into global coordinates using the quaternions. To obtain the element internal force, an equilibrium format is used to retrieve the elastic deformation separated from the rigid body motion (Krenk et al., 1999). The equilibrium displacement is found from the nodal positions and orientations, and the internal force vector is transformed into global coordinates using the quaternions. The external force vector consists of aerodynamic, gravity, and applied forces and is dependent on the configuration of the turbine.

For a given configuration $(\mathbf{p},\mathbf{q},\dot{\mathbf{u}},\ddot{\mathbf{u}})$ and a given external force $\mathbf{f}_{\text{ext}}$, say an initial guess, the system might not be in equilibrium, i.e., Equation (2.2) might not be satisfied. To find this equilibrium, increments of the positions and orientations $\delta\mathbf{u}$, velocities $\delta\dot{\mathbf{u}}$ and accelerations $\delta\ddot{\mathbf{u}}$ are found using the tangent relation, obtained from a variation of the equilibrium equation (2.2) and written as

$$\mathbf{M}(\mathbf{q})\delta\ddot{\mathbf{u}} + \mathbf{C}(\mathbf{q},\dot{\mathbf{u}})\delta\dot{\mathbf{u}} + \mathbf{K}(\mathbf{p},\mathbf{q},\dot{\mathbf{u}},\ddot{\mathbf{u}})\delta\mathbf{u} = \mathbf{r} \tag{2.4}$$

where $\mathbf{M}$, $\mathbf{C}$, and $\mathbf{K}$ are the tangent matrices for mass, damping/gyroscopic forces, and stiffness, respectively, and $\mathbf{r} = \mathbf{f}_{\text{ext}} - \mathbf{f}_{\text{iner}} - \mathbf{f}_{\text{damp}} - \mathbf{f}_{\text{int}}$ is the residual. The tangent mass and damping/gyroscopic matrices are largely equal to $\bar{\mathbf{M}}$ and $\bar{\mathbf{C}}$ in the equilibrium equation (2.2) but contain contributions from the inertial force, which are negligible because the formulation is in global coordinates. The tangent stiffness matrix consists of constitutive stiffness, geometric stiffness due to both internal and external forces, and inertial stiffness. The updating of the configuration is accomplished through Newton-Raphson iteration using Equation (2.4) combined with a suitable solution procedure (the Newmark method, generalised-α method (Chung and Hulbert, 1993), or a steady state solution (described in Section 4.1)) to predict velocities $\delta\dot{\mathbf{u}}$ and accelerations $\delta\ddot{\mathbf{u}}$ and reduce the problem to the determination of $\delta\mathbf{u}$. In each step the tangent matrices and the residual including the external force are updated to reflect the new configuration. The Newton-Raphson procedure is continued until equilibrium is sufficiently satisfied around $\mathbf{r} \approx \mathbf{0}$. In this way a geometrically nonlinear model is achieved from a linear finite element model through the updating of the orientation and length of the elements. Increments to the rotations in $\delta\mathbf{u}$, which are assumed infinitesimal, are for each node represented as a rotation pseudo-vector, whose direction determines the axis of rotation and whose length determines the magnitude of rotation. The quaternion for node number i is updated as

$$\mathbf{q}_i := \mathbf{quat}(\delta\mathbf{u}_{i,\text{rot}}) * \mathbf{q}_i \tag{2.5}$$

where $\delta\mathbf{u}_{i,\text{rot}}$ contains three rotations that are assumed infinitesimal and thus commute, and where this rotation vector is transformed by the function termed **quat** into a quaternion, which is used to update the nodal quaternion $\mathbf{q}_i$ employing the special quaternion product denoted by $*$ which maintains the unity of the quaternion (Krenk, 2009). The nodal positions $\mathbf{p}$ and nodal velocities $\dot{\mathbf{u}}$ and accelerations $\ddot{\mathbf{u}}$ are updated by regular addition of the positional part of $\delta\mathbf{u}$, $\delta\dot{\mathbf{u}}$ and $\delta\ddot{\mathbf{u}}$, respectively, as determined by the solution procedure.

2.3.2 Aerodynamics

The aerodynamic force in BHawC is calculated in a number of points on the blades positioned independently of the structural nodes with finer spacing near the blade tips. Blade element momentum theory is applied to determine the tangential and axial induced velocities in these aerodynamic calculation points, and Prandtl's tip loss correction as well as a correction for the thrust at high induction values are implemented. The blade element momentum theory is expanded to allow a skewed inflow and an unsteady inflow by filtering the induced velocities as described by Björck (2000).

The aerodynamic force is based on 3D corrected stationary airfoil data with lift, drag, and moment coefficients, but is corrected by a Beddoes-Leishman-type dynamic stall model described by Petersen et al. (1998). The dynamic stall model takes the circulatory and impulsive loading into account, and the effects of trailing edge separation of the flow are determined from an expression for the lift as function of the separation point position due to Øye (1991), replacing the original expression by Leishman and Beddoes (1986). For each calculation point the flow is described by four state variables. In addition, BHawC contains a model for the tower shadow, and it also calculates the aerodynamic forces on the nacelle and tower.

The unsteady effect of trailing edge separation is modelled by the position of the separation point f, related to the lift coefficient C_L as

$$C_L = C_{L,\mathrm{fa}}(\alpha) f + C_{L,\mathrm{fs}}(\alpha)(1-f) \tag{2.6}$$

where $C_{L,\mathrm{fa}}$ is the lift curve for fully attached flow, $C_{L,\mathrm{fs}}$ is the lift curve for fully separated flow, and α is the angle of attack. The dynamics of the flow separation is modelled as

$$\dot{f} = \frac{2W}{\tau_\mathrm{f} c}(f_\mathrm{st}(\alpha) - f) \tag{2.7}$$

where W is the relative wind speed, c is the chord length, τ_f is a constant, and f_st is the stationary separation point position obtained from Equation (2.6) with C_L taken as the stationary value.

2.3.3 Linearised model for modal analysis

The tangent relation in Equation (2.4) describes small perturbations to the equilibrium configuration and can therefore by used as the linearised equations of motion for the structural part in modal analysis [P3]. The linearisation of the aerodynamic force, contributing with aerodynamic damping and stiffness and a coupling to the aerodynamic state variables, is performed numerically [P4]. In the current implementation only the unsteady aerodynamic effect of trailing edge separation is included in the linearised model. The separation point positions f for all calculation points are collected in the vector $\mathbf{a}$, and the linearised version of Equation (2.7) is written as

$$\dot{\mathbf{x}} = \mathbf{A}_\mathrm{d}(\mathbf{p},\mathbf{q},\dot{\mathbf{u}},\mathbf{a})\mathbf{x} + \mathbf{C}_\mathrm{ua}(\mathbf{p},\mathbf{q},\dot{\mathbf{u}},\mathbf{a})\dot{\mathbf{y}} + \mathbf{K}_\mathrm{ua}(\mathbf{p},\mathbf{q},\dot{\mathbf{u}},\mathbf{a})\mathbf{y} \tag{2.8}$$

where $\mathbf{A}_\mathrm{d}$ is the aerodynamic system matrix, and $\mathbf{C}_\mathrm{ua}$ and $\mathbf{K}_\mathrm{ua}$ are the aerodynamic velocity and displacement coupling matrices, respectively, all determined by numerical linearisation about the equilibrium configuration $(\mathbf{p},\mathbf{q},\dot{\mathbf{u}},\ddot{\mathbf{u}},\mathbf{a})$ [P4]. The degrees of freedom $\mathbf{y}$ contain perturbations to both positions $\mathbf{p}$ and orientations $\mathbf{q}$, its derivatives $\dot{\mathbf{y}}$ and $\ddot{\mathbf{y}}$ contain perturbations to $\dot{\mathbf{u}}$ and $\ddot{\mathbf{u}}$, respectively, and $\mathbf{x}$ contains perturbations to the aerodynamic state variables $\mathbf{a}$.

The structural equations of motion from Equation (2.4) including aerodynamic forces become

$$\mathbf{M}(\mathbf{q})\ddot{\mathbf{y}} + \left(\mathbf{C}(\mathbf{q},\dot{\mathbf{u}}) + \mathbf{C}_{\mathrm{a}}(\mathbf{p},\mathbf{q},\dot{\mathbf{u}},\mathbf{a})\right)\dot{\mathbf{y}} + \left(\mathbf{K}(\mathbf{p},\mathbf{q},\dot{\mathbf{u}},\ddot{\mathbf{u}}) + \mathbf{K}_{\mathrm{a}}(\mathbf{p},\mathbf{q},\dot{\mathbf{u}},\mathbf{a})\right)\mathbf{y} + \mathbf{A}_{\mathrm{f}}(\mathbf{p},\mathbf{q},\dot{\mathbf{u}},\mathbf{a})\mathbf{x} = \mathbf{0} \tag{2.9}$$

where $\mathbf{A}_{\mathrm{f}}$ is the aerodynamic flow coupling matrix determined by numerical linearisation, and all matrices are evaluated at the equilibrium configuration $(\mathbf{p},\mathbf{q},\dot{\mathbf{u}},\ddot{\mathbf{u}},\mathbf{a})$. The implementation is described in more detail in Chapter 4.

The combined linearised structural and aerodynamic equations of motion ((2.8) and (2.9)) form the basis of the aeroelastic BHawC modal analysis. Currently, effects of dynamic inflow and speed and pitch control are not included in the modal analysis. The structural model is used in [P3] and the aeroelastic model is used in [P4]. In both cases the BHawC model is a 2.3 MW pitch-regulated wind turbine with three 45 m blades, hub height 80 m, and nominal speed 16 rpm. The model has 381 structural degrees of freedom and 153 aerodynamic state variables.

Chapter 3

Methods for modal analysis of periodic systems

There are three steps to modal analysis with a numerical model: obtaining a steady state, linearisation of the equations of motion, and decomposition of the linearised motion into modal contributions. The first and last of the steps are described in this chapter with emphasis on the modal decomposition. The linearisation step depends on the model and is not treated in this chapter.

The described methods are either already existing or combined from existing methods, but most of them have not seen extensive use in the wind turbine community. The description is based on a generic state-space model of a bladed rotor system and the methods are validated by numerical results using the models described in Chapter 2.

3.1 Steady state calculation

The simplest case of a steady state is that with no deflection of the structure, and it need not be calculated. In the case of a non-zero deflection the steady state can be found as a periodic steady state solution directly from the equations of motion, or by time simulation until a sufficient approximation to steady state is obtained. The direct steady state method is fairly simple to implement in isotropic conditions ([P3, P4], see Section 4.1 for details), because the rotor speed and the blade deflection in the rotating frame are constant, hence the inertia and aerodynamic forces depend only on the rotor speed and the deflection state, and it can be calculated for a single azimuth angle at a time.

In anisotropic conditions the task is more demanding, because the members of the turbine, both on the supporting and rotating structures, exhibit periodic motion, meaning that inertia, damping, and aerodynamic forces must be calculated over a period of rotor rotation concurrently. One way of enforcing a periodic solution is to apply the period shooting technique (Nayfeh and Balachandran, 1995), which however requires multiple integrations of the system over a period of rotation of the rotor, and is therefore computationally very demanding. Another way is to construct a finite difference solution (Nayfeh and Balachandran, 1995) for which the linearised

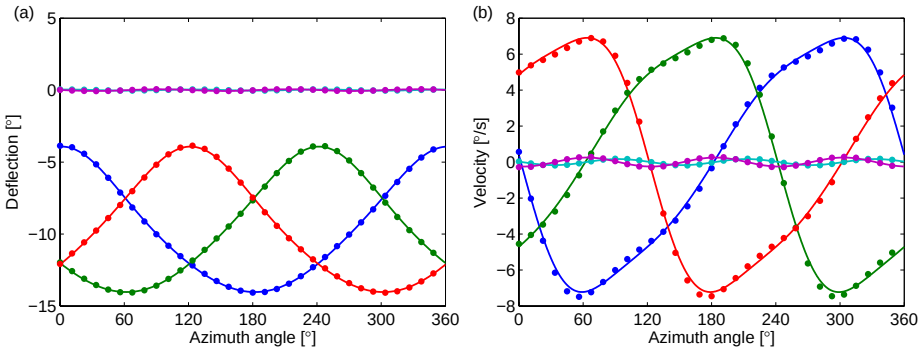

Figure 3.1: Anisotropic steady state calculation for the nonlinear simple flapwise model with rotor speed of 1.4 m/s and forcing simulating a logarithmic wind shear. Time simulation (—) and finite difference after six iterations using 32 points (•). Blades 1 (—), 2 (—), and 3 (—); nacelle tilt (—), and yaw (—).

equations of motion are written as

$$\dot{\mathbf{y}} = \mathbf{A}(t, \mathbf{y}, \dot{\mathbf{y}})\mathbf{y} + \mathbf{b}(t, \mathbf{y}, \dot{\mathbf{y}}) \tag{3.1}$$

where $\mathbf{y}$ is the state vector with N state variables, $\mathbf{A}$ is the linear system matrix, and $\mathbf{b}$ is the forcing vector. A periodic solution $\mathbf{y}(t+T) = \mathbf{y}(t)$, where T is the rotor period, is sought by discretising the period into m equal intervals with time points $t_i = ih$ and time step $h = T/m$. Equation (3.1) is written at the midpoint of interval i with the derivative approximated using a central difference scheme as $\dot{\mathbf{y}}(t_i - h/2) \approx (\mathbf{y}_i - \mathbf{y}_{i-1})/h$, and the other terms approximated by the mean value written as $\mathbf{A}(t_i - h/2)\mathbf{y}(t_i - h/2) \approx (\mathbf{A}_i\mathbf{y}_i + \mathbf{A}_{i-1}\mathbf{y}_{i-1})/2$ and $\mathbf{b}(t_i - h/2) \approx (\mathbf{b}_i + \mathbf{b}_{i-1})/2$, where the shorthand notation $\mathbf{y}_i = \mathbf{y}(t_i)$ is used. These approximate equations of motion for $i = 1, 2, \ldots, m$ are assembled in total form using $\mathbf{y}_0 = \mathbf{y}_m$ as

$$\hat{\mathbf{A}}\hat{\mathbf{y}} = \hat{\mathbf{b}} \tag{3.2}$$

where the expanded state vector with mN components is $\hat{\mathbf{y}} = \{\mathbf{y}_1^{\mathrm{T}}\ \mathbf{y}_2^{\mathrm{T}}\ \ldots\ \mathbf{y}_n^{\mathrm{T}}\}^{\mathrm{T}}$ and the coefficient matrix $\hat{\mathbf{A}}$ and forcing vector $\hat{\mathbf{b}}$ are given as

$$\hat{\mathbf{A}} = \begin{bmatrix} \mathbf{A}_1 - \frac{2}{h}\mathbf{I} & \mathbf{0} & \cdots & \mathbf{0} & \mathbf{A}_m + \frac{2}{h}\mathbf{I} \\ \mathbf{A}_1 + \frac{2}{h}\mathbf{I} & \mathbf{A}_2 - \frac{2}{h}\mathbf{I} & & \mathbf{0} & \mathbf{0} \\ & \ddots & \ddots & & \vdots \\ \mathbf{0} & & \mathbf{A}_{m-2} + \frac{2}{h}\mathbf{I} & \mathbf{A}_{m-1} - \frac{2}{h}\mathbf{I} & \mathbf{0} \\ \mathbf{0} & \cdots & \mathbf{0} & \mathbf{A}_{m-1} + \frac{2}{h}\mathbf{I} & \mathbf{A}_m - \frac{2}{h}\mathbf{I} \end{bmatrix}, \quad \hat{\mathbf{b}} = -\begin{Bmatrix} \mathbf{b}_m + \mathbf{b}_1 \\ \mathbf{b}_1 + \mathbf{b}_2 \\ \vdots \\ \mathbf{b}_{m-2} + \mathbf{b}_{m-1} \\ \mathbf{b}_{m-1} + \mathbf{b}_m \end{Bmatrix} \tag{3.3}$$

This system is solved using Newton-Raphson iteration updating $\hat{\mathbf{A}}$ and $\hat{\mathbf{b}}$ with the new value of $\hat{\mathbf{y}}$, and converges to the exact solution for an increasing number of time steps m.

Figure 3.1 shows a finite difference solution to a steady state caused by forcing simulating a logarithmic wind shear on the nonlinear simple flapwise model described in Section 2.1. Comparing to a time simulation the agreement for the deflections is better than for the velocities.

The advantage of the direct steady state method is that the solution is exactly periodic and that a solution can also be found in an unstable steady state, where

a time simulation would enter into a limit cycle oscillation or simply blow up. The direct steady state method is, however, complex to set up for a large model, and it has not been attempted here. One practical method to obtain an unstable steady state in isotropic conditions by time simulation is to increase the structural damping to make the equilibrium stable. In anisotropic conditions, however, this procedure would change the steady state because the elastic deformation is time-variant and thus dependent on the damping. Another approach is suggested by Riziotis et al. (2008) who use only the periodic part of the response growing in time, i.e., that with frequencies of multiples of the rotor speed. This approach could be problematic if the frequency of the mode causing the instability is close to a multiple of the rotor speed.

Modal analysis considers the free response of the system and depends only on the homogeneous part of the equations of motion. Therefore it is important to linearise as much of the various forces as possible to have them included in the homogeneous part and hence in the modal analysis. Details on the linearisation of the BHawC model are given in Section 4.2.

3.2 Modal analysis as an eigenvalue problem

The equations of motion linearised about a periodic steady state are typically cast in a second order form with mass, damping, and stiffness matrices for the structure, and in a first order form for the aerodynamics. To facilitate the modal analysis the homogeneous equations are written in first order form [P1] as

$$\dot{\mathbf{y}} = \mathbf{A}(t)\mathbf{y}, \quad \mathbf{A}(t+T) = \mathbf{A}(t) \tag{3.4}$$

where $\mathbf{y}$ is the state vector with N state variables consisting of the perturbations of the structural degrees of freedom and their velocities as well as the aerodynamic state variables and $\mathbf{A}$ is the T-periodic system matrix. A modal analysis cannot be directly performed on the periodic system, therefore the Lyapunov-Floquet (L-F) transformation $\mathbf{L}$, which transforms the system into a time-invariant one, is introduced as

$$\mathbf{y} = \mathbf{L}(t)\mathbf{z} \tag{3.5}$$

where $\mathbf{z}$ is the L-F transformed state vector. The time-invariant transformed system given as

$$\dot{\mathbf{z}} = \mathbf{A}_\mathrm{L}\mathbf{z}, \quad \mathbf{A}_\mathrm{L} = \mathbf{L}^{-1}(t)\big(\mathbf{A}(t)\mathbf{L}(t) - \dot{\mathbf{L}}(t)\big) \tag{3.6}$$

has the simple solution $\mathbf{z} = \mathrm{e}^{\mathbf{A}_\mathrm{L} t}\mathbf{z}(0)$ because the L-F transformed system matrix $\mathbf{A}_\mathrm{L}$ is constant.

A modal decomposition of the time-invariant system in Equation (3.6) is readily obtained from the standard eigenvalue analysis of the system matrix

$$\mathbf{A}_\mathrm{L} = \mathbf{V}_\mathrm{L}\mathbf{\Lambda}\mathbf{V}_\mathrm{L}^{-1} \tag{3.7}$$

where $\mathbf{V}_\mathrm{L}$ contains the eigenvectors of $\mathbf{A}_\mathrm{L}$ as columns and $\mathbf{\Lambda}$ is a diagonal matrix containing its eigenvalues, assuming that a complete set of linearly independent eigenvectors exist for $\mathbf{A}_\mathrm{L}$. This assumption is made in this thesis. A detailed discussion of the general Jordan decomposition applicable in the case of linearly dependent eigenvectors is made by Nayfeh and Balachandran (1995). The free response of

the system is found by inserting the modally decomposed system matrix of Equation (3.7) into the solution of Equation (3.6) and transforming back into the original coordinates using Equation (3.5) as

$$\mathbf{y} = \sum_{k=1}^{N} \mathbf{u}_k(t)\, \mathrm{e}^{\lambda_k t} q_k(0) \tag{3.8}$$

where $\mathbf{u}_k$ are the periodic mode shapes contained as columns in the matrix $\mathbf{U}(t) = \mathbf{L}(t)\mathbf{V}_\mathrm{L}$, $\lambda_k = \sigma_k + \mathrm{i}\omega_k$ with $\mathrm{i} = \sqrt{-1}$ are the eigenvalues containing the damping σ_k and frequency ω_k, and $q_k(0)$ is the initial content of mode number k. Note that the free response is a sum of modal contributions, like in the case of time-invariant systems, but the mode shape is periodic with the rotor period. The damping ratio is defined as

$$\zeta_k = \frac{-\sigma_k}{|\omega_k|\sqrt{1+\sigma_k^2/\omega_k^2}} \tag{3.9}$$

and the logarithmic decrement as

$$\delta_k = \frac{-2\pi\sigma_k}{|\omega_k|} \tag{3.10}$$

The following sections describe different approaches to obtaining the modally decomposed solution given in Equation (3.8), either by an explicit L-F transformation or with it implicitly built into the method.

3.3 Floquet analysis

Floquet theory (Coddington and Levinson, 1955) shows that an L-F transformation exists, but it does not provide an explicit means of obtaining it. Floquet analysis is an application of Floquet theory using a numerically integrated set of solutions to Equation (3.4) from which the modal decomposition is obtained. This section is divided into classical Floquet analysis, which is a straight-forward numerical implementation of Floquet theory, and implicit Floquet analysis which is an approximate implementation to efficiently extract the least damped modes of large systems.

3.3.1 Classical Floquet analysis

A fundamental solution of Equation (3.4) consists of N solutions obtained, e.g., by numerical integration, over $t \in [0; T]$ with linearly independent initial conditions written as

$$\boldsymbol{\varphi}(t) = [\boldsymbol{\varphi}_1(t) \quad \boldsymbol{\varphi}_2(t) \quad \dots \quad \boldsymbol{\varphi}_N(t)] \tag{3.11}$$

such that $\dot{\boldsymbol{\varphi}}(t) = \mathbf{A}(t)\boldsymbol{\varphi}(t)$. Because $\mathbf{A}$ is T-periodic, $\boldsymbol{\varphi}(t+T)$ is also a solution to Equation (3.4), $\dot{\boldsymbol{\varphi}}(t+T) = \mathbf{A}(t)\boldsymbol{\varphi}(t+T)$, and therefore $\boldsymbol{\varphi}(t+T)$ must be a linear combination of $\boldsymbol{\varphi}(t)$ written as

$$\boldsymbol{\varphi}(T) = \boldsymbol{\varphi}(0)\mathbf{C} \tag{3.12}$$

where $\mathbf{C}$ is the monodromy matrix, and $t = 0$ is introduced without loss of generality. Any particular solution within $t \in [0; T]$ can be written as a linear combination of the columns in the fundamental solution as $\mathbf{y} = \boldsymbol{\varphi}(t)(\boldsymbol{\varphi}^{-1}(0)\mathbf{y}(0))$, which indicates

that the fundamental solution contains all information about the dynamics of the system.

The principal result of Floquet theory is that the fundamental solution can be written as a product of a purely periodic matrix and a matrix exponential (Coddington and Levinson, 1955, see [P2] for details)

$$\boldsymbol{\varphi}(t) = \big(\mathbf{L}(t)\mathbf{L}^{-1}(0)\boldsymbol{\varphi}(0)\big)\,\mathrm{e}^{\mathbf{R}t} \tag{3.13}$$

where the system matrix $\mathbf{R}$ of this time-invariant system is defined in terms of the monodromy matrix as $\mathbf{C} = \mathrm{e}^{\mathbf{R}T}$, and the term $\mathbf{L}^{-1}(0)\boldsymbol{\varphi}(0)$ is introduced to make the L-F transformation independent of the particular choice of fundamental solution. The initial condition $\mathbf{L}(0)$ is arbitrary but can be selected to give physical meaning to the transformation. The L-F transformation can thus be written in terms of the fundamental solution and the eigenvalue decomposition $\mathbf{R} = \mathbf{V}\boldsymbol{\Lambda}\mathbf{V}^{-1}$ as

$$\mathbf{L}(t) = \boldsymbol{\varphi}(t)\mathbf{V}\mathrm{e}^{-\boldsymbol{\Lambda}t}\mathbf{V}^{-1}\boldsymbol{\varphi}^{-1}(0)\mathbf{L}(0) \tag{3.14}$$

and the system matrix of the corresponding time-invariant system is

$$\mathbf{A}_{\mathrm{L}} = \mathbf{L}^{-1}(0)\boldsymbol{\varphi}(0)\mathbf{R}\big(\mathbf{L}^{-1}(0)\boldsymbol{\varphi}(0)\big)^{-1} \tag{3.15}$$

which is similar to $\mathbf{R}$ and therefore has the same eigenvalues [P1]. The characteristic exponents λ_k obtained from the characteristic multipliers ρ_k, the eigenvalues of $\mathbf{C}$, as $\lambda_k = \ln(\rho_k)/T$ yield the modal frequencies and damping as

$$\begin{aligned} \omega_{\mathrm{p},k} &= \arg(\rho_k)/T\,, \quad \omega_{\mathrm{p},k} \in]-\Omega/2;\Omega/2] \\ \omega_k &= \omega_{\mathrm{p},k} + j_k\Omega \\ \sigma_k &= \ln(|\rho_k|)/T \end{aligned} \tag{3.16}$$

where the modal frequency ω_k is not unique because of the infinite branches of the complex logarithm and can be obtained by adding any integer multiple j_k of the rotor speed Ω to the principal frequency $\omega_{\mathrm{p},k}$. This choice of frequency is addressed in Section 3.6. The periodic mode shapes are obtained as

$$\mathbf{u}_k(t) = \boldsymbol{\varphi}(t)\mathbf{v}_k\mathrm{e}^{-\lambda_k t} \tag{3.17}$$

which also depend on the choice of frequency contained in λ_k, such that the solution in Equation (3.8) is not dependent on that choice.

Floquet analysis can be characterised as a time domain method, in that it relies on integration in time of the system equations and that the periodic mode shapes result in the time domain. These mode shapes can subsequently be described in the frequency domain by a Fourier transformation.

Floquet analysis can also be classified as a system identification method because it relies on the response of the system and not the system equations directly. It is, however, exact in the sense that the consistency between the response and the model is determined only by the precision of the integration algorithm. The response from a nonlinear model where the perturbations to the steady state are small can be used in the fundamental solution, thus avoiding the step of linearisation. This possibility, mentioned in [P2], is here applied to the simple flapwise model. Figure 3.2 shows the error in frequency from a Floquet analysis using the linear and nonlinear responses compared to the exact solution as function of initial condition

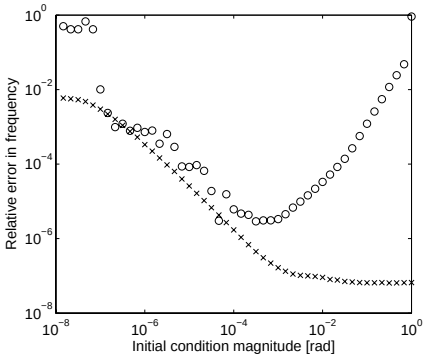

Figure 3.2: Error in frequency compared to exact solution as function of magnitude of initial condition of a Floquet analysis of the simple flapwise model. Linear response (×) and nonlinear response (∘).

magnitude. In each calculation the initial conditions have the same mechanical energy as the flapwise symmetric mode with the given deformation. The error using the linear response decreases with the magnitude of the initial condition because the signal to noise ratio decreases due to a constant error tolerance in the integration. The same is the case for the nonlinear response until around 10^{-3} rad where nonlinear effects become significant and introduce errors in the modal decomposition. Thus, this approach requires that one find this window in the magnitude of initial condition, where the precision is acceptable.

In Floquet analysis a number of authors use the state transition matrix $\mathbf{\Phi}(t_1,t_0)$ that maps the fundamental solution from one point in time to another, such that $\boldsymbol{\varphi}(t_1) = \mathbf{\Phi}(t_1,t_0)\boldsymbol{\varphi}(t_0)$ (Johnson, 1980). The relation between the state transition matrix after one period and the monodromy matrix is $\mathbf{C} = \boldsymbol{\varphi}^{-1}(0)\mathbf{\Phi}(T,0)\boldsymbol{\varphi}(0)$. The matrices are similar and have the same eigenvalues, which means that modal damping and frequency can be found from either of them. The eigenvectors $\mathbf{w}_k$ of $\mathbf{\Phi}(T,0)$ are related to the eigenvectors $\mathbf{v}_k$ of $\mathbf{C}$ as $\mathbf{w}_k = \boldsymbol{\varphi}(0)\mathbf{v}_k$, which must be taken into account in the calculation of the periodic mode shapes if the initial condition of the fundamental solution is not the identity matrix.

The practical applicability of Floquet analysis is very dependent on the rotor speed. For speeds tending to zero the rotor period tends to infinity but the integration time step must be held at a certain value to resolve the dynamics of the system, and thus the computation time tends to infinity. But at very low speeds the effects of rotation are negligible and the analysis might be replaced by several standstill analyses for different azimuth angles. Classical Floquet analysis is prohibitive, or at best impractical, for large systems, where a more efficient method such as implicit Floquet analysis, considered in the next section, should be used. Therefore the classical Floquet analysis is applied only to the simple flapwise model in [P1, P2].

3.3.2 Implicit Floquet analysis

Implicit Floquet analysis (Bauchau and Nikishkov, 2001) exploits the feature of the Arnoldi algorithm (see, e.g., Golub and van Loan (1989)) for eigenvalue extraction of a matrix, that it requests the product of this matrix with a vector. The matrix in question is the state transition matrix after a period, the vector is an initial condition

of the system, and the product is thereby the response after one period to the given initial condition. The Arnoldi algorithm successively determines the initial condition in each step such that all initial conditions form an orthogonal subspace after m Arnoldi steps written as

$$\mathbf{P} = [\mathbf{p}_1 \quad \mathbf{p}_2 \quad \dots \quad \mathbf{p}_m] \tag{3.18}$$

where the first initial condition $\mathbf{p}_1 = \varphi_1(0)$ is arbitrary. The algorithm also builds the projection of the transition matrix in the subspace, written as

$$\mathbf{H} = \mathbf{P}^{\mathrm{T}} \mathbf{\Phi}(T,0) \mathbf{P} \tag{3.19}$$

of size $m \times m$. If N Arnoldi steps were performed, requiring N integrations of the system over a period, $\mathbf{P}$ would constitute the initial conditions of a fundamental solution and classical Floquet analysis could be performed on either $\mathbf{\Phi}(T,0)$ or $\mathbf{H}$. But the eigenvalues of $\mathbf{H}$ approximate those of $\mathbf{\Phi}(T,0)$ with the characteristic multipliers of largest magnitude converging first, so after much fewer than N steps a good approximation of the lowest damped modes (the characteristic exponents with largest real part) can be obtained.

The m approximate modal frequencies $\tilde{\omega}_k$, damping $\tilde{\sigma}_k$, and mode shapes $\tilde{\mathbf{u}}_k$ are determined after m Arnoldi steps as

$$\begin{aligned} \tilde{\omega}_{\mathrm{p},k} &= \arg(\tilde{\rho}_k)/T \\ \tilde{\omega}_k &= \tilde{\omega}_{\mathrm{p},k} + j_k \Omega \\ \tilde{\sigma}_k &= \ln(|\tilde{\rho}_k|)/T \\ \mathbf{u}_k(t) &= [\varphi_1(t) \quad \varphi_2(t) \quad \dots \quad \varphi_m(t)]\, \tilde{\mathbf{w}}_k \mathrm{e}^{-\tilde{\lambda}_k t} \end{aligned} \tag{3.20}$$

where $\tilde{\rho}_k$ are the eigenvalues of $\mathbf{H}$ and $\tilde{\mathbf{w}}_k$ are its eigenvectors. The issues with frequency non-uniqueness described for classical Floquet analysis also apply to the implicit Floquet analysis.

The dynamics of the system is determined by the m-dimensional subspace projected system

$$\dot{\tilde{\mathbf{y}}} = \tilde{\mathbf{A}}_{\mathrm{L}} \tilde{\mathbf{y}} \tag{3.21}$$

where $\tilde{\mathbf{y}} = \mathbf{P}^{\mathrm{T}} \mathbf{y}$, with L-F transformation

$$\tilde{\mathbf{L}}(t) = \mathbf{P}^{\mathrm{T}} \varphi(t) \tilde{\mathbf{W}} \mathrm{e}^{-\tilde{\Lambda} t} \tilde{\mathbf{W}}^{-1} \left(\mathbf{P}^{\mathrm{T}} \varphi(0)\right)^{-1} \tilde{\mathbf{L}}(0) \tag{3.22}$$

and system matrix

$$\tilde{\mathbf{A}}_{\mathrm{L}} = \ln(\mathbf{H})/T = \tilde{\mathbf{W}} \tilde{\mathbf{\Lambda}} \tilde{\mathbf{W}}^{-1} \tag{3.23}$$

where $\tilde{\mathbf{\Lambda}}$ contains the characteristic exponents $\tilde{\lambda}_k = \ln(\tilde{\rho}_k)/T$ in the diagonal, $\tilde{\mathbf{W}}$ contains the eigenvectors of $\mathbf{H}$ as columns, and the initial condition $\tilde{\mathbf{L}}(0)$ is arbitrary.

The advantage of the implicit Floquet analysis is that it has the same qualities as classical Floquet analysis, but that it makes the treatment of larger systems possible due to the reduced computation time. Hence it is used in [P3, P4] on the BHawC model. Figure 3.3 shows the convergence of the modes as function of the Arnoldi step [P3] where 19 modes are converged after 50 steps. An equivalent classical Floquet analysis would require 762 integrations. The modes with lowest damping, which are obtained from an implicit Floquet analysis, are the most important modes with regard to stability, and for a purely structural model they typically correspond to the

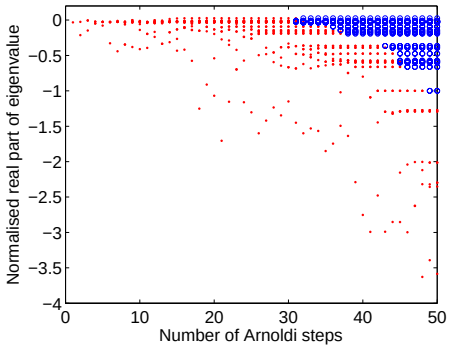

Figure 3.3: Normalised real part of implicit Floquet characteristic exponents of the structural BHawC model as function of Arnoldi steps. Non-converged eigenvalues (•) and converged eigenvalues (○). From [P3, Fig. 3].

modes with lowest frequency which describe the most important dynamics of the system.

Another advantage of the implicit Floquet analysis is that the number of Arnoldi steps, i.e., system integrations, necessary for a given number of modes to converge is believed to be independent of the detail, i.e., number of state variables, of the model and is instead a characteristic of the system dynamics. So the computational burden increases only in view of the larger system matrices to integrate, whereas for a classical (or even Fast) Floquet analysis it would also increase the number of integrations. For example, 50 Arnoldi steps are required to extract the 19 modes with lowest frequency of the structural model [P3], and 56 steps are required to extract the 19 modes with lowest damping (including the 14 modes with lowest frequency) of the aeroelastic model [P4] which has more state variables. This hypothesis needs to be confirmed by analyses with models of different complexity.

3.4 Hill's method

Floquet theory shows that the free response of a system with a periodic system matrix contains a mode shape periodic with the same period (cf. Equation (3.8) and see [P1] for more details). Therefore the system matrix and periodic mode shapes can be expressed as the Fourier series

$$\begin{aligned} \mathbf{A}(t) &= \sum_{l=-\infty}^{\infty} \mathcal{A}_l \, \mathrm{e}^{\mathrm{i}l\Omega t} \\ \mathbf{u}_k(t) &= \sum_{l=-\infty}^{\infty} u_{k,l} \, \mathrm{e}^{\mathrm{i}l\Omega t} \end{aligned} \tag{3.24}$$

where $\mathcal{A}_l$ and $u_{k,l}$ contain the harmonic components with frequency $l\Omega$ of $\mathbf{A}$ and $\mathbf{u}_k$, respectively. Inserting the expansion of the mode shape into the solution given in Equation (3.8), then inserting this expression and the expansion of the system matrix into Equation (3.4), and finally collecting coefficients of equal harmonics yields the eigenvalue problem (Xu and Gasch, 1995, see [P2] for more details)

$$(\hat{\mathbf{A}} - \lambda_{k,j}\mathbf{I})\,\hat{u}_{k,j} = \mathbf{0} \tag{3.25}$$

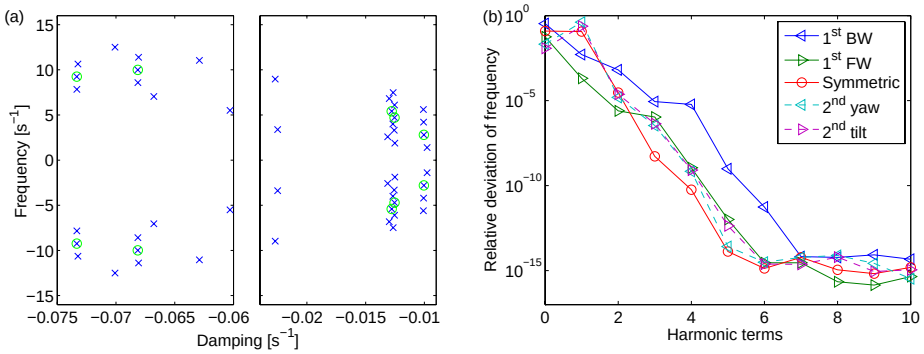

Figure 3.4: Hill's method applied to the simple flapwise model. (a) Eigenvalues (×) and basis eigenvalues (○) for two harmonic terms included in the expansion; (b) error in frequency for different numbers of harmonic terms compared to the solution with eleven terms.

where $\hat{\mathbf{A}}$ is of infinite size and $\hat{u}_{k,j}$ is of infinite length. For each mode k there exists an infinite number of eigenvalues $\lambda_{k,j}$ with the same damping values and with frequencies differing by multiples of the rotor speed Ω. Similarly, there exist infinitely many eigenvectors $\hat{u}_{k,j}$ containing the harmonic components of the periodic mode shape. These components are shifted integer multiples of the rotor speed in frequency between different values of j. Because all pairs of $\lambda_{k,j}$ and $\hat{u}_{k,j}$ produce the same solution, only one pair need be included.

Hill's method is applied to the simple flapwise model in [P2], where the infinite-dimension eigenvalue problem of Equation (3.25) is truncated to include a finite number of terms in the expansion. This truncation introduces errors in $\lambda_{k,j}$ and $\hat{u}_{k,j}$ such that the eigenvalues belonging to one mode are then in general not exactly equal in the real part, neither differing exactly by Ω in the imaginary part, nor do the eigenvectors contain the exact same components [P2]. This situation is illustrated in Figure 3.4(a) where the inclusion of two harmonic terms should yield five complex conjugate eigenvalues for each mode. But for the highest damped mode, for example, it is only possible to identify three eigenvalues, where the remaining two eigenvalues contain significant errors caused by the truncation. This observation indicates that eigenvalues that are centred in frequency, also termed the basis eigenvalues (Christensen and Santos, 2005), contain the most precise solution, because the harmonic components that are included in the truncated eigenvector $\hat{u}_{k,j}$ are those with the largest relative magnitude [P2] (see also Section 3.6). The figure also shows that it can be difficult to identify the basis eigenvalue, especially for a low number of terms included. Figure 3.4(b) shows that the solution using the basis eigenvalues converges for an increasing number of terms included. Choosing which eigenvalue to use for each mode also determines the modal frequency, which is non-unique like in Floquet analysis. This choice is addressed in Section 3.6.

The periodic mode shape is thus given by Equation (3.24) with $l = -m,\ldots,m$, where m is the number of harmonic terms included. Because the method operates directly on the periodic mode shape, this might be considered the L-F transformation, $\mathbf{L}(t) = \mathbf{U}(t)$, and the time-invariant system matrix becomes $\mathbf{A}_\mathrm{L} = \mathbf{\Lambda}$, which is already diagonalised.

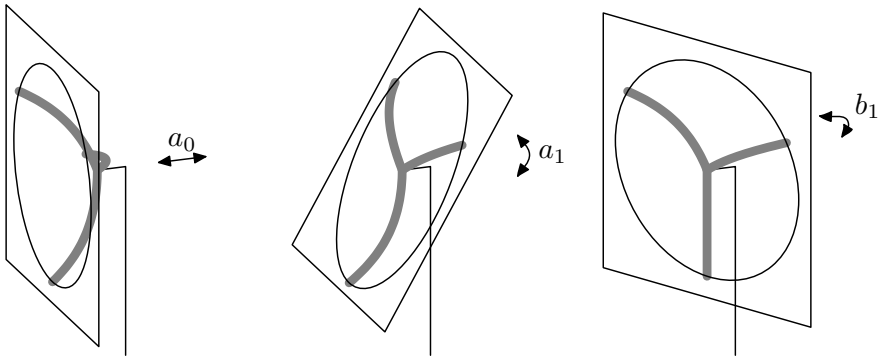

Figure 3.5: Multi-blade coordinates for flapwise motion of a three-bladed rotor.

Hill's method can be characterised as a frequency domain method because the Fourier series of the system matrix is used and because the periodic mode shape results in frequency domain. Eliminating the need for time integration of the system makes Hill's method fast in use when applying the computationally efficient Fast Fourier Transform algorithm. The expanded eigenvalue problem does, however, become very large for large systems, which necessitates a formulation in sparse matrices and a reliable solver that can retrieve selected modes, e.g., with lowest damping. Friedmann (1986) notes that Hill's method is not convenient for implementation on computers in comparison with Floquet analysis. He does not substantiate this statement, but he might be referring to the problem with the large eigenvalue problem or to the problem with choosing which eigenvalue to use for each mode. In this work, Hill's method has been applied only to a model of small dimension because, indeed, the reliability of the sparse eigenvalue solver was not satisfactory.

3.5 Coleman transformation approach

Coleman (1943) introduces a transformation to describe the degrees of freedom on a bladed rotor in the inertial, or non-rotating, frame. The transformation makes the system matrix time-invariant when the system is isotropic, and it is thus a special case of the L-F transformation [P1]. What makes the Coleman transformation especially useful is that it is known a priori for a given system and that it is based on a physically meaningful coordinate transformation.

The transformation uses multi-blade coordinates which for a three bladed rotor are given as

$$a_0 = \frac{1}{3}\sum_{j=1}^{3} u_j\,, \quad a_1 = \frac{2}{3}\sum_{j=1}^{3} \cos(\psi_j) u_j\,, \quad b_1 = \frac{2}{3}\sum_{j=1}^{3} \sin(\psi_j) u_j \tag{3.26}$$

where $\psi_j = \psi_1 + 2\pi(j-1)/3$ is the azimuth angle for blade number j and u_j are a set of state variables, which are identical in the local blade frame. For u_j representing flapwise motion and $\psi_j = 0$ for blade j pointing down, Figure 3.5 shows that a_0 is symmetric flapwise motion, a_1 is tilting motion of the rotor, and b_1 is yawing motion of the rotor. For u_j representing edgewise motion, a_0 is the symmetric edgewise

motion coupling to the drivetrain, a_1 is horizontal motion of the rotor, and b_1 is vertical motion of the rotor.

The inverse transformations of those in Equation (3.26) are collected in matrix form as

$$\mathbf{u} = \mathbf{B}_u(t)\mathbf{z} \tag{3.27}$$

with $\mathbf{u} = \{u_1\ u_2\ u_3\}^{\mathrm{T}}$, $\mathbf{z} = \{a_0\ a_1\ b_1\}^{\mathrm{T}}$ and

$$\mathbf{B}_u(t) = \begin{bmatrix} 1 & \cos(\psi_1(t)) & \sin(\psi_1(t)) \\ 1 & \cos(\psi_2(t)) & \sin(\psi_2(t)) \\ 1 & \cos(\psi_3(t)) & \sin(\psi_3(t)) \end{bmatrix} \tag{3.28}$$

where $\mathbf{B}_u$ has the convenient properties $\mathbf{B}_u^{-1}(t) = \boldsymbol{\mu}\mathbf{B}_u^{\mathrm{T}}(t)$ and $\dot{\mathbf{B}}_u(t) = \mathbf{B}_u(t)\,\bar{\boldsymbol{\omega}}$ with $\boldsymbol{\mu}$ and $\bar{\boldsymbol{\omega}}$ constant matrices known a priori in isotropic conditions (Hansen, 2003). The transformation matrix in Equation (3.28) can be expanded into a matrix $\mathbf{B}(t)$ including transformations for all sets of corresponding state variables on the blades, and including simple rotational transformations for state variables on the non-bladed rotating members, e.g. the shaft, as well as including the identity transformation for state variables on non-rotating members. Thus, the matrix $\mathbf{B}(t)$ transforms the original state variables into the inertial frame, which makes an isotropic system time-invariant. After the system is transformed into the inertial frame, a standard eigenvalue analysis of the transformed system matrix given by Equation (3.6) with $\mathbf{B}(t) = \mathbf{L}(t)$ yields the modal frequencies and damping, and the eigenvectors in multi-blade coordinates. This approach is used for modal analysis in [P1–P5].

The advantages of using the Coleman transformation for modal decomposition are that the approach is simple, fast, and physically based, such that there is no ambiguity with respect to the frequencies. But it only allows an exact modal analysis of isotropic systems. In case of anisotropic systems the Coleman transformation still makes the system less time-variant, and the approach can be used in combination with the methods mentioned previously. Applying the Coleman transformation before using Hill's method [P2] results in fewer harmonic terms needed in the expansion to give a good approximation to the solution. In combination with Floquet analysis the Coleman transformation provides no saving in computation time, on the contrary it might ruin the sparsity of the system matrices and increase the computation time, but it is useful for identification of the modal frequency.

3.6 Identification of modal frequency

As seen in the previous sections the L-F transformations associated with Floquet analysis and Hill's method are not unique, which means that the frequency content in the solution is arbitrarily divided between the eigenvalue and the periodic mode shape.

For an isotropic system the Coleman transformation provides an L-F transformation which is unique and known a priori for a given system, and which transforms the system into the inertial frame. To give physical meaning to the modal frequency determined from Floquet analysis and Hill's method it is defined as that which can be measured in the inertial frame, i.e. for an isotropic system the L-F transformation is chosen to be equal to the Coleman transformation [P1]. This choice is done by requiring that the periodic mode shape for components in the inertial frame be constant as is the case for a system described in multi-blade coordinates.

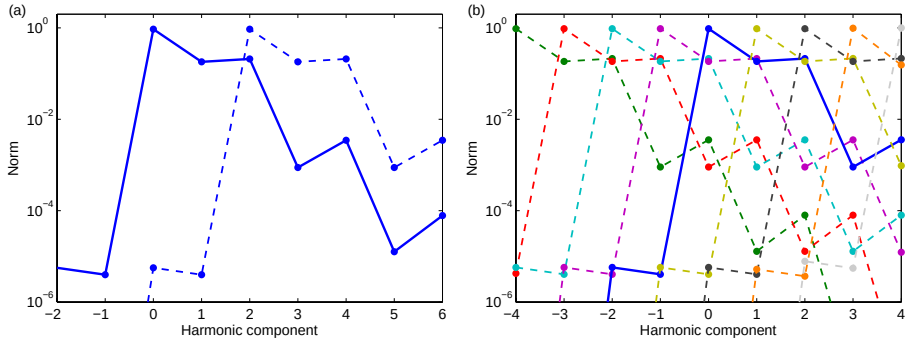

Figure 3.6: Norm of harmonic components of periodic mode shape in multi-blade coordinates for the simple flapwise model with anisotropic rotor. (a) Floquet analysis, principal (– –) and identified (—) mode shapes; (b) Hill's method, mode shapes of basis (—) and other (– –) eigenvalues. The norm is calculated from the amplitude of the position parts in the mode shape. The spectrum is discrete and represented by the dots; the lines are drawn only to aid in separating the series.

By extension of this principle to anisotropic conditions the periodic mode shape for anisotropic systems is required to be as constant as possible for state variables in the inertial frame [P1]. In this way, for mildly anisotropic systems, the frequencies will be close to those obtained using the Coleman transformation on a corresponding isotropic system, but the periodic mode shapes will correctly reflect the anisotropy of the system.

That the modal frequency is not uniquely determined in Floquet analysis and Hill's method is a consequence of the ability of these methods to handle anisotropic systems where the modal frequency in the general is not well defined, because the response on all members of the structure can contain an infinite number of harmonic components. In mildly anisotropic conditions, which is the typical case for wind turbines, the modal frequency can be uniquely defined by similarity to the isotropic condition, but for strongly anisotropic systems it is better to examine the frequency spectrum of the response of a single mode (see, e.g., [P1, Fig. 5]) because there might be several dominating frequencies, even in the inertial frame.

In practice, the frequency spectrum of the periodic mode shape for state variables on the supporting structure can be analysed to find the dominating harmonic component (j_k in Equation (3.16)) which must be extracted from the periodic mode shape and transferred to the modal frequency. If the periodic mode shape for the state variables on the rotor is given in multi-blade coordinates, these can also be used to determine the frequency content in the inertial frame. The frequency content is typically determined more precisely by including the rotor components because of their larger deflection. Thus, the Coleman transformation is useful for identification of the modal frequency in both Floquet analysis and Hill's method.

Even though, in principle, the process of frequency identification is similar for Floquet analysis and Hill's method, there are some practical differences. Figure 3.6 shows the norm of each harmonic component in the multi-blade coordinate mode shape from Floquet analysis and Hill's method with four harmonic terms included, applied to the simple flapwise model. In the Floquet analysis in Figure 3.6(a) a single periodic mode shape is calculated using the principal frequency, and this periodic

mode shape is then shifted -2Ω in frequency, such that the dominating component is at zero frequency. The modal frequency is then found by adding 2Ω to the principal frequency. In Hill's method in Figure 3.6(b) several periodic mode shapes are calculated, the choice between which both determines the modal frequency and the precision of the solution. Here, the one with the dominating component at zero frequency is used, which is also the one in the centre with the basis eigenvalue, where the harmonic components that are truncated in the average case are the ones with the smallest magnitude, providing the most precise eigenvalue. In Figure 3.6, however, the best representation of the mode shape is that with the dominating component at -2Ω, because the positive harmonic components in this case are dominant. Alternatively this mode shape could have been used and the frequency shifted like in Floquet analysis to have the dominating component at zero frequency.

3.7 Partial Floquet analysis

To overcome the difficulties of obtaining linearised systems for large, complex models and applying Floquet analysis to these systems, the partial Floquet analysis has been developed (Bauchau and Wang, 2008). It is a system identification method in that it applies Floquet analysis to a limited number of time signals of the free response obtained over relatively short time to perturbations about a periodic steady state. Concepts from signal analysis are incorporated to achieve an approximation to the modal parameters of the system. The method can be used with responses directly from the nonlinear model meaning that no analytical linearisation of the system equations is necessary. The method can also be applied to measurements, provided that the free response to an applied excitation can be measured without significant external disturbances.

3.7.1 Partial Floquet analysis on periodic systems

The underlying system is assumed to be of the form in Equation (3.4). The time signals used are typically displacements and are thus part of a column of a fundamental solution, but they can also be other signals representing the dynamics of the system. To estimate the transition matrix over a period, a signal h_s sampled with period Δt is divided into parts pertaining to each period l of rotor rotation as

$$\mathbf{h}_{s,l} = \{h_s(\Delta t + l\,T) \quad h_s(2\Delta t + l\,T) \quad \dots \quad h_s(m\Delta t + l\,T)\}^{\mathrm{T}} \tag{3.29}$$

A number N_h of these signals obtained over $n+1$ periods, $l = 0,\dots,n$, are assembled into two Hankel-type matrices $\mathbf{H}_0$ for $l = 0,\dots,n-1$ and $\mathbf{H}_1$ for $l = 1,\dots,n$, such that $\mathbf{H}_1 = \boldsymbol{\Phi}(T,0)\mathbf{H}_0$ of size $N_h m \times n$. In the case that $m = 1$, $N_h = N$, and $n = N$, where N is the number of state variables, then $\mathbf{H}_0$ is square and invertible, and the exact transition matrix over a period can be calculated as $\boldsymbol{\Phi}(T,0) = \mathbf{H}_1\mathbf{H}_0^{-1}$. In practice, the signals are not available for each state variable and not for such an extended time. Therefore time-shifted state variables ($m > 1$) are used to increase the statistical accuracy of an approximation to the state transition matrix over a period, determined as $\tilde{\boldsymbol{\Phi}}(T,0) = \mathbf{H}_1\mathbf{H}_0^{+}$, where $()^{+}$ denotes a Moore-Penrose pseudo-inverse. It is found using the singular value decomposition $\mathbf{H}_0 = \boldsymbol{\mathcal{U}}_r\boldsymbol{\mathcal{S}}_r\boldsymbol{\mathcal{V}}_r^{\mathrm{T}}$, where only the r largest singular values in $\boldsymbol{\mathcal{S}}_r$ are retained to eliminate noise, as $\mathbf{H}_0^{+} = \boldsymbol{\mathcal{V}}_r\boldsymbol{\mathcal{S}}_r^{-1}\boldsymbol{\mathcal{U}}_r^{\mathrm{T}}$. Similarly, to filter out noise of the Hankel-type matrices they are projected into the subspace

spanned by the r proper orthogonal modes contained in $\mathcal{U}_r$, such that the approximate transition matrix of size $r \times r$ becomes

$$\tilde{\mathbf{\Phi}}_r(T,0) = \mathcal{U}_r^{\mathrm{T}} \mathbf{H}_1 \mathcal{V}_r \mathcal{S}_r^{-1} \tag{3.30}$$

The modal damping and frequency are extracted from the eigenvalues ρ_k of $\tilde{\mathbf{\Phi}}_r(T,0)$ as

$$\begin{aligned} \tilde{\omega}_k &= \arg(\rho_k)/T + j_k\Omega \\ \tilde{\sigma}_k &= \ln(|\rho_k|)/T \end{aligned} \tag{3.31}$$

where the frequency is non-unique like in classical Floquet analysis. To validate the modal decomposition a reconstructed signal $\tilde{h}_s(t)$ is obtained as

$$\tilde{h}_s(t) = \sum_{k=1}^{r} \tilde{u}_{s,k}(t) \mathrm{e}^{\tilde{\lambda}_k t} \tag{3.32}$$

with $\tilde{\lambda}_k = \tilde{\sigma}_k + \mathrm{i}\tilde{\omega}_k$ by a curve fit using a least squares approximation to the original signal $h_s(t)$, determining the modal amplitudes $\tilde{u}_{s,k}$ which correspond to components of the periodic mode shape in Equation (3.8). The partial Floquet analysis as described above can extract one estimate of a complex conjugate mode for every two rotor periods contained in the signals. The method is applied to the simple edgewise model in [P5].

3.7.2 Partial Floquet analysis combined with the Coleman transformation

Application of the partial Floquet analysis shows that the number of periods contained in a signal before it has decayed to the noise level is rarely enough to get a reliable estimate of the most important modes. If, on the other hand, an underlying time-invariant system is analysed, the system period is arbitrary and may be selected as the time step to extract the maximum amount of information from the signal. The Coleman transformation provides a way to obtain a time-invariant system in isotropic conditions, and even though the conditions in a realistic case are not isotropic, using the Coleman transformed signals (called the Coleman post-processing in [P5]) in partial Floquet analysis under the assumption of a time-invariant system is typically a good approximation .

Figure 3.7 shows the modal frequencies and damping as function of the rank number r for a partial Floquet analysis using Coleman transformed signals. All four modes specifically excited can be identified at a rank of eight, and the reliability of the estimates is characterised by whether the parameters are independent of the rank number. The damping of the mode denoted by squares varies at low rank until a second mode with the same frequency and higher damping is identified at rank ten and above, meaning that the mode is not well represented by the linear model for the given combination of applied excitation and chosen signals.

The moving window analysis is introduced in [P5] as a way to qualitatively examine the nonlinearity of the system. A partial Floquet analysis is applied to a relatively short part of the signal, called the window, yielding the modal parameters of frequency, damping and signal amplitude. The window is then moved forward, say one time step, where a new analysis is performed. Continuing this process the modal parameters are obtained as function of time. Nonlinear behaviour is indicated

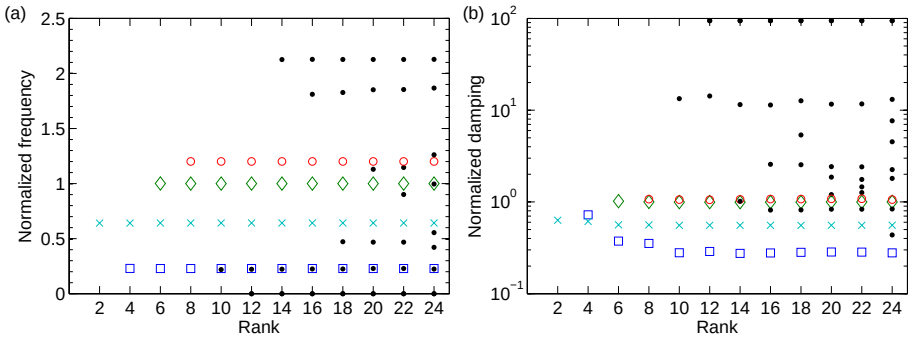

Figure 3.7: Normalised modal frequency (a) and damping (b) as function of rank number for a partial Floquet analysis of the BHawC model. Excited modes (□, ×, ◇, ○) and other estimates (•). Data from [P5, Fig. 12].

by a change in modal parameters over time, e.g., due to a change in vibration amplitude. For example, [P5, Fig. 9] shows that the effect of nonlinear damping applied to the simple edgewise model is clearly picked up as an increase in modal damping for high amplitude vibration.

In [P5] the partial Floquet analysis is applied to the Coleman transformed signals of the linearised and nonlinear versions of the simple edgewise model and the nonlinear BHawC model. The advantage of the method is that a modal analysis can be obtained from the nonlinear simulation tool as it is and that all dynamics of the system, e.g., unsteady aerodynamics and control, are included automatically. The drawback is that care must be taken to excite all relevant modes to a sufficient level, and that the modal parameters are estimated only in an approximate manner.

3.8 Comparison of methods

This chapter has reviewed different methods for modal analysis of structures with bladed rotors, of which some of the features are compared in Table 3.1.

The Coleman transformation of the system equations allows extraction of the modal parameters using standard eigenvalue analysis. It is a simple and efficient approach, but it only provides the exact solution for isotropic systems. Floquet analysis allows modal decomposition of an anisotropic system but it requires numerical integration of the system equations and yields a non-unique frequency, from which a physically meaningful modal frequency can, however, be identified. The implicit Floquet analysis is an efficient implementation requiring much fewer integrations than the classical analysis. Hill's method provides a solution equivalent to that from Floquet analysis and requires only a Fourier expansion of the system matrix. It does, however, set up a very large eigenvalue problem, that can be difficult to solve, and the process of frequency identification can be more difficult than for Floquet analysis. In the partial Floquet analysis signals from responses of the nonlinear model are used to estimate the modal parameters, meaning that no linearisation of the system equations is necessary. This method is effectively combined with a Coleman transformation of the signals, and the method can be used to qualitatively examine the nonlinearity of the system.

Method (Section)	Domain	System	Precision	Modes extracted
Coleman (3.5)	frequency	isotropic	exact	all
Classical Floquet (3.3.1)	time	anisotropic	determined by integration	all
Implicit Floquet (3.3.2)	time	anisotropic	determined by integration	least damped
Hill's method (3.4)	frequency	anisotropic	determined by number of harmonics	all
Partial Floquet (3.7.1)	time	anisotropic	approximate	most excited
Partial Floquet with Coleman (3.7.2)	time	isotropic (nonlinear)	approximate	most excited

Table 3.1: Comparison of features of methods for modal analysis of structures with bladed rotors.

The Coleman transformation approach is suitable for use in the initial stages of an analysis to quickly examine how the dynamics of the isotropic system depend on different parameters, such as rotor speed, pitch angle, and wind speed. To examine the effects of anisotropy, e.g. wind shear, yaw error, or rotor unbalance, on a large system such as BHawC the implicit Floquet analysis is preferred to Hill's method because it can use the already implemented time integration algorithm used for calculation of the nonlinear response, and the identification of the modal frequency poses less problems. Even though the identification of the modal frequency might seem like a trivial issue, it affects the value of the logarithmic decrement as well, and it determines whether the method is of practical use in the daily work. The implicit Floquet analysis is preferred to another efficient implementation, the Fast Floquet theory (Peters, 1994), for two reasons. Firstly, Fast Floquet theory is an exact method that reduces the computation time by a factor of three for a three-bladed turbine, whereas the implicit Floquet analysis in the current example gives a saving of more than factor 15 (even though it is an approximate method the calculated modes are determined more than precisely enough for practical purposes). Secondly, Fast Floquet theory is applicable only to isotropic rotors, whereas the implicit Floquet analysis is applicable with anisotropy on both rotor and external conditions. The partial Floquet analysis serves to validate the linearised model used with the Coleman transformation approach and implicit Floquet analysis, and to include effects of aerodynamics and control that would be arduous to include in the linear model.

Chapter 4

Implementation of modal analysis in BHawC

This chapter describes the main approach to modal analysis of a rotating wind turbine implemented for the BHawC model described in Chapter 2, using methods described in Chapter 3. In isotropic conditions the steady state can be obtained from a direct steady state calculation, and in isotropic or anisotropic conditions it can be obtained from a time simulation. The linearised equations of motion are obtained directly from the analytically linearised tangent matrices for the structural part and from a numerical linearisation for the aerodynamic part. For modal decomposition in isotropic conditions the Coleman transformation approach can be used, while the implicit Floquet analysis can be used in both isotropic and anisotropic conditions. A secondary approach based on the partial Floquet analysis of Section 3.7.2 is used for validation and special analyses and is not described further here.

The steps for producing the linearised BHawC model for modal analysis is outlined in Figure 4.1. To validate the linearised model, results are compared with corresponding results from the nonlinear BHawC model. The description contained in this chapter is an elaboration of the approaches to modal analysis used in [P3, P4].

4.1 Steady state calculation

In isotropic conditions the most efficient and precise way to calculate the steady state is by the direct method outlined in Section 3.1 and used in [P3, P4]. For a given constant rotor speed represented by the angular velocity vector $\mathbf{\Omega}$ and a given pitch angle, the motion on the blade is determined by

$$\begin{aligned}
\dot{\mathbf{u}}_{i,\text{tra}} &= \mathbf{\Omega} \times (\mathbf{p}_i - \mathbf{p}_{\text{hub}}) \\
\dot{\mathbf{u}}_{i,\text{rot}} &= \mathbf{\Omega} \\
\ddot{\mathbf{u}}_{i,\text{tra}} &= \mathbf{\Omega} \times \dot{\mathbf{u}}_{i,\text{tra}} \\
\ddot{\mathbf{u}}_{i,\text{rot}} &= \mathbf{0}
\end{aligned} \tag{4.1}$$

where $\dot{\mathbf{u}}_{i,\text{tra}}$ and $\dot{\mathbf{u}}_{i,\text{rot}}$ are the translational and rotational velocities of blade node i, respectively, $\mathbf{p}_i$ is the position of node i, and $\mathbf{p}_{\text{hub}}$ is the position of the hub centre. The equilibrium is found at a single azimuth angle at a time using Newton-Raphson iteration where the velocities and accelerations are updated from Equation 4.1 with

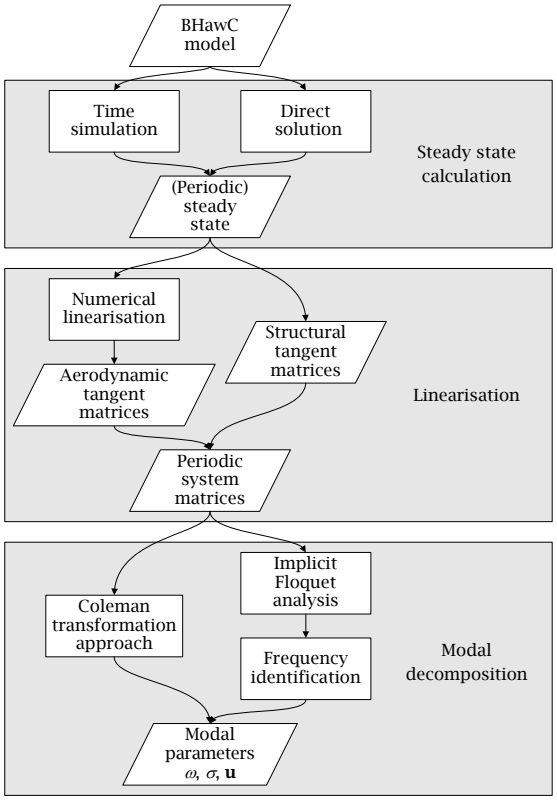

Figure 4.1: Flow chart of modal analysis implementation in BHawC. Parallelograms denote data and rectangles denote procedures.

the new value of $\mathbf{p}_i$. As a first approach only the deflection of the blades is included in the steady state calculation. The deflection of the rest of the structure has a minimal influence on the modal parameters.

In anisotropic conditions a standard time simulation is performed until an approximately steady state is reached. To accelerate the process, the damping is increased in the beginning of the simulation.

4.2 Linearisation

The analytically linearised structural tangent matrices of mass, damping, and stiffness are used during the equilibrium iteration (Equation 2.4) in the steady state calculation and are thus already available for modal analysis once the steady state is reached [P3].

Because of the rather complex dependence of the aerodynamic force on the orientation of the nodes, the aerodynamic force and unsteady aerodynamic equations are linearised numerically. This approach is also minimally dependent on the actual implementation of the structural and aerodynamic models, minimising the maintenance burden following changes to the model. The following description is based closely on [P4]. The aerodynamic force $\mathbf{f}_\mathrm{a}$ depends on the linearised structural degrees of freedom $\mathbf{y}$, their velocities $\dot{\mathbf{y}}$, and the aerodynamic state variables $\mathbf{x}$, and is

linearised as

$$\mathbf{f}_\mathrm{a} = \mathbf{f}_\mathrm{a,ss} + \frac{\partial \mathbf{f}_\mathrm{a}}{\partial \mathbf{y}}\mathbf{y} + \frac{\partial \mathbf{f}_\mathrm{a}}{\partial \dot{\mathbf{y}}}\dot{\mathbf{y}} + \frac{\partial \mathbf{f}_\mathrm{a}}{\partial \mathbf{x}}\mathbf{x} \tag{4.2}$$

where the subscript 'ss' denotes a steady state value and the Jacobian matrices yield the aerodynamic damping matrix $\mathbf{C}_\mathrm{a} = -\partial \mathbf{f}_\mathrm{a}/\partial \dot{\mathbf{y}}$, the aerodynamic stiffness matrix $\mathbf{K}_\mathrm{a} = -\partial \mathbf{f}_\mathrm{a}/\partial \mathbf{y}$, and the aerodynamic flow coupling matrix $\mathbf{A}_\mathrm{f} = -\partial \mathbf{f}_\mathrm{a}/\partial \mathbf{x}$. The matrices are approximated using a one-sided difference scheme, with column j of the aerodynamic stiffness matrix calculated as

$$\mathbf{K}_{\mathrm{a},j} \approx -\frac{\mathbf{f}_\mathrm{a}(\mathbf{u}_\mathrm{ss} + \Delta\mathbf{u}_j, \dot{\mathbf{u}}_\mathrm{ss}, \mathbf{a}_\mathrm{ss}) - \mathbf{f}_\mathrm{a}(\mathbf{u}_\mathrm{ss}, \dot{\mathbf{u}}_\mathrm{ss}, \mathbf{a}_\mathrm{ss})}{\Delta u} \tag{4.3}$$

where $\Delta\mathbf{u}_j$ is the displacement perturbation vector with one non-zero element of magnitude Δu at position j. Similarly, a column of the aerodynamic damping matrix is calculated as

$$\mathbf{C}_{\mathrm{a},j} \approx -\frac{\mathbf{f}_\mathrm{a}(\mathbf{u}_\mathrm{ss}, \dot{\mathbf{u}}_\mathrm{ss} + \Delta\dot{\mathbf{u}}_j, \mathbf{a}_\mathrm{ss}) - \mathbf{f}_\mathrm{a}(\mathbf{u}_\mathrm{ss}, \dot{\mathbf{u}}_\mathrm{ss}, \mathbf{a}_\mathrm{ss})}{\Delta \dot{u}} \tag{4.4}$$

where $\Delta\dot{\mathbf{u}}_j$ is the velocity perturbation vector with one non-zero element of magnitude $\Delta\dot{u}$ at position j. A column of the aerodynamic flow coupling matrix is calculated as

$$\mathbf{A}_{\mathrm{f},j} \approx -\frac{\mathbf{f}_\mathrm{a}(\mathbf{u}_\mathrm{ss}, \dot{\mathbf{u}}_\mathrm{ss}, \mathbf{a}_\mathrm{ss} + \Delta\mathbf{x}_j) - \mathbf{f}_\mathrm{a}(\mathbf{u}_\mathrm{ss}, \dot{\mathbf{u}}_\mathrm{ss}, \mathbf{a}_\mathrm{ss})}{\Delta x} \tag{4.5}$$

where $\Delta\mathbf{x}_j$ is the aerodynamic state perturbation vector with one non-zero element of magnitude Δx at position j. These aerodynamic matrices enter into the structural equations of motion which become

$$\mathbf{M}\ddot{\mathbf{y}} + (\mathbf{C} + \mathbf{C}_\mathrm{a})\dot{\mathbf{y}} + (\mathbf{K} + \mathbf{K}_\mathrm{a})\mathbf{y} + \mathbf{A}_\mathrm{f}\mathbf{x} = \mathbf{0} \tag{4.6}$$

The unsteady aerodynamic equations are determined from a similar numerical linearisation. In the current implementation only the unsteady effect of trailing edge separation, which is described by one state variable per calculation point, is included in the modal analysis (cf. Section 2.3.2). The following approach, however, extends to any state-space aerodynamic model. The linearised aerodynamic equation is written as

$$\dot{\mathbf{x}} + \mathbf{A}_\mathrm{d}\mathbf{x} + \mathbf{C}_\mathrm{ua}\dot{\mathbf{y}} + \mathbf{K}_\mathrm{ua}\mathbf{y} = \mathbf{0} \tag{4.7}$$

where the aerodynamic system matrix $\mathbf{A}_\mathrm{d}$ is a diagonal matrix obtained analytically from Equation (2.7) with elements

$$A_{\mathrm{d},i} = \frac{2W_i}{\tau_\mathrm{f} c_i} \tag{4.8}$$

where i denotes the number of the aerodynamic calculation point. The element (i,j) of the aerodynamic velocity coupling matrix $\mathbf{C}_\mathrm{ua}$ is found from Equation (2.7) as

$$C_{\mathrm{ua},ij} \approx \frac{2}{\tau_\mathrm{f} c_i} \frac{W_i(f_{\mathrm{ss},i} - f_{\mathrm{st},i}) - W_{\mathrm{ss},i}(f_{\mathrm{ss},i} - f_{\mathrm{st,ss},i})}{\Delta \dot{u}} \tag{4.9}$$

where the relative wind speed W_i and the stationary value of the separation point position $f_{\mathrm{st},i}$ are updated with the perturbation $\Delta\dot{u}$ to $\dot{u}_j$. Similarly, an element of the aerodynamic displacement coupling matrix $\mathbf{K}_\mathrm{ua}$ is calculated as

$$K_{\mathrm{ua},ij} \approx \frac{2}{\tau_\mathrm{f} c_i} \frac{W_i(f_{\mathrm{ss},i} - f_{\mathrm{st},i}) - W_{\mathrm{ss},i}(f_{\mathrm{ss},i} - f_{\mathrm{st,ss},i})}{\Delta u} \tag{4.10}$$

where W_i and $f_{\mathrm{st},i}$ are updated with the perturbation Δu to u_j. The magnitude of the perturbations are selected as $\Delta u = 10^{-5}\,\mathrm{m}$ and $\Delta \dot{u} = 10^{-4}\,\mathrm{m/s}$ for translational degrees of freedom, $\Delta u = 10^{-6}$ and $\Delta \dot{u} = 10^{-5}\,\mathrm{s}^{-1}$ for rotational degrees of freedom, and $\Delta x = 10^{-4}$ for the aerodynamic state variables (see Section 4.4).

The power-speed controller is currently not implemented in the linearised model. Thus, the generator rotor is allowed to move freely.

The combination of Equations (4.6) and (4.7) constitute the combined linearised aeroelastic equations of motion.

4.3 Modal decomposition

The current implementation contains two methods for modal decomposition: the Coleman transformation approach (cf. Section 3.5) for fast analysis of isotropic systems, and the implicit Floquet analysis (cf. Section 3.3.2) for examining anisotropic effects.

4.3.1 Coleman transformation approach

The Coleman transformation requires that the blade degrees of freedom be identical in their respective local blade reference frame, and therefore the equations of motion are transformed into substructure coordinates $\mathbf{y}_\mathrm{T}$ as

$$\begin{aligned} \mathbf{y} &= \mathbf{T}\,\mathbf{y}_\mathrm{T} \\ \mathbf{T} &= \mathbf{diag}(\mathbf{I}_{N_\mathrm{s}}, \mathbf{T}_\mathrm{r}, \mathbf{T}_{\mathrm{b}1}, \mathbf{T}_{\mathrm{b}2}, \mathbf{T}_{\mathrm{b}3}) \end{aligned} \tag{4.11}$$

where $\mathbf{T}$ is a block diagonal T-periodic matrix composed of the identity matrix $\mathbf{I}_{N_\mathrm{s}}$ sized by the number of degrees of freedom of the tower, nacelle, and drivetrain, $\mathbf{T}_\mathrm{r}$ transforming the degrees of freedom on the shaft and hub into a hub centre frame, and $\mathbf{T}_{\mathrm{b}j}$ transforming the degrees of freedom on blade number $j = 1,2,3$ into a local frame for blade j [P3].

The equations of motion are then brought into the inertial frame by the transformation [P3, P4]

$$\begin{aligned} \mathbf{y}_\mathrm{T} &= \mathbf{B}_\mathbf{y}\,\mathbf{z}_\mathbf{y} \\ \mathbf{B}_\mathbf{y} &= \mathbf{diag}(\mathbf{I}_{N_\mathrm{s}}, \mathbf{B}_\mathrm{r}, \mathbf{B}_\mathrm{b}) \\ \mathbf{x} &= \mathbf{B}_\mathbf{x}\mathbf{z}_\mathbf{x} \end{aligned} \tag{4.12}$$

where $\mathbf{z}_\mathbf{y}$ contains the inertial frame structural degrees of freedom, $\mathbf{B}_\mathbf{y}$ is the structural inertial frame transformation matrix including the Coleman transformation $\mathbf{B}_\mathrm{b}$ of the blade degrees of freedom and a simple rotational transformation $\mathbf{B}_\mathrm{r}$ of the shaft, $\mathbf{z}_\mathbf{x}$ is the inertial frame aerodynamic state vector, and $\mathbf{B}_\mathbf{x}$ is the aerodynamic Coleman transformation matrix. The periodic Coleman transformations $\mathbf{B}_\mathrm{b}$ and $\mathbf{B}_\mathbf{x}$ are composed of blocks of Equation (3.28) for each set of three corresponding degrees of freedom or state variables.

The first order form inertial frame equations of motion of the aeroelastic system given by Equations (4.6) and (4.7) become [P4]

$$\dot{\mathbf{z}}_3 = \mathbf{A}_\mathrm{B}\mathbf{z}_3 \tag{4.13}$$

where $\mathbf{z}_3 = \{\mathbf{z}_\mathbf{y}^\mathrm{T}\ \tilde{\mathbf{z}}_\mathbf{y}^\mathrm{T}\ \mathbf{z}_\mathbf{x}^\mathrm{T}\}^\mathrm{T}$ is the inertial frame state vector with $\tilde{\mathbf{z}}_\mathbf{y} = \dot{\mathbf{z}}_\mathbf{y} + \bar{\boldsymbol{\omega}}_\mathbf{y}\mathbf{z}_\mathbf{y}$, and the inertial frame system matrix is

$$\mathbf{A}_\mathrm{B} = \begin{bmatrix} -\bar{\boldsymbol{\omega}}_\mathbf{y} & \mathbf{I} & \mathbf{0} \\ -\mathbf{M}_\mathrm{B}^{-1}\mathbf{K}_\mathrm{B} & -\mathbf{M}_\mathrm{B}^{-1}\mathbf{C}_\mathrm{B} - \bar{\boldsymbol{\omega}}_\mathbf{y} & -\mathbf{M}_\mathrm{B}^{-1}\mathbf{A}_\mathrm{fB} \\ -\mathbf{K}_\mathrm{uaB} & -\mathbf{C}_\mathrm{uaB} & -\mathbf{A}_\mathrm{dB} - \bar{\boldsymbol{\omega}}_\mathbf{x} \end{bmatrix} \tag{4.14}$$

where $\bar{\boldsymbol{\omega}}_\mathbf{y} = \mathbf{B}_\mathbf{y}^{-1}\dot{\mathbf{B}}_\mathbf{y}$ and $\bar{\boldsymbol{\omega}}_\mathbf{x} = \mathbf{B}_\mathbf{x}^{-1}\dot{\mathbf{B}}_\mathbf{x}$ are constant matrices and the inertial frame transformed matrices are

$$\begin{aligned} \mathbf{M}_\mathrm{B} &= \mathbf{B}_\mathbf{y}^{-1}\mathbf{T}^\mathrm{T}\mathbf{M}\mathbf{T}\mathbf{B}_\mathbf{y} \\ \mathbf{C}_\mathrm{B} &= \mathbf{B}_\mathbf{y}^{-1}\mathbf{T}^\mathrm{T}\left((\mathbf{C}+\mathbf{C}_\mathrm{a})\mathbf{T} + 2\mathbf{M}\dot{\mathbf{T}}\right)\mathbf{B}_\mathbf{y} \\ \mathbf{K}_\mathrm{B} &= \mathbf{B}_\mathbf{y}^{-1}\mathbf{T}^\mathrm{T}\left((\mathbf{K}+\mathbf{K}_\mathrm{a})\mathbf{T} + (\mathbf{C}+\mathbf{C}_\mathrm{a})\dot{\mathbf{T}} + \mathbf{M}\ddot{\mathbf{T}}\right)\mathbf{B}_\mathbf{y} \\ \mathbf{A}_\mathrm{fB} &= \mathbf{B}_\mathbf{y}^{-1}\mathbf{T}^\mathrm{T}\mathbf{A}_\mathrm{f}\mathbf{B}_\mathbf{x} \\ \mathbf{A}_\mathrm{dB} &= \mathbf{B}_\mathbf{x}^{-1}\mathbf{A}_\mathrm{d}\mathbf{B}_\mathbf{x} \\ \mathbf{C}_\mathrm{uaB} &= \mathbf{B}_\mathbf{x}^{-1}\mathbf{C}_\mathrm{ua}\mathbf{T}\mathbf{B}_\mathbf{y} \\ \mathbf{K}_\mathrm{uaB} &= \mathbf{B}_\mathbf{x}^{-1}(\mathbf{K}_\mathrm{ua}\mathbf{T} + \mathbf{C}_\mathrm{ua}\dot{\mathbf{T}})\mathbf{B}_\mathbf{y} \end{aligned} \tag{4.15}$$

where the time-dependence of the matrices on the right-hand side is omitted to simplify the notation. If the system is isotropic, the system matrix $\mathbf{A}_\mathrm{B}$ is time-invariant and the modal parameters can be determined from eigenvalue analysis of $\mathbf{A}_\mathrm{B}$ extracted at steady state for a single azimuth angle as described in Section 3.2.

4.3.2 Implicit Floquet analysis

The implicit Floquet analysis is performed as described in Section 3.3.2 by integration of the aeroelastic system in second order form given by Equations (4.6) and (4.7)

$$\begin{bmatrix} \mathbf{M} & \mathbf{0} \\ \mathbf{0} & \mathbf{0} \end{bmatrix} \begin{Bmatrix} \ddot{\mathbf{y}} \\ \ddot{\mathbf{x}} \end{Bmatrix} + \begin{bmatrix} \mathbf{C}+\mathbf{C}_\mathrm{a} & \mathbf{0} \\ \mathbf{C}_\mathrm{ua} & \mathbf{I} \end{bmatrix} \begin{Bmatrix} \dot{\mathbf{y}} \\ \dot{\mathbf{x}} \end{Bmatrix} + \begin{bmatrix} \mathbf{K}+\mathbf{K}_\mathrm{a} & \mathbf{A}_\mathrm{f} \\ \mathbf{K}_\mathrm{ua} & \mathbf{A}_\mathrm{d} \end{bmatrix} \begin{Bmatrix} \mathbf{y} \\ \mathbf{x} \end{Bmatrix} = \begin{Bmatrix} \mathbf{0} \\ \mathbf{0} \end{Bmatrix} \tag{4.16}$$

over a period of rotor rotation using the generalised-α algorithm [P4]. The first initial condition is set to the first yaw standstill mode shape and the following are determined by the Arnoldi algorithm. In the steady state, the system matrices are extracted at a number of azimuth angles over a rotor rotation and then interpolated onto the integration time steps using a truncated Fourier series. The columns of the fundamental solution in Equation (3.11) are composed as $\boldsymbol{\varphi}_j = \{\mathbf{y}^\mathrm{T}\ \dot{\mathbf{y}}^\mathrm{T}\ \mathbf{x}^\mathrm{T}\}^\mathrm{T}$ obtained from the integration and used in the Arnoldi algorithm to build the approximation to the state transition matrix as well as to determine the modal parameters from Equation (3.20). The implicit Floquet analysis is continued until a desired number of modes are converged to within $10^{-10}\,\mathrm{s}^{-1}$ on the eigenvalue over the last three Arnoldi steps. Typically, around 20 modes are converged after around 50 steps [P3, P4]. The identification of the modal frequency utilises the periodic mode shape calculated for the tower top in lateral and longitudinal directions and for the blade tips in edgewise and flapwise directions transformed into multi-blade coordinates. The modal frequency is determined as the principal modal frequency plus the frequency of the dominant harmonic component in these five elements of the periodic mode shape where the tower components are weighted with a factor of 20. The periodic mode shape is then recalculated with the identified modal frequency.

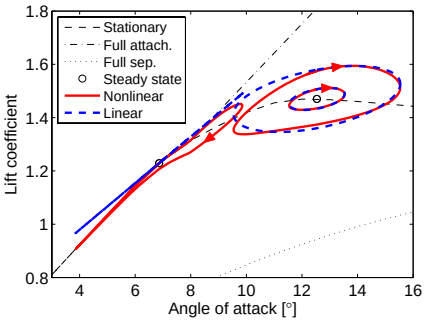

Figure 4.2: Lift coefficient as function of angle of attack for harmonic oscillation of the airfoil section around the length axis. From [P4, Fig. 1].

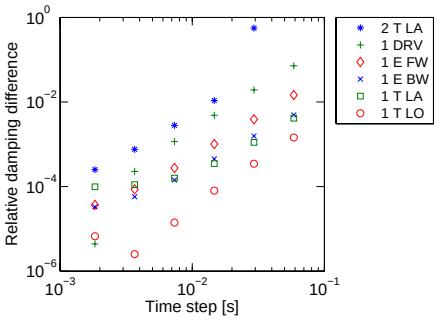

Figure 4.3: Relative damping difference of the implicit Floquet analysis compared to the Coleman approach for selected modes as function of the implicit Floquet integration time step. From [P4, Fig. 4].

A useful application of the linearised model is to provide a reduced order model for control design. The implicit Floquet analysis already provides a reduced model in the form of Equation (3.21), and a reduced model can be obtained from the Coleman approach by including only the modes with frequencies within the range of interest. But also more advanced methods for delivering optimal small models (reviewed by, e.g., Ersal et al. (2008)) should be investigated. The output matrix of a full state-space model also needs to be provided. The structural output of measurable forces and moments can be determined from the displacements using the shape functions of the finite element, accelerations can be determined from the state variables and the equations of motion, and the aerodynamic output such as angle of attack and relative wind speed can be determined from relations obtained during the numerical linearisation. This coupling to control design constitutes future work of this project.

4.4 Validation of model

A parameter study has been performed to examine the sensitivity of the modal parameters towards the perturbation magnitude used in the numerical linearisation in Equations (4.3), (4.4), (4.5), (4.9), and (4.10). For a variation in the translational perturbation magnitude between 10^{-6} m and 10^{-2} m, and the other perturbations scaled accordingly, a relative change of less than 10^{-6} is found in the modal frequencies and damping [P4, Sec. 4.2].

The linearisation of the dynamic stall model is validated by comparing the lift of an airfoil section subjected to harmonic pitching motion obtained from the linearised and the nonlinear models [P4]. Figure 4.2 shows the lift coefficient as function of angle of attack for two different mean values and two different amplitudes of the angle of attack. The linear and nonlinear models agree well for oscillations in angle of attack up to around 1°.

The convergence of the damping obtained from an implicit Floquet analysis of an isotropic system towards the results of the Coleman approach is shown in Figure 4.3 (the naming of the modes is explained in Chapter 5). The damping from

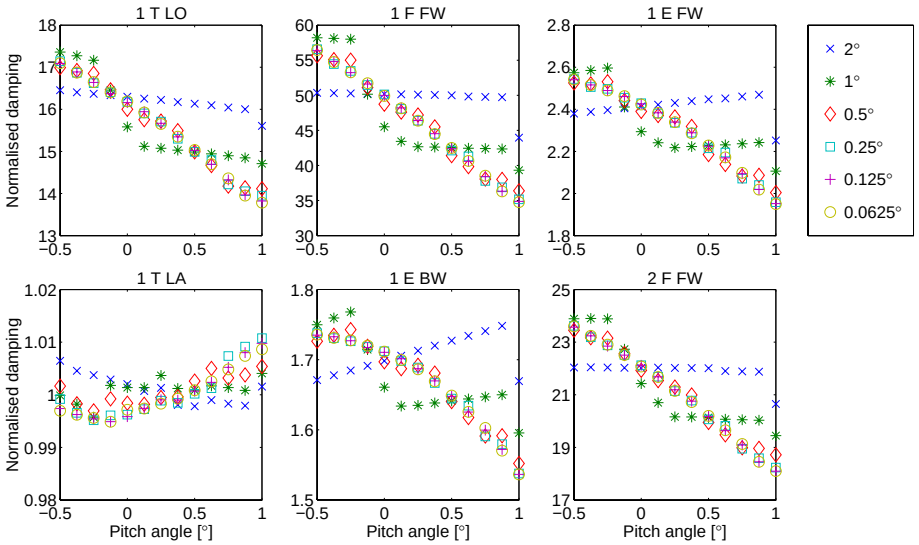

Figure 4.4: Normalised damping of selected modes as function of pitch angle for different values of spacing used for the linear interpolation in angle of attack. The damping is calculated for the aeroelastic BHawC model using the Coleman approach.

the implicit Floquet analysis converges with the error proportional to the time step squared until the relative error is around 10^{-4} where the convergence of the first lateral tower mode seemingly stalls. This discrepancy is, however, caused by a bad conditioning of the large eigenvalue problem set up by the Coleman approach and not a lack of convergence of the implicit Floquet analysis [P4].

During equilibrium iteration the aerodynamic profile coefficients are determined at a given angle of attack from linear interpolation between the values at fixed angles of attack determined initially using a shape-preserving spline. The default spacing between the fixed angles of attack is 1° between -10° and 30° and greater outside this interval. When the lift curves for fully attached and fully separated flow and the curve for the separation point position in Equation (2.6) are thus piecewise linear, the dynamic value of the lift coefficient becomes piecewise quadratic. This interpolation results in a wobbly lift curve with a non-continuous slope. In a time simulation the angle of attack changes quickly, thus averaging out this effect, but in a modal analysis in isotropic conditions the angle of attack is constant, and thus the damping can be affected. Figure 4.4 shows the damping of six modes as function of the pitch angle, which changes the angle of attack, for different values of spacing between the fixed angles of attack. The damping of all modes except the first lateral tower mode decreases with the pitch angle and the damping converges for decreasing spacing. For a spacing of 1° and 2° the change in damping is non-smooth or even contradicting the tendency for smaller values of the spacing. It is concluded that linear interpolation can be safely used with spacing of 0.1°. A better way to interpolate during iteration would be to use a shape-preserving spline (e.g. the monotone piecewise cubic interpolation described by Fritsch and Carlson (1980)) that gives a faithful representation of the slope.

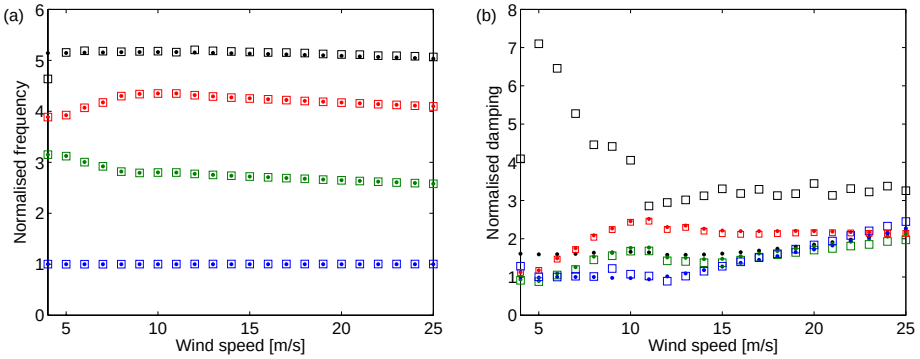

Figure 4.5: Frequencies (a) and damping (b) of the lowest damped quasi-steady aeroelastic modes calculated with the Coleman approach (•) and with a partial Floquet analysis (□). Modes 1 T LA (•, □), 1 E BW (•, □), 1 E FW (•, □), and 1 DRV (•, □).

In [P3, Fig. 2] the modal frequencies and damping as function of the rotor speed for the eleven modes with lowest frequency calculated with the linearised model are compared to a system identification of the nonlinear model. The agreement is good, though with some discrepancy for the drivetrain mode due to a bad estimate from the system identification. Figure 4.5 shows the modal frequencies and damping as function of wind speed determined from both the aeroelastic linear and nonlinear models using quasi-steady aerodynamics. The agreement between the frequencies is good, except for a discrepancy for the drivetrain mode (1 DRV) at 4 m/s. The agreement between the damping is very good for the first edgewise forward whirling mode (1 E FW) and fairly good for the first edgewise backward whirling (1 E BW) and lateral tower (1 T LA) modes. There is a large discrepancy for the drivetrain mode because the controller, which is not present in the linearised model, provides additional damping.

Chapter 5

Modal dynamics of wind turbines in isotropic conditions

The modal properties for a static structure, e.g., a wind turbine at standstill, are simple to interpret: the modal frequency gives the oscillation frequency for all degrees of freedom, with their relative amplitude described by the mode shape, and the decay of the oscillation given by the damping value. The solutions given by the methods outlined in Chapter 3 indicates that the situation is more complex for systems with bladed rotors, where a coordinate transformation is necessary to introduce the concept of modal analysis, and hence the mode shape becomes periodic.

This chapter focuses on the modal dynamics of a wind turbine with a three-bladed isotropic rotor operating in isotropic external conditions. For such a system the modal parameters are readily obtained from standard eigenvalue analysis of the system matrix after applying the Coleman transformation, as described in Section 3.5. Both structural and aeroelastic systems are considered together because they share the most important features, the aerodynamics mainly changing the damping of the system. First the characteristics of an isotropic steady state are described, then the effects of rotation, pitch angle, and nonlinearities on the modal dynamics are considered. The material presented here is not new and has already been described by, e.g., Hansen (2007), but it illustrates the implementation of the modal analysis on the BHawC model and it serves to establish a framework based on which anisotropic systems are analysed in Chapter 6.

5.1 An isotropic system

It is somewhat idealised to describe a wind turbine as an isotropic system. An isotropic rotor requires that all blades be manufactured identically to have the exact same mass and stiffness properties, and that they be mounted in perfect alignment. Operation in isotropic external conditions entails that no gravity field is present and that the wind field is constant in time, uniform, and aligned in tilt and yaw to be perpendicular to the rotor plane. This situation is not experienced on a wind turbine in the field, but the results of an isotropic modal analysis are simpler to interpret and contain the most important features of wind turbine modal dynamics.

Figure 5.1 shows the twelve lowest frequency mode shapes of the BHawC model at standstill. The modes essentially consist of different combinations of bend-

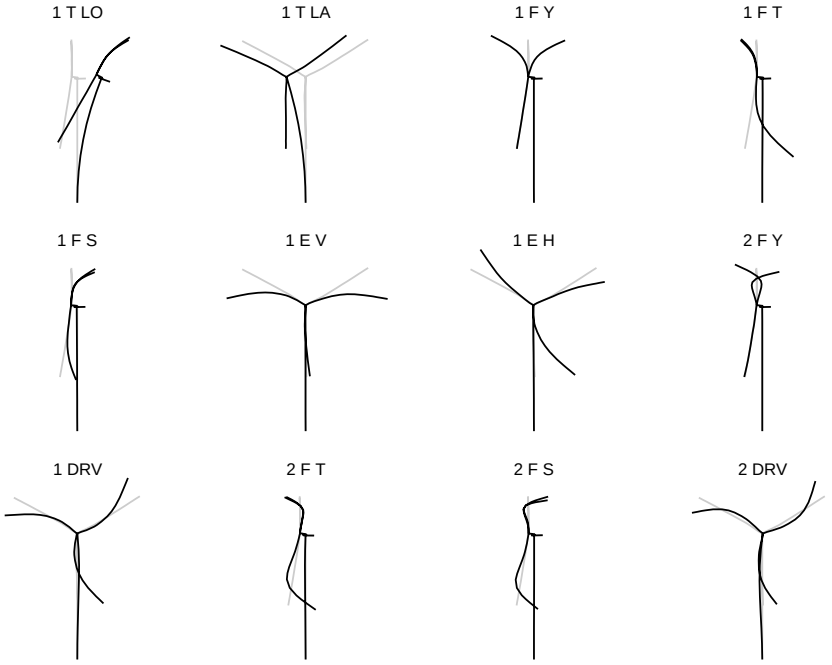

Figure 5.1: Lowest frequency standstill modes calculated for the structural BHawC model. Undeformed (grey) and deformed (black) structure.

ing modes of the substructures, mainly the tower and the blades. Starting from the lowest modal frequency, the tower modes are dominated by tower deflection and a small amount of blade deflection, especially of the blade pointing upwards. The tower modes appear in pairs: a longitudinal mode (1 T LO) with dominant tower motion perpendicular to the rotor plane and a lateral mode (1 T LA) with dominant tower motion parallel to the rotor plane. The rotor modes on three-bladed rotors appear in triples containing first edgewise blade deflection, first flapwise deflection, and likewise for higher deflection modes. Each triple consists of one symmetric mode and two asymmetric modes. The symmetric mode is an in-phase deflection of all three blades in the same direction, i.e., an in-phase fore-aft deflection for the flapwise modes (1 F S and 2 F S) and an in-phase deflection in the rotor plane coupling directly to the drivetrain for the edgewise modes (1 DRV and 2 DRV). The symmetric mode is characterised by dominant motion in the multi-blade coordinates a_0 in Equation (3.26) for each set of flapwise degrees of freedom along the blades. The azimuth angle in Equation (3.26) is defined as zero for blade 1 pointing downwards. Thereby the asymmetric flapwise modes consist of the tilt modes (1 F T and 2 F T) with dominant motion in the multi-blade coordinates a_1, and the yaw modes (1 F Y and 2 F Y) with dominant motion in b_1. The asymmetric modes for edgewise motion consist of a mode with horizontal blade motion (1 E H) dominated by the multi-blade coordinates a_1, and a mode with vertical blade motion (1 E V) dominated by b_1. At standstill the appearance of the asymmetric modes, i.e., how much the different blades participate in the motion, depends on the azimuth angle.

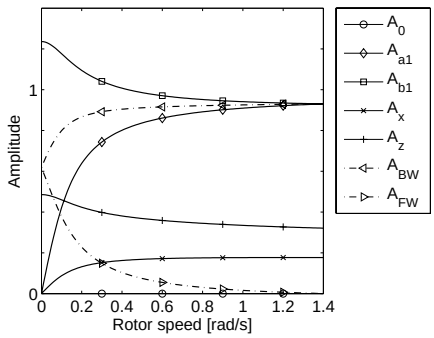

Figure 5.2: Modal amplitudes as function of rotor speed for the simple flapwise model. From [P1, Fig. 2(a)].

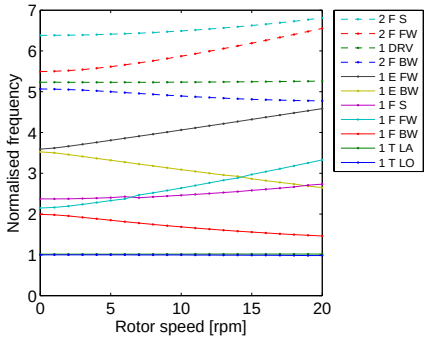

Figure 5.3: Frequencies as function of rotor speed for the structural BHawC model. Data from [P3, Fig. 2(a)].

5.2 Effects of rotation

At standstill the multi-blade coordinates mainly couple individually to the degrees of freedom on the support. When the rotor begins to rotate the inertia in the blade oscillation is transferred to another azimuth angle, which causes a coupling between the a_1 and b_1 coordinates, i.e., between tilt and yaw for flapwise motion and between edgewise horizontal and vertical motion. This phenomenon is illustrated in Figure 5.2 which shows the amplitude of the multi-blade eigenvector components as function of rotor speed for that mode of the simple flapwise model which at standstill is the first yaw mode. As the rotor speed increases, the yaw amplitude A_{b1} decreases and the tilt amplitude A_{a1} increases until the two amplitudes are equal. Also, the nacelle tilt motion A_x, which is zero at standstill, increases and the nacelle yaw motion A_z decreases. The motion of the blade given in multi-blade coordinates can be transformed back into the rotating frame using Equation (3.27) (Hansen, 2003) as

$$y_{ik} = \mathrm{e}^{\sigma_k t}\Big(A_{0,ik}\cos(\omega_k t + \varphi_{0,ik}) + A_{\mathrm{BW},ik}\cos\left((\omega_k + \Omega)t + \varphi_j + \varphi_{\mathrm{BW},ik}\right) + A_{\mathrm{FW},ik}\cos\left((\omega_k - \Omega)t - \varphi_j + \varphi_{\mathrm{FW},ik}\right)\Big) \quad (5.1)$$

where $\varphi_j = 2\pi(j-1)/3$, and the amplitudes $A_{0,ik}$, $A_{\mathrm{BW},ik}$, and $A_{\mathrm{FW},ik}$ and phases $\varphi_{0,ik}$, $\varphi_{\mathrm{BW},ik}$, and $\varphi_{\mathrm{FW},ik}$ for symmetric, backward whirling, and forward whirling motion, respectively, are determined by the multi-blade coordinate eigenvector [P1]. Equation (5.1) shows that for a single mode there are up to three harmonic components in the motion of the blade with frequencies ω_k and $\omega_k \pm \Omega$, while the motion of the supporting structure consists of a single harmonic with frequency ω_k. The amplitudes of these whirling components are also plotted in Figure 5.2, showing that at the maximum speed the mode is purely forward whirling. In a purely whirling mode the motion is identical for each blade with a phase shift of 120° between the blades. For edgewise motion it means that the centre of mass of the blades, or equivalently the reaction force, rotates against the rotor direction for the backward whirling mode and with the rotor direction for the forward whirling mode. A similar argument can be made with the reaction moment for flapwise motion.

Figure 5.3 shows a Campbell diagram with the normalised modal frequency of the eleven modes with lowest frequency as function of rotor speed of the structural

BHawC model operating with 0° pitch angle. The first longitudinal and lateral tower modes have a nearly identical frequency that is not affected by the rotor speed because the blade deflection is small. The mode which at standstill is the first yaw mode turns into the first flapwise backward whirling mode (1 F BW) of the rotating turbine, where the frequency decreases approximately with the rotor speed. This decrease in modal frequency ω_k means that the frequency $\omega_k + \Omega$ of the backward whirling component in Equation (5.1), which is dominant for this mode, remains approximately constant. Thus, the blade continues to oscillate mainly with its natural frequency for increasing rotor speed, while the oscillation of the support decreases in frequency. Conversely, the first tilt mode at standstill turns into a dominantly forward whirling mode (1 F FW) with the frequency increasing approximately with the frequency of the rotor speed. Again, as seen from Equation (5.1), the blade continues to oscillate mainly with the same frequency as at standstill. The frequency of the first symmetric flapwise mode (1 F S) increases slightly with the rotor speed due to centrifugal stiffening of the blade, an effect which is also seen on the flapwise whirling modes. The first asymmetric edgewise modes turn into backward and forward whirling modes (1 E BW and 1 E FW, respectively). There is no notable centrifugal stiffening of these modes because the centrifugal force rotates with the deflection in the rotor plane, approximately cancelling the stiffening effect. The symmetric edgewise mode is called the drivetrain mode because the motion of the blades couples directly to the drivetrain, which causes the large difference in frequency from the asymmetric first edgewise modes. The drivetrain is here modelled as free on the generator side. The second flapwise modes have the same characteristics of frequency splitting and centrifugal stiffening as the first flapwise modes.

The first flapwise forward whirling and symmetric modes shown in Figure 5.3 cross in frequency around 7 rpm. An analysis more finely spaced in the rotor speed would show that the modes do not actually cross but veer off from each other. At the point where they are close in frequency the mode shapes are similar, both containing significant amounts of forward whirling and symmetric motion. In the figure the labelling of the modes has been switched at the veering point so that the name of the mode corresponds to the dominating component for all rotor speeds. At around 14 rpm the first flapwise forward whirling and the first edgewise backward whirling modes cross in frequency. The mode shapes mix slightly but the modes do not veer because they are too incompatible with motion in different directions.

The damping rate σ_k does not change significantly with the rotor speed for operation at constant pitch angle. The damping ratio and logarithmic decrement, however, change due to the changes in frequency seen in Figure 5.3 (cf. Equations (3.9) and (3.10)).

Figure 5.4 shows the amplitudes of the three harmonic components of the blade and the constant component for the tower in the first flapwise forward whirling periodic mode shape. The zoom factor in the corner indicates how much each component has been enlarged. All components on the blade are mainly first bending modes, and the rigid body motion from the hub is seen at the root of the blade. The forward whirling flapwise component is dominant but there is also some backward whirling motion and slight symmetric motion coupling to the tower which deforms in a mix of first and second longitudinal bending modes. There is also a small amount of backward whirling edgewise motion because the first flapwise forward whirling and first edgewise backward whirling modes are close in frequency at 16 rpm (cf. Figure 5.3). The mode shape is shown here in frequency domain. In [P4, Figs. 9,11]

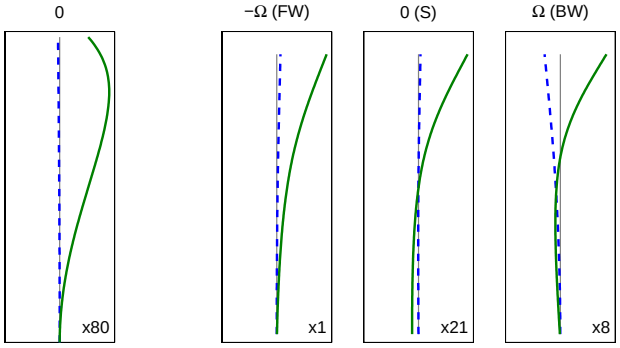

Figure 5.4: Amplitudes of harmonic components of the first flapwise forward whirling periodic mode shape for the structural BHawC model operating at 16 rpm. Left: Tower lateral (– –) and longitudinal (—); right: blades edgewise (– –) and flapwise (—). From [P3, Fig. 5].

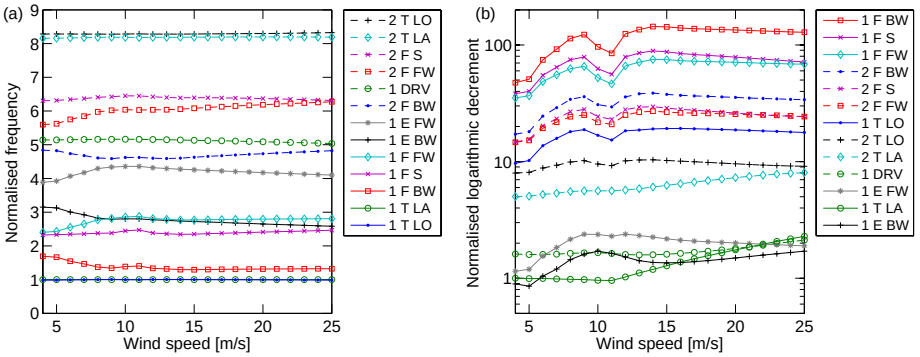

Figure 5.5: Frequencies (a) and damping (b) (log.scale) for the aeroelastic BHawC model as function of wind speed. The legend entries are ordered after the sequence at 4 m/s. From [P4, Fig. 3]

there are examples of aeroelastic mode shapes in time domain as function of azimuth angle.

5.3 Effects of pitch angle

In normal operation the controller on a wind turbine changes rotor speed and pitch angle depending on the wind speed to optimise power production while staying within rated power and speed. In the present work the controller dynamics are not included in the modal analysis, thus the pitch angle and generator speed are for a given wind speed kept constant at the values shown in [P4, Fig. 2]. Figure 5.5(a) shows the normalised frequencies of the 13 lowest frequency modes of the aeroelastic BHawC model as function of wind speed. Until 8 m/s the pitch angle is constant and the speed varies approximately linearly with the wind speed, so the figure resembles a Campbell diagram with frequency splitting of the asymmetric modes. From 11 m/s the speed remains constant and the pitch angle turns towards feather

which reduces the frequency of the edgewise modes because of increased flapwise motion and conversely increases the frequency of the flapwise modes because of increased edgewise motion.

The modal damping shown in Figure 5.5(b) is composed of structural and aerodynamic damping. The aerodynamic damping is determined mainly by the direction of blade motion and the slope of the lift curve which is constant for the angles of attack experienced in most of the normal operating range (the influence of the direction on motion on the aerodynamic damping is described by Rasmussen et al. (1999) and Hansen (2007) and stated in [P4, Eq. (29)]). Edgewise motion results in low aerodynamic damping, hence the first lateral tower mode and first edgewise modes have low modal damping. Flapwise motion at the low angles of attack experienced in normal operation results in a high aerodynamic damping as seen for the flapwise modes in the figure. The dip in damping at 11 m/s is caused by the angle of attack moving into an area with flow separation. This change in damping is complemented by a small change in frequency for the very highly damped first flapwise modes. The change in pitch angle above 11 m/s introduces flapwise motion to the first lateral tower mode, increasing the damping, and conversely reduces flapwise motion for the flapwise modes, slightly decreasing the damping.

The damping of the first lateral tower mode and the first drivetrain mode in Figure 5.5(b) do not precisely represent that of the real turbine because the speed controller, which affects the damping of these modes, is not included in the modal analysis (cf. Figure 4.5).

5.4 Effects of nonlinearity

The linearisation of the equations of motion is an approximation that is valid for small amplitude vibrations and might not be reasonable for larger amplitudes. Modal analysis relies on the linear principle of superposition for decomposition into modes, thus the concept of modes is not well-defined for nonlinear systems. For small nonlinearities, linear system identification methods can be used to give an approximation of the modal parameters' dependency on some parameter causing the nonlinearity.

The analyses performed in [P5] with the moving window partial Floquet analysis (cf. Section 3.7.2) show that nonlinear effects on a wind turbine in normal operation are modest. Figure 5.6 shows the damping of the four lowest damped modes as function of time (starting time for the moving window) for a decaying free response. It is seen that the damping for the tower mode is higher in the beginning of the signal and decreases to a steady value. This time-variance of the damping is an indication of nonlinear behaviour caused by the high vibration amplitude in the beginning of the signal. The higher damping is associated with heavy pitching action, indicating that the nonlinearity is caused by the power-speed controller.

The linear analytical methods are valuable for predicting the onset of vibrations caused by instability phenomena, but at larger vibration amplitudes they fail to correctly assess the motion. Such an assessment could be valuable for determining the severeness of an instability, ranging between slightly increased fatigue loads and a crash. Often nonlinear effects have a tendency of limiting the unstable behaviour by entry into a stable limit cycle oscillation (Thomsen, 2003).

One possible source of nonlinear effects on a wind turbine is the geometric nonlinearity caused by large deflections of the blades. In normal operation it is not very

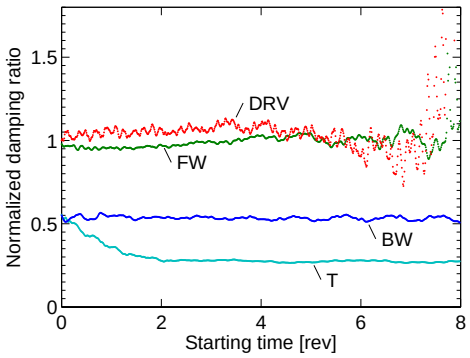

Figure 5.6: Damping ratio as function of time in a moving window analysis of the nonlinear aeroelastic BHawC model. First lateral tower (T), first edgewise backward and forward whirling (BW and FW, respectively), and first drivetrain (DRV) modes. From [P5, Fig. 14].

significant, but in unstable behaviour and for future larger turbines with more flexible blades it could have an effect. Another cause of nonlinearity comes from the aerodynamics where the profile coefficients affecting the damping vary with the angle of attack. In [P4, Fig. 1] the linearised unsteady lift is shown to be a good approximation for a variation in the angle of attack of 1°, but for a variation of 3° the discrepancies between the linear and nonlinear models are significant. This effect of the lift is only significant around stall, because the lift curve is linear for small angles of attack. But future blades possibly more flexible in torsion could experience larger variations in angle of attack invalidating the linear models.

Chapter 6

Effects of anisotropy

This chapter describes the effects of anisotropy on the steady state and modal dynamics of a wind turbine. Anisotropy is caused by either an unbalance on the rotor or asymmetric external conditions such as wind shear, yaw error, and gravity. In anisotropic conditions the steady state is periodic and the response of a single mode contains an infinite number of harmonics making the modal analysis more complex than described in the previous chapter. There is a qualitative difference between anisotropic external conditions, where the periodic mode shape in the inertial frame coordinates contains harmonics of multiples of three times the rotor speed, and an anisotropic rotor, where the mode shape contains harmonics of all multiples of the rotor speed.

At standstill, modal analysis of an anisotropic system can be performed using standard eigenvalue analysis. But once the rotor rotates the anisotropy causes unbalanced couplings between the rotor and the support structure such that a time-invariant system cannot be obtained by a simple physically based coordinate transformation. The L-F transformation must be obtained using a general method such as Floquet analysis or Hill's method. Even though they are not treated here, two-bladed rotors are inherently subject to anisotropic effects due to their lack of balance.

6.1 An anisotropic system

A rotor anisotropy can be caused by a mass or stiffness unbalance from a production irregularity or a material such as ice deposited on one blade, or by a pitch misalignment from production or from a fault in the control system. Anisotropic external conditions arise from gravity forces or asymmetric wind flow caused by wind shear, nacelle tilt, terrain slope, yaw error, or tower shadow. Cyclic pitch is considered an external anisotropy because each blade is pitched at the same angle at a given azimuth angle.

The frequency spectrum of a steady state due to an anisotropic rotor contains all multiples of the rotor speed, which is realised from a Fourier expansion of the forcing on the blades which is periodic with the rotor period. Figure 6.1(a) shows the frequency spectrum of a steady state calculated by time simulation with the BHawC model where one blade has an added mass. The amplitudes present for all harmonic

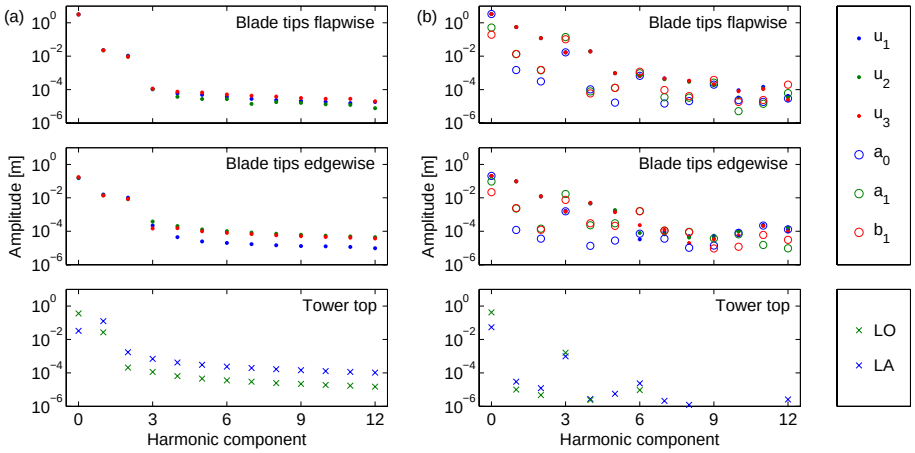

Figure 6.1: Amplitude frequency spectra of periodic steady states. (a) Anisotropic rotor, isotropic external conditions; (b) Isotropic rotor, anisotropic external conditions. Tower top and blade motion, as well as multi-blade motion in (b). The figures are Fourier transforms of (a) [P3, Fig. 6] and (b) [P4, Fig. 5].

components both on the tower and on the blades decrease gradually with increasing frequency.

For anisotropic external conditions the steady state response of the blades due to the period forcing contains all multiples of the rotor speed written as

$$u_j = \sum_{l=1}^{\infty} \left(A_l \cos(l\psi_j) + B_l \sin(l\psi_j) \right) + A_0 \tag{6.1}$$

for a generic degree of freedom on blade j, where $\psi_j = \psi_1 + 2\pi(j-1)/3$. If the rotor is isotropic, however, the coupling to the supporting structure is independent of the azimuth angle and can be described directly in multi-blade coordinates using the Coleman transformation. Inserting Equation (6.1) into Equation (3.26) the corresponding generic steady state response in multi-blade coordinates becomes

$$\begin{aligned}
a_0 &= \sum_{l=1}^{\infty} \left(A_l \cos(3l\psi_1) + B_l \sin(3l\psi_1) \right) + A_0 \\
a_1 &= \sum_{l=1}^{\infty} \left((A_{3l-1} + A_{3l+1}) \cos(3l\psi_1) + (B_{3l+1} + B_{3l-1}) \sin(3l\psi_1) \right) + A_1 \\
b_1 &= \sum_{l=1}^{\infty} \left((B_{3l-1} - B_{3l+1}) \cos(3l\psi_1) + (A_{3l-1} - A_{3l+1}) \sin(3l\psi_1) \right) + B_1
\end{aligned} \tag{6.2}$$

using the Werner formulas for products of trigonometric functions and identities for sums of trigonometric functions of angle multiples (Johnson, 1980, pp. 347). It is seen that the isotropic rotor acts as a filter on the forcing from the anisotropic external conditions and only allows harmonics of multiples of three to couple to the support (Bir and Jonkman, 2007).

Figure 6.1(b) shows a steady state calculated by time simulation with the BHawC model in extreme wind shear. The steady state response in the blade frame contains

all harmonics, while the response in the inertial frame given by tower and multi-blade coordinates consists mainly of harmonic components that are multiples of 3Ω, including the mean with zero frequency. The small content of other harmonics is due to transient motion that has not damped away.

The simplest approach to considering anisotropy in modal analysis is based on the steady state calculated with isotropic conditions obtained as an average of the anisotropic conditions. The periodic forcing due to the anisotropy can then be considered an external force exciting modes with a modal frequency close to a multiple of the rotor speed for an anisotropic rotor or a multiple of three times the rotor speed for anisotropic external conditions. This approach corresponds to describing the additional steady state motion due to anisotropy linearly, because the model is linearised about the averaged isotropic steady state. By considering the nonlinear anisotropic steady state, however, the model can be linearised at each azimuth angle over a rotor rotation, for which the conditions might vary substantially if the deflection varies. Thus, the periodic steady state is included in the modal analysis, and only non-periodic forcing, such as turbulence, need be considered an external source of excitation. This latter approach for modal analysis of anisotropic systems is followed in this chapter.

6.2 Rotor anisotropy

The response of a single mode of a system with an anisotropic rotor can contain an infinite number of harmonic terms, differing in frequency by the rotor speed, for degrees of freedom both on the supporting structure and on the blades [P1]. This response is the most general result of Equation (3.8) written as a sum of harmonic components [P3, Eq. (24)]

$$\mathbf{y} = \sum_{k=1}^{N} \sum_{j=-\infty}^{\infty} \mathcal{U}_{jk} \mathrm{e}^{(\sigma_k + \mathrm{i}(\omega_k + j\Omega))t} q_k(0) \tag{6.3}$$

where $\mathcal{U}_{jk}$ is the component of the Fourier transform of $\mathbf{u}_k$ with frequency $j\Omega$. Note that Equation (5.1) is a special case of this expression for $j = -1, 0, 1$.

The dynamics can be studied from the periodic mode shape alone or from the frequency spectrum of the response of a pure excitation of the mode constructed from the modal frequency and the periodic mode shape [P1]. Figure 6.2 shows the amplitude and phase of the harmonic components in the periodic mode shape of the first forward whirling mode of the simple flapwise model with the scale in the bottom showing the frequencies in the response. The constant components of the support degrees of freedom, which are the only ones present in isotropic conditions, are still dominant. But there is also a significant component at -2Ω and a discernible component at $+2\Omega$. For the blade degrees of freedom, in addition to the backward and forward whirling components at $\pm\Omega$, respectively, present in isotropic conditions, there is also a component at $+3\Omega$. All harmonic components on the blades are forward whirling for negative harmonic components and backward whirling for positive harmonic components, where the direction of the whirl is determined from the phase difference. The non-zero components on the support occupy even harmonics and the non-zero components on the blades occupy odd harmonics. This tendency is caused by the separation of the symmetric degree of freedom, multi-blade coordinate a_0, and the other asymmetric degrees of freedom which do not

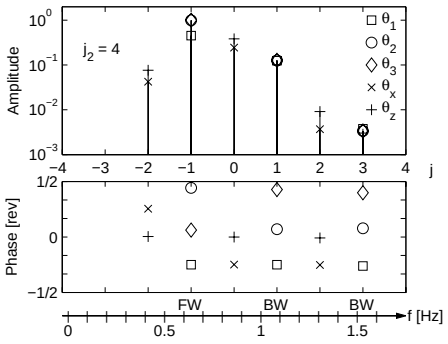

Figure 6.2: Amplitudes and phases of the first flapwise forward whirling mode with frequency $f = 0.864$ Hz of the simple flapwise model with an anisotropic rotor. The bottom scale shows the frequencies in the response. Data from [P1, Fig. 5(b)].

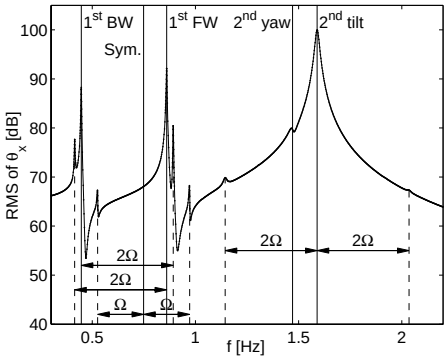

Figure 6.3: Root-mean-square values of the steady state nacelle tilt response due to a harmonic excitation on the same degree of freedom on the simple flapwise model with an anisotropic rotor. $\Omega = 0.223$ Hz. Data from [P1, Fig. 6].

couple in this simple model. For a more complex model, in general all components on all degrees of freedom will be non-zero.

The frequency content of the periodic mode shape is directly related to the frequency response of the system which is shown in Figure 6.3 containing the steady-state tilt response of the simple flapwise model due to excitation on this degree of freedom. Because the response contains multiple harmonic components, its root-mean-square value is shown. There are peaks at all the modal frequencies except for the symmetric flapwise mode because it does not contain any tilt motion. But there is also a peak at 2Ω below the first forward whirling modal frequency corresponding to the additional harmonic component at -2Ω in Figure 6.2. Similar trends are seen for the other modes in Figure 6.3. The frequency response is calculated using a brute force approach by simulation until steady state for different excitation frequencies. A better, more analytical approach would be to calculate the frequency response directly from the mode shapes incorporating the concept of a transfer function for periodic systems (Wereley and Hall, 1991, Irretier, 1999, Bittanti and Colaneri, 2000), which has an output containing multiple harmonic components for a single harmonic in the input.

Figure 6.4 shows the amplitudes of the harmonic components of the first flapwise forward whirling periodic mode shape obtained from an implicit Floquet analysis of the BHawC model with a mass unbalance on the rotor. For the blade, in addition to the harmonic components at $-\Omega$, 0, and Ω, there is a significant component at $+2\Omega$. For the tower the dominant component is at -2Ω instead of at 0. Both the blade and the tower have non-zero harmonic components at all harmonics. The rotor anisotropy can also affect the modal damping [P3].

Another source of rotor anisotropy not examined here is a pitch offset of one blade. The offset would change the aerodynamic forces on the blade resulting in a change of the steady state, and it would also change the stiffness coupling to the rest of the structure. If some part of the blade were operating in separated flow, the

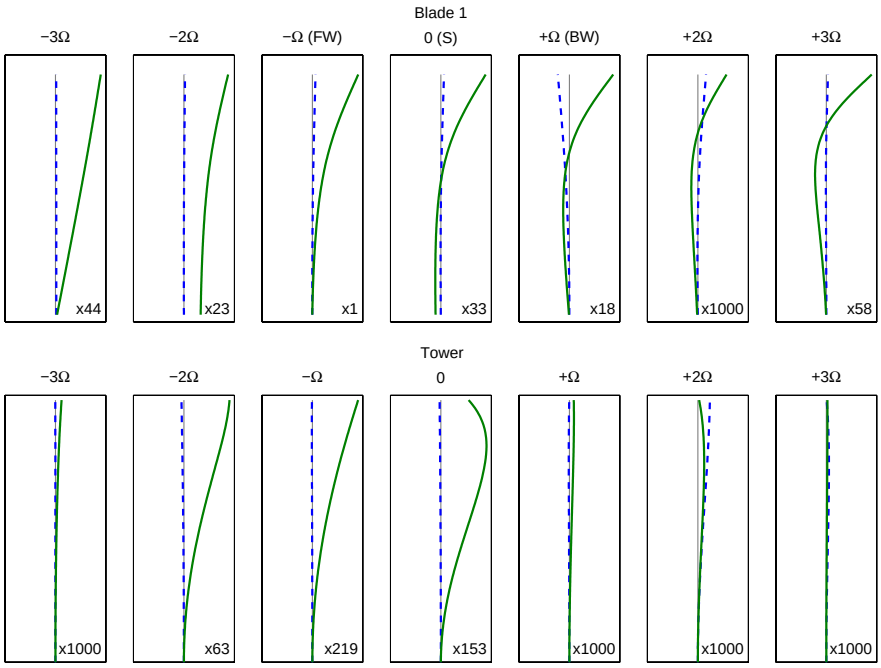

Figure 6.4: Amplitudes of harmonic components of the first flapwise forward whirling periodic mode shape for the structural BHawC model with blade 1 covered with ice. Top: blade 1 edgewise (– –) and flapwise (—); bottom: tower lateral (– –) and longitudinal (—). From [P3, Fig. 7].

curvature of the lift coefficient would result in a changed aerodynamic damping on this blade, which could affect the modal damping [P4].

6.3 External anisotropy

An external anisotropy is caused by gravity forces and more importantly by a non-uniform inflow due to wind shear and tower shadow, and an oblique inflow due to yaw error, nacelle tilt, and terrain slope.

Figure 6.5 shows the amplitudes of the harmonic components of the first flapwise forward whirling periodic mode shape obtained from an implicit Floquet analysis on the aeroelastic BHawC model operating in extreme wind shear with a power coefficient of 0.55 [P4]. The mode shape of the tower in addition to the constant component contains harmonic components at multiples of three times the rotor speed, which in this case have a negligibly small amplitude. The blade mode shape contains harmonics at all multiples of the rotor speed. In addition to the harmonic components present in isotropic conditions there is a significant component at -2Ω. Additionally it is seen that this symmetric mode contains a considerable amount of forward whirling motion with a ratio between the blade tip BW, S, and FW components of $2:1:17$, while the ratio for the same mode in isotropic conditions is $17:1:45$. Conversely, the first flapwise forward whirling mode contains considerable symmetric motion with a ratio of $1:2:12$ compared to $1:18:9$ in isotropic conditions. These results indicate that almost purely symmetric or whirling modes

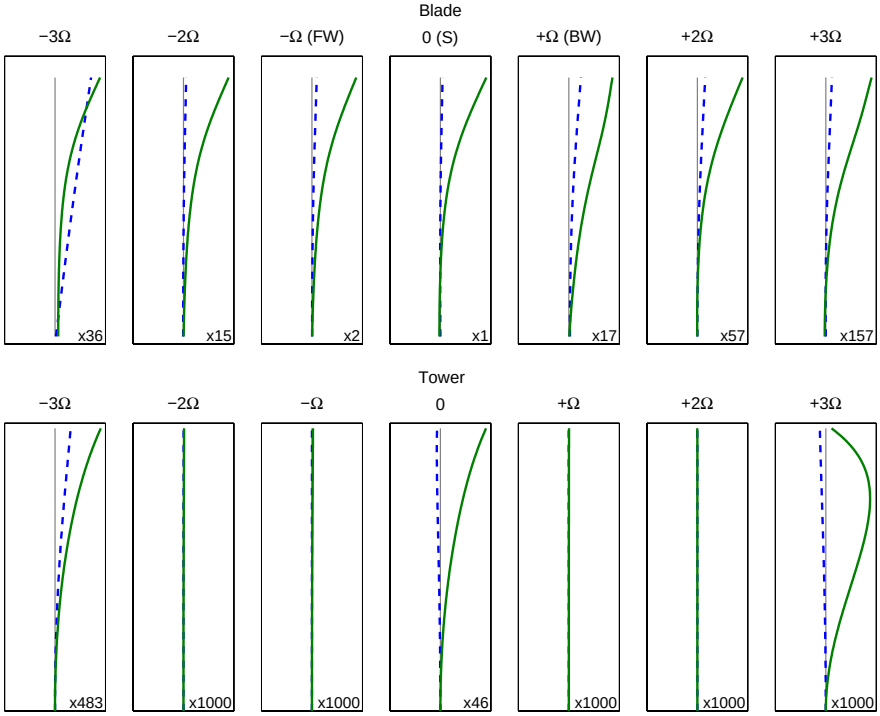

Figure 6.5: Amplitudes of harmonic components of the first flapwise symmetric whirling periodic mode shape for the BHawC model operating in extreme shear. Top: blade edgewise (– –) and flapwise (—); bottom: tower lateral (– –) and longitudinal (—). Data for blade from [P4, Fig. 11(b)].

are not likely to exist in external anisotropic conditions. The frequency content of the periodic mode shape, consisting of harmonics at multiples of three times the rotor speed on the tower and of all harmonics on the blades, is consistent with the steady state response shown in Figure 6.1(b).

Operation in wind shear gives a variation in the angle of attack, which can result in a change of the local aerodynamic damping. Figure 6.6 shows the lift coefficient as function of the angle of attack for different radial positions on the blade in extreme shear conditions at 11 m/s where the angle of attack is highest. There is a small curvature of the lift due to beginning separation of the flow, which affects the damping (Hansen, 2007, see [P4] for details). The modal frequencies and damping obtained from an implicit Floquet analysis are shown in Figure 6.7 for both isotropic and extreme shear conditions. The frequencies are almost unchanged by the wind shear but the damping of the first flapwise symmetric and backward whirling modes increases while the damping of the first longitudinal tower mode decreases. This difference in damping can be explained by the interaction between the response of a single mode and the local aerodynamic damping determined by the angle of attack. The work performed by the aerodynamic forces gives an indication of the aerodynamic damping and can be estimated from the local quasi-steady aerodynamic damping of an airfoil section weighted with the mode shape amplitude. Figure 6.8 shows this aerodynamic work integrated over the blade length as function of azimuth angle where the modal damping can be estimated from the area within the

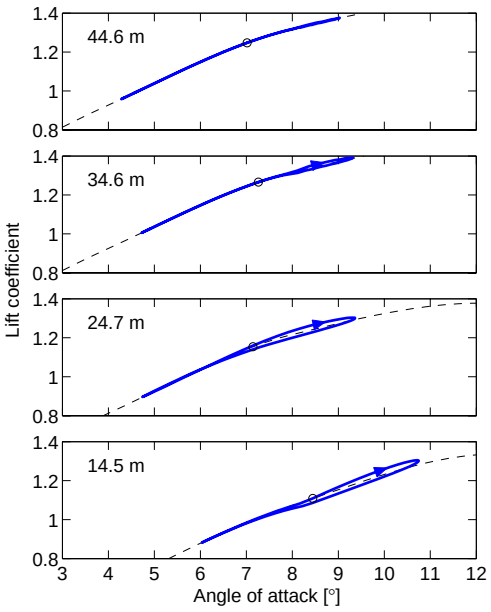

Figure 6.6: Lift coefficient as function of angle of attack for different radial positions. Profile data (– –), working point in isotropic condition (○) and working points in extreme shear condition (—). From [P4, Fig. 12(a)].

curve. In shear conditions the increase in local damping when the blade is pointing down to the right outweighs the decrease when the blade is pointing up to the left, which explains the increase in modal damping seen in Figure 6.7. The decrease in modal damping of the first longitudinal tower mode can be explained similarly [P4, Sec. 4.3]. At operation in stall with angles of attack around maximum with a large curvature of the lift these changes in modal damping are amplified [P4, Fig. 13], confirming that they are caused by the curvature of the lift.

Figure 6.9 shows the amplitude of flapwise motion in the first flapwise symmetric mode shape as function of azimuth angle in isotropic and extreme shear conditions. Figure 6.9(b) is a time domain version of the frequency domain plot in the upper part of Figure 6.5. In isotropic conditions the mode shape is almost constant during a rotor rotation. In shear conditions it varies considerably with minimum around 120° caused by the low damping around 0° when the blade is pointing downwards and with maximum around 320° caused by the low damping around 180° when the blade is pointing up. Thus, the variation in damping caused by the wind shear can significantly influence the periodic mode shape.

Cyclic pitch also causes a periodic variation in angle attack and might affect the damping in a similar way to that described for the wind shear. Another effect which should be investigated is the influence of yaw error on flutter speed due to the increased relative wind speed when the blade is moving against the wind at the upward position. Other sources of external anisotropy include the change in the wind field due to the wake of an upwind turbine reaching parts of the rotor and slowly changing turbulence which can be approximated as periodic to allow a modal analysis.

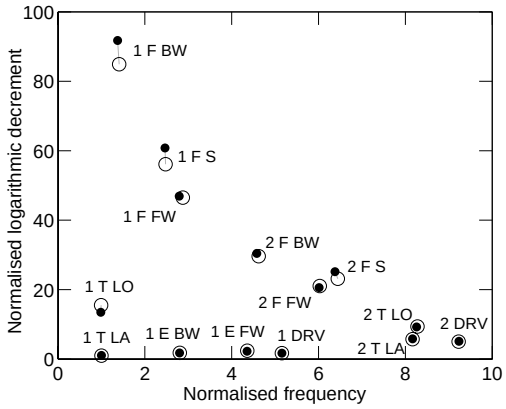

Figure 6.7: Modal damping and frequencies for the aeroelastic BHawC model in normal operation at 11 m/s normalised with the values for the first lateral tower mode of the isotropic condition. Isotropic (○) and extreme shear (•) conditions. From [P4, Fig. 6].

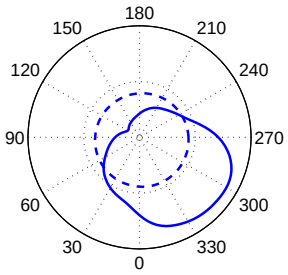

Figure 6.8: Local quasi-steady aerodynamic damping weighted with the mode shape amplitude and integrated over the blade length as function of azimuth angle. First flapwise symmetric mode of the aeroelastic BHawC model in isotropic (- -) and extreme shear (—) conditions. From [P4, Fig. 10(b)].

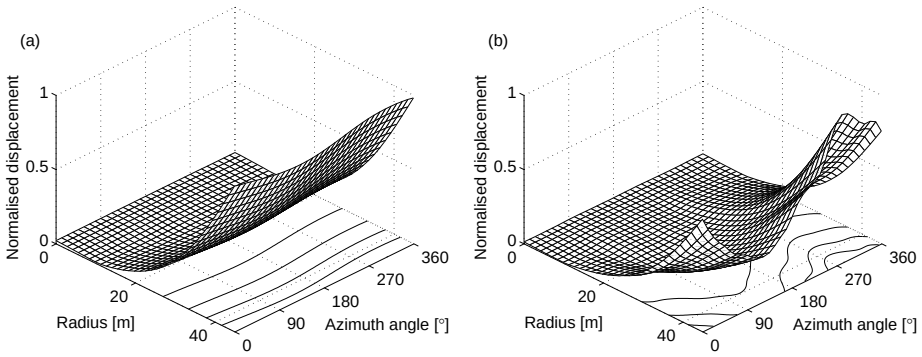

Figure 6.9: Amplitude of blade displacement perpendicular to the rotor plane in the first flapwise symmetric mode of the aeroelastic BHawC model as function of radius and azimuth angle in normal operation. Isotropic (a) and extreme shear (b) conditions. From [P4, Fig. 11(b)].

Chapter 7

Conclusion

This thesis has developed methods for aeroelastic modal analysis of wind turbines and their most important modal dynamics, determining the dynamic response. The main contributions of this thesis are a rigourous application of two of these methods for an existing complex aeroelastic wind turbine code and new insight into the modal dynamics in anisotropic conditions.

Modal analysis consists of three steps: location of a steady state, linearisation about the steady state, and modal decomposition of the motion. In isotropic conditions the steady state is characterised by a constant deflection of the turbine members. In anisotropic conditions caused by, e.g., a rotor unbalance or wind shear, the steady state becomes periodic. The linearisation of the model is preferably obtained analytically, but for complex models it can be advantageous to obtain it numerically or as part of a system identification method based on the nonlinear model.

The rotation of the rotor makes the system equations for a wind turbine periodic. A modal decomposition of such a time-periodic system can be defined for an equivalent time-invariant system obtained by the Lyapunov-Floquet transformation. The inverse transformation yields a mode shape that is periodic in the original coordinates. The Coleman transformation, which describes the rotor in the inertial frame, is an analytical example of the Lyapunov-Floquet transformation for isotropic systems, and it enables modal decomposition using standard eigenvalue analysis. Floquet analysis provides a modal decomposition of an anisotropic system from a fundamental solution obtained by numerical integration. Hill's method obtains the modal decomposition from an expanded eigenvalue problem using the Fourier expansion of the system matrix. The Coleman approach provides a unique modal frequency measured in the inertial frame, in which the mode shape is constant. The non-unique modal frequency obtained from Floquet analysis and Hill's method is chosen such that the periodic mode shape is as constant as possible for degrees of freedom measured in the inertial frame.

This thesis has presented a modal analysis tool based directly on the nonlinear aeroelastic code BHawC. The linearised structural equations of motion consist of the tangent matrices used during iteration in time simulations, and the linearised aerodynamics, including the unsteady effect of trailing edge separation, are obtained from numerical linearisation. The Coleman approach provides a fast modal analysis of an isotropic system and is useful for parameter studies. The implicit Floquet analysis is an efficient method extracting the least damped modes with a reduced computational effort compared to classical Floquet analysis. It is used to

examine anisotropic effects. The tool is validated by comparison of results from the Coleman approach and the Floquet analysis on a model of a 2.3 MW turbine. It is also validated against results from a system identification with the partial Floquet method on the nonlinear model. The partial Floquet method can estimate the modal parameters of lightly damped modes and is also used to obtain the correct damping of modes affected by the controller, which is not included in the linearised model.

Results from a system identification of the nonlinear model of the 2.3 MW turbine in normal operation show that the nonlinear effects in most cases are small, however, the damping of the first lateral tower mode in one case increases at high amplitude of vibration, indicating nonlinear behaviour of the controller.

Linear modal analyses on a three-bladed wind turbine in isotropic conditions show that the periodic mode shape is constant for components in the inertial frame and contains up to three harmonic components for blade components in the rotating frame. The periodic mode shape for a turbine with an anisotropic rotor can contain an infinite number of harmonics with frequencies that are multiples of the rotor speed. Thus, the response to a pure excitation of a single mode contains multiple harmonic components. The rotor unbalance also causes a small change in modal frequency and a small change in the damping of some modes. The periodic mode shape for a wind turbine with an isotropic rotor operating in anisotropic conditions also contains an infinite number of harmonics, but the frequencies are multiples of three times the rotor speed for degrees of freedom measured in the inertial frame. Extreme wind shear causes a variation in the steady state angle of attack, which affects the local aerodynamic damping when the flow is separated. Through interaction with the periodic mode shape the modal damping of the first longitudinal tower mode decreases slightly and the modal damping of the flapwise modes increases.

To further validate the findings of this thesis the presented modal analysis tool should be further developed to include the full BHawC unsteady aerodynamic and dynamic wake models. To become a full aeroservoelastic model, a linearised controller needs to be incorporated. For control design it would be useful to provide reduced models and to calculate transfer functions, which also give additional insight into the modal dynamics. An effort should be put into examining how to provide useful transfer functions based on the response of an anisotropic system with multiple output frequencies for a single input frequency.

The results of the modal analyses show that the error committed by performing an isotropic analysis compared to a more realistic anisotropic analysis are small for the 2.3 MW turbine. The analyses in anisotropic conditions have, however, provided additional insight into the turbine dynamics. There are still anisotropic effects that need to be examined, e.g., the influence of yaw error on flutter speed and the effect of cyclic pitch on modal damping. These and other sources of and measures against instabilities will be more important for future wind turbines with larger and more flexible rotors.

Bibliography

O.A. Bauchau and Y.G. Nikishkov. An implicit Floquet analysis for rotorcraft stability evaluation. *Journal of the American Helicopter Society*, 46(3):200–209, 2001.

O.A. Bauchau and J. Wang. Efficient and robust approaches to the stability analysis of large multibody systems. *Journal of Computational and Nonlinear Dynamics*, 3:011001, 2008. doi:10.1115/1.2397690.

G. Bir and J. Jonkman. Aeroelastic instabilities of large offshore and onshore wind turbines. *Journal of Physics: Conference Series*, 75(1), 2007. doi:10.1088/1742-6596/75/1/012069.

S. Bittanti and P. Colaneri. Invariant representations of discrete-time periodic systems. *Automatica*, 36(12):1777–1793, 2000. doi:10.1016/S0005-1098(00)00087-X.

A. Björck. Aerforce: Subroutine package for unsteady blade-element/momentum calculations. Technical Report FFA TN 2000-07, Flygtekniska Forsöksanstalten, 2000. Available from <cvi.se>.

T.G. Carne and A.R. Nord. Modal testing of a rotating wind turbine. Technical Report SAND82-0631, Sandia National Laboratories, 1983. Available from <windpower.sandia.gov>.

R.H. Christensen and I.F. Santos. Design of active controlled rotor-blade systems based on time-variant modal analysis. *Journal of Vibration and Control*, 11(6): 801–828, 2005. doi:10.1177/1077546305054596.

J. Chung and G.M. Hulbert. A time integration algorithm for structural dynamics with improved numerical dissipation: The generalized-α method. *Journal of Applied Mechanics*, 60(2):371–376, 1993.

E.A. Coddington and N. Levinson. *Theory of Ordinary Differential Equations*. McGraw-Hill, New York, 1955.

R.P. Coleman. Theory of self-excited mechanical oscillations of hinged rotor blades. Technical Report NACA-WR-L-308, Langley Research Center, 1943.

R.P. Coleman and A.M. Feingold. Theory of ground vibrations of a two-blade helicopter rotor on anisotropic flexible supports. Technical Report NACA-TN-1184, Langley Research Center, 1947.

P. Crimi. A method for analyzing the aeroelastic stability of a helicopter rotor in forward flight. NASA Report CR-1332, National Advisory Committe for Aeronautics, 1969.

T. Ersal, H.K. Fathy, D.G. Rideout, L.S. Louca, and J.L. Stein. A review of proper modeling techniques. *Journal of Dynamic Systems, Measurement, and Control*, 130: 061008, 2008. doi:10.1115/1.2977484.

G. Floquet. Sur les équations différentielles linéaires à coefficients périodiques (on linear differential equations with periodic coefficients). *Annales scientifiques de l'École Normale Supérieure*, 2(12):47–88, 1883. Available from <numdam.org>.

P.P. Friedmann. Numerical methods for determining the stability and response of periodic systems with applications to helicopter rotor dynamics and aeroelasticity. *Computers & Mathematics with Applications*, 12A(1):131–48, 1986.

F.N. Fritsch and R.E. Carlson. Monotone piecewise cubic interpolation. *SIAM Journal on Numerical Analysis*, 17:238–246, 1980.

C.P. Fuehne. Application of generalized Floquet theory to ground resonance data. In *Proceedings of American Helicopter Society 56th Annual National Forum*, Virginia Beach VA, USA, 2000.

G.H. Golub and C.F. van Loan. *Matrix Computations*. Johns Hopkins University Press, Baltimore, second edition, 1989.

C. Hammond and R. Doggett, Jr. Determination of subcritical damping by moving-block/randomdec applications. Technical Report NASA-SP-415, NASA Langley Research Center, 1975.

M.H. Hansen. Improved modal dynamics of wind turbines to avoid stall-induced vibrations. *Wind Energy*, 6:179–195, 2003. doi:10.1002/we.79.

M.H. Hansen. Aeroelastic stability analysis of wind turbines using an eigenvalue approach. *Wind Energy*, 7:133–143, 2004. doi:10.1002/we.116.

M.H. Hansen. Aeroelastic instability problems for wind turbines. *Wind Energy*, 10 (6):551–577, 2007. doi:10.1002/we.242.

M.H. Hansen, K. Thomsen, P. Fuglsang, and T. Knudsen. Two methods for estimating aeroelastic damping of operational wind turbine modes from experiments. *Wind Energy*, 9(1):179–191, 2006. doi:10.1002/we.187.

G.W. Hill. On the part of the motion of the lunar perigee which is a function of the mean motions of the sun and moon. *Acta Mathematica*, 8(1):1–36, 1886. doi:10.1007/BF02417081.

H. Irretier. Mathematical foundations of experimental modal analysis in rotor dynamics. *Mechanical Systems and Signal Processing*, 13(2):183–191, 1999.

W. Johnson. A perturbation solution of helicopter rotor flapping stability. Technical Report NASA TM X-62165, Ames Research Center, 1972. Available from <ntrs.nasa.gov>.

W. Johnson. *Helicopter Theory*. Dover Publications, 1980.

B. Kirchgässner. ARLIS – a program system for aeroelastic analysis of rotating linear systems. In *Proceedings of European Wind Energy Conference*, pages 253–258, Hamburg, Germany, 1984.

S. Krenk. *Non-linear Modeling and Analysis of Solids and Structures*. Cambridge University Press, Cambridge, 2009.

S. Krenk, C. Vissing-Jørgensen, and L. Thesbjerg. Efficient collapse analysis techniques for framed structures. *Computers and Structures*, 72:481–496, 1999.

N.M. Krylov and N.N. Bogolyubov. *Introduction to non-linear mechanics*. Princeton University Press, 1947.

J.G. Leishman and T.S. Beddoes. A generalized model for airfoil unsteady aerodynamic behaviour and dynamic stall using the indicial method. In *Proceedings of 42nd Annual Forum of the American Helicopter Society*, Washington DC, USA, 1986.

K. Liu. Identification of linear time-varying systems. *Journal of Sound and Vibration*, 206:487–505, 1997.

O.J. Lowis. The stability of rotor blade flapping motion at high tip speed ratios. Technical Report R. & M. No. 3544, Aeronautical Research Council, 1963.

A.M. Lyapunov. Sur une série relative à la théorie des équations différentielles linéaires à coefficients périodiques (on a series concerning the theory of linear differential equations with periodic coefficients). *Comptes rendus de l'Académie des Sciences, Paris*, CXXIII:1248–1252, 1896.

L. Meirovitch. *Methods of Analytical Dynamics*. McGraw-Hill, New York, 1970.

A.H. Nayfeh and B. Balachandran. *Applied Nonlinear Dynamics*. Wiley, New York, 1995.

A.H. Nayfeh and D.T. Mook. *Nonlinear Oscillations*. John Wiley & Sons, New York, 1979.

P.E. Nikravesh. *Computer-Aided Analysis of Mechanical Systems*. Prentice-Hall, New Jersey, 1988.

D.A. Peters. Fast Floquet theory and trim for multi-bladed rotorcraft. *Journal of the American Helicopter Society*, 39(4):82–89, 1994.

D.A. Peters and K.H. Hohenemser. Application of the Floquet transition matrix to problems of lifting rotor stability. *Journal of the American Helicopter Society*, 16 (2):25–33, 1971.

J.T. Petersen. *Kinematically Nonlinear Finite Element Model of a Horizontal Axis Wind Turbine. Part 1: Mathematical Model and Results*. PhD thesis, Risø National Laboratory, DK-4000 Roskilde, Denmark, 1990. Available from <risoe.dk>.

J.T. Petersen, H.Aa. Madsen, A. Björck, P. Enevoldsen, S. Øye, H. Ganander, and D. Winkelaar. Prediction of dynamic loads and induced vibrations in stall. Technical Report Risø-R-1045, Risø National Laboratory, 1998. Available from <risoe.dk>.

F. Rasmussen, J.T. Petersen, and H.Aa. Madsen. Dynamic stall and aerodynamic damping. *Journal of Solar Energy Engineering*, 121:150–155, 1999. doi:10.1115/1.2888426.

V.A. Riziotis, S.G. Voutsinas, E.S. Politis, and P.K. Chaviaropoulos. Aeroelastic stability of wind turbines: The problem, the methods and the issues. *Wind Energy*, 7 (4):373–392, 2004. doi:10.1002/we.133.

V.A. Riziotis, E.S. Politis, S.G. Voutsinas, and P.K. Chaviaropoulos. Stability analysis of pitch-regulated, variable-speed wind turbines in closed loop operation using a linear eigenvalue approach. *Wind Energy*, 11(5):517–535, 2008. doi:10.1002/we.276.

S.C. Sinha and R. Pandiyan. Analysis of quasilinear dynamical systems with periodic coefficients via Liapunov-Floquet transformation. *International Journal of Non-Linear Mechanics*, 29(5):687–702, 1994.

J.J. Thomsen. *Vibrations and Stability*. Springer, Berlin, second edition, 2003.

T.G. van Engelen and H. Braam. TURBU offshore, computer program for frequency domain analysis of horizontal axis offshore wind turbines. Technical Report ECN-C–04-079, Energy Research Centre of the Netherlands, 2004. Available from <ecn.nl>.

X. Wang and D.A. Peters. Generalized Floquet theory for analysis of numerical or experimental rotor response data. *Proceedings of the 24th European Rotorcraft Forum, Marseilles, France*, September 1998.

N.M. Wereley and S.R. Hall. Linear time periodic systems: Transfer function, poles, transmission zeroes and directional properties. In *American Control Conference*, Boston MA, USA, June 1991.

E.T. Whittaker and G.N. Watson. *A Course of Modern Analysis*. Cambridge University Press, London, fourth edition, 1927.

J. Xu and R. Gasch. Modale behandlung linearer periodisch zeitvarianter bewegungsgleichungen (modal analysis of linear periodically time-variant equations of motion). *Archive of Applied Mechanics*, 65:178–193, 1995.

V.A. Yakubovich and V.M. Starzhinskii. *Linear Differential Equations with Periodic Coefficients*. Wiley, New York, 1975.

S. Øye. Dynamic stall simulated as time lag of separation. In *Proceedings of 4th IEA Symposium on Aerodynamics of Wind Turbines*, Rome, Italy, 1991.

Publications P1–P5

P1

On the similarity of the Coleman and Lyapunov-Floquet transformations for modal analysis of bladed rotor structures

Journal of Sound and Vibration, 327:424–439, 2009.
doi:10.1016/j.jsv.2009.07.007

Errata:

p. 434, Fig. 5(b):
The values '$0,1,\ldots,8$' on the upper abscissa for j should be '$1,2,\ldots,9$'.

p. 437, Equation (54b), component (4,5) of $\mathbf{C}(t)$:
'$3\Omega J_{\mathrm{b}}$' should be '$-3\Omega J_{\mathrm{b}}$'.

Journal of Sound and Vibration 327 (2009) 424–439

Contents lists available at ScienceDirect

Journal of Sound and Vibration

journal homepage: www.elsevier.com/locate/jsvi

On the similarity of the Coleman and Lyapunov–Floquet transformations for modal analysis of bladed rotor structures

P.F. Skjoldan [a,*], M.H. Hansen [b]

[a] Loads, Aerodynamics and Control, Siemens Wind Power A/S, Dybendalsvænget 3, DK-2630 Taastrup, Denmark
[b] National Laboratory for Sustainable Energy, Risø – Technical University of Denmark, Frederiksborgvej 399, DK-4000 Roskilde, Denmark

ARTICLE INFO

Article history:
Received 4 December 2008
Received in revised form
27 May 2009
Accepted 13 July 2009
Handling Editor: M.P. Cartmell
Available online 14 August 2009

ABSTRACT

Structures with isotropic bladed rotors can be modally analyzed by eigenvalue analysis of time-invariant Coleman transformed equations of motion related to the inertial frame or by Floquet analysis of the periodic equations of motion. The Coleman transformation is here shown to be a special case of the Lyapunov–Floquet (L–F) transformation which transforms system equations of structures with anisotropic bladed rotors into a time-invariant system using the transition matrix and Floquet eigenvectors as a basis. The L–F transformation is not unique, whereby eigensolutions of the time-invariant system are not directly related to the modal frequencies and mode shapes observed in the inertial frame. This modal frequency indeterminacy is resolved by requiring the periodic mode shapes from the L–F approach to be as similar as possible to the mode shapes from the Coleman approach. For an anisotropic rotor the Floquet analysis yields a periodic mode shape that contains harmonics of integer multiples of the rotor speed for inertial state variables. These harmonic components show up as resonance frequencies on the sides of the corresponding modal frequency in a computed frequency response function of a simple three-bladed turbine with an anisotropic rotor.

1. Introduction

The Coleman and Lyapunov–Floquet (L–F) transformations can be used to obtain time-invariant system equations for modal and stability analysis of structures with bladed rotors, e.g. wind turbines and helicopters. This paper explores a similarity of these transformations and uses the physical basis of the Coleman transformation to resolve the indeterminacy of the modal frequencies in Floquet analysis due to the non-uniqueness of the L–F transformation.

Coleman [1] introduces a transformation of the coordinates of bladed rotors into multi-blade coordinates describing the rotor motion in the inertial frame of reference. The periodic coefficients can thereby be eliminated in the system equations for isotropic rotors, where the blades are identical and symmetrically mounted. Feingold [2] extends the work by Coleman to show that the periodic coefficients can also be eliminated in the equations of inplane motion for two-bladed rotors if the rotor support is symmetric. Coleman and Feingold [3] show that for two-bladed rotors with an asymmetric support, the Coleman transformation yields system equations containing periodic terms that have a frequency of two times the rotor speed. They use Floquet theory [4] to show that the solution to a linear periodic system can be written as a set of exponential functions containing the characteristic exponents (each representing a frequency and damping) multiplied by a corresponding set of periodic functions that contain harmonics with integer multiples of the system frequency. Any

* Corresponding author. Tel.: +45 44774865.
E-mail address: peter.skjoldan@siemens.com (P.F. Skjoldan).

0022-460X/$ - see front matter © 2009 Elsevier Ltd. All rights reserved.
doi:10.1016/j.jsv.2009.07.007

periodic function can be represented by a Fourier series, which is used in Hill's method to derive the characteristic exponents from Hill's determinant (see, e.g. [5–7]) as Coleman and Feingold do in their stability analysis of two-bladed rotors.

The development of digital numerical analysis allows direct application of Floquet theory by computation of the transition matrix from the time integration of the system equations. The transition matrix gives the *monodromy matrix* whose eigenvalues are the Floquet multipliers that determine the characteristic exponents with non-unique frequencies. Early Floquet analyses are performed on helicopters by Lowis [8] using a rectangular ripple method and Peters and Hohenemser [9] using a predictor–corrector integration scheme. Attempts to reduce the immense computational effort required by Floquet analysis on larger systems are done by Friedmann et al. [10] who develop an efficient numerical scheme to obtain the transition matrix from a single integration, and by Sinha and Pandiyan [11] who approximate the transition matrix based on an expansion of the system matrix in Chebyshev polynomials. Peters [12] shows with *fast Floquet theory* that the transition matrix computed until $1/B$ of the system period for an isotropic rotor with B blades can be used to generate the transition matrix for the full period. Bauchau and Nikishkov [13] use elements of the Arnoldi eigenvalue algorithm to perform *implicit Floquet analysis* yielding the most important eigensolutions from a limited number of system matrix integrations. Concepts of system identification from experimental signal analysis are applied by Quaranta et al. [14] to project the state variables of a large multi-body dynamical system by proper orthogonal decomposition into a smaller subspace before applying Floquet analysis. Bauchau and Wang [15] use a similar approach, *partial Floquet analysis*, to approximate the monodromy matrix from an incomplete transition matrix.

The modal frequencies and damping of the vibration modes of the periodic system can be determined from the Floquet multipliers. The infinity of solution branches to the complex logarithm yields frequencies given by a principal value plus an integer multiple of the system frequency. The traditional approach for resolving this frequency indeterminacy is based on Fourier analysis of the set of periodic functions in the Floquet solution [16,17], which are herein referred to as the *periodic mode shapes*. This method is contained in several different Floquet approaches [15,18,19]. Nagabhushanam and Gaonkar [20] suggest an automatic modal identification method, where the integer factor of the frequency indeterminacy is determined by using that the ratio of the velocity and position parts of the dominating degree of freedom in the Floquet eigenvectors is an estimate of the modal frequency. Peters and Hohenemser [9] increase the magnitude of the system periodicity in small increments starting from zero, where the frequencies are unique, until the desired value, and thus obtain the modal frequencies by continuation.

In this paper, the traditional method for resolving the frequency indeterminacy is substantiated by showing a similarity between the modal dynamics of an isotropic rotor obtained by eigenvalue analysis of the Coleman transformed system equations and the modal dynamics obtained by Floquet analysis. The comparison is based on *Lyapunov's reducibility theorem* [21] stating that the periodic Lyapunov–Floquet (L–F) transformation eliminates the periodic coefficients in the system equations. The L–F transformation is not unique, because it depends on the non-unique characteristic exponents. The choice of integer factors on the rotor speed added to the characteristic exponents can be considered as a choice of reference frame into which the state variables are L–F transformed, and in which the frequencies are then measured. Modal frequencies are herein defined to be measured in the inertial frame, whereby they can be directly compared to the modal frequencies obtained from the eigenvalues of the Coleman transformed system equations. The inertial state variables in the periodic mode shape obtained from the Coleman transformed equations are constant; therefore the modal frequencies are chosen such that the harmonic components of the inertial state variables in the periodic mode shape become as constant as possible. In the comparison of the two approaches for an isotropic rotor, the same results are obtained. This frequency identification approach in Floquet analysis is, however, applicable to a system with anisotropic rotor and support.

The paper is arranged as follows: Section 2 contains the theory of modal analysis using the Coleman transformation and using Floquet analysis. The similarity of the two approaches is shown and used as a basis for resolving the frequency indeterminacy. Section 3 contains a numerical example that compares the two approaches for an isotropic rotor and uses Floquet analysis for an anisotropic rotor. Section 4 contains the conclusions.

2. Modal analysis of structures with bladed rotors

The linear equations of motion for small vibrations of a structure with a bladed rotor operating at constant mean rotor speed with small overlaid variations can be written as a set of first-order equations:

$$\dot{\mathbf{x}} = \mathbf{A}(t)\mathbf{x}, \quad \mathbf{A}(t+T) = \mathbf{A}(t) \tag{1}$$

where $(\dot{})$ denotes the time derivative, $\mathbf{A}$ is the periodic system matrix, $T = 2\pi/\Omega$ is the period corresponding to the mean rotor speed Ω, and $\mathbf{x}$ is the state vector for a rotor with B blades:

$$\mathbf{x} = \{x_{1,1} \cdots x_{1,N_b} \;\; x_{2,1} \cdots x_{2,N_b} \;\; \cdots \;\; x_{B,1} \cdots x_{B,N_b} \;\; x_{s,1} \cdots x_{s,N_s}\}^T \tag{2}$$

where an integer as the first index on x denotes the blade number and "s" as the first index denotes *inertial state variables* of the rotor support. The total number of state variables for a B-bladed rotor system is $N = BN_b + N_s$, where N_b is the number of *rotor state variables* in the rotating frame for a single blade and N_s is the number of inertial state variables of the rotor support. It is assumed that all blades have identical sets of state variables. Note that the state variables for an

aeroservoelastic model of a wind turbine or helicopter may consist of generalized coordinates and velocities of structural motion, state variables of the unsteady aerodynamic model, and state variables of the controller.

2.1. Coleman transformation approach

The Coleman transformation for a rotor with B blades is [12,16]

$$\mathbf{x} = \mathbf{B}(t)\mathbf{z}_\mathrm{B}$$

$$\mathbf{B}(t) = \begin{bmatrix} \mathbf{I}_{N_\mathrm{b}} & \mathbf{I}_{N_\mathrm{b}}\cos\psi_1 & \mathbf{I}_{N_\mathrm{b}}\sin\psi_1 & \cdots & \mathbf{I}_{N_\mathrm{b}}\cos\tilde{B}\psi_1 & \mathbf{I}_{N_\mathrm{b}}\sin\tilde{B}\psi_1 & -\mathbf{I}_{N_\mathrm{b}} & \mathbf{0} \\ \mathbf{I}_{N_\mathrm{b}} & \mathbf{I}_{N_\mathrm{b}}\cos\psi_2 & \mathbf{I}_{N_\mathrm{b}}\sin\psi_2 & \cdots & \mathbf{I}_{N_\mathrm{b}}\cos\tilde{B}\psi_2 & \mathbf{I}_{N_\mathrm{b}}\sin\tilde{B}\psi_2 & \mathbf{I}_{N_\mathrm{b}} & \mathbf{0} \\ \mathbf{I}_{N_\mathrm{b}} & \mathbf{I}_{N_\mathrm{b}}\cos\psi_3 & \mathbf{I}_{N_\mathrm{b}}\sin\psi_3 & \cdots & \mathbf{I}_{N_\mathrm{b}}\cos\tilde{B}\psi_3 & \mathbf{I}_{N_\mathrm{b}}\sin\tilde{B}\psi_3 & -\mathbf{I}_{N_\mathrm{b}} & \mathbf{0} \\ \vdots & \vdots & \vdots & & \vdots & \vdots & \vdots & \vdots \\ \mathbf{I}_{N_\mathrm{b}} & \mathbf{I}_{N_\mathrm{b}}\cos\psi_B & \mathbf{I}_{N_\mathrm{b}}\sin\psi_B & \cdots & \mathbf{I}_{N_\mathrm{b}}\cos\tilde{B}\psi_B & \mathbf{I}_{N_\mathrm{b}}\sin\tilde{B}\psi_B & (-\mathbf{I}_{N_\mathrm{b}})^B & \mathbf{0} \\ \mathbf{0} & \mathbf{0} & \mathbf{0} & \cdots & \mathbf{0} & \mathbf{0} & \mathbf{0} & \mathbf{I}_{N_\mathrm{s}} \end{bmatrix} \tag{3}$$

where $\tilde{B} = (B-1)/2$ for B odd and $\tilde{B} = (B-2)/2$ for B even, $\psi_j = \Omega t + 2\pi(j-1)/B$ is the mean azimuth angle to blade number $j = 1, 2, \ldots, B$, and $\mathbf{I}_{N_\mathrm{b}}$ and $\mathbf{I}_{N_\mathrm{s}}$ are identity matrices of sizes N_b and N_s. The vector $\mathbf{z}_\mathrm{B}$ contains the BN_b state variables in multi-blade coordinates and N_s inertial state variables as

$$\mathbf{z}_\mathrm{B} = \{a_{0,1}\cdots a_{0,N_\mathrm{b}}\ \ a_{1,1}\cdots a_{1,N_\mathrm{b}}\ \ b_{1,1}\cdots b_{1,N_\mathrm{b}}\ \ \cdots\ \ a_{\tilde{B},1}\cdots a_{\tilde{B},N_\mathrm{b}}\ \ b_{\tilde{B},1}\cdots b_{\tilde{B},N_\mathrm{b}}\ \ b_{B/2,1}\cdots b_{B/2,N_\mathrm{b}}\ \ x_{\mathrm{s},1}\cdots x_{\mathrm{s},N_\mathrm{s}}\}^\mathrm{T} \tag{4}$$

and describes the rotor motion in the inertial frame. The second last column block in $\mathbf{B}$ and coordinates $b_{B/2,1}$ to $b_{B/2,N_\mathrm{b}}$ occur only for B even. Details on how multi-blade coordinates describe the motion of a three-bladed wind turbine rotor in the inertial frame are discussed in [22,23].

Insertion of (3) into (1) shows that the Coleman transformed system equation becomes

$$\dot{\mathbf{z}}_\mathrm{B} = \mathbf{A}_\mathrm{B}\mathbf{z}_\mathrm{B} \tag{5}$$

where

$$\mathbf{A}_\mathrm{B} = \mathbf{B}^{-1}(t)\mathbf{A}(t)\mathbf{B}(t) - \mathbf{B}^{-1}(t)\dot{\mathbf{B}}(t) \tag{6}$$

The transformed system matrix $\mathbf{A}_\mathrm{B}$ will be time-invariant if the rotor is *isotropic*, i.e. it has three or more blades with equal properties and has symmetric inter-blade couplings such that the coupling to the support depends only on the azimuth angle and not the blade number, as shown in Appendix A. This important feature of the Coleman transformation enables the use of traditional eigenvalue analysis for the modal decomposition of the dynamics of these particular rotors.

2.1.1. Modal decomposition of transient solution

A transient solution of the time-invariant Coleman transformed system equation (5) for an isotropic rotor with a constant system matrix $\mathbf{A}_\mathrm{B}$ is

$$\mathbf{z}_\mathrm{B} = \mathrm{e}^{\mathbf{A}_\mathrm{B}t}\mathbf{z}_\mathrm{B}(0) \tag{7}$$

where $\mathbf{z}_\mathrm{B}(0) = \mathbf{B}^{-1}(0)\mathbf{x}(0)$ are the inverse transformed initial conditions (i.e. the disturbance of the structure away from its operating point). The Coleman transformed system matrix can be written in terms of its Jordan form as $\mathbf{A}_\mathrm{B} = \mathbf{V}_\mathrm{B}\mathbf{\Lambda}_\mathrm{B}\mathbf{V}_\mathrm{B}^{-1}$ whereby the transient solution (7) becomes

$$\mathbf{z}_\mathrm{B} = \mathbf{V}_\mathrm{B}\,\mathrm{e}^{\mathbf{\Lambda}_\mathrm{B}t}\mathbf{V}_\mathrm{B}^{-1}\mathbf{z}_\mathrm{B}(0) \tag{8}$$

If the eigenvectors $\mathbf{v}_{B,k}$ of $\mathbf{A}_\mathrm{B}$ are all linearly independent, $\mathbf{\Lambda}_\mathrm{B}$ is a diagonal matrix containing the eigenvalues $\lambda_{B,k}$ of $\mathbf{A}_\mathrm{B}$, and the eigenvectors $\mathbf{v}_{B,k}$ form the columns of $\mathbf{V}_\mathrm{B}$ (see [24] for the case of repeated eigenvalues with linearly dependent eigenvectors).

The transient solution (8) can be transformed into the original coordinates by (3) as

$$\mathbf{x} = \mathbf{U}_\mathrm{B}(t)\,\mathrm{e}^{\mathbf{\Lambda}_\mathrm{B}t}\mathbf{q}_\mathrm{B}(0) \tag{9}$$

where

$$\mathbf{q}_\mathrm{B}(0) = \mathbf{V}_\mathrm{B}^{-1}\mathbf{B}^{-1}(0)\mathbf{x}(0) \tag{10}$$

is a constant vector representing the modal content of the initial conditions $\mathbf{x}(0)$, and

$$\mathbf{U}_\mathrm{B}(t) = \mathbf{B}(t)\mathbf{V}_\mathrm{B} \tag{11}$$

is a periodic mode shape matrix. This modal interpretation becomes clearer if the Jordan form $\mathbf{\Lambda}_B$ is diagonal, whereby (9) can be decomposed as

$$\mathbf{x} = \sum_{k=1}^{N} \mathbf{u}_{B,k}(t)\, e^{\lambda_{B,k} t} q_{B,k}(0) \tag{12}$$

where $\mathbf{u}_{B,k}(t) = \mathbf{B}(t)\mathbf{v}_{B,k}$ is a periodic mode shape of mode number k in the original coordinates. It can be shown by expanding (12) for state variable number i on blade number j that the rotor state variables can contain B different harmonic components (see [23] for details on a three-bladed rotor) written as

$$x_{ik} = e^{\sigma_{B,k} t} \left(A_{0,ik} \cos(\omega_{B,k} t + \varphi_{0,ik}) + \sum_{n=1}^{\tilde{B}} \left(A_{\mathrm{BW}n,ik} \cos\left((\omega_{B,k} + n\Omega)t + \frac{2\pi n}{B}(j-1) + \phi_{\mathrm{BW}n,ik} \right) + A_{\mathrm{FW}n,ik} \cos\left((\omega_{B,k} - n\Omega)t - \frac{2\pi n}{B}(j-1) + \phi_{\mathrm{FW}n,ik} \right) \right) + A_{B/2,ik} \cos(\omega_{B,k} t + \phi_{B/2,ik}) \right) q_{B,k}(0) \tag{13}$$

where $\sigma_{B,k}$ and $\omega_{B,k}$ are the modal damping and frequency, respectively, given by the eigenvalue $\lambda_{B,k} = \sigma_{B,k} + \mathrm{i}\omega_{B,k}$ with $\mathrm{i} = \sqrt{-1}$. The amplitudes are determined from the components of the eigenvector $\mathbf{v}_{B,k}$ in multi-blade coordinates (4) as $A_{0,ik} = |a_{0,ik}|$, $A_{B/2,ik} = |b_{B/2,ik}|$ (for B even only) and

$$\begin{aligned} A_{\mathrm{BW}n,ik} &= \tfrac{1}{2}\sqrt{(\mathrm{Re}(a_{n,ik}) + \mathrm{Im}(b_{n,ik}))^2 + (\mathrm{Re}(b_{n,ik}) - \mathrm{Im}(a_{n,ik}))^2} \\ A_{\mathrm{FW}n,ik} &= \tfrac{1}{2}\sqrt{(\mathrm{Re}(a_{n,ik}) - \mathrm{Im}(b_{n,ik}))^2 + (\mathrm{Re}(b_{n,ik}) + \mathrm{Im}(a_{n,ik}))^2} \end{aligned} \tag{14}$$

where $a_{n,ik}$ and $b_{n,ik}$ are the cosine and sine components of $\mathbf{v}_{B,k}$, respectively. The constant phases $\phi_{0,ik}$, $\phi_{\mathrm{BW}n,ik}$, $\phi_{\mathrm{FW}n,ik}$, and $\phi_{B/2,ik}$ in (13) are also given by the eigenvector [23]. The amplitudes with subscript BW denote the backward whirling components, where for $n = 1$ the reaction force due to this rotor motion rotates against the direction of the rotor. Conversely, the FW amplitudes represent the forward whirling components, where for $n = 1$ the reaction force rotates in the direction of rotor rotation. For $n > 1$ the reaction forces cancel out and these components are called reactionless.

2.2. Lyapunov–Floquet transformation approach

Floquet theory enables the solution of the linear equation system (1) directly without elimination of the periodic coefficients. Any transient solution at any time t can be formed from N linearly independent solutions of (1) over a single period $t \in [0; T]$ [6]. These solutions $\boldsymbol{\varphi}_k(t)$ are collected in the columns of an $N \times N$ matrix called the *fundamental matrix* of the system:

$$\boldsymbol{\varphi}(t) = [\boldsymbol{\varphi}_1(t)\ \ \boldsymbol{\varphi}_2(t)\ \ \cdots\ \ \boldsymbol{\varphi}_N(t)], \quad \dot{\boldsymbol{\varphi}}(t) = \mathbf{A}(t)\boldsymbol{\varphi}(t) \tag{15}$$

The solutions may be found by numerical solution of (1) with N linearly independent initial conditions collected as columns in the matrix $\boldsymbol{\varphi}(0)$. Lyapunov's reducibility theorem [25] states that there exists a transformation of the original coordinates $\mathbf{x}$ that renders the periodic system (1) time-invariant. This Lyapunov–Floquet transformation can be defined as [26,11,27]

$$\mathbf{x} = \mathbf{L}(t)\mathbf{z}, \quad \mathbf{L}(t) = \boldsymbol{\varphi}(t)\, e^{-\mathbf{R}t} \boldsymbol{\varphi}^{-1}(0)\mathbf{L}(0) \tag{16}$$

where $\mathbf{R}$ is a constant non-singular matrix.

To show that the Lyapunov–Floquet transformation (16) eliminates the periodic terms of the system equations, it is substituted into (1) leading to

$$\dot{\mathbf{z}} = \mathbf{L}^{-1}(t)(\mathbf{A}(t)\mathbf{L}(t) - \dot{\mathbf{L}}(t))\mathbf{z} \tag{17}$$

which by differentiation of $\mathbf{L}$ and use of $\dot{\boldsymbol{\varphi}}(t) = \mathbf{A}(t)\boldsymbol{\varphi}(t)$ can be rewritten as

$$\dot{\mathbf{z}} = \mathbf{A}_L \mathbf{z} \tag{18}$$

where

$$\mathbf{A}_L = \mathbf{L}^{-1}(0)\boldsymbol{\varphi}(0)\mathbf{R}\boldsymbol{\varphi}^{-1}(0)\mathbf{L}(0) \tag{19}$$

is the time-invariant Lyapunov–Floquet transformed system matrix. Note that it is given by the constant matrix $\mathbf{R}$, and the choices of initial conditions for the fundamental matrix $\boldsymbol{\varphi}(0)$ and transformation matrix $\mathbf{L}(0)$.

If the constant matrix $\mathbf{R}$ is defined in terms of the *monodromy matrix*

$$\mathbf{C} \equiv \boldsymbol{\varphi}^{-1}(t)\boldsymbol{\varphi}(t+T) \tag{20}$$

as

$$\mathbf{C} = e^{\mathbf{R}T} \tag{21}$$

then the Lyapunov–Floquet transformation $\mathbf{L}$ can be shown to be periodic with period T by combining (16), (20), (21), and $\mathbf{R} = \mathbf{V}\boldsymbol{\Lambda}\mathbf{V}^{-1}$.

The monodromy matrix can be written in terms of its Jordan form $\mathbf{C} = \mathbf{P}\mathbf{J}\mathbf{P}^{-1}$ where $\mathbf{J}$ contains the eigenvalues ρ_k of $\mathbf{C}$ in the diagonal. The eigenvalues are named *characteristic* or *Floquet multipliers*. Eq. (21) shows that $\mathbf{R}$ is determined as the matrix logarithm

$$\mathbf{R} = \frac{1}{T}\ln(\mathbf{C}) = \frac{1}{T}\mathbf{P}\ln(\mathbf{J})\mathbf{P}^{-1} \tag{22}$$

which exists because $\mathbf{C}$ is non-singular [28]; however, $\mathbf{R}$ may not be unique. There can be two causes of non-uniqueness of the matrix logarithm [29]: first, the similarity transformation matrix $\mathbf{V}$ of the Jordan decomposition $\mathbf{R} = \mathbf{V}\boldsymbol{\Lambda}\mathbf{V}^{-1}$ can have an infinity of solutions if the Jordan form $\mathbf{J}$ of $\mathbf{C}$ is non-diagonal. Second, even if $\mathbf{J}$ is diagonal, the complex scalar logarithm is non-unique, which is the case relevant for practical applications.

2.2.1. Modal decomposition of transient solution

A transient solution of the time-invariant Lyapunov–Floquet transformed system Eq. (18) is

$$\mathbf{z} = \mathrm{e}^{\mathbf{A}_\mathrm{L} t}\mathbf{z}(0) \tag{23}$$

where $\mathbf{z}(0) = \mathbf{L}^{-1}(0)\mathbf{x}(0)$ are the inverse transformed initial conditions. The transformed system matrix (19) can be Jordan decomposed as

$$\mathbf{A}_\mathrm{L} = \mathbf{V}_\mathrm{L}\boldsymbol{\Lambda}\mathbf{V}_\mathrm{L}^{-1} \tag{24}$$

where $\mathbf{V}_\mathrm{L} = \mathbf{L}^{-1}(0)\boldsymbol{\varphi}(0)\mathbf{V}$ and the Jordan form of $\mathbf{A}_\mathrm{L}$ is $\boldsymbol{\Lambda}$, because $\mathbf{A}_\mathrm{L}$ is a similarity transform of $\mathbf{R}$ (19). The transient solution (23) then becomes

$$\mathbf{z} = \mathbf{V}_\mathrm{L}\,\mathrm{e}^{\boldsymbol{\Lambda} t}\mathbf{V}_\mathrm{L}^{-1}\mathbf{z}(0) \tag{25}$$

Note the similarity between this expression and (8). The transient solution (25) can be modally decomposed and written in the original coordinates using (16) as

$$\mathbf{x} = \mathbf{U}(t)\,\mathrm{e}^{\boldsymbol{\Lambda} t}\mathbf{q}(0) \tag{26}$$

where the initial modal coordinates are

$$\mathbf{q}(0) = \mathbf{V}_\mathrm{L}^{-1}\mathbf{L}^{-1}(0)\mathbf{x}(0) = \mathbf{V}^{-1}\boldsymbol{\varphi}^{-1}(0)\mathbf{x}(0) \tag{27}$$

and the periodic mode shape matrix is

$$\mathbf{U}(t) = \mathbf{L}(t)\mathbf{V}_\mathrm{L} = \mathbf{L}(t)\mathbf{L}^{-1}(0)\boldsymbol{\varphi}(0)\mathbf{V} \tag{28}$$

The periodicity of $\mathbf{U}$ follows from the periodicity of $\mathbf{L}$.

The matrix $\mathbf{R}$ defined by (21) from the monodromy matrix $\mathbf{C}$ is still undetermined due to the indeterminacy of the matrix logarithm in (22). However, when $\mathbf{J}$ (the Jordan form of $\mathbf{C}$) is diagonal, then $\boldsymbol{\Lambda}$ (the Jordan form of $\mathbf{R}$) will also be diagonal with the elements

$$\lambda_k = \frac{1}{T}\ln(\rho_k) \tag{29}$$

which are called the *characteristic exponents* of the monodromy matrix $\mathbf{C}$, and the similarity transformation matrix $\mathbf{P}$ that brings $\mathbf{C}$ to its Jordan form $\mathbf{J}$ will also bring $\mathbf{R}$ to its Jordan form $\boldsymbol{\Lambda}$, i.e. $\mathbf{V} = \mathbf{P}$. Furthermore, the diagonal property of $\boldsymbol{\Lambda}$ shows that the modal decomposition (26) can be written as

$$\mathbf{x} = \sum_{k=1}^{N} \mathbf{u}_k(t)\,\mathrm{e}^{\lambda_k t} q_k(0) \tag{30}$$

where $\mathbf{u}_k(t) = \mathbf{L}(t)\mathbf{L}^{-1}(0)\boldsymbol{\varphi}(0)\mathbf{v}_k$ is a periodic mode shape of mode number k in the original coordinates and $q_k(0)$ is its modal content in the initial condition.

The characteristic exponents (29) are given by the complex logarithm

$$\lambda_k = \sigma_k + \mathrm{i}\omega_k = \frac{1}{T}\ln(|\rho_k|) + \mathrm{i}\frac{1}{T}(\arg(\rho_k) + j_k 2\pi), \quad j_k \in \mathbb{Z} \tag{31}$$

where σ_k and ω_k are the real and imaginary parts of λ_k, respectively. The integers j_k in the imaginary parts are undetermined for each mode, i.e. the modal frequencies ω_k are not determined uniquely. A physical explanation to this indeterminacy is that frequencies depend on the observer's frame of reference, which is defined by a Lyapunov–Floquet transformation that is non-unique due to its dependency on $\mathbf{R}$ (16). The frequency indeterminacy is now resolved by *defining modal frequencies as those frequencies observed in frequency responses measured in the inertial frame of reference*.

2.2.2. Resolving the indeterminacy of the modal frequencies

Principal Floquet exponents $\lambda_{\mathrm{p},k} = \sigma_k + \mathrm{i}\omega_{p,k}$ are defined by the modal damping σ_k and principal frequencies $\omega_{p,k}$ which are given by

$$\begin{aligned} \sigma_k &= \frac{1}{T}\ln(|\rho_k|) \\ \omega_{p,k} &= \frac{1}{T}\arg(\rho_k), \quad \omega_{p,k} \in \left]-\frac{1}{2}\Omega;\frac{1}{2}\Omega\right] \end{aligned} \tag{32}$$

where $\arg(\rho_k) \in]-\pi;\pi]$ is implied. The complex logarithm (31) shows that the modal frequency ω_k is undetermined to within an integer multiple of the rotor speed:

$$\omega_k = \omega_{p,k} + j_k\Omega \tag{33}$$

where the indeterminacy for mode number k is denoted by the integer j_k. The transient response (30) to a pure excitation of mode k (obtainable by setting $q_k(0) = 1$ and all other initial modal components equal zero) can thereby be written as

$$\mathbf{x}_k(t) = \mathbf{u}_k(t)\,\mathrm{e}^{(\lambda_{\mathrm{p},k}+\mathrm{i}j_k\Omega)t} \tag{34}$$

where the periodic mode shape is given by (16) and (28) as

$$\begin{aligned} \mathbf{u}_k(t) &= \mathbf{L}(t)\mathbf{L}^{-1}(0)\boldsymbol{\varphi}(0)\mathbf{v}_k\,\mathrm{e}^{-(\lambda_{\mathrm{p},k}+\mathrm{i}j_k\Omega)t} \\ &= \boldsymbol{\varphi}(t)\mathbf{v}_k\,\mathrm{e}^{-(\lambda_{\mathrm{p},k}+\mathrm{i}j_k\Omega)t} = \mathbf{u}_{p,k}(t)\,\mathrm{e}^{-\mathrm{i}j_k\Omega t} \end{aligned} \tag{35}$$

where $\mathbf{u}_{p,k}(t) = \boldsymbol{\varphi}(t)\mathbf{v}_k\,\mathrm{e}^{-\lambda_{\mathrm{p},k}t}$ is the *principal periodic mode shape*. Both the periodic mode shape $\mathbf{u}_k$ and the exponential term in the solution (34) depend on the chosen integers j_k. As the exponent has different signs in (34) and (35), the contributions from j_k cancel, and the same transient solution is obtained independent of the values of j_k. Hence, a modal frequency of mode number k can be defined freely within an integer multiple of Ω, a choice that also determines the observer's frame of reference. The observer of the modal frequencies (33) is placed in the inertial frame of reference, which makes the modal frequencies similar to those obtained by the Coleman transformation approach, where the periodic mode shapes are constant for the non-transformed inertial state variables. The objective of the suggested approach is therefore to make the inertial state variables in the periodic mode shapes constant, or as constant as possible.

The Fourier expansion of the principal periodic mode shape $\mathbf{u}_{p,k}(t)$ contains only harmonics of an integer multiple of Ω because $\mathbf{u}_{p,k}$ is T-periodic, and it can be expressed for state variable i as

$$u_{p,ik}(t) = \sum_{j=-\infty}^{\infty} \mathscr{U}_{p,j,ik}\,\mathrm{e}^{\mathrm{i}2\pi jt/T} = \sum_{j=-\infty}^{\infty} \mathscr{U}_{p,j,ik}\,\mathrm{e}^{\mathrm{i}j\Omega t} \tag{36}$$

where $\mathscr{U}_{p,j,ik}$ are the Fourier coefficients.[1] Using (35) and (36), the periodic mode shape corresponding to the modal frequency (33) can be written as

$$u_{ik}(t) = \sum_{j=-\infty}^{\infty} \mathscr{U}_{p,j,ik}\,\mathrm{e}^{\mathrm{i}(j-j_k)\Omega t} \tag{37}$$

By selecting the undetermined integer j_k for mode k as the index of the largest Fourier coefficient

$$j_k = \{j_k \in \mathbb{Z} | \mathscr{U}_{\mathrm{p},j_k,ik} \geqslant \mathscr{U}_{p,j,ik}\ \forall \mathrm{j} \in \mathbb{Z}\} \tag{38}$$

the largest harmonic component in the periodic mode shape (37) is removed. Note the index i must correspond to a state variable in the inertial frame. In the case of an isotropic rotor, $\mathscr{U}_{p,j,ik}$ is non-zero only for one j_k, and u_{ik} is constant for inertial state variables. If the rotor has any anisotropy, internally or externally, then $\mathscr{U}_{p,j,ik}$ will have several non-zero components for inertial state variables, but the periodic mode shape $u_{ik}(t)$ is made as constant as possible using (38) to select j_k.

Johnson [16, p. 374] describes the above method in the following way: "One way to mechanize this choice of frequencies is to require that the mean value of the eigenvector have the largest magnitude; then the harmonic of largest magnitude in the eigenvector corresponding to the principal value of the eigenvalue gives the frequency $n2\pi/T$", where "eigenvector" refers to the periodic mode shape and n is j_k. The periodic mode shape has the largest mean value in time, when it is not oscillating. Johnson's statement is, however, in this context only valid when considering the inertial state variables, because the rotor state variable harmonics can be non-zero at other frequencies than the harmonics of the inertial state variables.

2.2.3. Similarity of Coleman and Lyapunov–Floquet transformations

For an isotropic rotor, the Lyapunov–Floquet transformed solution (23) must be identical to the Coleman transformed solution (7) when written in the original coordinates. Using the Jordan decomposed forms of the time-invariant system

[1] The frequency resolution of the Fourier series (36) must be exactly Ω implying that the Fast Fourier Transforms of the principal periodic mode shapes are computed from fundamental solutions obtained in 2^n time steps over the period T, where n is an integer.

matrices, this equality of the solutions becomes

$$\mathbf{B}(t)\mathbf{V}_\mathrm{B}\,\mathrm{e}^{\mathbf{\Lambda}_\mathrm{B}t}(\mathbf{B}(0)\mathbf{V}_\mathrm{B})^{-1}\mathbf{x}(0)=\mathbf{L}(t)\mathbf{V}_\mathrm{L}\,\mathrm{e}^{\mathbf{\Lambda}_\mathrm{B}t}(\mathbf{L}(0)\mathbf{V}_\mathrm{L})^{-1}\mathbf{x}(0) \tag{39}$$

where the Jordan forms $\mathbf{\Lambda}$ and $\mathbf{\Lambda}_\mathrm{B}$ are identical for the two approaches, because the modal frequencies in the Lyapunov–Floquet transformed solution are resolved in the inertial frame as in the Coleman transformation solution.

The initial values of the Lyapunov–Floquet transformation (16) $\mathbf{L}(0)$ can be chosen arbitrarily. Choosing $\mathbf{L}(0)=\mathbf{B}(0)$, the two similarity transformation matrices of the Jordan decomposed forms must be equal, $\mathbf{V}_\mathrm{B}=\mathbf{V}_\mathrm{L}$, to satisfy (39) at $t=0$, whereby also the transformations become equal, $\mathbf{L}(t)=\mathbf{B}(t)$, for all $t\in\mathbb{R}$.

Hence, the Coleman and Lyapunov–Floquet transformations are identical for an isotropic rotor when the Lyapunov–Floquet system matrix $\mathbf{R}$ is corrected for the initial conditions used in the fundamental solution (19), and when the Coleman transformation is used as initial condition for the Lyapunov–Floquet transformation. Thus, the Coleman transformation can be viewed as a special case of the Lyapunov–Floquet transformation which also renders systems with anisotropic rotors time-invariant.

3. Application to a wind turbine with hinged blades

A structural model of a wind turbine with a minimum degrees of freedom able to represent some of its fundamental structural dynamics is considered. Fig. 1 illustrates the turbine with three rigid flap-hinged blades and a rigid nacelle that can tilt and yaw on a rigid tower. The state vector is

$$\mathbf{x}=\{\theta_1,\dot\theta_1,\theta_2,\dot\theta_2,\theta_3,\dot\theta_3,\theta_x,\dot\theta_x,\theta_z,\dot\theta_z\}^\mathrm{T} \tag{40}$$

where θ_j is the flap-hinge angle of blade j, and θ_x and θ_z are the tilt and yaw angles of the nacelle, respectively.

The rotor is assumed to be mass balanced and gravity is neglected, whereby the model can be linearized around the steady-state equilibrium with constant rotor speed and zero deflection angles. In case of gravity, or a mass unbalance, this linearization is also valid if the deflections in the periodic equilibrium are not too large. The system equations are written in first-order form (1) with a periodic system matrix (55) in Appendix A. Dissipation is included in the model by viscous damping forces.

To investigate anisotropy, different values for the blade stiffnesses G_1, G_2, and G_3 can be applied. This type of anisotropy is chosen to avoid changing the steady-state equilibrium. Table 1 shows the model parameters chosen to represent a generic multi-MW turbine.

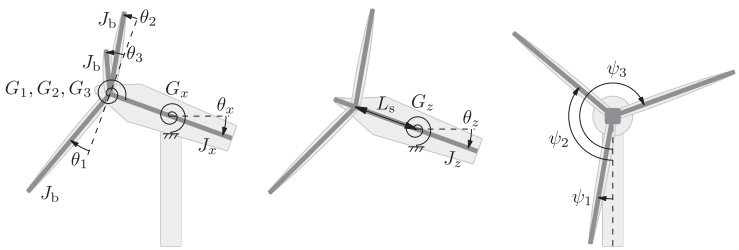

Fig. 1. A wind turbine with flapwise hinged rigid blades and a rigid nacelle able to tilt and yaw yielding five rotational degrees of freedom: θ_1, θ_2, θ_3, θ_x, and θ_z.

Table 1
Model parameters for a multi-MW generic wind turbine.

Blade moment of inertia about root	J_b	$4\times10^6\,\mathrm{kg\,m^2}$
Nacelle/tower tilt moment of inertia	J_x	$8\times10^6\,\mathrm{kg\,m^2}$
Nacelle/tower yaw moment of inertia	J_z	$6\times10^6\,\mathrm{kg\,m^2}$
Blade stiffness	G_b	$8\times10^7\,\mathrm{N\,m}$
Nacelle/tower tilt stiffness	G_x	$7\times10^8\,\mathrm{N\,m}$
Nacelle/tower yaw stiffness	G_z	$4\times10^8\,\mathrm{N\,m}$
Blade damping	c_b	$1\times10^5\,\mathrm{kg\,m^2\,s^{-1}}$
Nacelle/tower tilt damping	c_x	$1\times10^6\,\mathrm{kg\,m^2\,s^{-1}}$
Nacelle/tower yaw damping	c_z	$8\times10^5\,\mathrm{kg\,m^2\,s^{-1}}$
Blade mass	m_b	$12\times10^3\,\mathrm{kg}$
Distance from tower top to hub	L_s	4 m

3.1. Isotropic rotor

The case of an isotropic rotor, $G_1 = G_2 = G_3 = G_b$, is studied to show the similarity of the Coleman and Lyapunov–Floquet transformation approaches.

3.1.1. Coleman transformation approach

Eigenvalue analysis of the time-invariant system matrix (56) in Appendix A yields modal frequencies, damping, and eigenvectors in multi-blade coordinates. The state variables based on these coordinates are

$$\mathbf{z}_B = \{a_0, \tilde{a}_0, a_1, \tilde{a}_1, b_1, \tilde{b}_1, \theta_x, \dot{\theta}_x, \theta_z, \dot{\theta}_z\}^T \tag{41}$$

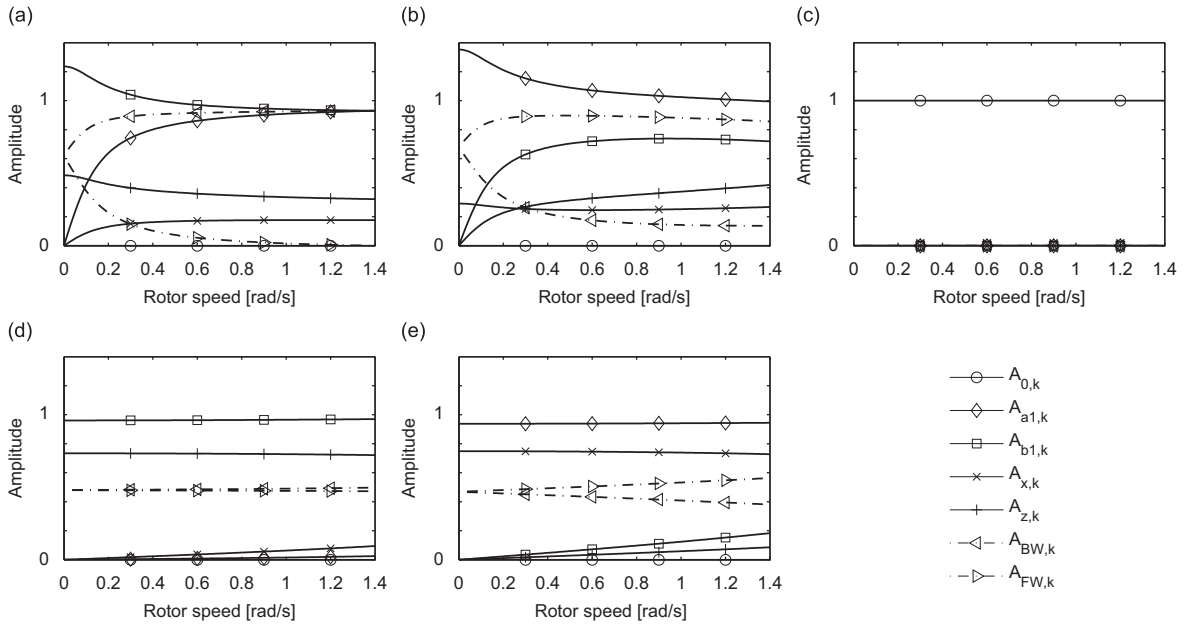

Fig. 2. Normalized modal amplitudes and whirling amplitudes versus rotor speed Ω. (a) First BW mode; (b) first FW mode; (c) symmetric mode; (d) second yaw mode; and (e) second tilt mode.

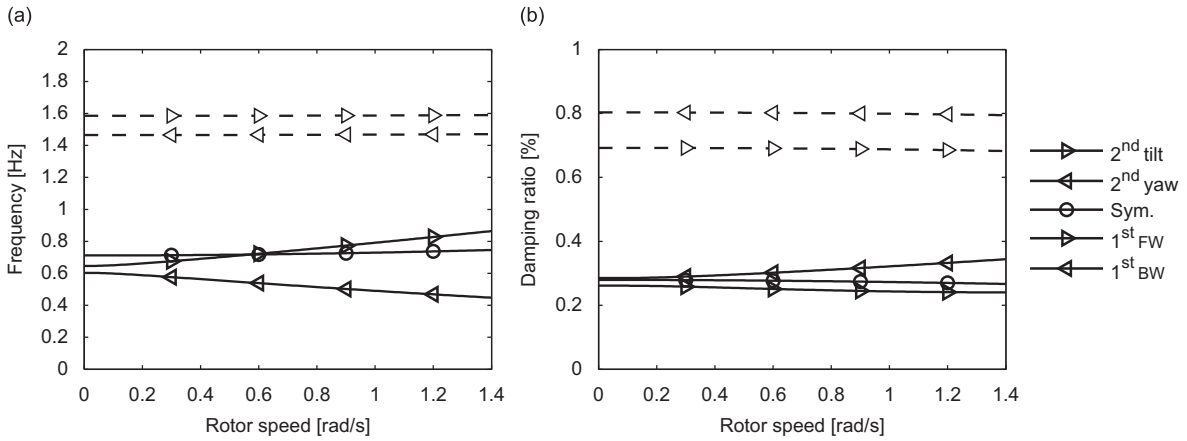

Fig. 3. (a) Campbell diagram with modal frequencies $f_k = \omega_k/2\pi$ versus rotor speed Ω. (b) Damping ratios (approx. $-\sigma_k/\omega_k$ for small damping values) versus rotor speed Ω.

where $\tilde{a}_0$, $\tilde{a}_1$, and $\tilde{b}_1$ are linear combinations of multi-blade positions and velocities (cf. Eq. (46) in Appendix A). The azimuth angle ψ_j for blade j is defined as zero for the blade pointing downwards (see Fig. 1), which means that the coordinate a_1 in (3) is rotor tilt motion, b_1 is yaw motion, and a_0 is the symmetric flap of the rotor.

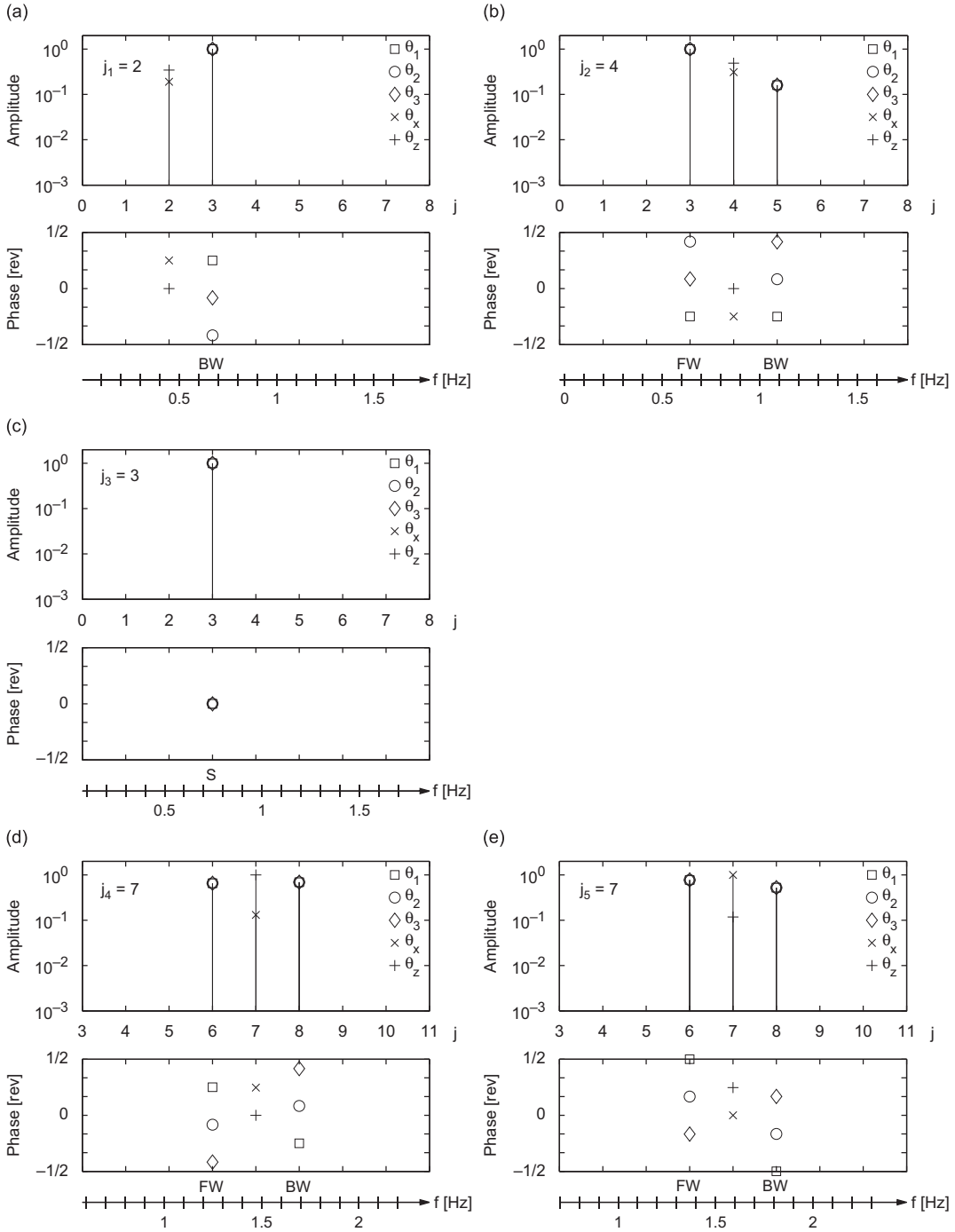

Fig. 4. Amplitudes (log. scale) and phases of harmonic components $\mathscr{U}_{p,j,ik}$ (36) in the principal periodic mode shape for the isotropic rotor at $\Omega = 1.4\,\mathrm{rad/s}$. The bottom scale shows the frequencies in the response measured in the inertial system as $(j - j_k)\Omega + \omega_k = j\Omega + \omega_{p,k}$ using (35). (a) First BW mode; (b) first FW mode; (c) symmetric mode; (d) second yaw mode; and (e) second tilt mode.

Fig. 2 shows the normalized modal amplitudes as function of rotor speed, where $A_{0,k}$, $A_{a_1,k}$, $A_{b_1,k}$, $A_{x,k}$, and $A_{y,k}$ are absolute values of the eigenvector components and $A_{\mathrm{BW},k}$ and $A_{\mathrm{FW},k}$ are obtained from (14) omitting subscripts $n = i = 1$. The tilt $A_{a_1,k}$ and yaw $A_{b_1,k}$ components represent rotor motion in the inertial frame, mutually exclusive to the whirling components $A_{\mathrm{BW},k}$ and $A_{\mathrm{FW},k}$ that represent rotor motion in the rotating frame. The first yaw mode (lowest frequency at standstill) develops into a mainly backward whirling mode for increasing rotor speed, whereas the first tilt mode develops into a mainly forward whirling mode. The second yaw and tilt modes with similar amounts of forward and backward whirling at all rotor speeds remain yaw and tilt modes. The symmetric mode has only the $A_{0,3}$ component and does not couple to the nacelle in this model with an isotropic rotor.

Fig. 3(a) shows the modal frequencies as function of rotor speed in a Campbell diagram. The frequency of the symmetric mode increases with the speed due to centrifugal stiffening, which derives from terms proportional to Ω^2 in the stiffness matrix (54c). The frequencies of the two lowest asymmetric modes split as they develop into backward and forward whirling modes, while the modal frequencies of the two highest asymmetric modes remain constant due to the small whirling amplitudes in these modes. Fig. 3(b) shows the damping ratios, which vary mainly due to the change in frequency.

3.1.2. Lyapunov–Floquet transformation approach

The periodic system equations (1) with (55) are integrated 10 times for linearly independent initial conditions $\boldsymbol{\varphi}(0) = \mathbf{I}$ to obtain the fundamental solution matrix (15) and monodromy matrix (20). Eigenvalue analysis of the monodromy matrix yields 10 distinct characteristic multipliers with linearly independent eigenvectors, whereby the system can be modally decomposed. The characteristic exponents (29) provide the principal frequencies $\omega_{p,k}$ in the interval $]-\Omega/2;\Omega/2]$ and damping σ_k using (32). The principal periodic mode shapes $\mathbf{u}_{p,k}$ are computed from (35) with $j_k = 0$.

Fig. 4(a) shows the amplitudes and phases of the Ω-harmonic components in the principal periodic mode shape of the first BW mode at the rated rotor speed $\Omega = 1.4\,\mathrm{rad/s}$. The modal frequency is determined from (38) using the dominating inertial component θ_z as $\omega_{\mathrm{p},1} + 2\Omega \approx 0.45\,\mathrm{Hz}$. The modal frequency of the first FW mode shape is similarly determined as $\omega_{\mathrm{p},2} + 4\Omega \approx 0.86\,\mathrm{Hz}$ from Fig. 4(b).

The direction of the rotor whirl can be determined from the phases of the individual blades. If the difference in phase between all blades is less than $\pi/3$, the harmonic is termed symmetric (S); otherwise it is termed backward whirling (BW) or forward whirling (FW) depending on the order of the phases of the individual blades (cf. Eq. (13)). The dominating rotor state variable harmonics in Figs. 4(a) and (b) thereby identify the first BW and first FW modes, respectively.

The phases in Fig. 4(c) show that the motion of the rotor state variables is symmetric, which means that they oscillate with the modal frequency. Thus, in the absence of any motion of the inertial state variables, the modal frequency is determined from the rotor component θ_1 as $\omega_{\mathrm{p},3} + 3\Omega \approx 0.75\,\mathrm{Hz}$.

The mode in Fig. 4(d) is termed the second yaw mode because θ_z is the most dominating inertial component, and because the BW and FW components are similar in magnitude, whereby the mode cannot be characterized as whirling. The modal frequency is determined from the θ_z component as $\omega_{\mathrm{p},4} + 7\Omega \approx 1.47\,\mathrm{Hz}$. Similarly, the mode in Fig. 4(e) is termed the second tilt mode from the dominating θ_x component and has modal frequency $\omega_{\mathrm{p},5} + 7\Omega \approx 1.59\,\mathrm{Hz}$.

The amplitudes of the Ω-harmonic components in the principal periodic mode shape are listed in Table 2. They are equal to the modal amplitudes obtained from the Coleman transformation approach shown in Fig. 2 for $\Omega = 1.4\,\mathrm{rad/s}$.

3.2. Anisotropic rotor

An anisotropy is applied to the blade stiffnesses as $G_1 = 1.1G_\mathrm{b}$ and $G_2 = G_3 = 0.95G_\mathrm{b}$ such that the mean stiffness is not changed. The modal frequencies determined from the Lyapunov–Floquet transformation approach change less than 0.5 percent compared to the isotropic case. Fig. 5(a) shows the amplitudes of the Ω-harmonic components in the principal periodic mode shape of the first BW mode. The mode shape now contains several Ω-harmonics, whereas there are at most three Ω-harmonics in the isotropic case. Similar results are obtained for the other asymmetric modes in Figs. 5(b, d, e).

Fig. 5(c) shows that the symmetric mode is not pure, i.e. there are whirling components in the mode shape. The stiffness anisotropy causes several Ω-harmonics in the symmetric mode shape for state variables in both the inertial and rotating

Table 2
For the isotropic rotor: modal frequencies and normalized amplitudes obtained from a Fourier transform of the periodic mode shape.

Mode	First BW	Sym.	First FW	Second tilt	Second yaw
f_k (Hz)	0.448	0.746	0.864	1.470	1.590
$A_{0,k}$ (f_k)	0.0000	1.0000	0.0000	0.0000	0.0000
$A_{\mathrm{BW},k}$ $(f_k + \Omega/2\pi)$	1.0000	0.0000	0.1605	0.6895	0.5228
$A_{\mathrm{FW},k}$ $(f_k - \Omega/2\pi)$	0.0002	0.0000	1.0000	0.6545	0.7748
$A_{x,k}$ (f_k)	0.1898	0.0000	0.3115	0.1310	1.0000
$A_{z,k}$ (f_k)	0.3449	0.0000	0.4888	1.0000	0.1181

Amplitudes $A_{0,k}$, $A_{\mathrm{BW},k}$, and $A_{\mathrm{FW},k}$ are obtained from θ_1 and $A_{x,k}$ and $A_{z,k}$ from θ_x and θ_z, respectively. In parentheses are noted the frequencies of the harmonic components, $\Omega/2\pi = 0.223\,\mathrm{Hz}$.

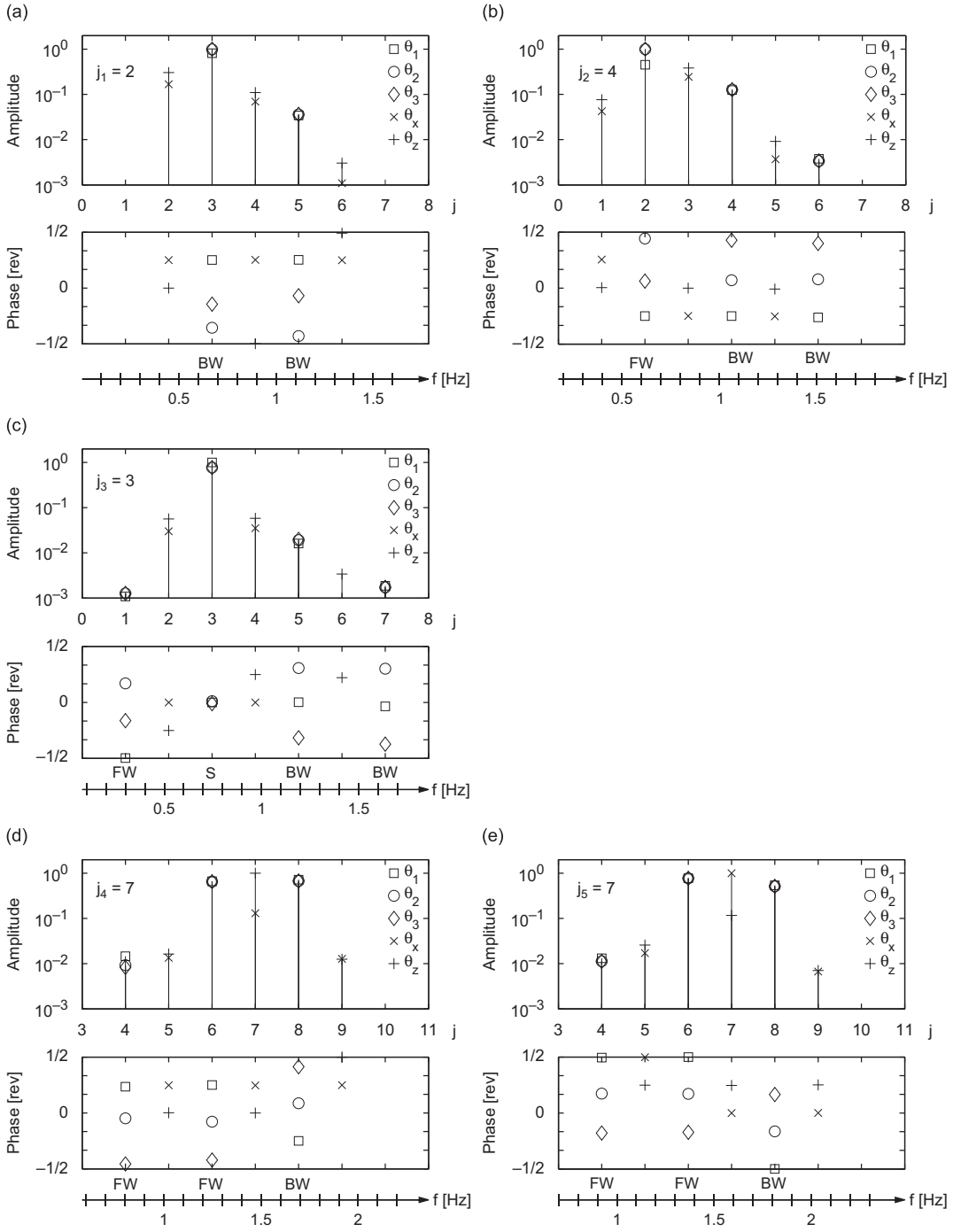

Fig. 5. Amplitudes (log. scale) and phases of harmonic components $\mathscr{U}_{p,j,ik}$ (36) in the principal periodic mode shape for the anisotropic rotor at $\Omega = 1.4\,\mathrm{rad/s}$. The bottom scale shows the frequencies in the response measured in the inertial system as $(j - j_k)\Omega + \omega_k = j\Omega + \omega_{p,k}$ using (35). (a) First BW mode; (b) first FW mode; (c) symmetric mode; (d) second yaw mode; and (e) second tilt mode.

frames, unlike the isotropic case involving only one harmonic in the rotor state variables. The symmetric mode has BW rotor components at even multiples of Ω above the symmetric rotor harmonic (the difference between the symmetric and the BW harmonics is an even number) and FW rotor components at even multiples of Ω below it.

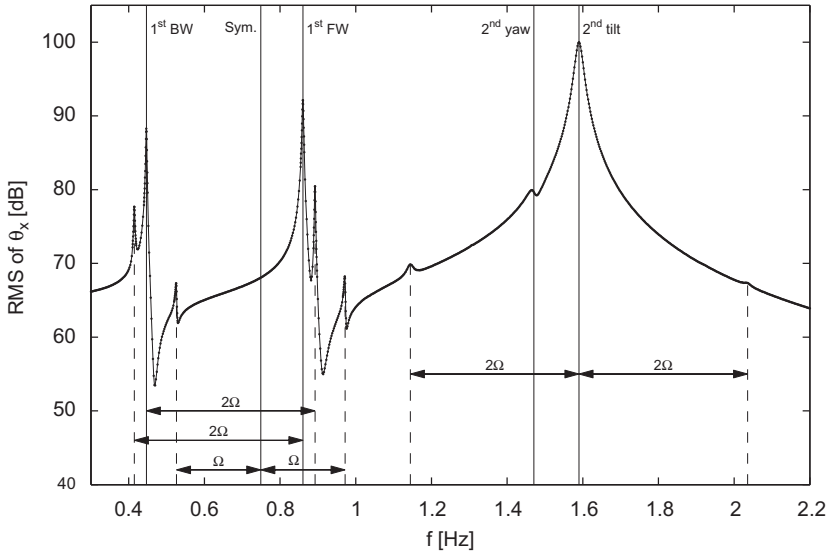

Fig. 6. RMS values of the steady-state nacelle tilt response θ_x (containing multiple harmonics) due to a harmonic excitation on the same degree of freedom for the anisotropic rotor and $\Omega = 1.4\,\mathrm{rad/s} = 0.223\,\mathrm{Hz}$.

The asymmetric mode shapes in Figs. 5(a, b, d, e) have BW and FW rotor components next to the dominating inertial component as in the isotropic case (cf. Eq. (13)). Additionally, the anisotropy creates BW rotor components at odd multiples of Ω above the dominating inertial component and FW rotor components at odd multiples of Ω below it. For all modes the inertial components appear between the whirling rotor components with an interval of 2Ω.

To study the effect of the additional harmonic components in the periodic mode shapes of the anisotropic rotor, the steady-state tilt response θ_x due to a harmonic excitation on θ_x is computed for a range of frequencies by a brute force approach using time integrations until a steady-state is reached for each excitation frequency. Steady state is here defined as the case where the frequency spectra of the response in two successive time intervals of 64 excitation periods are similar, with a maximum relative difference of 1 percent between the frequency components that have amplitudes larger than 0.1 percent of the maximum amplitude. These steady states may contain multiple harmonics, and the response is therefore represented by the rms value taken over the 64 excitation periods.

Fig. 6 shows peaks in the response at the modal frequencies denoted by the solid lines, except for the symmetric mode, due to the asymmetry of the excitation. The first smaller peak at $f_2 - 2\Omega = 0.41\,\mathrm{Hz}$ matches the harmonic at 2Ω below the dominating harmonic component of θ_x in the mode shape of the first FW mode in Fig. 5(b). Likewise, the peak at $f_1 + 2\Omega = 0.89\,\mathrm{Hz}$ is 2Ω above the frequency of the dominating harmonic of θ_x in the first BW mode shape in Fig. 5(a). The peaks around the symmetric modal frequency at $f_3 - \Omega = 0.53\,\mathrm{Hz}$ and $f_3 + \Omega = 0.97\,\mathrm{Hz}$ correspond respectively to the harmonics of θ_x at $\mp\Omega$ around the dominating rotor harmonic in Fig. 5(c). The two peaks at $f_5 - 2\Omega = 1.14\,\mathrm{Hz}$ and $f_5 + 2\Omega = 2.04\,\mathrm{Hz}$ correspond respectively to the harmonics of θ_x at $\mp 2\Omega$ around the dominating harmonic of θ_x in the second tilt mode shape in Fig. 5(d). The response has a small peak at the second yaw modal frequency because θ_x motion is involved only slightly in this mode, as seen by the amplitude of θ_x being much smaller than that of θ_z in the dominating harmonic in Fig. 5(e). This forced response analysis confirms the validity of predicting important aspects of the response by using the modal frequencies and periodic mode shapes. The obtained insight about Ω-harmonics in the periodic mode shape and their relation to the modal characteristics (symmetric or whirling rotor modes) can be used to understand frequency spectra and identify modes in measured or simulated time series of design determining loads.

4. Conclusion

In this paper, two methods for modally analyzing structures with bladed rotors are considered: the Coleman transformation approach and the Lyapunov–Floquet (L–F) transformation approach. The Coleman transformation is a special case of the L–F transformation for an isotropic rotor. The Coleman approach transforms rotor state variables into the inertial frame of reference and makes the system equations of structures with an isotropic rotor time-invariant, enabling eigenvalue analysis. The L–F approach is applicable to any periodic system but introduces an indeterminacy on the system frequencies and the transformation yielding a time-invariant system. Based on the similarity of the Coleman and the L–F approaches, the modal frequencies in the L–F approach are chosen such that the periodic mode shapes become as constant as possible for inertial state variables. In the example with a three-bladed wind turbine with an isotropic rotor the modal frequencies obtained using both approaches are identical. When introducing a rotor anisotropy to the blade stiffnesses,

meaningful modal frequencies are still obtained. However, state variables in the periodic mode shape, both in the rotor and in the inertial frame, now contain multiple harmonics that lead to multiple resonance frequencies for a single mode.

Acknowledgment

This work has been partially supported by the Danish Ministry of Science, Technology and Innovation through the Industrial PhD programme.

Appendix A

The equations of motion of a structure with a bladed rotor linearized about a steady state can be written in second-order form as

$$\mathbf{M}(t)\ddot{\mathbf{y}} + \mathbf{C}(t)\dot{\mathbf{y}} + \mathbf{K}(t)\mathbf{y} = \mathbf{0} \tag{42}$$

where $\mathbf{y}$ contains the generalized coordinates of the system, and the matrices $\mathbf{M}$, $\mathbf{C}$, and $\mathbf{K}$ are the periodic mass, gyroscopic/damping, and stiffness matrices, respectively. For an isotropic rotor, these periodic matrices of the second-order equations can all be written in a generic form as

$$\mathbf{G}(t) = \begin{bmatrix} \mathbf{G}_\mathrm{b} & \mathbf{G}_{bb,1} & \mathbf{G}_{bb,2} & \cdots & \mathbf{G}_{bb,2} & \mathbf{G}_{bb,1} & \mathbf{G}_{bs,1}(t) \\ \mathbf{G}_{bb,1} & \mathbf{G}_\mathrm{b} & \mathbf{G}_{bb,1} & \cdots & \mathbf{G}_{bb,3} & \mathbf{G}_{bb,2} & \mathbf{G}_{bs,2}(t) \\ \mathbf{G}_{bb,2} & \mathbf{G}_{bb,1} & \mathbf{G}_\mathrm{b} & \cdots & \mathbf{G}_{bb,4} & \mathbf{G}_{bb,3} & \mathbf{G}_{bs,3}(t) \\ \vdots & \vdots & \vdots & \ddots & \vdots & \vdots & \vdots \\ \mathbf{G}_{bb,2} & \mathbf{G}_{bb,3} & \mathbf{G}_{bb,4} & \cdots & \mathbf{G}_\mathrm{b} & \mathbf{G}_{bb,1} & \mathbf{G}_{bs,B-1}(t) \\ \mathbf{G}_{bb,1} & \mathbf{G}_{bb,2} & \mathbf{G}_{bb,3} & \cdots & \mathbf{G}_{bb,1} & \mathbf{G}_\mathrm{b} & \mathbf{G}_{bs,B}(t) \\ \mathbf{G}_{sb,1}(t) & \mathbf{G}_{sb,2}(t) & \mathbf{G}_{sb,3}(t) & \cdots & \mathbf{G}_{sb,B-1} & \mathbf{G}_{sb,B} & \mathbf{G}_\mathrm{s} \end{bmatrix} \tag{43}$$

where $\mathbf{G}_\mathrm{b}$ and $\mathbf{G}_\mathrm{s}$ are constant matrices describing the internal forces in the individual blades and the support and

$$\begin{aligned} \mathbf{G}_{sb,i}(t) &= \mathbf{G}^c_{\mathrm{sb}} \cos\psi_i + \mathbf{G}^s_{\mathrm{sb}} \sin\psi_i \\ \mathbf{G}_{bs,i}(t) &= \mathbf{G}^c_{\mathrm{bs}} \cos\psi_i + \mathbf{G}^s_{\mathrm{bs}} \sin\psi_i \end{aligned} \tag{44}$$

where $\mathbf{G}^s_{\mathrm{bs}}$, $\mathbf{G}^c_{\mathrm{bs}}$, $\mathbf{G}^s_{\mathrm{sb}}$, and $\mathbf{G}^c_{\mathrm{sb}}$ are constant matrices describing the coupling forces between blades of the rotor and its support. The constant matrices $\mathbf{G}_{bb,i}$ describe the coupling forces between blades j and $j+i$.

A.1. Coleman transformation of first-order state space equations

The Coleman transformation of state variables (3) implies that the generalized coordinates and velocities are transformed as

$$\mathbf{y} = \mathbf{B}_2\mathbf{z}_2 \quad \text{and} \quad \dot{\mathbf{y}} = \mathbf{B}_2\tilde{\mathbf{z}}_2 \tag{45}$$

where the Coleman transformation matrix $\mathbf{B}_2$ is given by (3) with half sized $\mathbf{I}_{N_\mathrm{b}}$ and $\mathbf{I}_{N_\mathrm{s}}$ corresponding to the number of generalized coordinates, and not state variables. The vector $\tilde{\mathbf{z}}_2$ represents the Coleman transformed generalized velocities, which are related to the time derivatives of the Coleman transformed generalized coordinates as

$$\tilde{\mathbf{z}}_2 = \bar{\omega}_2\mathbf{z}_2 + \dot{\mathbf{z}}_2 \tag{46}$$

where $\bar{\omega}_2$ is the constant matrix relating the Coleman transformation matrix and its derivative [23] as

$$\dot{\mathbf{B}}_2(t) = \mathbf{B}_2(t)\bar{\omega}_2 \tag{47}$$

Using that $\ddot{\mathbf{y}} = \mathbf{B}_2\bar{\omega}_2\tilde{\mathbf{z}}_2 + \mathbf{B}_2\dot{\tilde{\mathbf{z}}}_2$ and (46), the Coleman transformation of the second-order equations (42) becomes

$$\mathbf{M}_\mathrm{B}\dot{\tilde{\mathbf{z}}}_2 + \mathbf{M}_\mathrm{B}\bar{\omega}_2\tilde{\mathbf{z}}_2 + \mathbf{C}_\mathrm{B}\tilde{\mathbf{z}}_2 + \mathbf{K}_\mathrm{B}\mathbf{z}_2 = \mathbf{0} \tag{48}$$

where $\mathbf{M}_\mathrm{B} = \mathbf{B}_2^{-1}\mathbf{M}\mathbf{B}_2$, $\mathbf{C}_\mathrm{B} = \mathbf{B}_2^{-1}\mathbf{C}\mathbf{B}_2$, and $\mathbf{K}_\mathrm{B} = \mathbf{B}_2^{-1}\mathbf{K}\mathbf{B}_2$ are Coleman transformed system matrices.

Eqs. (46) and (48) can be rewritten in matrix form as

$$\begin{Bmatrix} \dot{\mathbf{z}}_2 \\ \dot{\tilde{\mathbf{z}}}_2 \end{Bmatrix} = \begin{bmatrix} -\bar{\omega}_2 & \mathbf{I} \\ -\mathbf{M}_\mathrm{B}^{-1}\mathbf{K}_\mathrm{B} & -\mathbf{M}_\mathrm{B}^{-1}\mathbf{C}_\mathrm{B} - \bar{\omega}_2 \end{bmatrix} \begin{Bmatrix} \mathbf{z}_2 \\ \tilde{\mathbf{z}}_2 \end{Bmatrix} \tag{49}$$

where $\{\mathbf{z}_2^\mathrm{T}, \tilde{\mathbf{z}}_2^\mathrm{T}\}$ contains the multi-blade state variables and original support state variables.

To use the Coleman transformation given by (3), this multi-blade state vector and the original state vector containing the general coordinates $\mathbf{y}$ and velocities $\dot{\mathbf{y}}$ must be permuted as

$$\mathbf{x} = \mathbf{P}_{\mathrm{x}} \begin{Bmatrix} \mathbf{y} \\ \dot{\mathbf{y}} \end{Bmatrix}, \quad \mathbf{z} = \mathbf{P}_{\mathrm{x}} \begin{Bmatrix} \mathbf{z}_2 \\ \dot{\mathbf{z}}_2 \end{Bmatrix} \tag{50}$$

where the permutation matrix $\mathbf{P}_{\mathrm{x}}$ orders the state variables in $\mathbf{x}$ as given by (2). The Coleman transformed system matrix (6) thereby becomes

$$\mathbf{A}_{\mathrm{B}} = \mathbf{P}_{\mathrm{x}} \begin{bmatrix} -\tilde{\boldsymbol{\omega}}_2 & \mathbf{I} \\ -\mathbf{M}_{\mathrm{B}}^{-1}\mathbf{K}_{\mathrm{B}} & -\mathbf{M}_{\mathrm{B}}^{-1}\mathbf{C}_{\mathrm{B}} - \tilde{\boldsymbol{\omega}}_2 \end{bmatrix} \mathbf{P}_{\mathrm{x}}^{\mathrm{T}} \tag{51}$$

where the matrices $\mathbf{M}_{\mathrm{B}}$, $\mathbf{C}_{\mathrm{B}}$, and $\mathbf{K}_{\mathrm{B}}$ are time-invariant for isotropic rotors, as seen by derivation of the Coleman transformation of the generic matrix (43) after substantial algebraic manipulation using the trigonometric addition formulas and identities for sums of harmonics of evenly spaced angles [16]:

$$\mathbf{G}_{\mathrm{B}} = \mathbf{B}_2^{-1}\mathbf{G}\mathbf{B}_2 = \begin{bmatrix} \mathbf{G}_{\mathrm{B},0} & \mathbf{0} & \mathbf{0} & \mathbf{0} & \mathbf{0} & \cdots & \mathbf{0} & \mathbf{0} & \mathbf{0} & \mathbf{0} \\ \mathbf{0} & \mathbf{G}_{\mathrm{B},1} & \mathbf{0} & \mathbf{0} & \mathbf{0} & \cdots & \mathbf{0} & \mathbf{0} & \mathbf{0} & \mathbf{G}_{\mathrm{bs}}^{c} \\ \mathbf{0} & \mathbf{0} & \mathbf{G}_{\mathrm{B},1} & \mathbf{0} & \mathbf{0} & \cdots & \mathbf{0} & \mathbf{0} & \mathbf{0} & \mathbf{G}_{\mathrm{bs}}^{s} \\ \mathbf{0} & \mathbf{0} & \mathbf{0} & \mathbf{G}_{\mathrm{B},2} & \mathbf{0} & \cdots & \mathbf{0} & \mathbf{0} & \mathbf{0} & \mathbf{0} \\ \mathbf{0} & \mathbf{0} & \mathbf{0} & \mathbf{0} & \mathbf{G}_{\mathrm{B},2} & \cdots & \mathbf{0} & \mathbf{0} & \mathbf{0} & \mathbf{0} \\ \vdots & \vdots & \vdots & \vdots & \vdots & \ddots & \vdots & \vdots & \vdots & \vdots \\ \mathbf{0} & \mathbf{0} & \mathbf{0} & \mathbf{0} & \mathbf{0} & \cdots & \mathbf{G}_{\mathrm{B},\tilde{B}} & \mathbf{0} & \mathbf{0} & \mathbf{0} \\ \mathbf{0} & \mathbf{0} & \mathbf{0} & \mathbf{0} & \mathbf{0} & \cdots & \mathbf{0} & \mathbf{G}_{\mathrm{B},\tilde{B}} & \mathbf{0} & \mathbf{0} \\ \mathbf{0} & \mathbf{0} & \mathbf{0} & \mathbf{0} & \mathbf{0} & \cdots & \mathbf{0} & \mathbf{0} & \mathbf{G}_{\mathrm{B},B/2} & \mathbf{0} \\ \mathbf{0} & \frac{B}{2}\mathbf{G}_{\mathrm{sb}}^{c} & \frac{B}{2}\mathbf{G}_{\mathrm{sb}}^{s} & \mathbf{0} & \mathbf{0} & \cdots & \mathbf{0} & \mathbf{0} & \mathbf{0} & \mathbf{G}_{\mathrm{s}} \end{bmatrix} \tag{52}$$

where the first B diagonal entries are defined by

$$\mathbf{G}_{\mathrm{B},i} = \mathbf{G}_{\mathrm{b}} + \sum_{n=1}^{\tilde{B}} 2\cos(2\pi i n/B)\mathbf{G}_{\mathrm{bb},n} + (-1)^i \mathbf{G}_{\mathrm{bb},B/2} \tag{53}$$

with $i = 0, 1, \ldots, \tilde{B}$ for B odd and $i = 0, 1, \ldots, \tilde{B}, B/2$ for B even.

A.2. Second-order system matrices of wind turbine with three flap-hinged blades

The mass matrix $\mathbf{M}$, gyroscopic/damping matrix $\mathbf{C}$, and stiffness matrix $\mathbf{K}$ for the wind turbine with flap-hinged blades in Fig. 1 are given by

$$\mathbf{M}(t) = \begin{bmatrix} J_{\mathrm{b}} & 0 & 0 & J_{\mathrm{b}}\cos\psi_1 & -J_{\mathrm{b}}\sin\psi_1 \\ 0 & J_{\mathrm{b}} & 0 & J_{\mathrm{b}}\cos\psi_2 & -J_{\mathrm{b}}\sin\psi_2 \\ 0 & 0 & J_{\mathrm{b}} & J_{\mathrm{b}}\cos\psi_3 & -J_{\mathrm{b}}\sin\psi_3 \\ J_{\mathrm{b}}\cos\psi_1 & J_{\mathrm{b}}\cos\psi_2 & J_{\mathrm{b}}\cos\psi_3 & J_x + \frac{3}{2}J_{\mathrm{b}} + J_0 & 0 \\ -J_{\mathrm{b}}\sin\psi_1 & -J_{\mathrm{b}}\sin\psi_2 & -J_{\mathrm{b}}\sin\psi_3 & 0 & J_z + \frac{3}{2}J_{\mathrm{b}} + J_0 \end{bmatrix} \tag{54a}$$

$$\mathbf{C}(t) = \begin{bmatrix} c_1 & 0 & 0 & -2\Omega J_{\mathrm{b}}\sin\psi_1 & -2\Omega J_{\mathrm{b}}\cos\psi_1 \\ 0 & c_2 & 0 & -2\Omega J_{\mathrm{b}}\sin\psi_2 & -2\Omega J_{\mathrm{b}}\cos\psi_2 \\ 0 & 0 & c_3 & -2\Omega J_{\mathrm{b}}\sin\psi_3 & -2\Omega J_{\mathrm{b}}\cos\psi_3 \\ 0 & 0 & 0 & c_x & 3\Omega J_{\mathrm{b}} \\ 0 & 0 & 0 & 3\Omega J_{\mathrm{b}} & c_z \end{bmatrix} \tag{54b}$$

$$\mathbf{K}(t) = \begin{bmatrix} G_1 + \Omega^2 J_{\mathrm{b}} & 0 & 0 & 0 & 0 \\ 0 & G_2 + \Omega^2 J_{\mathrm{b}} & 0 & 0 & 0 \\ 0 & 0 & G_3 + \Omega^2 J_{\mathrm{b}} & 0 & 0 \\ \Omega^2 J_{\mathrm{b}}\cos\psi_1 & \Omega^2 J_{\mathrm{b}}\cos\psi_2 & \Omega^2 J_{\mathrm{b}}\cos\psi_3 & G_x & 0 \\ -\Omega^2 J_{\mathrm{b}}\sin\psi_1 & -\Omega^2 J_{\mathrm{b}}\sin\psi_2 & -\Omega^2 J_{\mathrm{b}}\sin\psi_3 & 0 & G_z \end{bmatrix} \tag{54c}$$

where $J_0 = 3m_b L_s^2$ and $\psi_j = \Omega t + 2\pi(j-1)/3$. The periodic system matrix of the first-order equations (1) can be derived from

$$\mathbf{A}(t) = \mathbf{P}_x \begin{bmatrix} \mathbf{0} & \mathbf{I} \\ -\mathbf{M}^{-1}(t)\mathbf{K}(t) & -\mathbf{M}^{-1}(t)\mathbf{C}(t) \end{bmatrix} \mathbf{P}_x^T \tag{55}$$

Extracting the generic form of these system matrices, the Coleman transformed system matrix of the first-order equations can be derived from (51) and (52) as

$$\mathbf{A}_B = \begin{bmatrix} 0 & 1 & 0 & 0 & & \\ -\frac{G_b}{J_b} - \Omega^2 & -\frac{c_b}{J_b} & 0 & 0 & & \\ 0 & 0 & 0 & 1 & & \\ 0 & 0 & -\frac{G_b}{J_b} - \frac{3G_b}{2J_0+2J_x} - \Omega^2 & -c_b\left(\frac{3}{2J_0+2J_x} + \frac{1}{J_b}\right) & & \\ 0 & 0 & \Omega & 0 & & \\ 0 & 0 & 0 & \Omega & & \\ 0 & 0 & 0 & 0 & & \\ 0 & 0 & \frac{3G_b}{2J_0+2J_x} & \frac{3c_b}{2J_0+2J_x} & & \\ 0 & 0 & 0 & 0 & & \\ 0 & 0 & 0 & 0 & & \end{bmatrix}$$

$$\begin{bmatrix} 0 & 0 & 0 & 0 & 0 & 0 \\ 0 & 0 & 0 & 0 & 0 & 0 \\ -\Omega & 0 & 0 & 0 & 0 & 0 \\ 0 & -\Omega & \frac{G_x}{J_0+J_x} & \frac{c_x}{J_0+J_x} & 0 & 2\Omega \\ 0 & 1 & 0 & 0 & 0 & 0 \\ -\frac{G_b}{J_b} - \frac{3G_b}{2J_0+2J_z} - \Omega^2 & -c_b\left(\frac{3}{2J_0+2J_z} + \frac{1}{J_b}\right) & 0 & 2\Omega & -\frac{G_z}{J_0+J_z} & -\frac{c_z}{J_0+J_z} \\ 0 & 0 & 0 & 1 & 0 & 0 \\ 0 & 0 & -\frac{G_x}{J_0+J_x} & -\frac{c_x}{J_0+J_x} & 0 & 0 \\ 0 & 0 & 0 & 0 & 0 & 1 \\ -\frac{3G_b}{2J_0+2J_z} & -\frac{3c_b}{2J_0+2J_z} & 0 & 0 & -\frac{G_z}{J_0+J_z} & -\frac{c_z}{J_0+J_z} \end{bmatrix} \tag{56}$$

References

[1] R.P. Coleman, Theory of self-excited mechanical oscillations of hinged rotor blades, Technical Report NACA-WR-L-308, Langley Research Center, 1943, available from ⟨ntrs.nasa.gov⟩.
[2] A.M. Feingold, Theory of mechanical oscillations of rotors with two hinged blades, Technical Report NACA-WR-L-312, Langley Research Center, 1943, available from ⟨ntrs.nasa.gov⟩.
[3] R.P. Coleman, A.M. Feingold, Theory of ground vibrations of a two-blade helicopter rotor on anisotropic flexible supports, Technical Report NACA-TN-1184, Langley Research Center, 1947, available from ⟨ntrs.nasa.gov⟩.
[4] G. Floquet, Sur les équations différentielles linéaires à coefficients périodiques (on linear differential equations with periodic coefficients), *Annales scientifiques de l'École Normale Supérieure* 2 (12) (1883) 47–88.
[5] E.T. Whittaker, G.N. Watson, *A Course of Modern Analysis*, fourth ed., Cambridge University Press, London, 1927.
[6] L. Meirovitch, *Methods of Analytical Dynamics*, McGraw-Hill, New York, 1970.
[7] K.G. Lindh, P.W. Likins, Infinite determinant methods for stability analysis of periodic-coefficient differential equations, *AIAA Journal* 8 (4) (1970) 680–686.
[8] O.J. Lowis, The stability of rotor blade flapping motion at high tip speed ratios, Technical Report R. & M. No. 3544, Aeronautical Research Council, 1963, available from ⟨aerade.cranfield.ac.uk⟩.
[9] D.A. Peters, K.H. Hohenemser, Application of the Floquet transition matrix to problems of lifting rotor stability, *Journal of the American Helicopter Society* 16 (2) (1971) 25–33.
[10] P. Friedmann, C.E. Hammond, T.-H. Woo, Efficient numerical treatment of periodic systems with application to stability problems, *International Journal for Numerical Methods in Engineering* 11 (1977) 1117–1136.
[11] S.C. Sinha, R. Pandiyan, Analysis of quasilinear dynamical systems with periodic coefficients via Liapunov–Floquet transformation, *International Journal of Nonlinear Mechanics* 29 (5) (1994) 687–702.
[12] D.A. Peters, Fast Floquet theory and trim for multi-bladed rotorcraft, *Journal of the American Helicopter Society* 39 (4) (1994) 82–89.

[13] O.A. Bauchau, Y.G. Nikishkov, An implicit Floquet analysis for rotorcraft stability evaluation, *Journal of the American Helicopter Society* 46 (3) (2001) 200–209.
[14] G. Quaranta, P. Mantegazza, P. Masarati, Assessing the local stability of periodic motions for large multibody non-linear systems using proper orthogonal decomposition, *Journal of Sound and Vibration* 271 (2004) 1015–1038.
[15] O.A. Bauchau, J. Wang, Efficient and robust approaches to the stability analysis of large multibody systems, *Journal of Computational and Nonlinear Dynamics* 3 (2008).
[16] W. Johnson, *Helicopter Theory*, Princeton University Press, New Jersey, 1980.
[17] J. Dugundji, J.H. Wendell, Some analysis methods for rotating systems with periodic coefficients, *AIAA Journal* 21 (6) (1983) 890–897.
[18] J.H. Milgram, I. Chopra, Air resonance of hingeless rotor helicopters in trimmed forward flight, *Journal of the American Helicopter Society* 39 (4) (1994) 46–58.
[19] D. Lee, D.H. Hodges, M.J. Patil, Multi-flexible-body dynamic analysis of horizontal axis wind turbines, *Wind Energy* 5 (4) (2002) 281–300.
[20] J. Nagabhushanam, G.H. Gaonkar, Automatic identification of modal damping from Floquet analysis, *Journal of the American Helicopter Society* 40 (2) (1995) 39–42.
[21] V.A. Yakubovich, V.M. Starzhinskii, *Linear Differential Equations with Periodic Coefficients*, Wiley, New York, 1975.
[22] M.H. Hansen, Aeroelastic instability problems for wind turbines, *Wind Energy* 10 (2007) 551–577.
[23] M.H. Hansen, Improved modal dynamics of wind turbines to avoid stall-induced vibrations, *Wind Energy* 6 (2003) 179–195.
[24] A.H. Nayfeh, B. Balachandran, *Applied Nonlinear Dynamics*, Wiley, New York, 1995.
[25] A.M. Lyapunov, *The General Problem of Stability of Motion*, Taylor & Francis Ltd., London, 1992.
[26] E.A. Coddington, N. Levinson, *Theory of Ordinary Differential Equations*, McGraw-Hill, New York, 1955.
[27] P. Montagnier, C.C. Paige, R.J. Spiteri, Real Floquet factors of linear time-periodic systems, *System & Control Letters* 50 (2003) 251–262.
[28] F.R. Gantmacher, *The Theory of Matrices*, Vol. 1, Chelsea Publishing Company, New York, 1959.
[29] W.J. Culver, On the existence and uniqueness of the real logarithm of a matrix, *Proceedings of the American Mathematical Society* 17 (1966) 1146–1151.

P2

Modal Dynamics of Wind Turbines with Anisotropic Rotors

In *Proceedings of 47th AIAA Aerospace Sciences Meeting*, Orlando FL, USA, 2009.

Errata:

p. 1: 'period of oscillation' should be 'period of rotation'

p. 14: Ref. [2] is listed incorrectly, instead it should read
M.H. Hansen. Aeroelastic stability analysis of wind turbines using an eigenvalue approach. *Wind Energy*, 7:133–143, 2004.

47th AIAA Aerospace Sciences Meeting Including The New Horizons Forum and Aerospace Exposition
5 - 8 January 2009, Orlando, Florida

AIAA 2009-1036

Modal Dynamics of Wind Turbines with Anisotropic Rotors

Peter F. Skjoldan*

Siemens Wind Power A/S, Taastrup, DK-2630, Denmark.

Equations of motion for wind turbines contain periodic terms due to the rotor rotation. For a three-bladed isotropic rotor the traditional approach for conducting modal analysis is to use the Coleman transformation to yield a time-invariant system. Eigenvalue analysis of this system produces frequencies, damping and mode shapes. When the rotor is anisotropic, e.g. due to a difference in blade stiffness, the periodic terms are not completely removed by the Coleman transformation and an eigenvalue problem cannot be set up in this way. Modal analysis can be performed using Floquet analysis or using Hill's method where the equation system is expanded to obtain eigenvalues and -vectors of a selected number of terms in a Fourier series. The modal solutions for the isotropic rotor contain harmonic terms of the eigenfrequency and terms with frequencies of the rotor speed plus and minus the eigenfrequency. Applying an anisotropy on the rotor creates additional harmonic terms in the solutions. Through a numerical example of a simple structural model of a wind turbine the modal dynamics are illustrated using the different methods.

I. Introduction

This paper deals with some of the solution methods for the eigenvalue problem of a rotating three-bladed wind turbine with an anisotropic rotor and the resulting modal dynamics.

Modal analysis of wind turbines is used extensively in aeroelastic stability tools. These tools set up an eigenvalue problem for the equations of motion to give frequencies, damping ratios and mode shapes.

Equations of motion for a rotating wind turbine contain periodic coefficients due to the rotor rotation. The periodic terms can be eliminated by use of the Coleman transformation[1] if the rotor is isotropic. This is the approach used by most recent wind turbine stability tools.[2–4] Others[5–7] use Floquet analysis to solve the equations with periodic coefficients. This method has been used extensively on helicopters[8] and relies on numerical simulation through one period of oscillation for a number of different initial conditions equal to the number of states of the system. It is applicable to an anisotropic rotor. The use of the Coleman transformation and Floquet analysis is reviewed by Dugundji and Wendell[9] and by Johnson.[10] A method which has not been used in wind turbine stability tools is Hill's method.[11,12] It expands the equation system to obtain eigenvalues and -vectors of a selected number of terms in a Fourier series. This solution converges for an increasing number of terms included.

The periodic coefficients in the equations of motion cause the mode shapes to vary in time periodically, which can be interpreted as the motion consisting of different harmonic components. For an isotropic rotor these harmonic components give a symmetric motion and forward and backward whirling motion[13] of the blades. The frequency of the symmetric motion is the eigenfrequency, whereas the forward and backward whirling motions oscillate with the eigenfrequency minus and plus the rotor speed, respectively.

In this paper modal analysis is performed on an anisotropic rotor revealing harmonic components in addition to those present in the isotropic case. These components have frequencies of multiples of two times the rotor speed plus and minus the frequencies present in the isotropic case.

The next section describes how the equations of motion are set up for a wind turbine. Then the methods of the Coleman transformation, Floquet analysis and Hill's method are reviewed. An example of the methods

*Ph.D. student, Loads, Aerodynamics and Control, E R WP EN 432, Dybendalsvænget 3. Ph.D. study in cooperation with Risø DTU National Laboratory for Sustainable Energy, Frederiksborgvej 399, P.O.B. 49, DK-4000 Roskilde, Denmark.

applied to a simple model shows the differences in modal properties between an isotropic and an anisotropic rotor, where the anisotropy is caused by a difference in blade stiffness.

II. Wind turbine structural dynamics

The linearized equations of motion for a rotating wind turbine can be written as

$$\mathbf{M}(t)\ddot{\mathbf{y}}(t) + \mathbf{C}(t)\dot{\mathbf{y}}(t) + \mathbf{K}(t)\mathbf{y}(t) = \mathbf{0} \tag{1}$$

where $\mathbf{y}(t)$ are the degrees of freedom (DOF) measured about an equilibrium state, $\mathbf{M}(t)$ is the mass matrix, $\mathbf{C}(t)$ is the combined gyroscopic and damping matrix, and $\mathbf{K}(t)$ is the stiffness matrix. The equilibrium state is defined by a constant mean rotor speed Ω at a specific operating point, but small variations in the rotor speed can be accommodated by one or several DOF describing the shaft rotation. The matrices are periodic with period $T = 2\pi/\Omega$: $\mathbf{M}(t+T) = \mathbf{M}(t), \mathbf{C}(t+T) = \mathbf{C}(t), \mathbf{K}(t+T) = \mathbf{K}(t)$.

The equations of motion are of second order and Eq. (1) is therefore written in the first order standard form

$$\dot{\mathbf{x}}(t) = \tilde{\mathbf{A}}(t)\mathbf{x}(t) \tag{2}$$

where

$$\mathbf{x}(t) = \mathbf{P}\begin{Bmatrix}\mathbf{y}(t)\\ \dot{\mathbf{y}}(t)\end{Bmatrix} \tag{3}$$

$$\tilde{\mathbf{A}}(t) = \mathbf{P}\begin{bmatrix}\mathbf{0} & \mathbf{I}\\ -\mathbf{M}^{-1}(t)\mathbf{K}(t) & -\mathbf{M}^{-1}(t)\mathbf{C}(t)\end{bmatrix}\mathbf{P}^{\mathrm{T}} \tag{4}$$

$$\tilde{\mathbf{A}}(t+T) = \tilde{\mathbf{A}}(t) \tag{5}$$

and $\mathbf{P}$ is a permutation matrix that makes the position and velocity states belonging to a given DOF follow immediately after each other in the state vector $\mathbf{x}(t)$.[14] The size of the system matrix is $N \times N$, where $N/2$ is the number of DOF and N is the number of states of the system.

III. Isotropic rotor

An isotropic rotor allows for elimination of the periodic coefficients from the system matrix by use of the Coleman transformation. This transformation uses *multiblade coordinates* to describe the motion of the rotor as a whole in an inertial frame of reference instead of through coordinates belonging to the individual rotating blades.[10,13] The multiblade states $\mathbf{z}(t)$ are introduced by the transformation[13]

$$\mathbf{x}(t) = \mathbf{B}(t)\mathbf{z}(t)\,, \quad \mathbf{B}(t) = \begin{bmatrix}\mathbf{I}_{N_\mathrm{b}} & \mathbf{I}_{N_\mathrm{b}}\cos(\psi_1) & \mathbf{I}_{N_\mathrm{b}}\sin(\psi_1) & \mathbf{0}\\ \mathbf{I}_{N_\mathrm{b}} & \mathbf{I}_{N_\mathrm{b}}\cos(\psi_2) & \mathbf{I}_{N_\mathrm{b}}\sin(\psi_2) & \mathbf{0}\\ \mathbf{I}_{N_\mathrm{b}} & \mathbf{I}_{N_\mathrm{b}}\cos(\psi_3) & \mathbf{I}_{N_\mathrm{b}}\sin(\psi_3) & \mathbf{0}\\ \mathbf{0} & \mathbf{0} & \mathbf{0} & \mathbf{I}_{N_\mathrm{s}}\end{bmatrix} \tag{6}$$

where $\psi_j = \Omega t + 2\pi(j-1)/3$ is the mean azimuth angle to blade number $j = 1, 2, 3$. The number of states of each blade is N_b and the number of states measured in the inertial frame is N_s, such that $N = 3N_\mathrm{b} + N_\mathrm{s}$.

Insertion of Eq. (6) into Eq. (2) shows that the Coleman transformed system equation becomes

$$\dot{\mathbf{z}}(t) = \mathbf{A}(t)\mathbf{z}(t) \tag{7}$$

where

$$\mathbf{A}(t) = \mathbf{B}^{-1}(t)\tilde{\mathbf{A}}(t)\mathbf{B}(t) - \mathbf{B}^{-1}(t)\dot{\mathbf{B}}(t) \tag{8}$$

This transformed system matrix will be time-invariant if the three-bladed rotor is isotropic,[13,15] i.e., the blades are identical and modeled by identical states in their individual rotating frames. This important feature of the Coleman transformation of systems with isotropic three-bladed rotors enables the use of traditional eigenvalue analysis for modal decomposition of their dynamics. Thus, modal frequencies ω_k and

damping σ_k are obtained from the eigenvalues $\lambda_k = \sigma_k + \mathrm{i}\omega_k$ of $\mathbf{A}$. The motion is then described as a sum of modal solutions by solving Eq. (7) and transforming back to the physical coordinates using Eq. (6) as

$$\mathbf{x}(t) = \sum_{k=1}^{N} \mathbf{B}(t)\mathbf{v}_k e^{\lambda_k t} \tag{9}$$

The eigenvectors $\mathbf{v}_k$ of $\mathbf{A}$ are given in multiblade coordinates for the blade states and physical coordinates for the inertial states as

$$\mathbf{v}_k = \{a_{0,1} \quad \dots \quad a_{0,N_\mathrm{b}} \quad a_{1,1} \quad \dots \quad a_{1,N_\mathrm{b}} \quad b_{1,1} \quad \dots \quad b_{1,N_\mathrm{b}} \quad x_{\mathrm{s},1} \quad \dots \quad x_{\mathrm{s},N_\mathrm{s}}\}^\mathrm{T} \tag{10}$$

where $a_{0,i}$ describe the symmetric, $a_{1,i}$ the tilt, and $b_{1,i}$ the yaw motion of the rotor. The eigenvalues λ_k and eigenvectors $\mathbf{v}_k$ of dynamic modes are complex conjugate and thus act in pairs in Eq. (9) to give real modal solutions. When the terms in Eq. (9) are expanded,[13] it is realized that the motion is comprised of three harmonic components for state i of mode k on blade j given by

$$\begin{aligned} x_{ik}(t) = e^{\sigma_k t}\big(\quad & A_{0,ik}\cos(\omega_k t + \varphi_{0,ik}) \\ & + A_{\mathrm{BW},ik}\cos((\omega_k + \Omega)t + 2\pi(j-1)/3 + \varphi_{\mathrm{BW},ik}) \\ & + A_{\mathrm{FW},ik}\cos((\omega_k - \Omega)t - 2\pi(j-1)/3 + \varphi_{\mathrm{FW},ik})\ \big) q_k(0) \end{aligned} \tag{11}$$

where 0 denotes a symmetric motion, BW denotes a backward whirling motion and FW a forward whirling motion and $q_k(0)$ is the content of mode k in the initial conditions. The amplitudes are determined as

$$\begin{aligned} A_{0,ik} &= \sqrt{\left(\mathrm{Re}\left(a_{0,ik}\right)\right)^2 + \left(\mathrm{Im}\left(a_{0,ik}\right)\right)^2} \\ A_{\mathrm{BW},ik} &= \tfrac{1}{2}\sqrt{\left(\mathrm{Re}\left(a_{1,ik}\right) + \mathrm{Im}\left(b_{1,ik}\right)\right)^2 + \left(\mathrm{Re}\left(b_{1,ik}\right) - \mathrm{Im}\left(a_{1,ik}\right)\right)^2} \\ A_{\mathrm{FW},ik} &= \tfrac{1}{2}\sqrt{\left(\mathrm{Re}\left(a_{1,ik}\right) - \mathrm{Im}\left(b_{1,ik}\right)\right)^2 + \left(\mathrm{Re}\left(b_{1,ik}\right) + \mathrm{Im}\left(a_{1,ik}\right)\right)^2} \end{aligned} \tag{12}$$

and $\varphi_{0,ik}$, $\varphi_{\mathrm{BW},ik}$ and $\varphi_{\mathrm{FW},ik}$ are phases, also given by the eigenvector $\mathbf{v}_k$.[13]

IV. Anisotropic rotor

The periodic coefficients in the system matrix of an anisotropic rotor cannot be completely eliminated by the Coleman transformation, and the system in Eq. (7) becomes time-variant. One option for obtaining an eigenvalue problem is the Lyapunov-Floquet transformation,[14,16] another is the use of Hill's method. In both approaches the Coleman transformed system equations are used.

A. Floquet analysis

Floquet analysis yields the solution of a linear system of equations such as Eq. (7) directly without elimination of the periodic coefficients. Thus, it does not rely on any symmetry and can be applied to an anisotropic rotor. As there are many good references to Floquet theory[10,12,17,18] and its application, it is only briefly reviewed here following a recent approach of Skjoldan and Hansen.[14]

Numerical simulation of Eq. (7) with linearly independent initial conditions yields N linearly independent solutions. These solutions are collected as columns of an $N \times N$ matrix called the *fundamental matrix* of the system, given as

$$\boldsymbol{\varphi}(t) = \begin{bmatrix} \boldsymbol{\varphi}_1(t) & \boldsymbol{\varphi}_2(t) & \dots & \boldsymbol{\varphi}_N(t) \end{bmatrix} \tag{13}$$

with $\boldsymbol{\varphi}(0) = \mathbf{I}$. Any transient solution $\mathbf{z}(t)$ with initial conditions $\mathbf{z}(0)$ can now be written as a linear combination of the fundamental set of solutions as

$$\mathbf{z}(t) = \boldsymbol{\varphi}(t)\mathbf{z}(0) \tag{14}$$

The *monodromy matrix* is defined as

$$\mathbf{C} \equiv \boldsymbol{\varphi}^{-1}(0)\boldsymbol{\varphi}(T) = \boldsymbol{\varphi}(T) \tag{15}$$

and contains all information about the stability of the system.

The decomposition of the transient solution of Eq. (14) into components of modal motion is obtained by introduction of the *Lyapunov-Floquet transformation*

$$\mathbf{z}(t) = \mathbf{L}(t)\mathbf{z}_{\mathrm{LF}}(t) \tag{16}$$

where $\mathbf{z}_{\mathrm{LF}}(t)$ are new states of the system. By choosing $\mathbf{L}(t)$ as follows, the system in Eq. (7) with periodic coefficients is made time-invariant in states $\mathbf{z}_{\mathrm{LF}}(t)$:

$$\mathbf{L}(t) = \boldsymbol{\varphi}(t)e^{-\mathbf{R}t} \tag{17}$$

where

$$\mathbf{R} = \frac{1}{T}\ln(\mathbf{C}) \tag{18}$$

and $\mathbf{L}(t)$ can be shown to be periodic with period T. The solution in the transformed states $\mathbf{z}_{\mathrm{LF}}(t)$, when $\boldsymbol{\varphi}(t)$ is eliminated by use of Eq. (14) and Eq. (17), becomes

$$\mathbf{z}_{\mathrm{LF}}(t) = e^{\mathbf{R}t}\mathbf{z}(0) \tag{19}$$

To extract the modal properties, the time-invariant system matrix $\mathbf{R}$ is decomposed into

$$\mathbf{R} = \mathbf{V}\boldsymbol{\Lambda}\mathbf{V}^{-1} \tag{20}$$

where $\mathbf{V}$ contains the eigenvectors $\mathbf{v}_k$ as columns and $\boldsymbol{\Lambda}$ contains the eigenvalues λ_k in the diagonal, k being the index of the mode. Then, Eq. (19) can be decomposed into a sum of modal solutions transformed back to multiblade coordinates using Eq. (16) as

$$\mathbf{z}(t) = \sum_{k=1}^{N} \mathbf{r}_k(t)e^{\lambda_k t}q_k(0) \tag{21}$$

where $\mathbf{r}_k(t)$ are the multiblade coordinate periodic mode shapes determined using Eq. (17) and Eq. (20) as

$$\mathbf{r}_k(t) = \mathbf{L}(t)\mathbf{v}_k = \boldsymbol{\varphi}(t)\mathbf{v}_k e^{-\lambda_k t} \tag{22}$$

and $q_k(0)$ is the content of mode k in the initial conditions given by

$$\mathbf{q}(0) = \mathbf{V}^{-1}\mathbf{z}(0) \tag{23}$$

The solution described in physical coordinates is determined by inserting Eq. (21) into Eq. (6) as

$$\mathbf{x}(t) = \sum_{k=1}^{N} \mathbf{u}_k(t)e^{\lambda_k t}q_k(0) \tag{24}$$

where $\mathbf{u}_k(t)$ are the periodic mode shapes

$$\mathbf{u}_k(t) = \mathbf{B}(t)\boldsymbol{\varphi}(t)\mathbf{v}_k e^{-\lambda_k t} \tag{25}$$

The eigenvalues λ_k of $\mathbf{R}$ contain the frequency ω_k and damping σ_k as $\lambda_k = \sigma_k + \mathrm{i}\omega_k$. The eigenvalues are obtained from Eq. (18) as $\lambda_k = \ln(\rho_k)/T$ where ρ_k are the eigenvalues of the monodromy matrix. Because the complex logarithm has an infinite number of branches, the imaginary part of λ_k is undetermined to within an integer multiple of $2\pi/T$. Thus, the modal frequency is determined from the principal frequency $\omega_{\mathrm{p}\,k}$ by adding an integer multiple j_k of the rotor speed Ω:

$$\sigma_k = \frac{1}{T}\ln(|\rho_k|) \tag{26}$$

$$\omega_{\mathrm{p}\,k} = \frac{1}{T}\arg(\rho_k) \qquad \omega_{\mathrm{p}\,k} \in \,]-\tfrac{1}{2}\Omega;\tfrac{1}{2}\Omega] \tag{27}$$

$$\omega_k = \omega_{\mathrm{p}\,k} + j_k\Omega \qquad j_k \in \mathbb{Z} \tag{28}$$

The choice of modal frequency is discussed in section IV.C.

B. Hill's method

In the previous section, Floquet theory determined the form of the solution to the periodically time-varying system of Eq. (7). To avoid the numerical integration of the equations of motion, in this section a more analytical approach known as Hill's method is followed.[11,19]

The solution form from Floquet theory given by Eq. (21) for one mode inserted into Eq. (7) gives

$$\dot{\mathbf{r}}_k(t) = (\mathbf{A}(t) - \lambda_k \mathbf{I})\mathbf{r}_k(t) \tag{29}$$

As both the system matrix and the mode shapes are periodic with period $T = 2\pi/\Omega$ they can be written as Fourier series

$$\mathbf{A}(t) = \sum_{l=-\infty}^{\infty} \mathbf{A}_l e^{\mathrm{i}l\Omega t} \tag{30}$$

$$\mathbf{r}_k(t) = \sum_{j=-\infty}^{\infty} \mathbf{v}_{k,j} e^{\mathrm{i}j\Omega t} \tag{31}$$

where $\mathbf{A}_l$ and $\mathbf{v}_{k,j}$ are the coefficients with frequency $l\Omega$ and $j\Omega$ of the Fourier transforms of $\mathbf{A}(t)$ and $\mathbf{r}_k(t)$, respectively. These expansions are inserted into Eq. (29) which gives

$$\left(\sum_{j=-\infty}^{\infty} \sum_{l=-\infty}^{\infty} \mathbf{A}_l e^{\mathrm{i}(j+l)\Omega t} - \sum_{j=-\infty}^{\infty} (\lambda_k + \mathrm{i}j\Omega) e^{\mathrm{i}j\Omega t} \right) \mathbf{v}_{k,j} = \mathbf{0} \tag{32}$$

and the coefficients of equal harmonic terms are equated to yield an infinite number of equations written in a *hypermatrix* form as

$$(\hat{\mathbf{A}} - \lambda_{k,m}\mathbf{I})\hat{\mathbf{v}}_{k,m} = \mathbf{0} \tag{33}$$

where

$$\hat{\mathbf{A}} = \begin{bmatrix} \ddots & \vdots & & \vdots & \vdots & \vdots & & \vdots & \\ \cdots & \mathbf{A}_0 + \mathrm{i}n\Omega\mathbf{I} & \cdots & \mathbf{A}_{-n+1} & \mathbf{A}_{-n} & \mathbf{A}_{-n-1} & \cdots & \mathbf{A}_{-2n} & \cdots \\ & \vdots & \ddots & \vdots & \vdots & \vdots & & \vdots & \\ \cdots & \mathbf{A}_{n-1} & \cdots & \mathbf{A}_0 + \mathrm{i}\Omega\mathbf{I} & \mathbf{A}_{-1} & \mathbf{A}_{-2} & \cdots & \mathbf{A}_{-n-1} & \cdots \\ \cdots & \mathbf{A}_n & \cdots & \mathbf{A}_1 & \mathbf{A}_0 & \mathbf{A}_{-1} & \cdots & \mathbf{A}_{-n} & \cdots \\ \cdots & \mathbf{A}_{n+1} & \cdots & \mathbf{A}_2 & \mathbf{A}_1 & \mathbf{A}_0 - \mathrm{i}\Omega\mathbf{I} & \cdots & \mathbf{A}_{-n+1} & \cdots \\ & \vdots & & \vdots & \vdots & \vdots & \ddots & \vdots & \\ \cdots & \mathbf{A}_{2n} & \cdots & \mathbf{A}_{n+1} & \mathbf{A}_n & \mathbf{A}_{n-1} & \cdots & \mathbf{A}_0 - \mathrm{i}n\Omega\mathbf{I} & \cdots \\ & \vdots & & \vdots & \vdots & \vdots & & \vdots & \ddots \end{bmatrix}, \quad \hat{\mathbf{v}}_{k,m} = \begin{Bmatrix} \vdots \\ \mathbf{v}_{k,m,-n} \\ \vdots \\ \mathbf{v}_{k,m,-1} \\ \mathbf{v}_{k,m,0} \\ \mathbf{v}_{k,m,1} \\ \vdots \\ \mathbf{v}_{k,m,n} \\ \vdots \end{Bmatrix} \tag{34}$$

and the index m refers to one of the infinite number of eigenvalues and eigenvectors representing the physical mode with modal frequency λ_k. Because the size of $\hat{\mathbf{A}}$ is infinite, the same matrix is obtained by adding any integer multiple of $\mathrm{i}j\Omega\mathbf{I}$. Thus, $\hat{\mathbf{A}}$ has an infinite number of eigenvalues differing by integer multiples of $\mathrm{i}j\Omega$. These eigenvalues are written

$$\lambda_{k,m} = \lambda_k + \mathrm{i}m\Omega \tag{35}$$

where λ_k is the eigenvalue with the modal frequency as imaginary part, also called the *basis eigenvalue*.

The middle block equation of Eqs. (33) for the eigensolution with the basis eigenvalue $\lambda_{k,0} = \lambda_k$ is written as

$$\ldots + \mathbf{A}_1\mathbf{v}_{k,0,-1} + (\mathbf{A}_0 - \lambda_k\mathbf{I})\,\mathbf{v}_{k,0,0} + \mathbf{A}_{-1}\mathbf{v}_{k,0,1} + \ldots = \mathbf{0} \tag{36}$$

and the block equation m blocks above for the eigensolution with eigenvalue $\lambda_{k,m}$ using Eq. (35) is written as

$$\ldots + \mathbf{A}_1\mathbf{v}_{k,m,-m-1} + (\mathbf{A}_0 - \lambda_k\mathbf{I})\,\mathbf{v}_{k,m,-m} + \mathbf{A}_{-1}\mathbf{v}_{k,m,-m+1} + \ldots = \mathbf{0} \tag{37}$$

It is seen by comparison of these two equations that

$$\mathbf{v}_{k,m,j-m} = \mathbf{v}_{k,0,j} \tag{38}$$

which means that the eigenvector $\hat{\mathbf{v}}_{k,m}$ has the same Fourier components as the basis eigenvector $\hat{\mathbf{v}}_{k,0}$, but they are shifted $m\Omega$ downwards in frequency. Thus, all eigensolutions with the same value of k produce the same solution, and only one of them need be included.

In practice the infinite dimension problem is truncated to include harmonic terms up to $\pm n\Omega$, and the original problem in N unknowns is thus expanded to $(2n+1)N$ unknowns. The truncation introduces errors in the eigensolution because only a limited number of harmonic terms in the periodic mode shapes are included. The eigenvalues belonging to one mode are then in general not exactly equal in the real part, neither differing exactly Ω in the imaginary part, nor do the eigenvectors contain the exact same components. For a given value of n, the approximation is best for m around zero, i.e. the basis eigenvalues and values close to it, because the harmonic components that are excluded are high in frequency and therefore usually low in magnitude.

The solution in physical coordinates is found by inserting Eq. (31) into Eq. (21) and using Eq. (6) as

$$\mathbf{x}(t) = \sum_{k=1}^{N} \mathbf{u}_k(t) e^{\lambda_k t} q_k(0) \tag{39}$$

and the periodic mode shapes are given by

$$\mathbf{u}_k(t) = \sum_{l=-1}^{1} \sum_{j=-n}^{n} \mathbf{B}_l \mathbf{v}_{k,0,j} e^{\mathrm{i}(j+l)\Omega t} = \sum_{j=-n-1}^{n+1} \mathbf{u}_{k,j} e^{\mathrm{i}j\Omega t} \tag{40}$$

with the Coleman transformation matrix expressed as the Fourier series $\mathbf{B}(t) = \sum_{l=-1}^{1} \mathbf{B}_l e^{\mathrm{i}l\Omega t}$ and $\mathbf{u}_{k,j}$ being the coefficient with frequency $j\Omega$ when the periodic mode shape is expressed as a Fourier series. The solution contains two more harmonic terms with frequencies $\pm(n+1)\Omega$ than the eigenvector because the Coleman transformed equations are used.

C. Determination of modal frequency

Floquet theory describes the form of the solution to a system with periodic coefficients in Eq. (21). It implies that oscillation contained in a modal solution derives from both the eigenfrequency ω_k of λ_k as well as from the time-dependent periodic mode shape $\mathbf{r}_k(t)$ without constraint on the distribution between the two. This non-uniqueness of the frequency is characteristic of both the solutions obtained by Floquet analysis, where any integer multiple of the rotor speed can be added to the principal frequency, and Hill's method, which yields $2n+1$ different frequencies for each mode. The solution for an isotropic rotor obtained by Coleman transformation is a special case of Floquet theory, however the modal frequency is implicitly given as the one to which corresponds a constant mode shape when given in multiblade coordinates, i.e. defined in the inertial frame. This concept can be extended to the case of a moderately anisotropic rotor by defining the modal frequency as the one to which corresponds the most constant mode shape in multiblade coordinates. The advantage of using the multiblade coordinate mode shape is that the dominant oscillation by similarity to the isotropic case will be with the same frequency for all states. In contrast, in physical coordinates the dominant motion of rotor states can differ from the dominant motion of inertial states by the rotor speed.

In Floquet analysis, the periodic mode shape given by Eq. (22) and calculated with $j_k = 0$ can be expanded in a Fourier series and the integer j_k in Eq. (28) can be identified as the j in the frequency $j\Omega$ of the most dominant Fourier component. This method is described by Johnson[10] and has been applied by several researchers.[20–22] The basis eigenvalue containing the modal frequency can in Hill's method be identified by requiring that the corresponding eigenvector $\hat{\mathbf{v}}_{k,m}$ have the most dominant component $\mathbf{v}_{k,m,j}$ for $j = 0$.

V. Numerical example

A structural model of a wind turbine with a minimum degrees of freedom able to represent some of its fundamental structural dynamics is considered. Figure 1 illustrates the turbine with three rigid flap-hinged

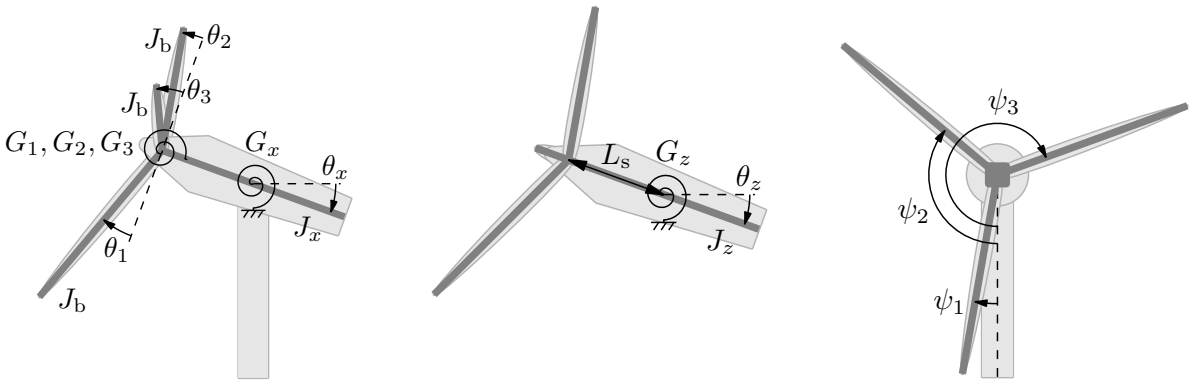

(a) Side view (b) Top view (c) Front view

Figure 1. A wind turbine with flapwise hinged rigid blades and a rigid nacelle able to tilt and yaw yielding five rotational degrees of freedom: θ_1, θ_2, θ_3, θ_x and θ_z.

Blade moment of inertia about root	J_b	$4{\times}10^6\,\mathrm{kg\,m^2}$
Nacelle/tower tilt moment of inertia	J_x	$8{\times}10^6\,\mathrm{kg\,m^2}$
Nacelle/tower yaw moment of inertia	J_z	$6{\times}10^6\,\mathrm{kg\,m^2}$
Blade stiffness	G_b	$8{\times}10^7\,\mathrm{N\,m}$
Nacelle/tower tilt stiffness	G_x	$7{\times}10^8\,\mathrm{N\,m}$
Nacelle/tower yaw stiffness	G_z	$4{\times}10^8\,\mathrm{N\,m}$
Blade damping	c_b	$1{\times}10^5\,\mathrm{kg\,m^2\,s^{-1}}$
Nacelle/tower tilt damping	c_x	$1{\times}10^6\,\mathrm{kg\,m^2\,s^{-1}}$
Nacelle/tower yaw damping	c_z	$8{\times}10^5\,\mathrm{kg\,m^2\,s^{-1}}$
Blade mass	m_b	$12{\times}10^3\,\mathrm{kg}$
Distance from tower top to hub	L_s	$4\,\mathrm{m}$

Table 1. Model parameters for a multi-MW generic wind turbine.

blades and a rigid nacelle that can tilt and yaw on a rigid tower. The model thus contains the three rotor DOF θ_1, θ_2 and θ_3 and the two inertial DOF θ_x and θ_z, and the state vector is given as

$$\mathbf{x}(t) = \{\theta_1, \dot{\theta}_1, \theta_2, \dot{\theta}_2, \theta_3, \dot{\theta}_3, \theta_x, \dot{\theta}_x, \theta_z, \dot{\theta}_z\}^{\mathrm{T}} \tag{41}$$

The rotor is assumed to be mass balanced and gravity is neglected, whereby the model can be linearized around the equilibrium at constant rotor speed with zero angles. The system equations can be written in first order form of Eq. (2) and Coleman transformed to yield the periodic system matrix given in the appendix.

Table 1 shows the parameters of the model chosen to correspond to the dynamics of a generic multi-MW turbine.

A. Isotropic rotor

The modal analysis of a three-bladed wind turbine with an isotropic rotor can be performed using the Coleman transformation method outlined in section III. Figure 2 shows the frequencies of the five modes of the model in a Campbell diagram as function of the rotor speed. The modes have been identified according to the dominant component of the harmonics defined in Eq. (11) which are shown in figure 3. The two modes with lowest frequencies at standstill are the first yaw and tilt modes, respectively. For increasing rotation speed they develop into whirling modes with the characteristic splitting of the frequencies[13] seen in figure 2. The symmetric mode denoted 0 has no coupling between the blades and the nacelle in this model. The frequency increase of this mode is due to the centrifugal stiffness. The two modes with highest frequency

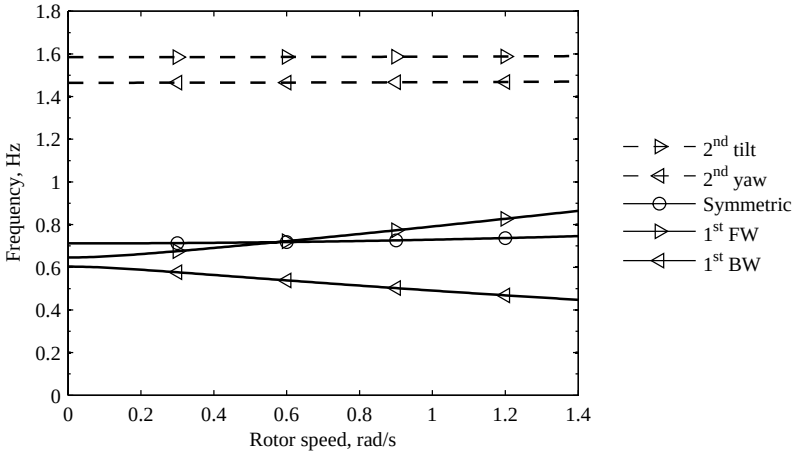

Figure 2. Campbell diagram with modal frequencies $f = \omega/2\pi$ versus rotor speed Ω.

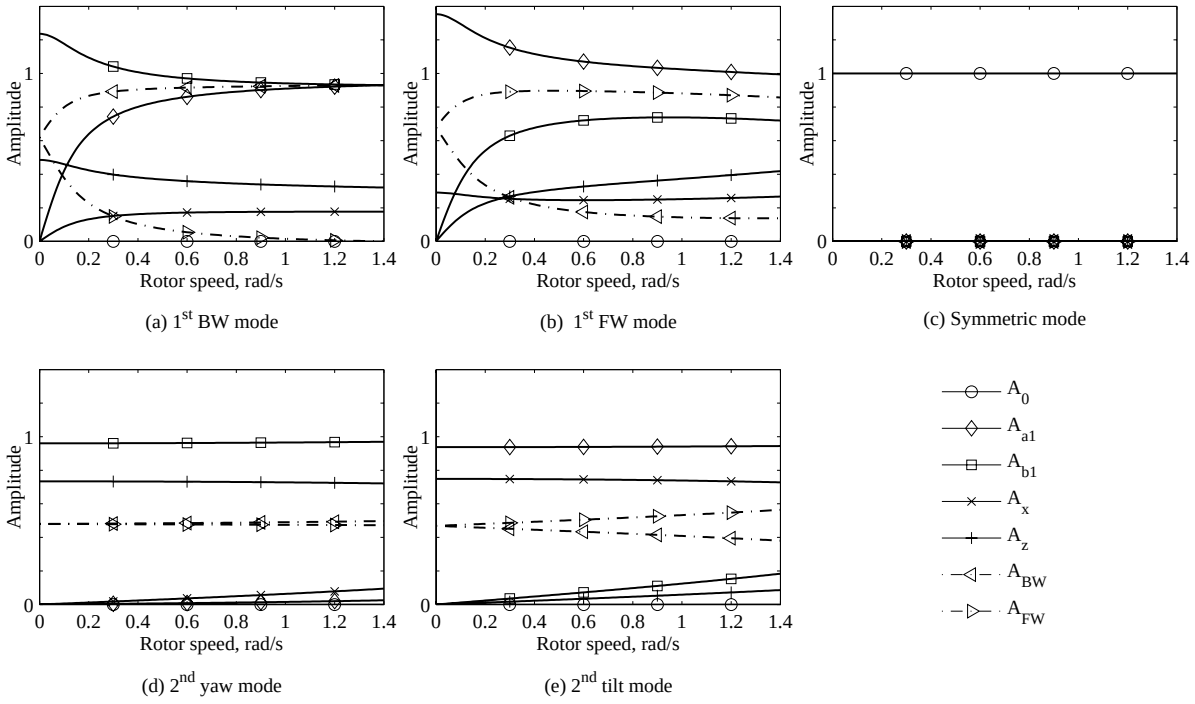

Figure 3. Amplitudes of harmonic modes $A_0, A_{\mathrm{BW}}, A_{\mathrm{FW}}$ and tower modes A_x, A_z of the five modes of the system.

are the second yaw and tilt modes, where the harmonic components do not change significantly when the rotor rotates.

B. Anisotropic rotor

In this section an anisotropic rotor with a stiffness asymmetry is considered. The rotor has a 10 % increase in stiffness on blade 1 and a 5 % decrease in stiffness on blades 2 and 3, such that the mean stiffness is the same as on the isotropic rotor.

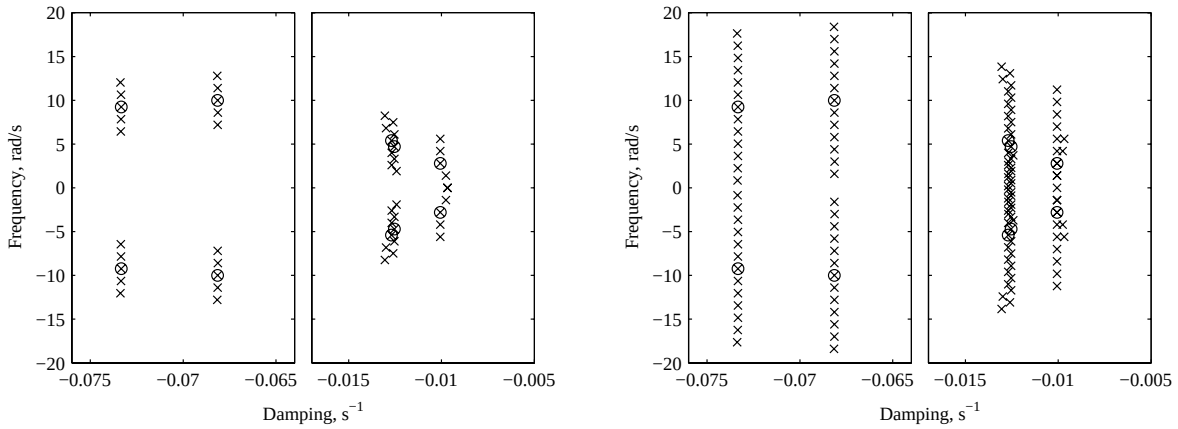

(a) 2 harmonic terms

(b) 6 harmonic terms

Figure 4. All eigenvalues obtained from Hill's method for different numbers of harmonics terms n included in the eigenvalue problem. $\times$ eigenvalues, $\otimes$ eigenvalues with modal frequency (basis eigenvalues). Anisotropic rotor at rotor speed 1.4 rad/s.

1. Floquet analysis

Floquet analysis is performed by numerical integration of Eq. (7) with the system matrix of Eq. (42) using the Runge-Kutta algorithm ode45 in Matlab. The monodromy matrix is found from Eq. (15) from which eigenvalue analysis provides damping and principal frequencies. The principal periodic mode shapes are then calculated in multiblade coordinates from Eq. (22) using the eigenvalues with principal frequencies and written as Fourier series. For each mode, the modal frequency is found from Eq. (28) with j_k given by the j in the Fourier series component with frequency $j\Omega$ that has the largest norm.

2. Hill's method

Hill's method is applied by computing the Fourier coefficients of the system matrix $\mathbf{A}(t)$ in Eq. (42). The highest frequency in $\mathbf{A}(t)$ is 2Ω, so the Fourier components $\mathbf{A}_l$ are non-zero only for $l \in \{-2, \ldots, 2\}$ and can be evaluated numerically using the Fast Fourier Transform algorithm. The eigenvalues are obtained from the system hypermatrix in Eq. (33) for different numbers of harmonic terms n included. The eigenvalues are shown at the rated rotor speed 1.4 rad/s in figure 4(a) for $n = 2$ and in figure 4(b) for $n = 6$. It can be difficult to determine which eigenvalues belonging to the same mode when the modes are close in damping, which is seen for both values of n. Therefore it is important that only the basis eigenvalues are considered. The basis eigenvalue for each mode is found as the one where the largest norm of the Fourier components $\mathbf{v}_{k,m,j}$ of the corresponding multiblade coordinate mode shape occurs for $j = 0$.

3. Convergence of eigenvalues

Both Floquet analysis and Hill's method are approximative because the first one relies on numerical integration of the system equations and the second one solves an approximation to the exact eigenvalue problem. The quality of these approximations is investigated first by looking at the convergence of the eigenvalues as the approximation is improved.

The modes computed for the anisotropic rotor have mode shapes similar to the isotropic case, so the modes are named in the same way. Figure 5 shows the deviation in the eigenvalues compared to a reference solution. The reference is the most precise approximation used, for Floquet analysis an absolute error tolerance of 10^{-16} (determining the integration time step) is used, and for Hill's method $n = 11$ harmonic terms are included in the hypermatrix system in Eq. (33). The difference between the eigenvalues of the reference solutions of the two methods are on the order 10^{-13}. Figure 5(a) shows that the eigenvalues computed with Floquet analysis converge steadily towards those of the reference solution when decreasing

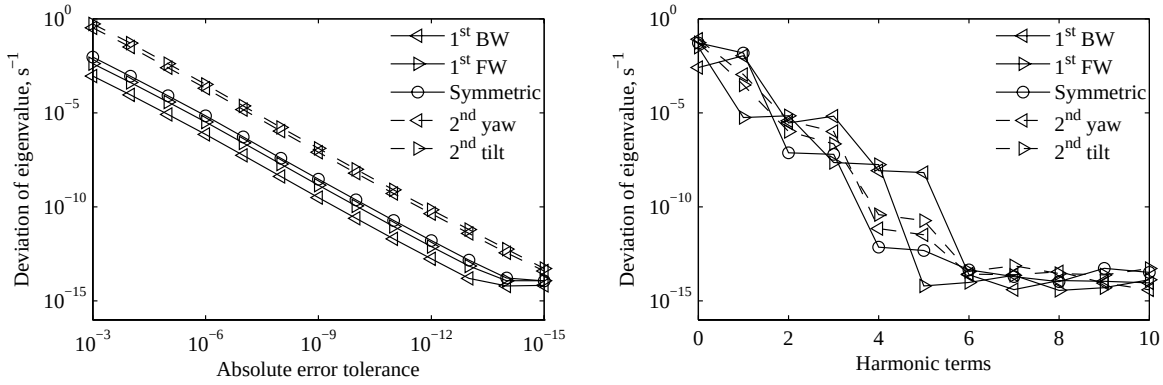

(a) Floquet analysis

(b) Hill's method

Figure 5. Absolute value of the deviation of the eigenvalues λ of each mode for (a) different absolute error tolerances in the integration and (b) different numbers of harmonic terms included in the eigenvalue problem. The deviations are calculated relative to reference solution with (a) a tolerance of 10^{-16} and (b) 11 harmonic terms. In the Floquet analysis a relative tolerance of 1000 times the absolute tolerance is used. Anisotropic rotor at rotor speed 1.4 rad/s.

Mode	1st BW	1st FW	Symmetric	2nd yaw	2nd tilt
Frequency, Hz	0.447	0.749	0.860	1.471	1.590
Deviation from isotropic case, %	0.20	0.41	0.45	0.03	0.006
Damping, s^{-1}	0.0101	0.0125	0.0127	0.0733	0.0681
Deviation from isotropic case, %	4.1	0.36	2.7	0.08	0.03

Table 2. Modal frequencies $f = \omega/2\pi$ and damping σ of the wind turbine with anisotropic rotor at rotor speed 1.4 rad/s.

the integration error tolerance. Figure 5(b) shows that no further increase in accuracy of the eigenvalues with these parameters computed with Hill's method is obtained by including more than 6 harmonic terms.

The frequencies and damping for the reference solutions using Floquet analysis and Hill's method are shown in Table 2. The change in frequency with respect to the isotropic rotor is small, but for the whirling modes the change in damping is considerable.

4. Modal dynamics

Figure 6 shows the amplitudes $\mathbf{u}_{k,j}$ of the Fourier components in the periodic mode shape for the first whirling modes calculated with Hill's method and $n = 6$. The same results can be obtained with Floquet analysis by Fourier transformation of the periodic mode shapes.[14] The different components have frequencies $\lambda_k + j\Omega$ in the solution given by Eq. (39) and Eq. (40), which is indicated with the frequency scale in the bottom of the figure. These frequencies would show up as peaks in a frequency response function. In figure 6(a) for the first BW mode the most dominant components, with frequencies λ_k and $\lambda_k + \Omega$, were also present in the isotropic case (*cf.* figure 3). However, the amplitude of the different blades is not the same, because the stiffness of the blades is not the same. In addition, more harmonic terms have appeared at higher frequencies. Figure 6(b) shows that the first FW mode has harmonic components at $\lambda_k - 2\Omega$ and at $\lambda_k + 2\Omega$ and above, in addition to the ones present in the isotropic case. The symmetric mode shown in figure 7, which had only blade motion at the modal frequency in the isotropic case, now has significant motion of the nacelle at $\lambda_k \pm \Omega$ and of the blades at $\lambda_k + 2\Omega$. Figure 8 shows the Fourier components for the second yaw and tilt modes. The components not present in the isotropic case, at frequencies $\lambda_k - 2\Omega$ and below and at $\lambda_k + 2\Omega$ and above, are somewhat smaller in magnitude than the corresponding ones for the first whirling modes.

It is general for all modes, that motion of the inertial states and the rotor states does not occur at the same frequency. Thus, for the first whirling and second yaw and tilt modes the inertial states oscillate with the modal frequency plus an even number multiple of the rotor speed and the rotor states oscillate with

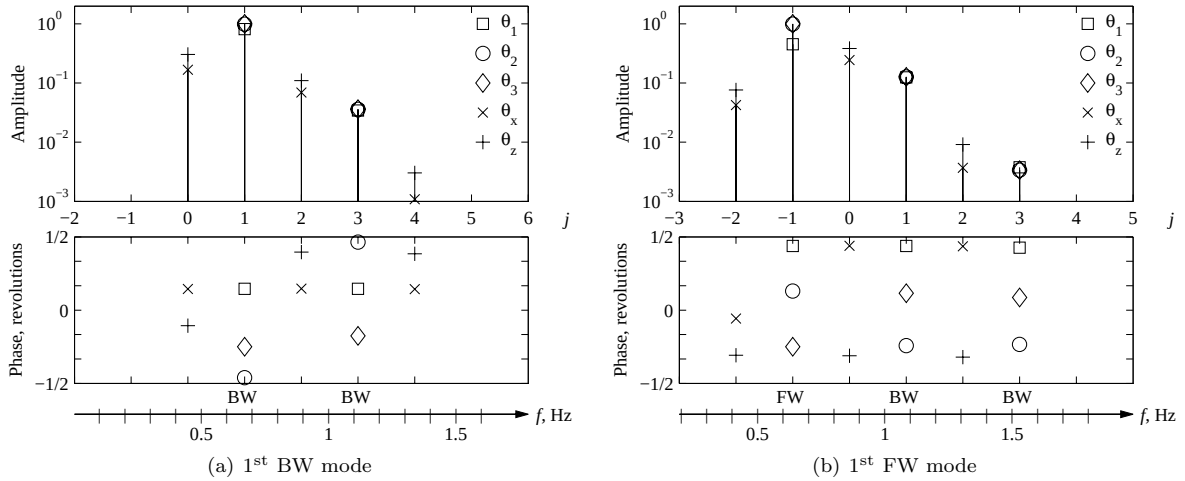

(a) 1st BW mode (b) 1st FW mode

Figure 6. Amplitudes and phases of harmonic components $\mathbf{u}_{k,j}$ with frequencies $j\Omega$ in the periodic mode shape and frequency scale for the modal solution. Anisotropic rotor at rotor speed 1.4 rad/s.

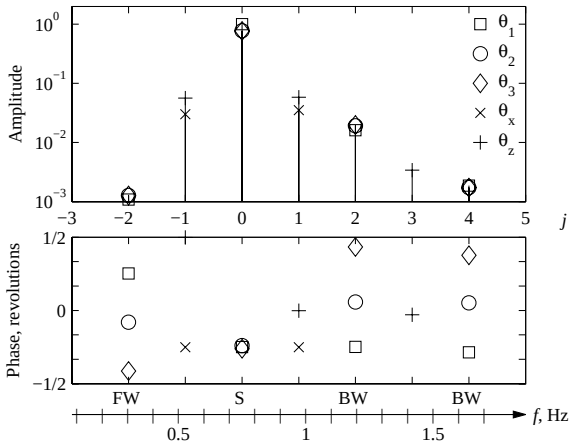

Figure 7. Amplitudes and phases of harmonic components $\mathbf{u}_{k,j}$ with frequencies $j\Omega$ in the periodic mode shape and frequency scale for the modal solution. Anisotropic rotor at rotor speed 1.4 rad/s, symmetric mode.

the modal frequency plus an odd number multiple of the rotor speed. Oppositely, for the symmetric mode the rotor states oscillate with the modal frequency plus an even number multiple of the rotor speed and the inertial states oscillate with the modal frequency plus an odd number multiple of the rotor speed. The rotor components at frequencies below the modal frequency are always BW and at frequencies above the modal frequency always FW as indicated in figures 6-8 below the phase plot. This observation complies with Eq. (12) and extends it to more harmonic components.

VI. Discussion

Floquet analysis and Hill's method produce similar results in modal analysis, with the periodic mode shape is given in time domain and in frequency domain, respectively. Hill's method is faster because it avoids numerical integration, but the size of the eigenvalue problem might be very large. One advantage of Floquet analysis is that the full nonlinear equations can be used to produce the fundamental solution, thus avoiding an explicit linearization of the equations of motion. The problem of the non-uniqueness of the frequency is inherent for both methods, but it can be solved without greater effort for small to moderate magnitudes of

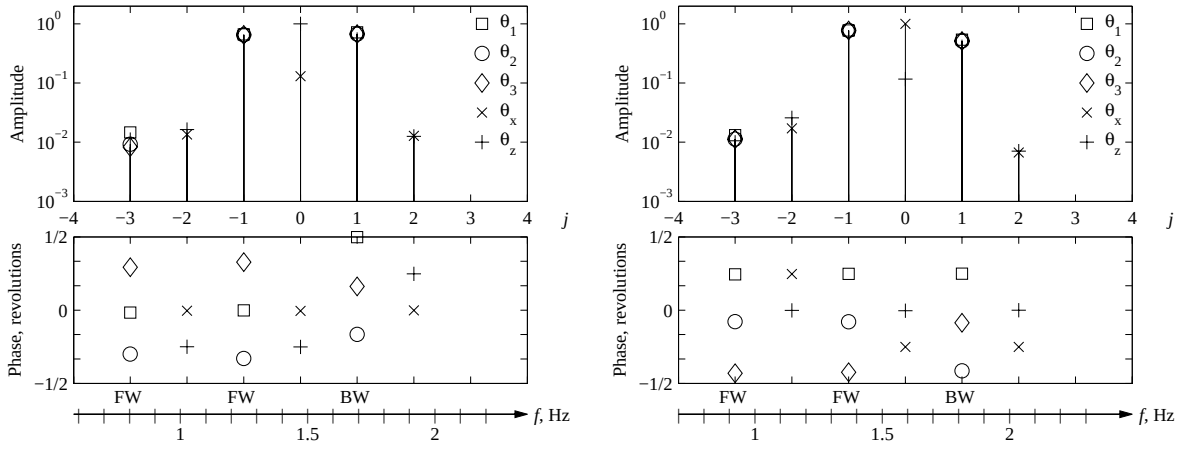

(a) 2nd yaw mode (b) 2nd tilt mode

Figure 8. Amplitudes and phases of harmonic components $\mathbf{u}_{k,j}$ with frequencies $j\Omega$ in the periodic mode shape and frequency scale for the modal solution. Anisotropic rotor at rotor speed 1.4 rad/s.

anisotropy.

The error of the eigenvalues found from Floquet analysis is consistently larger for some modes than for others as shown in figure 5(a), a tendency not observed in Hill's method. These errors are probably introduced through the numerical integration of the equations of motion, but it is difficult to say from the example in this paper, whether the modes that have highest error are characterized by high frequency or high damping.

The appearance of additional harmonic components in the response of the turbine with an anisotropic rotor is mostly interesting for the blade DOF, as this additional motion can introduce couplings with the unsteady aerodynamics in an aeroelastic model. The most notable change is that the first BW mode amplitude at $\lambda_k + 3\Omega$ in figure 6(a) is 4% of that at $\lambda_k\Omega$ for the blades.

It seems that the anisotropy affects the whirling modes the most, which is evidenced both by the change in damping and by the magnitude of the additional harmonic terms in the mode shape. However, it could also be that the least damped modes are affected most. It is difficult to draw conclusions from a model with only five modes, therefore further work must be done to apply these methods to a more complex model. It will also be interesting to see, whether quantitatively similar results are obtained from other sources of anisotropy such as rotor mass unbalance, gravity, non-uniform inflow.

VII. Conclusion

Modal analysis of a wind turbine with an anisotropic rotor can be performed using Floquet analysis or Hill's method. Both methods yield similar results and the non-uniqueness in the frequency, inherent of methods based on Floquet theory, can be resolved using a common approach for both methods: the modal frequency is chosen such that the corresponding mode shape in multiblade coordinates is as constant as possible. Modal analysis of a wind turbine with an isotropic rotor by use of the Coleman transformation results in periodic mode shapes with up to three harmonic components. The analysis of an anisotropic rotor with a difference in blade stiffness shows additional harmonic components in the periodic mode shape and thus in the response. The amplitude of additional harmonic components for the blades is up to a few percent of the blade amplitudes in the isotropic case. These additional harmonic terms, though small, might cause new couplings to the unsteady aerodynamics in an aeroelastic model.

Appendix

The Coleman transformed system matrix of Eq. (7) for the wind turbine in the example can be written as a sum of a time-invariant part and a time-variant part that is proportional to the stiffness anisotropy as

$$\mathbf{A}(t) = \mathbf{A}_\mathrm{i} + \Delta G_1 \mathbf{A}_\mathrm{a}(t) \tag{42}$$

where ΔG_1 is the increase in stiffness of blade 1 compared to the isotropic case such that $G_1 = G_\mathrm{b} + \Delta G_1$, $G_2 = G_3 = G_\mathrm{b} - \Delta G_1/2$. The matrices are given as

$$\mathbf{A}_\mathrm{i} = \begin{bmatrix}
0 & 1 & 0 & 0 \\
-\frac{G_\mathrm{b}}{J_\mathrm{b}} - \Omega^2 & -\frac{c_\mathrm{b}}{J_\mathrm{b}} & 0 & 0 \\
0 & 0 & 0 & 1 \\
0 & 0 & -\frac{G_\mathrm{b}}{J_\mathrm{b}} - \frac{3G_\mathrm{b}}{2J_0+2J_x} - \Omega^2 & -c_\mathrm{b}\left(\frac{3}{2J_0+2J_x} + \frac{1}{J_\mathrm{b}}\right) \\
0 & 0 & \Omega & 0 \\
0 & 0 & 0 & \Omega \\
0 & 0 & 0 & 0 \\
0 & 0 & \frac{3G_\mathrm{b}}{2J_0+2J_x} & \frac{3c_\mathrm{b}}{2J_0+2J_x} \\
0 & 0 & 0 & 0 \\
0 & 0 & 0 & 0
\end{bmatrix}$$

$$\begin{bmatrix}
0 & 0 & 0 & 0 & 0 & 0 \\
0 & 0 & 0 & 0 & 0 & 0 \\
-\Omega & 0 & 0 & 0 & 0 & 0 \\
0 & -\Omega & \frac{G_x}{J_0+J_x} & \frac{c_x}{J_0+J_x} & 0 & 2\Omega \\
0 & 1 & 0 & 0 & 0 & 0 \\
-\frac{G_\mathrm{b}}{J_\mathrm{b}} - \frac{3G_\mathrm{b}}{2J_0+2J_z} - \Omega^2 & -c_\mathrm{b}\left(\frac{3}{2J_0+2J_z} + \frac{1}{J_\mathrm{b}}\right) & 0 & 2\Omega & -\frac{G_z}{J_0+J_z} & -\frac{c_z}{J_0+J_z} \\
0 & 0 & 0 & 1 & 0 & 0 \\
0 & 0 & -\frac{G_x}{J_0+J_x} & -\frac{c_x}{J_0+J_x} & 0 & 0 \\
0 & 0 & 0 & 0 & 0 & 1 \\
-\frac{3G_\mathrm{b}}{2J_0+2J_z} & -\frac{3c_\mathrm{b}}{2J_0+2J_z} & 0 & 0 & -\frac{G_z}{J_0+J_z} & -\frac{c_z}{J_0+J_z}
\end{bmatrix} \tag{43}$$

and

$$\mathbf{A}_\mathrm{a}(t) = \begin{bmatrix}
0 & 0 & 0 & 0 & 0 & 0 & 0 & 0 & 0 & 0 \\
0 & 0 & -\frac{\cos(\Omega t)}{2J_\mathrm{b}} & 0 & -\frac{\sin(\Omega t)}{2J_\mathrm{b}} & 0 & 0 & 0 & 0 & 0 \\
0 & 0 & 0 & 0 & 0 & 0 & 0 & 0 & 0 & 0 \\
-\frac{(3J_\mathrm{b}+2(J_0+J_x))\cos(\Omega t)}{2J_\mathrm{b}(J_0+J_x)} & 0 & -\frac{(3J_\mathrm{b}+2(J_0+J_x))\cos(2\Omega t)}{4J_\mathrm{b}(J_0+J_x)} & 0 & -\frac{(3J_\mathrm{b}+2(J_0+J_x))\sin(2\Omega t)}{4J_\mathrm{b}(J_0+J_x)} & 0 & 0 & 0 & 0 & 0 \\
0 & 0 & 0 & 0 & 0 & 0 & 0 & 0 & 0 & 0 \\
-\frac{(3J_\mathrm{b}+2(J_0+J_z))\sin(\Omega t)}{2J_\mathrm{b}(J_0+J_z)} & 0 & -\frac{(3J_\mathrm{b}+2(J_0+J_z))\sin(2\Omega t)}{4J_\mathrm{b}(J_0+J_z)} & 0 & \frac{(3J_\mathrm{b}+2(J_0+J_z))\cos(2\Omega t)}{4J_\mathrm{b}(J_0+J_z)} & 0 & 0 & 0 & 0 & 0 \\
0 & 0 & 0 & 0 & 0 & 0 & 0 & 0 & 0 & 0 \\
\frac{3\cos(\Omega t)}{2(J_0+J_x)} & 0 & \frac{3\cos(2\Omega t)}{4(J_0+J_x)} & 0 & \frac{3\sin(2\Omega t)}{4(J_0+J_x)} & 0 & 0 & 0 & 0 & 0 \\
0 & 0 & 0 & 0 & 0 & 0 & 0 & 0 & 0 & 0 \\
-\frac{3\sin(\Omega t)}{2(J_0+J_z)} & 0 & -\frac{3\sin(2\Omega t)}{4(J_0+J_z)} & 0 & \frac{3\cos(2\Omega t)}{4(J_0+J_z)} & 0 & 0 & 0 & 0 & 0
\end{bmatrix} \tag{44}$$

where $J_0 = 3m_\mathrm{b}L_\mathrm{s}^2$.

Acknowledgments

This work has been partially supported by the Danish Ministry of Science, Technology and Innovation through the Industrial PhD programme.

References

[1]Coleman, R. P. and Feingold, A. M., "Theory of self-excited mechanical oscillations of helicopter rotors with hinged blades," NACA Report 1351, National Advisory Committe for Aeronautics, 1958.

[2]Hansen, M., Gaunaa, M., and Madsen, H., "A Beddoes-Leishman type dynamic stall model in state-space and indicial formulations," Tech. Rep. Risø-R-1354(EN), Risø National Laboratory, 2004.

[3]Riziotis, V., Voutsinas, S., Politis, E., and Chaviaropoulos, P., "Aeroelastic stability of wind turbines: The problem, the methods and the issues," *Wind Energy*, Vol. 7, No. 4, 2004, pp. 373–392.

[4]van Engelen, T. G. and Braam, H., "Turbu Offshore, computer program for frequency domain analysis of horizontal axis offshore wind turbines," Tech. Rep. ECN-C–04-079, Energy Research Centre of the Netherlands, Postbus 1, NL-1755 ZG Petten, 2004.

[5]Kirchgässner, B., "ARLIS – A Program System for Aeroelastic Analysis of Rotating Linear Systems," *Proceeding of 1984 European Wind Energy Conference*, EWEA, 1984, pp. 253–258.

[6]Matthies, H. and Nath, C., "Dynamic stability of periodic solutions of large scale nonlinear systems," *Computer Methods in Applied Mechanics and Engineering*, Vol. 48, No. 2, 1985, pp. 191–202.

[7]Stol, K., Balas, M., and Bir, G., "Floquet Modal Analysis of a Teetered-Rotor Wind Turbine," *Journal of Solar Energy Engineering*, Vol. 124, 2002, pp. 364–371.

[8]Friedmann, P., "Numerical methods for the treatment of periodic systems with applications to structural dynamics and helicopter rotor dynamics," *Computers and Structures*, Vol. 35, No. 4 Special Issue: Frontiers in Computational Mechanics, 1990, pp. 329–347.

[9]Dugundji, J. and Wendell, J. H., "Some analysis methods for rotating systems with periodic coefficients," *AIAA Journal*, Vol. 21, No. 6, June 1983, pp. 890–897.

[10]Johnson, W., *Helicopter Theory*, Dover Publications, 1980.

[11]Xu, J. and Gasch, R., "Modale Behandlung linearer periodisch zeitvarianter Bewegungsgleichungen (Modal analysis of linear periodically time-variant equations of motion)," *Archive of Applied Mechanics*, Vol. 65, 1995, pp. 178–193.

[12]Meirovitch, L., *Methods of Analytical Dynamics*, McGraw-Hill, New York, 1970.

[13]Hansen, M. H., "Improved modal dynamics of wind turbines to avoid stall-induced vibrations," *Wind Energy*, Vol. 6, 2003, pp. 179–195.

[14]Skjoldan, P. F. and Hansen, M. H., "Modal dynamics of structures with bladed rotors using the Coleman and Lyapunov-Floquet transformations," *Under review*, 2008.

[15]Peters, D. A., "Fast Floquet theory and trim for multi-bladed rotorcraft," *Journal of the American Helicopter Society*, Vol. 39, No. 4, 1994, pp. 82–89.

[16]Sinha, S. and Pandiyan, R., "Analysis of quasilinear dynamical systems with periodic coefficients via Liapunov-Floquet transformation," *International Journal of Non-Linear Mechanics*, Vol. 29, No. 5, 1994, pp. 687–702.

[17]Coddington, E. A. and Levinson, N., *Theory of Ordinary Differential Equations*, McGraw-Hill, New York, 1955.

[18]Nayfeh, A. H. and Balachandran, B., *Applied Nonlinear Dynamics*, Wiley-VCH, Weinheim, 2004.

[19]Christensen, R. and Santos, I., "Design of active controlled rotor-blade systems based on time-variant modal analysis," *Journal of Vibration and Control*, Vol. 11, No. 6, 2005, pp. 801–828.

[20]Milgram, J. H. and Chopra, I., "Air resonance of hingeless rotor helicopters in trimmed forward flight," *Journal of the American Helicopter Society*, Vol. 39, No. 4, 1994, pp. 46–58.

[21]Lee, D., Hodges, D. H., and Patil, M. J., "Multi-flexible-body Dynamic Analysis of Horizontal Axis Wind Turbines," *Wind Energy*, Vol. 5, No. 4, 2002, pp. 281–300.

[22]Bauchau, O. A. and Wang, J., "Efficient and Robust Approaches to the Stability Analysis of Large Multibody Systems," *Journal of Computational and Nonlinear Dynamics*, Vol. 3, 2008.

P3

Implicit Floquet analysis of wind turbines using tangent matrices of a nonlinear aeroelastic code

Wind Energy. Accepted for publication, delivered to production 15th February 2011.

Implicit Floquet analysis of wind turbines using tangent matrices of a nonlinear aeroelastic code

P. F. Skjoldan
Loads, Aerodynamic and Control
Siemens Wind Power A/S
Dybendalsvænget 3, DK-2630 Taastrup, Denmark

M. H. Hansen
Wind Energy Division,
National Laboratory for Sustainable Energy, Risø DTU,
Frederiksborgvej 399, DK-4000 Roskilde, Denmark

October 28, 2010

Abstract

The aeroelastic code BHawC for calculation of the dynamic response of a wind turbine uses a nonlinear finite element formulation. Most wind turbine stability tools for calculation of the aeroelastic modes are, however, based on separate linearised models. This paper presents an approach to modal analysis where the linear structural model is extracted directly from BHawC using the tangent system matrices when the turbine is in a steady state. A purely structural modal analysis of the periodic system for an isotropic rotor operating at a stationary steady state is performed by eigenvalue analysis after describing the rotor degrees of freedom in the inertial frame with the Coleman transformation. For general anisotropic systems implicit Floquet analysis, which is less computationally intensive than classical Floquet analysis, is used to extract the least damped modes.

Both methods are applied to a model of a three-bladed 2.3 MW Siemens wind turbine. Frequencies match individually and with a modal identification on time simulations with the nonlinear model. The implicit Floquet analysis performed for an anisotropic system in a periodic steady state shows that the response of a single mode contains multiple harmonic components differing in frequency by the rotor speed.

Keywords: modal analysis; Floquet analysis; rotor dynamics

1 Introduction

Today, advanced nonlinear finite element codes [1, 2, 3] are routinely used for load calculations on wind turbines. Most wind turbine stability tools for calculation of the aeroelastic modes are, however, based on separate linearised models. Stability analysis can be divided into three steps: First a calculation of the steady state, then a linearisation of the equations of motion about the steady state, and last a modal analysis to extract modal frequencies, damping, and mode shapes. This paper presents an approach to structural modal analysis applicable to any periodic steady state where the linearisation is obtained directly from the nonlinear wind turbine aeroelastic code BHawC [3].

The equations of motion for a wind turbine operating at a constant mean rotor speed contain periodic coefficients, preventing direct eigenvalue analysis of the system. Most recent wind turbine stability tools [4, 5, 6, 7] incorporate the Coleman transformation, also known as the multi-blade coordinate transformation, which describes the rotor degrees of freedom in the inertial frame. This transformation eliminates the periodic coefficients if the system is isotropic, i.e., the rotor consists of identical symmetrically mounted blades, and the environment conditions are symmetric. Floquet analysis is, however, applicable to anisotropic systems and any periodic steady state. It requires integration of the equations of motion over a period of rotor rotation, as many times as there are state variables in the system. Due to the computational burden of this approach it has only been applied to reduced or simplified wind turbine models with a limited number of degrees of freedom [8, 9, 10]. One way to reduce the computation time is Fast Floquet Theory [11] where only one third of the integrations are necessary for a three-bladed isotropic rotor. Another way is to use implicit Floquet analysis [12] where the least damped modes can be extracted after a limited number of integrations.

Stol et al. [13] compare the Coleman transformation approach applied to a periodic steady state, where the remaining periodic coefficients are averaged away, with Floquet analysis and find small differences in modal frequencies and damping, concluding that it is not necessary to use Floquet analysis.

Another approach to modal analysis is system

identification [14, 15, 16] which operates on the response from numerical simulations or measurements, and no knowledge of the system equations is needed to extract the modal properties. The accuracy of the methods is, however, limited and depends on the chosen excitation.

In this paper, tangent matrices for mass, damping, and stiffness are extracted from the aeroelastic code BHawC. If the system is isotropic and the steady state is stationary, the Coleman transformation is applied before extracting the modal parameters by eigenvalue analysis. For an anisotropic system, implicit Floquet analysis is used for the modal analysis. When the system is isotropic the response of a single mode contains a single harmonic component for tower degrees of freedom and up to three components for the blades. The response of a single mode in the anisotropic system on both blades and tower contains multiple harmonic components differing in frequency by the rotor speed.

Section 2 of this paper describes the BHawC model and Section 3 explains the methods for modal analysis, the Coleman transformation approach, implicit Floquet analysis and also partial Floquet analysis, a system identification technique. In Section 4 the methods are applied to model of a wind turbine. Section 5 discusses the approaches and Section 6 concludes the paper.

2 Structural model

The BHawC wind turbine aeroelastic code [3] is based on a structural finite element model sketched in Figure 1, where the main structural parts, tower, nacelle, shaft, hub, and blades, are modelled as two-node 12-degrees of freedom Timoshenko beam elements. The code uses a co-rotational formulation, where each element has its own coordinate system that rotates with the element. The elastic deformation is described in the element frame, while the movement of the element coordinate system accounts for rigid body motion. In this way, a geometrically nonlinear model is obtained using linear finite elements.

The configuration of the system, defined by nodal positions $\mathbf{p}$ and orientations $\mathbf{q}$, nodal velocities $\dot{\mathbf{u}}$ (of both positions and orientations) and nodal accelerations $\ddot{\mathbf{u}}$ must satisfy the equilibrium equation given in global coordinates as

$$\mathbf{f}_{\text{iner}}(\mathbf{p},\mathbf{q},\dot{\mathbf{u}},\ddot{\mathbf{u}}) + \mathbf{f}_{\text{damp}}(\mathbf{q},\dot{\mathbf{u}}) + \mathbf{f}_{\text{int}}(\mathbf{p},\mathbf{q}) = \mathbf{f}_{\text{ext}} \quad (1)$$

where $\mathbf{f}_{\text{iner}}$, $\mathbf{f}_{\text{damp}}$, $\mathbf{f}_{\text{int}}$, and $\mathbf{f}_{\text{ext}}$ are the inertial, damping, internal, and external force vectors, respectively, and $\dot{(\,)} = \mathrm{d}/\mathrm{d}t$ denotes a time derivative. The inertial forces depend on the acceleration of masses, the damping force is given by viscous damping, the internal force is due to elastic forces, and the external force contains the aerodynamic force [17]. To find this equilibrium configuration, increments of the positions and orientations $\delta\mathbf{u}$, velocities $\delta\dot{\mathbf{u}}$ and accelerations $\delta\ddot{\mathbf{u}}$ are found by Newton-Raphson iteration with the tangent relation obtained from the variation of Equation (1) as

$$\mathbf{M}(\mathbf{q})\delta\ddot{\mathbf{u}} + \mathbf{C}(\mathbf{q},\dot{\mathbf{u}})\delta\dot{\mathbf{u}} + \mathbf{K}(\mathbf{p},\mathbf{q},\dot{\mathbf{u}},\ddot{\mathbf{u}})\delta\mathbf{u} = \mathbf{r} \quad (2)$$

where $\mathbf{M}$, $\mathbf{C}$, and $\mathbf{K}$ are the tangent mass, damping/gyroscopic, and stiffness matrices, respectively, and $\mathbf{r} = \mathbf{f}_{\text{ext}} - \mathbf{f}_{\text{iner}} - \mathbf{f}_{\text{damp}} - \mathbf{f}_{\text{int}}$ is the residual. The stiffness matrix is composed of constitutive, geometric, and inertial stiffness. The orientation of the nodes $\mathbf{q}$ is described by quaternions, also known as Euler parameters [18], a general four-parameter representation equivalent to a rotation matrix, which for node number i is updated as

$$\mathbf{q}_i := \mathbf{quat}(\delta\mathbf{u}_{i,\text{rot}}) * \mathbf{q}_i \quad (3)$$

where $\delta\mathbf{u}_{i,\text{rot}}$ contains three rotations that are assumed infinitesimal and thus commute, and where this rotation pseudo-vector is transformed by the function termed **quat** into a quaternion, which is used to update the nodal quaternion $\mathbf{q}_i$ employing the special quaternion product denoted by $*$ which maintains the unity of the quaternion. The nodal positions $\mathbf{p}$, nodal velocities $\dot{\mathbf{u}}$, and accelerations $\ddot{\mathbf{u}}$ are updated by regular addition of the positional part of $\delta\mathbf{u}$, $\delta\dot{\mathbf{u}}$ and $\delta\ddot{\mathbf{u}}$, respectively. All components in $\mathbf{p}$, $\mathbf{q}$, and $\delta\mathbf{u}$ are absolute and described in a global frame.

The present work considers small perturbations in position and orientation $\mathbf{y}$, velocity $\dot{\mathbf{y}}$, and acceleration $\ddot{\mathbf{y}}$ to a steady state with constant mean rotor speed Ω defined by $(\mathbf{p}_{\text{ss}}, \mathbf{q}_{\text{ss}}, \dot{\mathbf{u}}_{\text{ss}}, \ddot{\mathbf{u}}_{\text{ss}})$, the steady

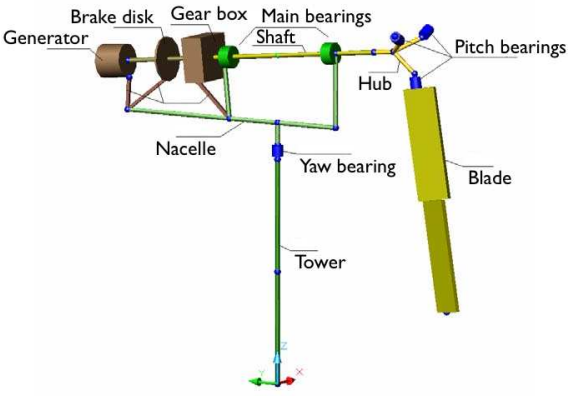

Figure 1: Sketch of BHawC model substructures.

state positions, orientations, velocities, and accelerations, respectively, all periodic with the rotor period $T = 2\pi/\Omega$. The linearised equations of motion are obtained from Equation (2) at $\mathbf{r} \approx \mathbf{0}$ as

$$\mathbf{M}(\mathbf{q}_{\mathrm{ss}})\ddot{\mathbf{y}} + \mathbf{C}(\mathbf{q}_{\mathrm{ss}}, \dot{\mathbf{u}}_{\mathrm{ss}})\dot{\mathbf{y}} + \mathbf{K}(\mathbf{p}_{\mathrm{ss}}, \mathbf{q}_{\mathrm{ss}}, \dot{\mathbf{u}}_{\mathrm{ss}}, \ddot{\mathbf{u}}_{\mathrm{ss}})\mathbf{y} = \mathbf{0} \quad (4)$$

where the matrices $\mathbf{M}$, $\mathbf{C}$, and $\mathbf{K}$ are the T-periodic tangent system matrices which are employed in the modal analysis described in the next section.

3 Methods

In this section four methods for modal analysis of structures with rotors are presented.

3.1 Coleman approach

The Coleman transformation requires identical degrees of freedom on each blade, and therefore the equations of motion (4) in global coordinates are first transformed into substructure coordinates $\mathbf{y}_{\mathrm{T}}$. The transformation is

$$\begin{aligned} \mathbf{y} &= \mathbf{T}\,\mathbf{y}_{\mathrm{T}} \\ \mathbf{T} &= \mathbf{diag}(\mathbf{I}_{N_{\mathrm{s}}}, \mathbf{T}_{\mathrm{r}}, \mathbf{T}_{\mathrm{b}1}, \mathbf{T}_{\mathrm{b}2}, \mathbf{T}_{\mathrm{b}3}) \end{aligned} \quad (5)$$

where $\mathbf{T}$ is a block diagonal time-variant matrix composed of the identity matrix $\mathbf{I}_{N_{\mathrm{s}}}$ sized by the number of degrees of freedom of the tower, nacelle, and drivetrain, $\mathbf{T}_{\mathrm{r}}$ transforming the degrees of freedom on the shaft and hub into a hub centre frame, and $\mathbf{T}_{\mathrm{b}j}$ transforming the degrees of freedom on blade number $j = 1, 2, 3$ into a local frame for blade j. The rotation matrices are obtained in the periodic steady state, and thus $\mathbf{T}$ is T-periodic.

The time-variant transformation into inertial frame coordinates $\mathbf{z}$ is

$$\begin{aligned} \mathbf{y}_{\mathrm{T}} &= \mathbf{B}\,\mathbf{z} \\ \mathbf{B} &= \mathbf{diag}(\mathbf{I}_{N_{\mathrm{s}}}, \mathbf{B}_{\mathrm{r}}, \mathbf{B}_{\mathrm{b}}) \end{aligned} \quad (6)$$

where $\mathbf{B}_{\mathrm{r}}$ is a simple rotational transformation of the shaft and hub, and $\mathbf{B}_{\mathrm{b}}$ is the Coleman transformation introducing multi-blade coordinates for a three-bladed rotor [11, 19] as

$$\mathbf{B}_{\mathrm{b}} = \begin{bmatrix} \mathbf{I}_{N_{\mathrm{b}}} & \mathbf{I}_{N_{\mathrm{b}}} \cos\psi_1 & \mathbf{I}_{N_{\mathrm{b}}} \sin\psi_1 \\ \mathbf{I}_{N_{\mathrm{b}}} & \mathbf{I}_{N_{\mathrm{b}}} \cos\psi_2 & \mathbf{I}_{N_{\mathrm{b}}} \sin\psi_2 \\ \mathbf{I}_{N_{\mathrm{b}}} & \mathbf{I}_{N_{\mathrm{b}}} \cos\psi_3 & \mathbf{I}_{N_{\mathrm{b}}} \sin\psi_3 \end{bmatrix} \quad (7)$$

where $\psi_j = \Omega t + 2\pi(j-1)/3$ is the mean azimuth angle to blade number j, and N_{b} is the number of degrees of freedom on each blade. The inertial frame coordinate vector

$$\mathbf{z} = \{\mathbf{y}_{\mathrm{s}}^{\mathrm{T}}\ \mathbf{z}_{\mathrm{r}}^{\mathrm{T}}\ \mathbf{a}_0^{\mathrm{T}}\ \mathbf{a}_1^{\mathrm{T}}\ \mathbf{b}_1^{\mathrm{T}}\}^{\mathrm{T}} \quad (8)$$

contains the untransformed coordinates for tower, nacelle, and drivetrain $\mathbf{y}_{\mathrm{s}}$, the coordinates for shaft and hub $\mathbf{z}_{\mathrm{r}}$ measured in a non-rotating frame aligned with the hub, and the multi-blade symmetric coordinates $\mathbf{a}_0$, cosine coordinates $\mathbf{a}_1$, and sine coordinates $\mathbf{b}_1$. Details on how multi-blade coordinates describe the motion of a wind turbine rotor in the inertial frame are discussed in [20, 21].

The Coleman transformed equations are obtained by first inserting Equation (5) into (4), then converting to first order form and last introducing the inertial frame transformation in Equation (6) as $\mathbf{y}_{\mathrm{T}2} = \mathbf{diag}(\mathbf{B}, \mathbf{B})\mathbf{z}_2$ where $\mathbf{y}_{\mathrm{T}2} = \{\mathbf{y}^{\mathrm{T}}\ \dot{\mathbf{y}}^{\mathrm{T}}\}^{\mathrm{T}}$ and $\mathbf{z}_2 = \{\mathbf{z}^{\mathrm{T}}\ \tilde{\mathbf{z}}^{\mathrm{T}}\}^{\mathrm{T}}$ are the state vector in substructure and inertial frames, respectively, with $\tilde{\mathbf{z}} = \dot{\mathbf{z}} + \bar{\omega}\mathbf{z}$ and the constant matrix $\bar{\omega} = \mathbf{B}^{-1}\dot{\mathbf{B}}$. The result is

$$\begin{aligned} \dot{\mathbf{z}}_2 &= \mathbf{A}_{\mathrm{B}}\mathbf{z}_2 \\ \mathbf{A}_{\mathrm{B}} &= \begin{bmatrix} -\bar{\omega} & \mathbf{I} \\ -\mathbf{M}_{\mathrm{B}}^{-1}\mathbf{K}_{\mathrm{B}} & -\mathbf{M}_{\mathrm{B}}^{-1}\mathbf{C}_{\mathrm{B}} - \bar{\omega} \end{bmatrix} \end{aligned} \quad (9)$$

where $\mathbf{A}_{\mathrm{B}}$ is the Coleman transformed system matrix and

$$\begin{aligned} \mathbf{M}_{\mathrm{B}} &= \mathbf{B}^{-1}\mathbf{T}^{\mathrm{T}}\mathbf{M}\,\mathbf{T}\,\mathbf{B} \\ \mathbf{C}_{\mathrm{B}} &= \mathbf{B}^{-1}\mathbf{T}^{\mathrm{T}}(\mathbf{C}\,\mathbf{T} + 2\,\mathbf{M}\,\dot{\mathbf{T}})\mathbf{B} \\ \mathbf{K}_{\mathrm{B}} &= \mathbf{B}^{-1}\mathbf{T}^{\mathrm{T}}(\mathbf{K}\,\mathbf{T} + \mathbf{C}\,\dot{\mathbf{T}} + \mathbf{M}\,\ddot{\mathbf{T}})\mathbf{B} \end{aligned} \quad (10)$$

are the Coleman transformed mass, damping/gyroscopic, and stiffness matrices, respectively. If the system is isotropic, then $\mathbf{A}_{\mathrm{B}}$ is time-invariant and a transient solution of Equation (9) is

$$\mathbf{z}_2 = \mathrm{e}^{\mathbf{A}_{\mathrm{B}}t}\mathbf{z}_2(0) = \mathbf{V}\mathrm{e}^{\mathbf{\Lambda}t}\mathbf{q}(0) \quad (11)$$

where $\mathbf{\Lambda}$ is a diagonal matrix containing the eigenvalues of $\mathbf{A}_{\mathrm{B}}$, $\mathbf{V}$ contains the corresponding eigenvectors as columns and $\mathbf{q}(0) = \mathbf{V}^{-1}\mathbf{z}_2(0)$ are the initial conditions in modal coordinates. It is assumed that all eigenvectors are linearly independent.

The blade motion given in the inertial frame in Equation (11) can be transformed back into the rotating frame using Equation (6) as [21]

$$\begin{aligned} y_{\mathrm{T,ik}} = \mathrm{e}^{\sigma_k t}\Big(& A_{0,ik}\cos(\omega_k t + \varphi_{0,ik}) \\ & + A_{\mathrm{BW},ik}\cos\big((\omega_k + \Omega)t + \varphi_j + \varphi_{\mathrm{BW},ik}\big) \\ & + A_{\mathrm{FW},ik}\cos\big((\omega_k - \Omega)t - \varphi_j + \varphi_{\mathrm{FW},ik}\big)\Big) \end{aligned} \quad (12)$$

where $\varphi_j = 2\pi(j-1)/3$, σ_k and ω_k are the modal damping and frequency of mode number k, respectively, given by the eigenvalue $\lambda_k = \sigma_k + \mathrm{i}\omega_k$ with $\mathrm{i} = \sqrt{-1}$. The amplitudes for degree of freedom number i are determined from the components of the eigenvector $\mathbf{v}_k$ given in multi-blade coordinates

of Equation (8) as $A_{0,ik} = |a_{0,ik}|$ and

$$A_{\mathrm{BW},ik} = \tfrac{1}{2}\big((\mathrm{Re}\,(a_{1,ik}) + \mathrm{Im}\,(b_{1,ik}))^2 + (\mathrm{Re}\,(b_{1,ik}) - \mathrm{Im}\,(a_{1,ik}))^2\big)^{1/2} \tag{13}$$

$$A_{\mathrm{FW},ik} = \tfrac{1}{2}\big((\mathrm{Re}\,(a_{1,ik}) - \mathrm{Im}\,(b_{1,ik}))^2 + (\mathrm{Re}\,(b_{1,ik}) + \mathrm{Im}\,(a_{1,ik}))^2\big)^{1/2} \tag{14}$$

where the subscripts 0, BW, and FW denote symmetric, backward whirling, and forward whirling motion, respectively.

3.2 Classical Floquet analysis

Floquet analysis enables the solution of the periodic equations of motion directly without an explicit transformation. Equation (4) is written in first order form

$$\begin{aligned}\dot{\mathbf{y}}_2 &= \mathbf{A}\mathbf{y}_2\\ \mathbf{A} &= \begin{bmatrix}\mathbf{0} & \mathbf{I}\\ -\mathbf{M}^{-1}\mathbf{K} & -\mathbf{M}^{-1}\mathbf{C}\end{bmatrix}\end{aligned} \tag{15}$$

where $\mathbf{y}_2 = \{\mathbf{y}^{\mathrm{T}}\ \dot{\mathbf{y}}^{\mathrm{T}}\}^{\mathrm{T}}$ is the state vector and $\mathbf{A}$ is the T-periodic system matrix.

Floquet theory [22] states that the solution to Equation (15) is of the form

$$\mathbf{y}_2 = \mathbf{U}\mathrm{e}^{\mathbf{\Lambda} t}\mathbf{U}^{-1}(0)\mathbf{y}_2(0) \tag{16}$$

where $\mathbf{U}$ is a T-periodic matrix and $\mathbf{\Lambda}$ is a diagonal matrix. One way to construct this solution is to form a fundamental solution to Equation (15) as

$$\boldsymbol{\varphi} = \begin{bmatrix}\boldsymbol{\varphi}_1 & \boldsymbol{\varphi}_2 & \cdots & \boldsymbol{\varphi}_N\end{bmatrix} \tag{17}$$

over one period, $t \in [0; T]$, where N is the number of state variables, such that $\dot{\boldsymbol{\varphi}} = \mathbf{A}\boldsymbol{\varphi}$. The monodromy matrix defined as

$$\mathbf{C} = \boldsymbol{\varphi}^{-1}(0)\boldsymbol{\varphi}(T) \tag{18}$$

contains all modal properties, which can be extracted from the eigenvalue decomposition

$$\mathbf{C} = \mathbf{V}\mathbf{J}\mathbf{V}^{-1} \tag{19}$$

where $\mathbf{V}$ contains the column eigenvectors $\mathbf{v}_k$ of $\mathbf{C}$, which are all assumed to be linearly independent, and $\mathbf{J}$ is a diagonal matrix containing the eigenvalues ρ_k of $\mathbf{C}$, called the characteristic multipliers. The characteristic exponents $\lambda_k = \sigma_k + \mathrm{i}\omega_k$ contain the frequency ω_k and damping σ_k and are related to the characteristic multipliers as $\rho_k = \exp(\lambda_k T)$. Because the complex logarithm is not unique, the frequency is not determined uniquely, and the principal frequency $\omega_{\mathrm{p},k}$ and the damping σ_k are defined from the characteristic multipliers as

$$\begin{aligned}\sigma_k &= \frac{1}{T}\ln(|\rho_k|)\\ \omega_{\mathrm{p},k} &= \frac{1}{T}\arg(\rho_k)\end{aligned} \tag{20}$$

where $\arg(\rho_k) \in\ ]-\pi;\pi]$ is implied, resulting in $\omega_{\mathrm{p},k} \in\ ]-\Omega/2;\Omega/2]$. Any integer multiple of the rotor speed can be added to the principal frequency to obtain a more physically meaningful frequency [23, 24]

$$\omega_k = \omega_{\mathrm{p},k} + j_k\Omega \tag{21}$$

a choice which also affects the periodic modal matrix $\mathbf{U}$ in Equation (16). This matrix $\mathbf{U}$ contains the periodic mode shapes $\mathbf{u}_k$ and is given as [24]

$$\mathbf{u}_k = \boldsymbol{\varphi}\mathbf{v}_k\mathrm{e}^{-\lambda_k t} \tag{22}$$

where λ_k is selected using Equation (21) such that $\mathbf{u}_k$ is as constant as possible for degrees of freedom measured in the inertial frame.

Introducing the Fourier transform of the periodic mode shape

$$\mathbf{u}_k = \sum_{j=-\infty}^{\infty} \boldsymbol{\mathcal{U}}_{jk}\mathrm{e}^{\mathrm{i}j\Omega t} \tag{23}$$

the transient solution in Equation (16) can be written as a sum of harmonic components

$$\mathbf{y}_2 = \sum_{k=1}^{N}\sum_{j=-\infty}^{\infty} \boldsymbol{\mathcal{U}}_{jk}\mathrm{e}^{(\sigma_k + \mathrm{i}(\omega_k + j\Omega))t}q_k(0) \tag{24}$$

where $\mathbf{q}(0) = \mathbf{U}^{-1}(0)\mathbf{y}_2(0)$. Note that Equation (12) is a special case of this expression for $j = -1, 0, 1$.

3.3 Implicit Floquet analysis

The Implicit Floquet method is here described based on the detailed description in [12], which focuses on computation of the characteristic multipliers from the state transition matrix $\mathbf{\Phi}(T, 0)$. It can be defined in classical Floquet theory as

$$\boldsymbol{\varphi}(T) = \mathbf{\Phi}(T, 0)\,\boldsymbol{\varphi}(0) \tag{25}$$

Using Equation (18), the relationship between the state transition and monodromy matrices is derived as

$$\mathbf{\Phi}(T, 0) = \boldsymbol{\varphi}(0)\mathbf{C}\,\boldsymbol{\varphi}^{-1}(0) \tag{26}$$

showing that $\mathbf{\Phi}(T, 0)$ and $\mathbf{C}$ have identical eigenvalues (characteristic multipliers), and their eigenvectors are related as $\mathbf{v}_k = \boldsymbol{\varphi}^{-1}(0)\mathbf{w}_k$, where $\mathbf{w}_k$ are the eigenvectors of $\mathbf{\Phi}(T, 0)$.

The key feature of the state transition matrix is that it defines the solution $\mathbf{y}_2(T) = \mathbf{\Phi}(T,0)\mathbf{y}_2(0)$ for a time integration of the system equations (15) over one period T with initial conditions $\mathbf{y}_2(0)$. Hence, without knowing the state transition matrix, it is possible to obtain the product of it with an arbitrary vector (the initial state vector) by integration of (15) over one period. The Arnoldi algorithm [25] is a method to approximate the eigenvalues and eigenvectors of a matrix, say $\mathbf{\Phi}(T,0)$, using only the matrix multiplication with $\mathbf{\Phi}(T,0)$ to construct an m-sized subspace

$$\mathbf{P} = \begin{bmatrix}\mathbf{p}_1 & \mathbf{p}_2 & \dots & \mathbf{p}_m\end{bmatrix} \tag{27}$$

that satisfies the orthonormality condition

$$\mathbf{P}^{\mathrm{T}}\mathbf{P} = \mathbf{I}, \tag{28}$$

and where the eigenvalues $\tilde{\rho}_k$ of the subspace projected state transition matrix

$$\mathbf{H} = \mathbf{P}^{\mathrm{T}}\mathbf{\Phi}(T,0)\mathbf{P} \tag{29}$$

converge towards the eigenvalues ρ_k of $\mathbf{\Phi}(T,0)$ with the largest modulus as the size m of the subspace increases. The subspace eigenvectors $\tilde{\mathbf{w}}_k$ of $\mathbf{H}$ projected back to the full state space converge towards the eigenvectors $\mathbf{w}_k$ of $\mathbf{\Phi}(T,0)$, i.e., $\mathbf{w}_k \approx \mathbf{P}\tilde{\mathbf{w}}_k$.

The Arnoldi algorithm proceeds as follows:

Choose an arbitrary vector $\mathbf{p}_1$ with $|\mathbf{p}_1| = 1$
for $n = 1, 2, \dots, m$
  $\mathbf{a} := \mathbf{\Phi}(T,0)\,\mathbf{p}_n$
    (integration of (15) over $t \in [0;T]$)
  $\mathbf{b} := \mathbf{a}$
  for $j = 1, 2, \dots, n$
    $h_{j,n} := \mathbf{p}_j^{\mathrm{T}}\mathbf{a}$
    $\mathbf{b} := \mathbf{b} - h_{j,n}\mathbf{p}_j$
  end
  if $n < m$
    $h_{n+1,n} := |\mathbf{b}|$
    $\mathbf{p}_{n+1} := \mathbf{b}/h_{n+1,n}$
  end
  $\mathbf{p}_{n+1} := \mathbf{p}_{n+1} - \sum_{j=1}^{n}(\mathbf{p}_j^{\mathrm{T}}\mathbf{p}_{n+1})\mathbf{p}_j$
end

The last step in the n-loop is an explicit reorthogonalisation to eliminate an otherwise progressing skewness of the subspace basis and thereby ensure convergence of the algorithm [12]. Note that $\mathbf{H}$ with components $h_{j,n}$, $n = 1, \dots, m$, $j = 1, \dots, n$, is an upper Hessenberg matrix for which there exist efficient eigenvalue solvers. In practice the Arnoldi algorithm is continued until a desired number of eigenvalues $\tilde{\lambda}_k$ with largest modulus and their corresponding eigenvectors $\mathbf{P}\tilde{\mathbf{w}}_k$ of the state transition matrix $\mathbf{\Phi}(T,0)$ are converged to within a specific tolerance.

To construct the approximations to the periodic mode shapes (22), the $m \times m$ fundamental solution matrix $\tilde{\varphi}$ to the subspace projected system equations is written as

$$\tilde{\boldsymbol{\varphi}} = \mathbf{P}^{\mathrm{T}}\begin{bmatrix}\boldsymbol{\varphi}_1 & \boldsymbol{\varphi}_2 & \dots & \boldsymbol{\varphi}_m\end{bmatrix} \tag{30}$$

where $\boldsymbol{\varphi}_j$ is the solution of the full system (15) integrated over $t \in [0;T]$ for each initial condition $\mathbf{p}_j$, whereby $\tilde{\boldsymbol{\varphi}}(0) = \mathbf{I}$ due to (28). The eigenvectors $\tilde{\mathbf{v}}_k$ of the subspace projected monodromy matrix $\tilde{\mathbf{C}} = \tilde{\varphi}^{-1}(0)\tilde{\varphi}(T)$ are therefore identical to the eigenvectors $\tilde{\mathbf{w}}_k$ of the subspace projected state transition matrix (29). The periodic mode shapes in the subspace are therefore similar to Equation (22) given by

$$\tilde{\mathbf{u}}_k = \tilde{\varphi}\tilde{\mathbf{w}}_k \mathrm{e}^{-\tilde{\lambda}_k t} \tag{31}$$

which by projection back into the full state space using $\mathbf{u}_k = \mathbf{P}\tilde{\mathbf{u}}_k$ yields the approximated periodic mode shapes of the full system

$$\mathbf{u}_k \approx \begin{bmatrix}\boldsymbol{\varphi}_1 & \boldsymbol{\varphi}_2 & \dots & \boldsymbol{\varphi}_m\end{bmatrix}\tilde{\mathbf{w}}_k \mathrm{e}^{-\tilde{\lambda}_k t} \tag{32}$$

where $\tilde{\mathbf{w}}_k$ and $\tilde{\lambda}_k$ are the eigenvectors and characteristic exponents of $\mathbf{H}$, respectively.

3.4 Partial Floquet analysis

Partial Floquet analysis [23] is a system identification technique that operates on signals with the free response of the system, thus no knowledge of the system equations is necessary. The signals can be obtained by numerical simulation or from measurements.

Singular value decomposition is used to eliminate noise and extract the frequency and damping of the most dominant modes from a matrix similar to the monodromy matrix assembled from a limited number of signals spanning several periods. The entries in this matrix can only be sampled once per period for periodic systems, which limits the accuracy because the signal damps away, decreasing the signal to noise ratio. Time-invariant systems can, however, be sampled once per time step. Therefore, partial Floquet analysis is combined with Coleman transformation of the signals [26], such that the response resembles that of a time-invariant system. This approach increases the accuracy and the number of modes that can be extracted from a given signal. However, a careful choice of forcing, that excites all modes of interest to a sufficient level, is necessary to extract these modes accurately.

4 Numerical results

The modal analysis methods described in the previous sections are applied to a BHawC model of a

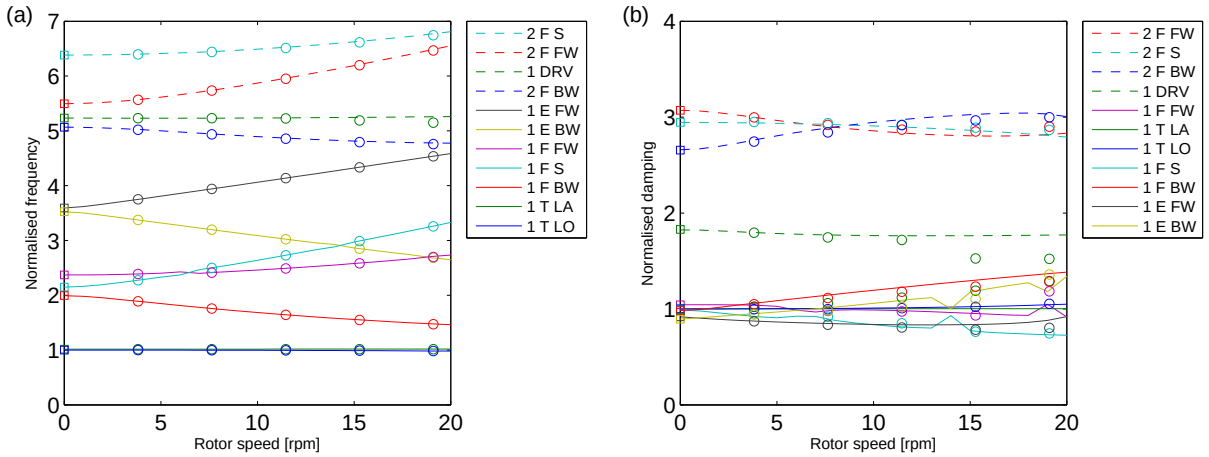

Figure 2: Frequency (a) and damping (b) as function of rotor speed. Standstill eigenvalue analysis (squares), Coleman approach (lines), partial Floquet analysis (circles). Legend entries are ordered after the sequence at 0 rpm.

2.3 MW wind turbine with three 45 m blades, hub height 80 m and nominal speed 16 rpm. The model has 381 structural degrees of freedom.

4.1 Isotropic system

The turbine is mounted with identical blades and runs in vacuum neglecting gravity forces, so the system is isotropic. The deflection of the blades due to centrifugal forces is therefore constant in the blade frame. The constant steady state is found at a given azimuth position by solving Equation (1) statically, including centrifugal forces from the constant rotor speed. In this way a steady state with no transients is obtained, and the system matrices become exactly periodic.

4.1.1 Coleman transformation approach

Because the system is isotropic, a modal analysis can be performed on the Coleman transformed system matrix. The system matrices $\mathbf{M}$, $\mathbf{C}$ and $\mathbf{K}$ from Equation (4) are extracted at a single azimuth angle and combined into the Coleman transformed system matrix of Equation (9) from which the modal frequencies, damping and eigenvectors given in the inertial frame are extracted. The time-invariance of the system matrix is checked by calculation for several azimuth angles.

Figure 2(a) shows the lowest modal frequencies as function of rotor speed where the frequency is normalised with the lowest modal frequency at 0 rpm. The modes are named according to their dominant motion determined from the eigenvector and the whirling amplitudes calculated from equations (13) and (14). The mode labels in Figure 2 first contain the index of that particular mode; then 'T' for tower, 'F' for blade flapwise, 'E' for blade edgewise or 'DRV' for drivetrain; then 'LO' for longitudinal, 'LA' for lateral, 'BW' for backward whirling, 'FW' for forward whirling or 'S' for symmetric. For comparison, frequencies extracted from time simulations with the nonlinear BHawC model using the partial Floquet method [26] are also shown. The agreement is within 0.4% except for modes coupling to the drivetrain, i.e., the drivetrain, edgewise, and lateral tower modes, where the discrepancy is up to 2% at the highest rotor speed, which is caused by a difficulty with keeping the rotor speed exactly constant in the nonlinear simulation due to the energy dissipated in the oscillation.

Figure 2(b) shows the damping as function of rotor speed where the logarithmic decrement is normalised with the value for the first tower longitudinal mode at 0 rpm. The agreement in damping between the results from the linear model and the partial Floquet analysis applied to the nonlinear model is within 6%, except for a discrepancy of up to 20% for modes coupling to the drivetrain. It must be noted that the purely structural damping of the modes is small, and thus a small absolute difference leads to a high relative difference. The results also show that damping is more difficult to estimate than frequency using system identification.

4.1.2 Implicit Floquet analysis

For the implicit Floquet analysis the system matrices in global coordinates in Equation (4) are extracted from the steady state at 16 azimuth an-

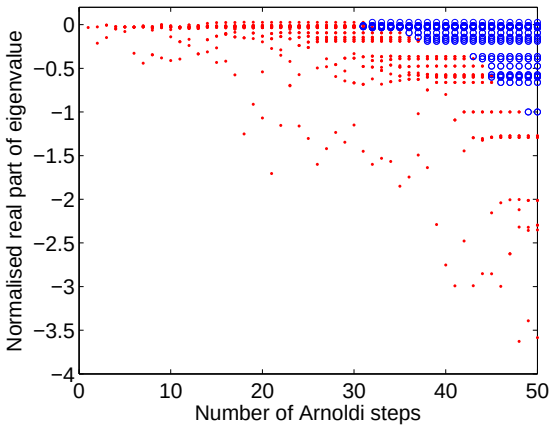

Figure 3: Magnitude of implicit Floquet characteristic multipliers as function of steps in Arnoldi algorithm. • non-converged eigenvalues, ○ converged eigenvalues.

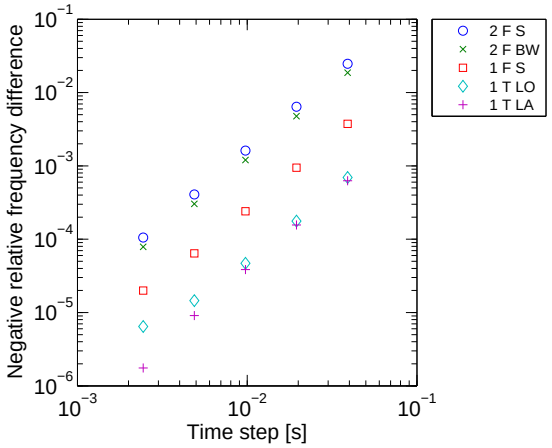

Figure 4: Relative difference in implicit Floquet frequency compared to Coleman approach frequency for selected modes as function of implicit Floquet integration time step.

gles equally spaced over a rotor rotation. For interpolation to other azimuth angles a least squares fit of a truncated Fourier series with 8 terms is used. The fundamental solutions in Equation (30) are integrated with a Newmark-type solver from initial conditions determined by the Arnoldi algorithm. The principal frequencies and damping are found from Equation (20) where ρ_k are taken as the eigenvalues of the approximated state transition matrix. Figure 3 shows the real part σ_k of the characteristic exponents calculated at each Arnoldi step for a steady state at 12 rpm using a time step of $\Delta t = T/1024 = 0.0049\,\mathrm{s}$. The scattering of the highest damping values shows that the highest damped modes are spurious and do not represent actual eigenmodes of the system due to the approximate nature of the implicit Floquet analysis. To exclude these modes from the results, only modes satisfying a strict convergence criterion, where the absolute change of both damping σ_k and principal frequency $\omega_{\mathrm{p},k}$ is less than 10^{-10} between three successive steps, are retained. After 50 Arnoldi steps 19 modes are converged. The modal frequencies are determined using Equation (21) by adding $j_k\Omega$ to the principal frequency, where $j_k\Omega$ is the single non-vanishing harmonic component in a Fourier transform of the periodic mode shape for degrees of freedom on the tower calculated from Equation (32) using the principal frequency $\omega_{\mathrm{p},k}$. The periodic mode shape components for degrees of freedom on the tower and nacelle calculated with the modal frequency ω_k are thus constant. A detailed description of the process of frequency identification is given in [24].

Figure 4 shows the difference in frequency calculated with the Coleman transformation approach and the implicit Floquet analysis with different integration time steps. The implicit Floquet results converge towards the Coleman transformation results for decreasing time steps, the error being roughly proportional to Δt^2. Predominantly the error increases with the modal frequency. A similar trend is seen for the damping.

Figure 5 shows the dominant harmonic components $\boldsymbol{\mathcal{U}}_{jk}$ in Equation (24) for the first flapwise forward whirling mode shape. The blade mode shape is transformed into substructure coordinates using Equation (5) and contains the rigid body motion of the hub. The zoom factor in the lower right corner indicates how much each component has been enlarged. The ground fixed components in the mode shape are constant, consistent with the solution from the Coleman transformation approach. The mode shape for the blade has harmonic components at $j = -1, 0, 1$, corresponding to the forward whirling, symmetric, and backward whirling components, respectively, in the Coleman transformation approach. Thus, in a pure excitation of this mode at 12 rpm, according to Equation (24) the tower vibrates with the normalised modal frequency $\omega' = 2.8$, and the blades dominantly vibrate with $\omega' - \Omega' = 2.2$ (FW), and to a lesser extent with $\omega' + \Omega' = 3.3$ (BW) and $\omega' = 2.8$ (S) (see Figure 2(a)).

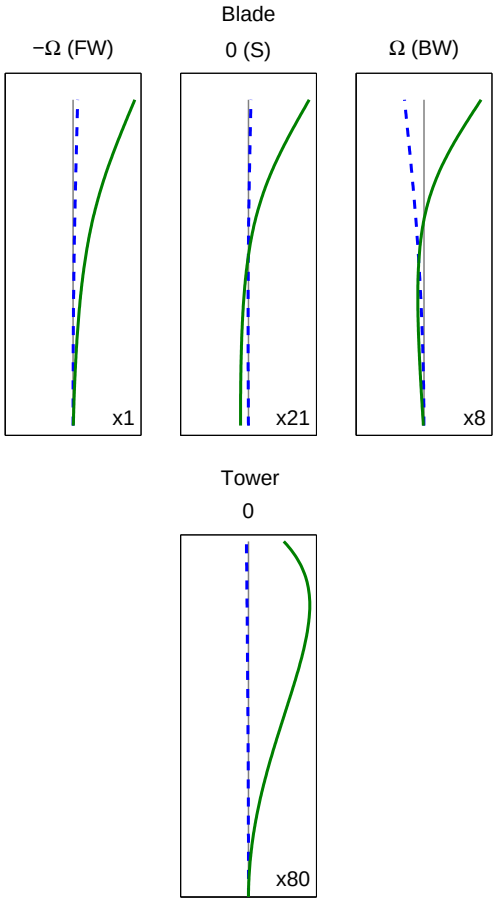

Figure 5: Amplitudes of harmonic components of the first flapwise forward whirling periodic mode shape for the isotropic rotor. Blades (top) — flapwise and - - edgewise, and tower (bottom) — longitudinal and - - lateral.

4.2 Anisotropic system

To investigate the effects of an anisotropic rotor on the modal properties, a mass of 485 kg due to ice coverage defined by DIN-1055-5 [27] is added along the length of blade 1. Figure 6 shows the resulting steady state when running the turbine at 16 rpm with a 10 m/s uniform wind field perpendicular to the rotor plane. Note that the wind is used only to drive the rotor and the modal analysis is still purely structural. The steady state varies periodically both for the tower and the blades, and the blade motion for blade 1 is different from that of blades 2 and 3. The steady state is determined from a time simulation until transients have damped away and system matrices are then extracted at each time step of the steady state simulation and interpolated onto integration time points using a truncated Fourier series with 8 terms. The implicit Floquet

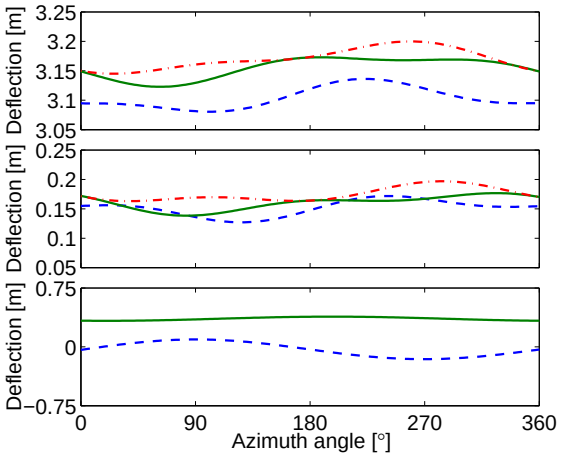

Figure 6: Steady state over one rotor period for the anisotropic rotor at 16 rpm. Blade tips flapwise (top) - - 1, — 2 and -·- 3 and edgewise (middle) - - 1, — 2 and -·- 3, and blade tips, tower top (bottom) — longitudinal and - - lateral.

analysis is carried out with an integration time step of $T/1024 = 0.0037$ s as described for the isotropic case. The frequencies are up to 4% lower than in the isotropic case due to the added mass on one blade. The change in damping is slightly more pronounced, up to a 17% decrease for the second flapwise forward whirling mode.

Figure 7 shows the harmonic components $\boldsymbol{u}_{jk}$ with frequencies $j\Omega$ of the first flapwise forward whirling mode shape for the tower and blade 1. The tower mode shape now has several harmonic components compared to only one in the isotropic case. The component at $j = 0$ is similar in shape to the corresponding one for the isotropic case, but now the dominant component is at $j = -2$, and there is also a significant component at $j = -1$.

For the mode shape of blade 1 the harmonic components at $j = -1, 0, 1$ are similar to the corresponding ones in the isotropic case. However, now the amplitude of the dominant flapwise component at $j = -1$ for blade 1 is three times as high as for blades 2 and 3, and blades 2 and 3 move close to in-phase and in counter-phase with blade 1, as shown in Figure 8. Thus, in a pure excitation of this mode the tower now vibrates dominantly with the normalised frequency $\omega' - 2\Omega' = 1.6$ in addition to the component at $\omega' = 2.8$. Blade 1 vibrates dominantly at $\omega' - \Omega' = 2.2$ as for the isotropic case and notably at $\omega' - 2\Omega' = 1.6$, $\omega' - 3\Omega' = 1.0$ and $\omega' + 3\Omega' = 4.5$ in addition to $\omega' + \Omega' = 3.3$ and $\omega' = 2.8$ as for the isotropic case.

The identification of the first flapwise forward whirling modal frequency is not done by making the

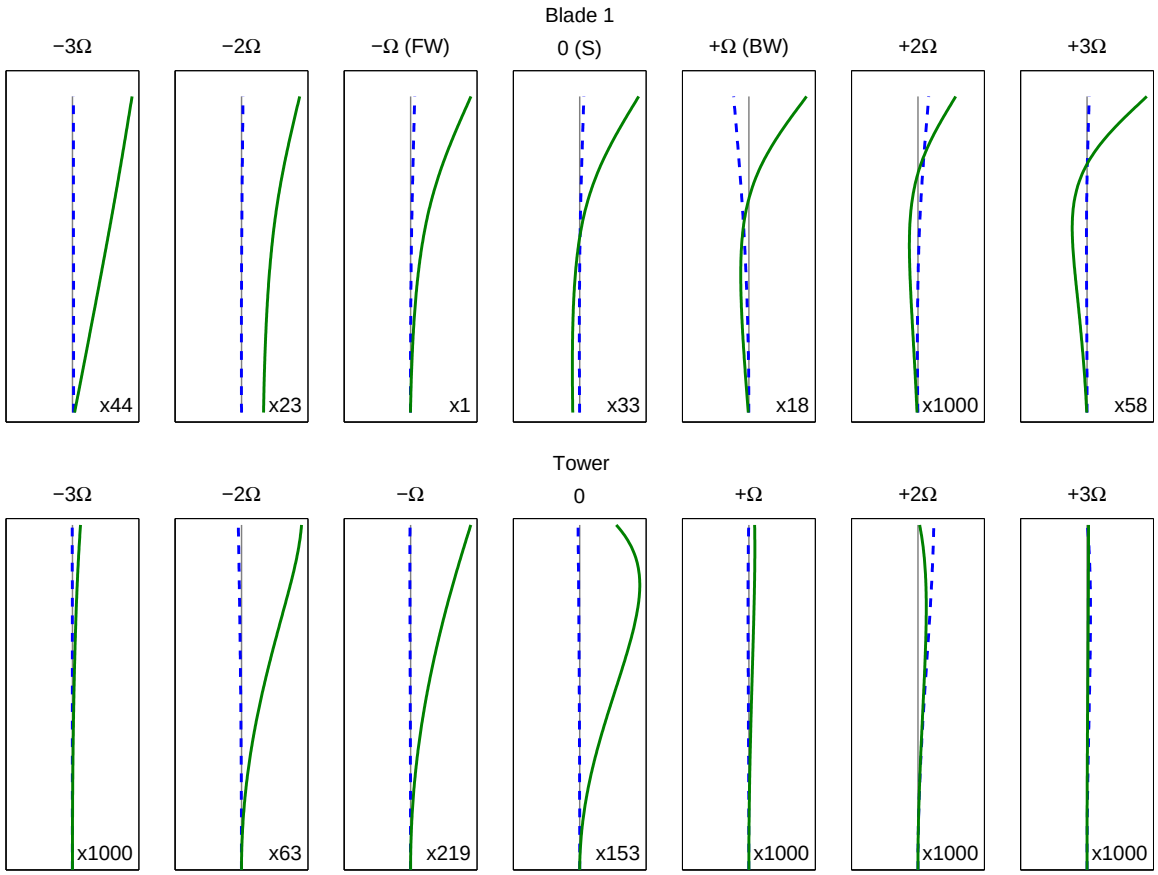

Figure 7: Amplitudes of harmonic components of the first flapwise forward whirling periodic mode shape for the anisotropic rotor with one blade covered with ice. Blade 1 (top) — flapwise, - - edgewise, and tower (bottom) — longitudinal and - - lateral.

tower mode shape as constant as possible, as in the isotropic case. Rather, the modal frequency is chosen to be close to the one for the similar mode in the isotropic case. A more suitable criterion to give this result is to require that the mode shape with the rotor degrees of freedom in multi-blade coordinates be as constant as possible [28].

The rotor with one ice-covered blade is an example of how an isotropic rotor can change the modal dynamics of the system. Other influences that could cause a similar behaviour is rotor stiffness unbalance, gravity loads, yaw error, and wind shear. A two-bladed rotor is inherently anisotropic and requires a general approach like Floquet analysis.

5 Discussion

This paper has presented several different methods for structural modal analysis of wind turbines. The Coleman approach is simple and fast, and its basis in a physical coordinate transformation means that the results are easily interpreted. Its speed makes it useful for doing parameter studies early in the design process. But it is only applicable to isotropic systems. Floquet analysis can be applied to examine special cases where anisotropic effects are suspected to change the modal parameters. The implicit Floquet analysis is an efficient implementation of Floquet analysis for systems with many degrees of freedom. In the example given, the most important modes are extracted after 50 integrations of the system over a rotor period, whereas 762 integrations would be needed for a classical Floquet analysis. Finally, the partial Floquet analysis, or another means of system identification, is useful to check the validity of the linearisation.

The work presented in this paper is part of an ongoing effort to obtain a full aeroelastic linear model of the nonlinear code BHawC. The approach presented in this paper is readily extendable to a linear aeroelastic model. The linear model will aid

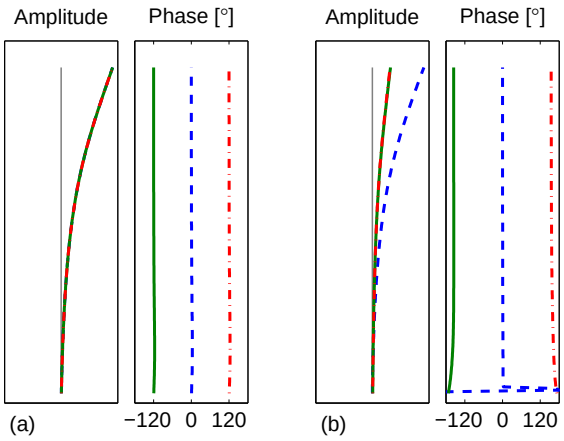

Figure 8: Amplitudes and phases of the harmonic component at $j = -1$ of the first flapwise forward whirling periodic mode shape for the isotropic rotor (a) and the anisotropic rotor (b). Blades - - 1, — 2 and -·- 3.

in the understanding of the loads obtained from a nonlinear response, of which many features can be explained from the linear modes.

6 Conclusion

Tangent matrices for structural modal analysis are extracted directly from the nonlinear model of a wind turbine in a steady state. When the system is isotropic the preferred approach is to use the Coleman transformation for describing the equations of motion in the inertial frame allowing direct eigenvalue analysis to extract the modal frequencies, damping, and mode shapes. When the system is anisotropic, implicit Floquet analysis, that reduces the computational burden associated with classical Floquet analysis, is applied to yield the lowest damped eigenmodes. The linearised model is validated from numerical results for a three-bladed turbine, showing a reasonable agreement for the frequencies and the damping between the Coleman approach and partial Floquet analysis on the response of the nonlinear model for modes not related to the drivetrain. The implicit Floquet results converge to the results from the Coleman approach with the deviation in frequency and damping roughly proportional to the square of the integration time step and increasing with the modal frequency. This finding shows the importance of precise time integration in implicit Floquet analysis. An analysis applied to an anisotropic system with one blade covered with ice shows a decrease in frequency up to 3% and changes in damping within 17%. It also reveals multiple harmonic components in the response of a single mode which will show up in measurements.

Acknowledgment

This work has been partially supported by the Danish Ministry of Science, Technology, and Innovation through the Industrial PhD programme.

References

[1] T.J. Larsen and A.M. Hansen. How 2 HAWC2, the user's manual. Technical Report Risø-R-1597(EN), Risø National Laboratory, Roskilde, Denmark, 2007.

[2] V.A. Riziotis and S.G. Voutsinas. Fatigue loads on wind turbines of different control strategies operating in complex terrain. *Journal of Wind Engineering and Industrial Aerodynamics*, 85(3):211–240, 2000.

[3] R. Rubak and J.T. Petersen. Monopile as part of aeroelastic wind turbine simulation code. In *Proceedings of Copenhagen Offshore Wind*, Denmark, October 2005.

[4] V.A. Riziotis, S.G. Voutsinas, E.S. Politis, and P.K. Chaviaropoulos. Aeroelastic stability of wind turbines: The problem, the methods and the issues. *Wind Energy*, 7(4):373–392, 2004. DOI:10.1002/we.133

[5] T.G. van Engelen and H. Braam. TURBU offshore, computer program for frequency domain analysis of horizontal axis offshore wind turbines. Technical Report ECN-C–04-079, Energy Research Centre of the Netherlands, 2004.

[6] M.H. Hansen. Aeroelastic stability analysis of wind turbines using an eigenvalue approach. *Wind Energy*, 7:133–143, 2004. DOI:10.1002/we.116

[7] G. Bir and J. Jonkman. Aeroelastic instabilities of large offshore and onshore wind turbines. *Journal of Physics: Conference Series*, 75(1), 2007.

[8] B. Kirchgässner. ARLIS – a program system for aeroelastic analysis of rotating linear systems. In *Proceedings of European Wind Energy Conference*, pages 253–258, Hamburg, Germany, 1984.

[9] H.G. Matthies and C. Nath. Dynamic stability of periodic solutions of large scale nonlinear

systems. *Computer Methods in Applied Mechanics and Engineering*, 48(2):191–202, 1985.

[10] K. Stol, M. Balas, and G. Bir. Floquet modal analysis of a teetered-rotor wind turbine. *Journal of Solar Energy Engineering*, 124:364–371, 2002.

[11] D.A. Peters. Fast Floquet theory and trim for multi-bladed rotorcraft. *Journal of the American Helicopter Society*, 39(4):82–89, 1994.

[12] O.A. Bauchau and Y.G. Nikishkov. An implicit Floquet analysis for rotorcraft stability evaluation. *Journal of the American Helicopter Society*, 46(3):200–209, 2001.

[13] K.A. Stol, H.-G. Moll, G. Bir, and H. Namik. A comparison of multi-blade coordinate transformation and direct periodic techniques for wind turbine control design. In *Proceedings of 47th AIAA Aerospace Sciences Meeting*, Orlando FL, USA, 2009.

[14] G.H. James III, T.G. Carne, and J.P. Lauffer. The natural excitation technique (NExT) for modal parameter extraction from operating wind turbines. Technical Report UC-261, Sandia National Laboratories, 1993.

[15] B. Marrant and Th. van Holten. System identification for the analysis of aeroelastic stability of wind turbine blades. In *Proceedings of European Wind Energy Conference*, London, UK, 2004.

[16] P.J. Murtagh and B. Basu. Identification of equivalent modal damping for a wind turbine at standstill using fourier and wavelet analysis. *Proceedings of the Institution of Mechanical Engineers, Part K: Journal of Multi-body Dynamics*, 221(4):577–589, 2007. DOI:10.1243/14644193JMBD90

[17] P.F. Skjoldan. *Aeroelastic modal dynamics of wind turbines including anisotropic effects*. PhD thesis, Technical University of Denmark, to be submitted.

[18] P.E. Nikravesh. *Computer-Aided Analysis of Mechanical Systems*. Prentice-Hall, New Jersey, 1988.

[19] W. Johnson. *Helicopter Theory*. Dover Publications, 1980.

[20] M.H. Hansen. Aeroelastic instability problems for wind turbines. *Wind Energy*, 10(6):551–577, 2007. DOI:10.1002/we.242

[21] M.H. Hansen. Improved modal dynamics of wind turbines to avoid stall-induced vibrations. *Wind Energy*, 6:179–195, 2003. DOI:10.1002/we.79

[22] L. Meirovitch. *Methods of Analytical Dynamics*. McGraw-Hill, New York, 1970.

[23] O.A. Bauchau and J. Wang. Efficient and robust approaches to the stability analysis of large multibody systems. *Journal of Computational and Nonlinear Dynamics*, 3, 2008. DOI:10.1115/1.2397690

[24] P.F. Skjoldan and M.H. Hansen. On the similarity of the Coleman and Lyapunov-Floquet transformations for modal analysis of bladed rotor structures. *Journal of Sound and Vibration*, 327:424–439, 2009. DOI:10.1016/j.jsv.2009.07.007

[25] G.H. Golub and C.F. van Loan. *Matrix Computations*. The Johns Hopkins University Press, Baltimore, MD, 3rd edition, 1996.

[26] P.F. Skjoldan and O.A. Bauchau. Determination of modal parameters in complex nonlinear systems. *Journal of Nonlinear and Computational Dynamics*, 2010. Accepted for publication.

[27] Richtlinie für Windenergieanlagen. Directive Reihe B, Heft 8, Deutsches Institut für Bautechnik, Berlin, Germany, 2004.

[28] P.F. Skjoldan. Modal dynamics of wind turbines with anisotropic rotors. In *Proceedings of 47th AIAA Aerospace Sciences Meeting*, Orlando FL, USA, 2009.

P4

Effects of extreme wind shear on aeroelastic modal damping of wind turbines

Wind Energy. Accepted for publication, submitted in revised form 28th February 2011.

Effects of extreme wind shear on aeroelastic modal damping of wind turbines

P. F. Skjoldan
Loads, Aerodynamics, and Control,
Siemens Wind Power A/S,
Dybendalsvænget 3, DK-2630 Taastrup, Denmark

M. H. Hansen
Wind Energy Division,
National Laboratory for Sustainable Energy, Risø DTU,
Frederiksborgvej 399, DK-4000 Roskilde, Denmark

February 28, 2011

Abstract

Wind shear is an important contributor to fatigue loads on wind turbines. Because it causes an azimuthal variation in angle of attack, it can also affect aerodynamic damping. In this paper a linearised model of a wind turbine, based on the nonlinear aeroelastic code BHawC, is used to investigate the effect of wind shear on the modal damping of the turbine. In isotropic conditions with a uniform wind field the modal properties can be extracted from the system matrix transformed into the inertial frame using the Coleman transformation. In shear conditions an implicit Floquet analysis, which reduces the computational burden associated with classical Floquet analysis, is used for modal analysis.

The methods are applied to a 2.3 MW three-bladed pitch-regulated wind turbine showing a difference in damping between isotropic and extreme shear conditions at rated wind speed when the turbine is operating closest to stall. The first longitudinal tower mode decreases slightly in damping while the first flapwise backward whirling and symmetric modes increase in damping. This change in damping is attributed to an interaction between the periodic blade mode shapes and the azimuth-dependent local aerodynamic damping in the shear condition caused by a beginning separation of the flow.

1 Introduction

This paper investigates the changes in modal damping of wind turbines caused by operation in conditions with extreme wind shear. Wind shear is an important factor in the periodic loading of a wind turbine contributing to the fatigue loads. It also gives an azimuthal variation in the inflow angle which affects the aerodynamic damping [1], particularly if the slope of the lift curve varies at the angles of attack experienced.

Wind turbine stability tools for calculation of the modal frequencies and damping most often do not take into account anisotropic effects like wind shear but to varying degrees assume isotropy. The rotor is in this context defined as isotropic if it has three or more identical and symmetrically mounted blades [2]. The external conditions are defined as isotropic if the wind profile is constant in time, uniform, and aligned in tilt and yaw to be perpendicular to the rotor plane, and if gravity and other asymmetric external forces are absent.

Most recent stability tools [3, 4, 5, 6] use the Coleman transformation to describe the equations of motion in the inertial frame, which renders the system equations time-invariant by eliminating the periodic terms caused by the rotor rotation, if the rotor and the external conditions are isotropic. Other researchers use Floquet analysis to include anisotropic effects in the modal analysis of two-bladed wind turbines [7, 8], which have an inherently anisotropic rotor, and of three-bladed wind turbines in anisotropic conditions [9].

Floquet analysis is demanding due to the heavy computational burden required by multiple integrations of the equations of motion over a period of rotation of the rotor, and due to the non-uniqueness of the determined frequencies. The issue of computation time is addressed in Fast Floquet Theory [10], where only one third of the integrations is necessary for a three-bladed isotropic rotor, and by implicit Floquet analysis [11], which extracts the least damped modes after a limited number of integrations. The non-uniqueness of the frequency is a consequence of the applicability of Floquet analysis to anisotropic conditions, and it can be resolved in isotropic and moderately anisotropic conditions, without ambiguity, by analysing the frequency content of the corresponding periodic mode shape [2, 7, 12].

The authors compare the Coleman transformation approach to Floquet analysis [2, 13], showing the existence of additional harmonic components in the periodic mode shape when the rotor is anisotropic. Stol et al. [9] examine anisotropic conditions due to operation in wind shear and idling in a yawed condition, and they

find small differences in modal damping between a Floquet analysis and an approximate solution based on the Coleman transformation.

This paper builds on a recent approach to structural modal analysis [13] and extends it to include aerodynamics. The structural linear equations of motion are extracted directly from the nonlinear finite element-based aeroelastic tool BHawC, and the aerodynamic force and unsteady aerodynamic equations are linearised numerically. The modal analysis is performed using the Coleman approach in isotropic conditions and using implicit Floquet analysis in both isotropic conditions and anisotropic conditions with wind shear. The effects of extreme wind shear are examined on a model of a three-bladed pitch-regulated 2.3 MW wind turbine, showing a small increase in damping of the first flapwise backward whirling and symmetric modes and a slight decrease in damping of the first longitudinal tower mode owing to the interaction between azimuth-dependent local aerodynamic damping, caused by the wind shear, and the periodic mode shape.

Section 2 describes the BHawC structural and aerodynamic modelling and linearisation. Section 3 summarises the Coleman approach and implicit Floquet analysis applied to this model. Section 4 presents the results of the modal analysis, and section 5 contains the conclusions.

2 Aeroelastic model

The first step in a modal analysis is to obtain a steady state, which possibly varies periodically with the rotor period. In the present work it is calculated with the aeroelastic code BHawC. The second step is the linearisation of the system equations to describe small perturbations to the steady state.

2.1 Steady state configuration

In BHawC [13, 14], the configuration of the system, defined by nodal positions $\mathbf{p}$ and orientations $\mathbf{q}$, nodal velocities $\dot{\mathbf{u}}$ and nodal accelerations $\ddot{\mathbf{u}}$, must satisfy the equilibrium equation in global coordinates given as

$$\mathbf{f}_{\text{iner}}(\mathbf{p},\mathbf{q},\dot{\mathbf{u}},\ddot{\mathbf{u}}) + \mathbf{f}_{\text{damp}}(\mathbf{q},\dot{\mathbf{u}}) + \mathbf{f}_{\text{int}}(\mathbf{p},\mathbf{q}) = \mathbf{f}_{\text{a}}(\mathbf{p},\mathbf{q},\dot{\mathbf{u}},\mathbf{a}) + \mathbf{f}_{\text{ext}} \tag{1}$$

where $\dot{(\,)} = \mathrm{d}/\mathrm{d}t$ denotes a time derivative and $\mathbf{f}_{\text{iner}}$, $\mathbf{f}_{\text{damp}}$, $\mathbf{f}_{\text{int}}$, and $\mathbf{f}_{\text{a}}$ are the inertial, damping, internal (elastic), and aerodynamic force vectors, respectively, and $\mathbf{f}_{\text{ext}}$ includes other external forces, e.g., gravity. The aerodynamic force depends on the structural degrees of freedom through the relative wind velocity vector in the airfoil frame and the transformation of the force into the global frame, as well as the aerodynamic state vector $\mathbf{a}$ describing the flow.

In BHawC the aerodynamic force $\mathbf{f}_{\text{a}}$ is determined using a Beddoes-Leishman-type unsteady aerodynamic model [15] in a number of aerodynamic calculation points positioned on each blade independently of the structural nodes. In the present work, the unsteady model is reduced to include the effects of trailing edge separation alone, thereby making it equivalent to the Øye dynamic stall model [16]. This effect is described by the position of the separation point f, related to the lift coefficient C_L as

$$C_L = C_{L,\text{fa}}(\alpha) f + C_{L,\text{fs}}(\alpha)(1-f) \tag{2}$$

where $C_{L,\text{fa}}$ is the lift curve for fully attached flow, $C_{L,\text{fs}}$ is the lift curve for fully separated flow, and α is the angle of attack. The stationary value of the separation point position $f_{\text{st}}(\alpha)$ can be calculated as f from Equation (2) by replacing C_L with $C_{L,\text{st}}(\alpha)$. The dynamics of the separation point position are modelled as

$$\dot{f} = \frac{2W}{\tau_{\text{f}} c}(f_{\text{st}}(\alpha) - f) \tag{3}$$

where W is the relative wind speed, c is the chord length, and τ_{f} is a time constant representing the lag in the boundary layer. Equation (3) is linear in f but nonlinear in $\mathbf{u}$ and $\dot{\mathbf{u}}$ because of their influence on the relative wind speed and the stationary separation point position through the angle of attack. The dynamic drag coefficient is determined as the induced drag due to the change in lift [15] as

$$C_D = C_{D,\text{st}}(\alpha) + \left(C_L - C_{L,\text{st}}(\alpha) - \eta_c C_{L,\text{st}}(\alpha)\left(\sqrt{f} - \sqrt{f_{\text{st}}(\alpha)}\right)\cos(\alpha)\right)\sin(\alpha) \tag{4}$$

where η_c is an efficiency factor.

To find an equilibrium configuration of the model satisfying Equation (1), increments of the positions and orientations $\delta\mathbf{u}$, velocities $\delta\dot{\mathbf{u}}$, and accelerations $\delta\ddot{\mathbf{u}}$ are found by Newton-Raphson iteration with the structural tangent relation determined from the variation of Equation (1) as

$$\mathbf{M}(\mathbf{q})\delta\ddot{\mathbf{u}} + \mathbf{C}(\mathbf{q},\dot{\mathbf{u}})\delta\dot{\mathbf{u}} + \mathbf{K}(\mathbf{p},\mathbf{q},\dot{\mathbf{u}},\ddot{\mathbf{u}})\delta\mathbf{u} = \mathbf{r} \tag{5}$$

where $\mathbf{M}$, $\mathbf{C}$, and $\mathbf{K}$ are the mass, damping/gyroscopic, and stiffness matrices, respectively, and $\mathbf{r} = \mathbf{f}_\mathrm{a} + \mathbf{f}_\mathrm{ext} - \mathbf{f}_\mathrm{iner} - \mathbf{f}_\mathrm{damp} - \mathbf{f}_\mathrm{int}$ is the residual. The iteration is continued until $\mathbf{r} \approx \mathbf{0}$. This equation can be used to find a periodic steady state configuration, which in isotropic conditions is characterised by constant deflections of the structure, constant rotor speed Ω, and constant position of the separation point. The steady state can be determined for different azimuth angles as a stationary solution to Equation (1) including centrifugal and aerodynamic forces determined from the constant rotation of the rotor. The steady state in anisotropic conditions is characterised by general periodic motion with period T, which then defines the *mean* rotor speed $\Omega = 2\pi/T$. This steady state cannot be determined at a single azimuth angle independently because the inertia and damping forces depend on the periodic motion. Rather, it is necessary to consider the whole rotor period at once, e.g., by use of a finite difference method. This approach is complex for a large model and is not attempted here. Instead, a time simulation in BHawC is carried out until the transients are sufficiently damped away, giving an approximation to the periodic steady state. In this paper the anisotropic condition is caused by the wind shear, but it can also include cyclic pitch.

2.2 Linearised motion

A linearised modal analysis considers small perturbations in structural position and orientation $\mathbf{y}$, velocity $\dot{\mathbf{y}}$, and acceleration $\ddot{\mathbf{y}}$, and in separation point position $\mathbf{x}$ and velocity $\dot{\mathbf{x}}$ to the steady state configuration $(\mathbf{p}_\mathrm{ss}, \mathbf{q}_\mathrm{ss}, \dot{\mathbf{u}}_\mathrm{ss}, \ddot{\mathbf{u}}_\mathrm{ss}, \mathbf{a}_\mathrm{ss}, \dot{\mathbf{a}}_\mathrm{ss})$ with constant mean rotor speed Ω. In this configuration $\mathbf{p}_\mathrm{ss}$, $\mathbf{q}_\mathrm{ss}$, $\dot{\mathbf{u}}_\mathrm{ss}$, and $\ddot{\mathbf{u}}_\mathrm{ss}$ are the periodic steady state structural positions, orientations, velocities, and accelerations, respectively, and $\mathbf{a}_\mathrm{ss}$ and $\dot{\mathbf{a}}_\mathrm{ss}$ contain the periodic steady state positions and velocities, respectively, of the separation point in all calculation points.

The aerodynamic force can be drawn out from the residual in Equation (5) and linearised about the steady state as

$$\mathbf{f}_\mathrm{a} = \mathbf{f}_\mathrm{a,ss} + \frac{\partial \mathbf{f}_\mathrm{a}}{\partial \mathbf{y}}\mathbf{y} + \frac{\partial \mathbf{f}_\mathrm{a}}{\partial \dot{\mathbf{y}}}\dot{\mathbf{y}} + \frac{\partial \mathbf{f}_\mathrm{a}}{\partial \mathbf{x}}\mathbf{x} \tag{6}$$

such that the linearised structural equations of motion for small-amplitude motion about the steady state from Equation (5) become

$$\mathbf{M}\,\ddot{\mathbf{y}} + (\mathbf{C} + \mathbf{C}_\mathrm{a})\dot{\mathbf{y}} + (\mathbf{K} + \mathbf{K}_\mathrm{a})\mathbf{y} + \mathbf{A}_\mathrm{f}\mathbf{x} = \mathbf{0} \tag{7}$$

with the aerodynamic damping matrix written as $\mathbf{C}_\mathrm{a} = -\partial \mathbf{f}_\mathrm{a}/\partial \dot{\mathbf{y}}$, the aerodynamic stiffness matrix as $\mathbf{K}_\mathrm{a} = -\partial \mathbf{f}_\mathrm{a}/\partial \mathbf{y}$, and the aerodynamic flow coupling matrix as $\mathbf{A}_\mathrm{f} = -\partial \mathbf{f}_\mathrm{a}/\partial \mathbf{x}$, all evaluated at the steady state. In the present work a numerical linearisation is preferred to an analytical one because of the fairly complicated dependence of the relative wind velocity on the structural degrees of freedom, and in order to make the linearisation independent of the implementation of the aerodynamics. Consequently, the present approach extends to any state-space aerodynamic model. The aerodynamic stiffness matrix is approximated using a one-sided difference scheme with column j calculated as

$$\mathbf{K}_{\mathrm{a},j} \approx -\frac{\mathbf{f}_\mathrm{a}(\mathbf{u}_\mathrm{ss} + \Delta\mathbf{u}_j, \dot{\mathbf{u}}_\mathrm{ss}, \mathbf{a}_\mathrm{ss}) - \mathbf{f}_\mathrm{a}(\mathbf{u}_\mathrm{ss}, \dot{\mathbf{u}}_\mathrm{ss}, \mathbf{a}_\mathrm{ss})}{\Delta u} \tag{8}$$

where $\Delta\mathbf{u}_j$ is the displacement perturbation vector with one non-zero element of magnitude Δu at position j. Similarly, a column of the aerodynamic damping matrix is calculated as

$$\mathbf{C}_{\mathrm{a},j} \approx -\frac{\mathbf{f}_\mathrm{a}(\mathbf{u}_\mathrm{ss}, \dot{\mathbf{u}}_\mathrm{ss} + \Delta\dot{\mathbf{u}}_j, \mathbf{a}_\mathrm{ss}) - \mathbf{f}_\mathrm{a}(\mathbf{u}_\mathrm{ss}, \dot{\mathbf{u}}_\mathrm{ss}, \mathbf{a}_\mathrm{ss})}{\Delta \dot{u}} \tag{9}$$

where $\Delta\dot{\mathbf{u}}_j$ is the velocity perturbation vector with one non-zero element of magnitude $\Delta\dot{u}$ at position j. A column of the aerodynamic flow coupling matrix is calculated as

$$\mathbf{A}_{\mathrm{f},j} \approx -\frac{\mathbf{f}_\mathrm{a}(\mathbf{u}_\mathrm{ss}, \dot{\mathbf{u}}_\mathrm{ss}, \mathbf{a}_\mathrm{ss} + \Delta\mathbf{x}_j) - \mathbf{f}_\mathrm{a}(\mathbf{u}_\mathrm{ss}, \dot{\mathbf{u}}_\mathrm{ss}, \mathbf{a}_\mathrm{ss})}{\Delta x} \tag{10}$$

where $\Delta\mathbf{x}_j$ is the aerodynamic state perturbation vector with one non-zero element of magnitude Δx at position j.

The linearised form of Equation (3) for all aerodynamic calculation points can be written as [5]

$$\dot{\mathbf{x}} + \mathbf{A}_\mathrm{d}\mathbf{x} + \mathbf{C}_\mathrm{ua}\dot{\mathbf{y}} + \mathbf{K}_\mathrm{ua}\mathbf{y} = \mathbf{0} \tag{11}$$

where the aerodynamic system matrix $\mathbf{A}_\mathrm{d}$ is a diagonal matrix obtained analytically from Equation (3) with elements

$$A_{\mathrm{d},i} = \frac{2W_i}{\tau_\mathrm{f} c_i} \tag{12}$$

where i denotes the number of the aerodynamic calculation point. The element (i, j) of the aerodynamic velocity coupling matrix $\mathbf{C}_{\mathrm{ua}}$ is calculated as

$$C_{\mathrm{ua},ij} \approx \frac{2}{\tau_{\mathrm{f}} c_i} \frac{W_i(f_{\mathrm{ss},i} - f_{\mathrm{st},i}) - W_{\mathrm{ss},i}(f_{\mathrm{ss},i} - f_{\mathrm{st,ss},i})}{\Delta \dot{u}} \tag{13}$$

where $W_{\mathrm{ss},i}$ and $f_{\mathrm{st,ss},i}$ are the steady state values of the relative wind speed and stationary separation point position of calculation point number i, respectively, and W_i and $f_{\mathrm{st},i}$ are updated with the perturbation $\Delta\dot{u}$ to $\dot{u}_j$ affecting W_i directly and $f_{\mathrm{st},i}$ through the angle of attack. Similarly, the aerodynamic displacement coupling matrix $\mathbf{K}_{\mathrm{ua}}$ is calculated as

$$K_{\mathrm{ua},ij} \approx \frac{2}{\tau_{\mathrm{f}} c_i} \frac{W_i(f_{\mathrm{ss},i} - f_{\mathrm{st},i}) - W_{\mathrm{ss},i}(f_{\mathrm{ss},i} - f_{\mathrm{st,ss},i})}{\Delta u} \tag{14}$$

where W_i and $f_{\mathrm{st},i}$ are updated with the perturbation Δu to u_j.

3 Modal analysis

A modal analysis extracting the modal frequencies, damping, and mode shapes can be performed using the Coleman approach if the rotor and external conditions are isotropic. In the general case of an anisotropic system Floquet analysis can be used. These two methods are summarised below with the addition of aerodynamics compared to the description in [13].

3.1 Coleman approach

To enable the use of the Coleman transformation, the structural equations of motion in Equation (7) are transformed into substructure coordinates $\mathbf{y}_{\mathrm{T}}$ given by the transformation $\mathbf{y} = \mathbf{T}\,\mathbf{y}_{\mathrm{T}}$, such that the degrees of freedom on each blade are equal in the local blade frame. The aeroelastic system is then transformed into the inertial frame coordinates given by

$$\begin{aligned} \mathbf{y}_{\mathrm{T}} &= \mathbf{B}_{\mathbf{y}} \mathbf{z}_{\mathbf{y}} \\ \mathbf{x} &= \mathbf{B}_{\mathbf{x}} \mathbf{z}_{\mathbf{x}} \end{aligned} \tag{15}$$

where $\mathbf{z}_{\mathbf{y}}$ are the inertial frame structural degrees of freedom, $\mathbf{B}_{\mathbf{y}}$ is the structural inertial frame transformation matrix including the Coleman transformation, $\mathbf{z}_{\mathbf{x}}$ are the inertial frame aerodynamic state variables, and $\mathbf{B}_{\mathbf{x}}$ is the aerodynamic Coleman transformation matrix. The Coleman transformation [17] describes the blade degrees of freedom in multi-blade coordinates by use of 1P harmonic functions. It is periodic with the rotor period such that $\mathbf{B}_{\mathbf{y}}(t+T) = \mathbf{B}_{\mathbf{y}}(t)$ and $\mathbf{B}_{\mathbf{x}}(t+T) = \mathbf{B}_{\mathbf{x}}(t)$.

The first order form inertial frame equations of motion of the aeroelastic system given by Equations (7) and (11) become

$$\dot{\mathbf{z}}_3 = \mathbf{A}_{\mathrm{B}}\, \mathbf{z}_3 \tag{16}$$

where $\mathbf{z}_3 = \{\mathbf{z}_{\mathbf{y}}^{\mathrm{T}}\ \tilde{\mathbf{z}}_{\mathbf{y}}^{\mathrm{T}}\ \mathbf{z}_{\mathbf{x}}^{\mathrm{T}}\}^{\mathrm{T}}$ is the inertial frame state vector with $\tilde{\mathbf{z}}_{\mathbf{y}} = \dot{\mathbf{z}}_{\mathbf{y}} + \bar{\boldsymbol{\omega}}_{\mathbf{y}} \mathbf{z}_{\mathbf{y}}$, and the inertial frame system matrix is

$$\mathbf{A}_{\mathrm{B}} = \begin{bmatrix} -\bar{\boldsymbol{\omega}}_{\mathbf{y}} & \mathbf{I} & \mathbf{0} \\ -\mathbf{M}_{\mathrm{B}}^{-1}\mathbf{K}_{\mathrm{B}} & -\mathbf{M}_{\mathrm{B}}^{-1}\mathbf{C}_{\mathrm{B}} - \bar{\boldsymbol{\omega}}_{\mathbf{y}} & -\mathbf{M}_{\mathrm{B}}^{-1}\mathbf{A}_{\mathrm{fB}} \\ -\mathbf{K}_{\mathrm{uaB}} & -\mathbf{C}_{\mathrm{uaB}} & -\mathbf{A}_{\mathrm{dB}} - \bar{\boldsymbol{\omega}}_{\mathbf{x}} \end{bmatrix} \tag{17}$$

where $\mathbf{B} = \mathbf{diag}(\mathbf{B}_{\mathbf{y}}, \mathbf{B}_{\mathbf{y}}, \mathbf{B}_{\mathbf{x}})$, $\bar{\boldsymbol{\omega}} = \mathbf{B}^{-1}\dot{\mathbf{B}}$ is a constant matrix, and the inertial frame transformed matrices are

$$\begin{aligned} \mathbf{M}_{\mathrm{B}} &= \mathbf{B}_{\mathbf{y}}^{-1}\mathbf{T}^{\mathrm{T}}\mathbf{M}\,\mathbf{T}\,\mathbf{B}_{\mathbf{y}} \\ \mathbf{C}_{\mathrm{B}} &= \mathbf{B}_{\mathbf{y}}^{-1}\mathbf{T}^{\mathrm{T}}\big((\mathbf{C}+\mathbf{C}_{\mathrm{a}})\mathbf{T} + 2\mathbf{M}\,\dot{\mathbf{T}}\big)\mathbf{B}_{\mathbf{y}} \\ \mathbf{K}_{\mathrm{B}} &= \mathbf{B}_{\mathbf{y}}^{-1}\mathbf{T}^{\mathrm{T}}\big((\mathbf{K}+\mathbf{K}_{\mathrm{a}})\mathbf{T} + (\mathbf{C}+\mathbf{C}_{\mathrm{a}})\dot{\mathbf{T}} + \mathbf{M}\,\ddot{\mathbf{T}}\big)\mathbf{B}_{\mathbf{y}} \\ \mathbf{A}_{\mathrm{fB}} &= \mathbf{B}_{\mathbf{y}}^{-1}\mathbf{T}^{\mathrm{T}}\mathbf{A}_{\mathrm{f}}\mathbf{B}_{\mathbf{x}} \\ \mathbf{A}_{\mathrm{dB}} &= \mathbf{B}_{\mathbf{x}}^{-1}\mathbf{A}_{\mathrm{d}}\mathbf{B}_{\mathbf{x}} \\ \mathbf{C}_{\mathrm{uaB}} &= \mathbf{B}_{\mathbf{x}}^{-1}\mathbf{C}_{\mathrm{ua}}\mathbf{T}\,\mathbf{B}_{\mathbf{y}} \\ \mathbf{K}_{\mathrm{uaB}} &= \mathbf{B}_{\mathbf{x}}^{-1}\mathbf{K}_{\mathrm{ua}}\mathbf{T} + \mathbf{C}_{\mathrm{ua}}\dot{\mathbf{T}}\,\mathbf{B}_{\mathbf{y}} \end{aligned} \tag{18}$$

If the system is isotropic, then $\mathbf{A}_\mathrm{B}$ is time-invariant [2], and a transient solution to Equation (16) transformed into substructure coordinates is

$$\mathbf{y}_{\mathrm{T}3} = \mathbf{B}\mathbf{V}\mathrm{e}^{\mathbf{\Lambda}t}\mathbf{q}(0) \tag{19}$$

where $\mathbf{y}_{\mathrm{T}3} = \{\mathbf{y}_\mathrm{T}^\mathrm{T}\ \dot{\mathbf{y}}_\mathrm{T}^\mathrm{T}\ \mathbf{x}^\mathrm{T}\}^\mathrm{T}$ is the substructure coordinate state vector, $\mathbf{\Lambda}$ is a diagonal matrix containing the eigenvalues $\lambda_k = \sigma_k + \mathrm{i}\omega$ of $\mathbf{A}_\mathrm{B}$ with $\mathrm{i} = \sqrt{-1}$ and damping σ_k and frequency ω_k of mode number k, $\mathbf{V}$ contains the corresponding eigenvectors as columns, and $\mathbf{q}(0) = \mathbf{V}^{-1}\mathbf{B}^{-1}(0)\mathbf{y}_{\mathrm{T}3}(0)$ are the initial conditions in modal coordinates. It is assumed that all eigenvectors are linearly independent, i.e., that $\mathbf{A}_\mathrm{B}$ has a diagonal Jordan form.

3.2 Implicit Floquet analysis

This section gives a summary of the implementation of the implicit Floquet method described in [13] and based on the original formulation in [11]. Floquet analysis enables the solution of periodic equations of motion directly without an explicit transformation when they are written in the form

$$\dot{\mathbf{y}}_3 = \mathbf{A}(t)\,\mathbf{y}_3 \tag{20}$$

where $\mathbf{y}_3$ is the state vector and $\mathbf{A}$ is the periodic system matrix in first order form satisfying $\mathbf{A}(t+T) = \mathbf{A}(t)$. Floquet theory [18] states that the solution to Equation (20) is of the form

$$\mathbf{y}_3 = \mathbf{U}(t)\,\mathrm{e}^{\mathbf{\Lambda}t}\,\mathbf{U}^{-1}(0)\,\mathbf{y}_3(0) \tag{21}$$

which is a decomposition of the solution into modal contributions consisting of periodic mode shapes $\mathbf{u}_k$ with period T contained as columns in the periodic mode shape matrix $\mathbf{U}$ and eigenvalues $\lambda_k = \sigma_k + \mathrm{i}\omega_k$ contained in the diagonal of $\mathbf{\Lambda}$, assuming that the system is diagonalisable. This solution is similar to the one given in Equation (19), with the difference that the periodic mode shape $\mathbf{BV}$ has a 1P azimuth-dependency from $\mathbf{B}$ due to the isotropic nature of the system, while $\mathbf{U}$ has an arbitrary integer-P azimuth-dependency caused by the anisotropy, e.g., wind shear.

This decomposition can be formed from a set of solutions $\boldsymbol{\varphi}_j$ found by integration of Equation (20) over one period with linearly independent initial conditions $\boldsymbol{\varphi}_j(0) = \mathbf{p}_j$, such that $\dot{\boldsymbol{\varphi}}_j(t) = \mathbf{A}(t)\,\boldsymbol{\varphi}_j(t)$ for $t \in [0;T]$. Classical Floquet analysis requires the computation of n solutions, where n is the number of state variables. To reduce this computational burden, the implicit Floquet analysis, which gives an approximate decomposition from a limited number of solutions $\boldsymbol{\varphi}_j$, is used. In the implicit Floquet analysis, the initial conditions $\boldsymbol{\varphi}_j(0)$ are determined successively by the Arnoldi algorithm such that after m integrations $\mathbf{P} = [\mathbf{p}_1\ \mathbf{p}_2\ \ldots\ \mathbf{p}_m]$ constitutes an orthogonal subspace. The subspace projected monodromy matrix is given as

$$\tilde{\mathbf{C}} = \mathbf{P}^\mathrm{T}\left[\boldsymbol{\varphi}_1(T) \quad \boldsymbol{\varphi}_2(T) \quad \ldots \quad \boldsymbol{\varphi}_m(T)\right] \tag{22}$$

and its eigenvalues, the characteristic multipliers ρ_k, are related to the characteristic exponents λ_k as $\rho_k = \mathrm{e}^{\lambda_k T}$ for mode number k. The m characteristic exponents are approximations to the m eigenvalues with the lowest damping in the solution in Equation (21). The frequency and damping are defined from the characteristic multipliers as

$$\begin{aligned} \sigma_k &= \frac{1}{T}\ln(|\rho_k|) \\ \omega_k &= \frac{1}{T}\arg(\rho_k) + j_k\Omega \end{aligned} \tag{23}$$

where the principal branch of the non-unique complex logarithm is used, such that $\arg(\rho_k) \in \,]-\pi;\pi]$, and j_k is an integer chosen to make the non-unique frequency more physically meaningful [2, 12]. The periodic mode shapes $\mathbf{u}_k$ are determined approximately as

$$\mathbf{u}_k(t) \approx [\boldsymbol{\varphi}_1(t)\ \boldsymbol{\varphi}_2(t)\ \ldots\ \boldsymbol{\varphi}_m(t)]\,\mathbf{v}_k\,\mathrm{e}^{-\lambda_k t} \tag{24}$$

where $\mathbf{v}_k$ are the eigenvectors of the monodromy matrix $\tilde{\mathbf{C}}$, and j_k, yielding λ_k from Equation (23), is selected such that $\mathbf{u}_k$ is as constant as possible for degrees of freedom measured in the inertial frame. The choice of j_k changes both the frequency ω_k and the mode shape $\mathbf{u}_k$ such that the solution in Equation (21) remains unaffected.

The state vector in Equation (20) is given as $\mathbf{y}_3 = \{\mathbf{y}^\mathrm{T}\ \dot{\mathbf{y}}^\mathrm{T}\ \mathbf{x}^\mathrm{T}\}^\mathrm{T}$, however it is not necessary to explicitly form the first order system matrix $\mathbf{A}$. Instead, the solutions φ_j are determined from the aeroelastic system

given by Equations (7) and (11) which is retained in global coordinates to exploit the sparsity of the system matrices for fast integration with a Newmark-type solver in the second order form

$$\begin{bmatrix} \mathbf{M} & \mathbf{0} \\ \mathbf{0} & \mathbf{0} \end{bmatrix} \begin{Bmatrix} \ddot{\mathbf{y}} \\ \ddot{\mathbf{x}} \end{Bmatrix} + \begin{bmatrix} \mathbf{C} + \mathbf{C}_\mathrm{a} & \mathbf{0} \\ \mathbf{C}_\mathrm{ua} & \mathbf{I} \end{bmatrix} \begin{Bmatrix} \dot{\mathbf{y}} \\ \dot{\mathbf{x}} \end{Bmatrix} + \begin{bmatrix} \mathbf{K} + \mathbf{K}_\mathrm{a} & \mathbf{A}_\mathrm{f} \\ \mathbf{K}_\mathrm{ua} & \mathbf{A}_\mathrm{d} \end{bmatrix} \begin{Bmatrix} \mathbf{y} \\ \mathbf{x} \end{Bmatrix} = \begin{Bmatrix} \mathbf{0} \\ \mathbf{0} \end{Bmatrix} \tag{25}$$

where the singularity of the combined mass matrix in the first term is circumvented by initially using $\mathbf{M}$ to find the accelerations $\ddot{\mathbf{y}}$ and setting the accelerations $\ddot{\mathbf{x}}$ explicitly to zero. In practice, the implicit Floquet analysis is continued by integrating Equation (25) over one period until a desired number of modes have converged to within a desired tolerance.

4 Numerical results

In this section the presented methods for modal analysis are applied to a BHawC model of a Siemens 2.3 MW pitch-regulated wind turbine with three 45 m blades, hub height 80 m, and nominal speed 16 rpm. The model has 381 structural degrees of freedom and 153 aerodynamic calculation points.

4.1 Harmonic pitching of airfoil section

The behaviour of the dynamic stall model is examined for a single aerodynamic calculation point and rigid body pitching motion of the airfoil, reducing Equation (11) to

$$\dot{f} = -\frac{K_{\alpha a}}{A_{\mathrm{d},i}} \alpha \tag{26}$$

where $K_{\alpha a}$ is the sum of the two elements in the substructure transformed matrix $\mathbf{K}_\mathrm{ua}\mathbf{T}$ coupling pitching motion of the two structural nodes surrounding the aerodynamic calculation point i to the separation f at this point. For harmonic oscillation of the angle of attack, $\alpha = A\sin(\omega t) + \alpha_\mathrm{ss}$, with amplitude A and frequency ω around the steady state angle of attack α_ss, Equation (26) has the solution

$$f = \frac{AK_{\alpha a,i}}{\sqrt{\omega^2 + A_{\mathrm{d},i}^2}} \sin\left(\omega t + \arctan(\omega / -A_{\mathrm{d},i})\right) \tag{27}$$

The linearisation of the lift coefficient about the steady state is found using Equation (2) as

$$C_L = C_{L,\mathrm{ss}}(\alpha) + \left(C'_{L,\mathrm{fa}}(\alpha) f_\mathrm{ss} + C'_{L,\mathrm{fs}}(\alpha)(1 - f_\mathrm{ss})\right)(\alpha - \alpha_\mathrm{ss}) + \left(C_{L,\mathrm{fa}}(\alpha) - C_{L,\mathrm{fs}}(\alpha)\right)(f - f_\mathrm{ss}) \tag{28}$$

where subscript 'ss' denotes steady state values, $()'$ denotes the derivative with respect to the angle of attack and all profile coefficients are evaluated at the steady state angle of attack α_ss.

Figure 1 shows the lift coefficient determined from the nonlinear model in Equation (3) compared to the linearised lift coefficient determined from Equations (26) and (27) for harmonic motion of the angle of attack and $\tau_\mathrm{f} = 6$ [15, p. 71]. For the calculation with a steady state angle of attack around 7° the lift coefficient determined from the nonlinear model follows the stationary curve for the small angles of attack, whereas it enters into the stall regime for the large amplitude resulting in a hysteresis loop due to the lag in the boundary layer. The linearised lift curve is tangent to the stationary lift curve because the linearization point is in fully attached flow. For the mean angle of attack around 12° the loop of the nonlinear lift coefficient at the large amplitude is shaped by the curvature of the stationary lift curve, while the linearised lift curve is an ellipse. The ellipse is inclined relative to the tangent of the stationary lift curve because the separation is delayed and the lift tends towards the value for fully attached flow whose lift curve has a higher slope. At the small amplitude and both mean angles of attack the lift coefficient of the linearised model agrees well with the nonlinear model, which means that the linearised model is suitable for representing vibrations with an amplitude in angle of attack up to around 1°.

4.2 Normal operation

Figure 2 shows the rotor speed and pitch angle (measured as negative towards feather) as function of hub height wind speed. These operating points are determined from BHawC time simulations until steady state with a wind profile constant in time defined by the power law $V = V_\mathrm{H}(z/z_\mathrm{H})^a$, where z is the height above ground, z_H is the hub height, V_H is the wind speed at hub height, and a is the wind shear exponent set to 0.2.

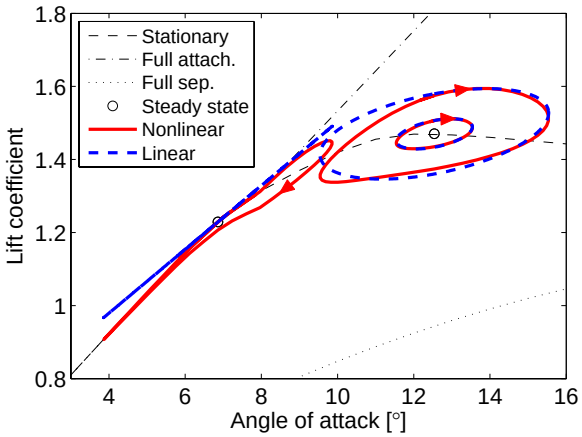

Figure 1: Lift coefficient as function of angle of attack for harmonic oscillations of the airfoil at 40.4 m radius around its pitch axis for combinations of two mean angles of attack and amplitudes of 1° and 3°. The curve for the low angle of attack and 1° amplitude follows the tangent and is thus not discernible. Wind speed 16 m/s, rotor speed 16 rpm, and reduced frequency $\omega c/(2W) = 0.1$.

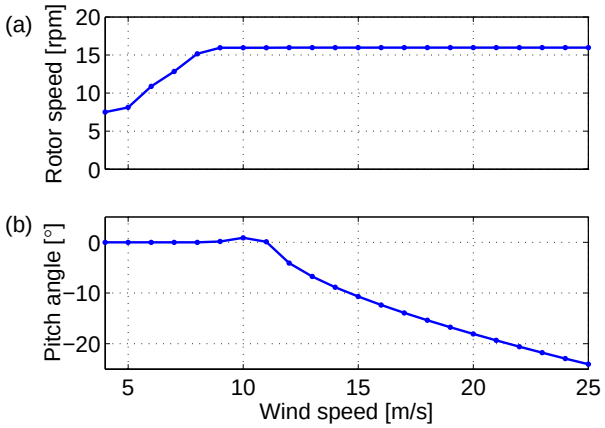

Figure 2: Rotor speed (a) and pitch angle (b) as function of wind speed in normal operation determined from BHawC time simulations to steady state.

An overview of the dynamic characteristics of the turbine at these operating points is provided by a modal analysis using the Coleman approach where the wind field is approximated as isotropic, and the system matrices in Equations (7) and (11) are extracted from a static steady state calculation including centrifugal and aerodynamic forces at a single azimuth angle. The time-invariance of the system matrix is checked by calculation for several azimuth angles. Figure 3(a) shows the normalised modal frequencies of the 14 modes with lowest frequency determined from the eigenvalues of the inertial frame transformed system matrix in Equation (17) as function of wind speed. The frequencies are normalised with the frequency of the first lateral tower mode. The labels first contain the index of the mode; then 'T' for tower, 'F' for blade flapwise, 'E' for blade edgewise or 'DRV' for drivetrain; then 'LO' for longitudinal, 'LA' for lateral, 'BW' for backward whirling, 'FW' for forward whirling or 'S' for symmetric. A detailed description of wind turbine modal dynamics is given in [19]. From 4 m/s to 9 m/s the figure resembles a Campbell diagram with a variation of the frequencies due to the variation in rotor speed, and for higher wind speeds the frequencies change due to the pitching of the blades. Figure 3(b) shows the logarithmic decrements normalised with respect to the first lateral tower mode as function of wind speed. The low damped modes are the first lateral tower mode and the edgewise backward and forward whirling modes. The drivetrain mode is in the modal analysis artificially low damped because the the drivetrain is modelled as free-free and the controller is not present to provide damping. The flapwise modes are highly damped with a dip in the damping around 11 m/s where the high angle of attack causes beginning separation of the flow.

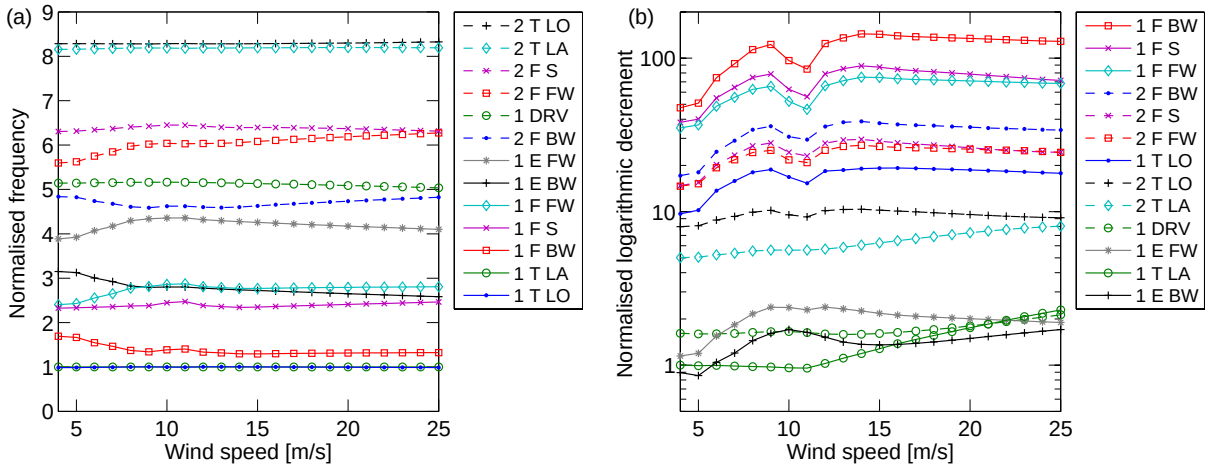

Figure 3: Modal frequencies (a) and logarithmic decrements (b) obtained from the Coleman approach as function of wind speed in normal operation. The values are normalised with the first lateral tower mode at 4 m/s. Labels are ordered after the sequence at 4 m/s.

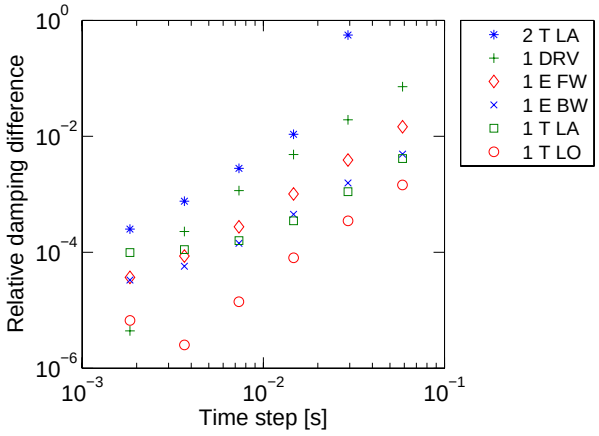

Figure 4: Relative damping difference of the implicit Floquet analysis compared to the Coleman approach for selected modes as function of the implicit Floquet integration time step.

The sensitivity towards the perturbation magnitude in the numerically linearised aerodynamic matrices in Equations (8)–(10), (13), and (14) is found to be a relative change of less than 10^{-6} in the modal frequencies and damping for variations of the perturbation magnitude between 10^{-6} and 10^{-2}.

To investigate the sensitivity of the Floquet analysis results with respect to the time step of the integration, the results of the Floquet analysis are compared to the Coleman approach, both in isotropic conditions at 16 rpm. An implicit Floquet analysis is performed using the system matrices of Equation (25) extracted at 64 azimuth angles over one rotor rotation in a steady state time simulation. The system of Equation (25) is integrated with a Newmark-type algorithm in time steps varying from $T/64$ to $T/2048$, where the system matrices are interpolated onto the integration time points using a truncated Fourier series with 14 harmonic terms. The integration is carried out over 56 rotation periods to yield 20 dynamic modes, including the 14 modes with lowest frequency, converged to within an absolute tolerance of 10^{-10} on the eigenvalues. The modal frequencies are identified from the frequency content in the periodic mode shapes in Equation (24) calculated for tower and blade degrees of freedom, the latter in multi-blade coordinates [2].

Figure 4 shows the difference in damping of the implicit Floquet analyses with different integration time steps relative to the Coleman approach. Using 64 time steps the solution is not precise enough to yield the second lateral tower mode. The error is approximately proportional to the time step squared and generally increases with the modal frequency. But when the error is around 10^{-4} the convergence for the first lateral

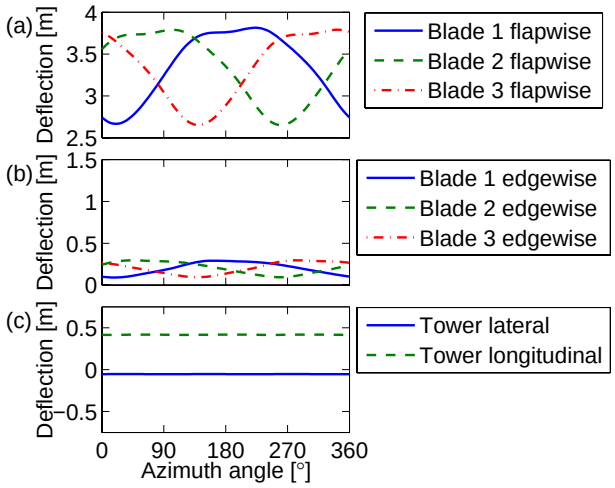

Figure 5: Steady state deflection over one rotor period in normal operation at 11 m/s and extreme shear condition. Blade tip motion flapwise (a) and edgewise (b), and tower top motion (c).

tower mode stalls, which is caused by a bad conditioning of the eigenvalue problem in the Coleman approach[1] and not a lack of convergence of the implicit Floquet analysis itself. The number of time steps for further analyses is selected as 512 as a compromise between precision and computation time.

4.3 Normal operation in extreme wind shear

The effects of extreme wind shear are examined at the operating point at 11 m/s, 16 rpm, and 0.1° pitch where the blades experience the largest angles of attack. The curvature of the lift coefficient at this point where flow separation has begun can affect the damping due to the large azimuthal variation of the lift slope. Simulations with the present model and previous work [20] show that gravity forces have a negligible effect on modal frequencies and damping, and are therefore excluded. For a wind shear exponent $a = 0.55$, which has been measured at the Høvsøre test site in Denmark under extremely stable atmospheric conditions [21], the steady state flapwise and edgewise deflections of the blade tips and the deflection of the tower top are shown as function of azimuth angle in Figure 5. The deflection of the blades varies significantly and is at maximum when the blade is pointing upwards (180° for blade one), while the deflection of the tower top is practically constant.

To extract the modal properties in these anisotropic conditions an implicit Floquet analysis is carried out. Figure 6 compares the modal frequencies and logarithmic decrements of the first 14 modes in the extreme shear condition and in an isotropic condition at the same wind speed, rotor speed and pitch angle, where the modal properties are calculated using the Coleman approach. The frequencies are almost unchanged by the wind shear but the damping of the flapwise modes increases slightly while the first longitudinal tower mode damping decreases slightly in the shear condition. This difference in damping can be explained by the interaction between modal vibration determined by the mode shape, and aerodynamic damping determined by the angle of attack. It is noted that the modal properties of the lowly damped modes, which are the modes observable from measurements, are unaffected by the wind shear.

Figure 7(a) shows the lift coefficient as function of angle of attack during one rotor rotation at different blade radii in the extreme shear operating condition compared to the corresponding constant operating point in the isotropic condition. The angle of attack in the shear condition varies towards the blade root due to the nacelle tilt and towards the tip due to the wind shear. On the outer part of the blade the angle of attack is lowest when the blade is pointing downwards and highest when the blade is pointing upwards. In both isotropic and shear conditions the airfoils are at the onset of separation with a small curvature of the lift. For the highest angles of attack in the shear condition the lag in the boundary layer is seen by a small opening of the curve. The lag is most apparent at the inner part of the blade where the relative wind speed is lower,

[1]The system matrix $\mathbf{A}$ is badly conditioned because of the large span in order of magnitude of the eigenvalues: the model contains extremely highly damped modes compared to which the physically relevant modes have an eigenvalue close to zero. The system matrix $\mathbf{A}_B$ is balanced as performed by the Matlab command 'eig', which improves the conditioning but cannot entirely eliminate the problem.

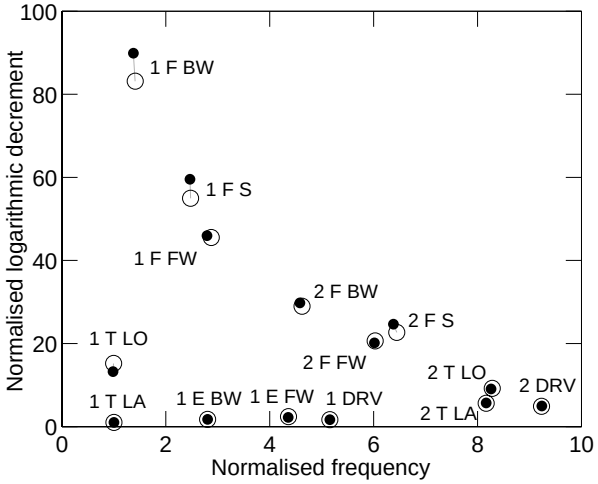

Figure 6: Logarithmic decrements and modal frequencies in normal operation at 11 m/s normalised with the values for the first lateral tower mode in normal operation at 4 m/s (cf. Figure 3). Isotropic (○) and extreme shear (●) conditions.

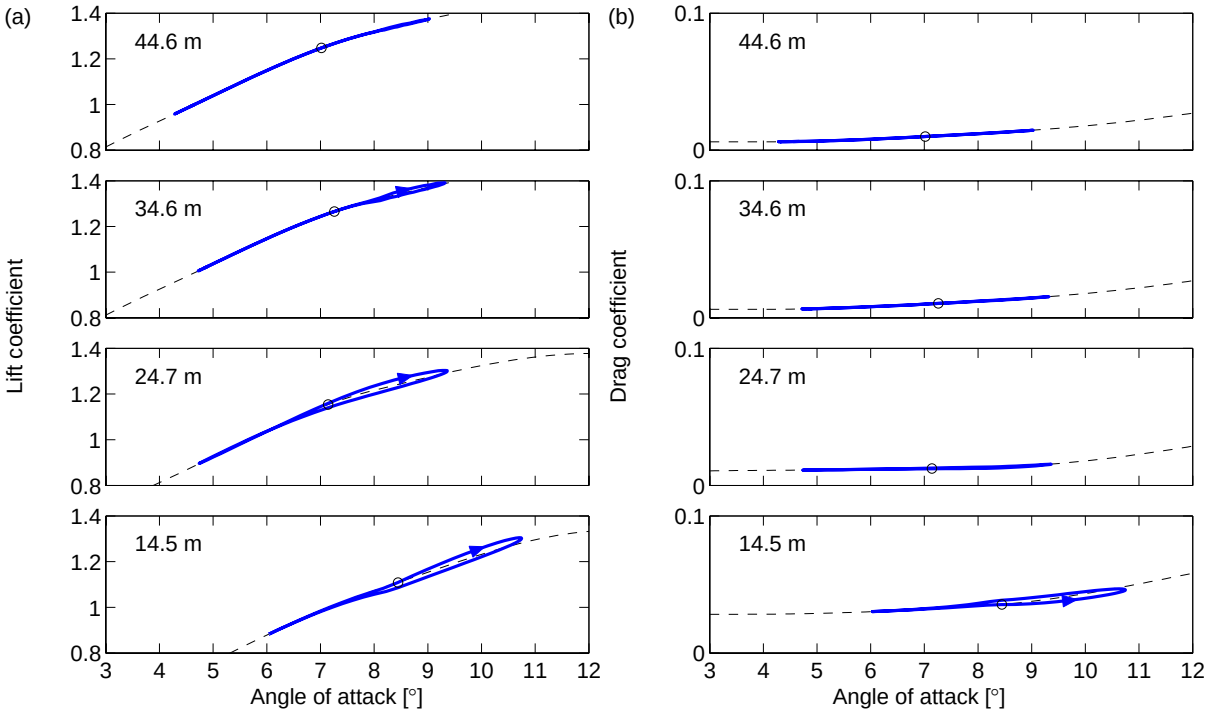

Figure 7: Lift coefficient (a) and drag coefficient (b) as function of angle of attack for different radial positions in normal operation at 11 m/s. Profile data (- - -), working point in isotropic condition (○) and working points in extreme shear condition (—).

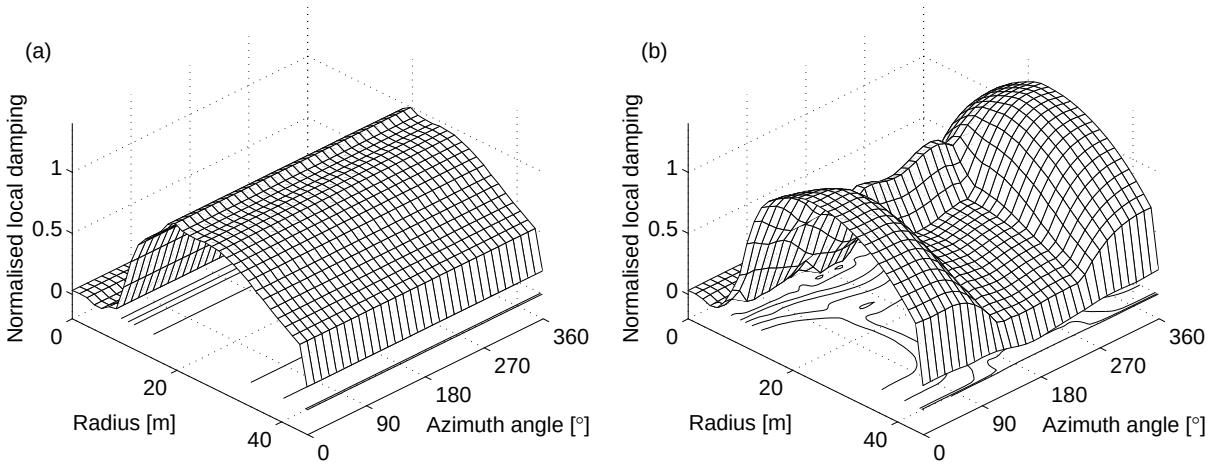

Figure 8: Local quasi-steady aerodynamic damping for motion perpendicular to the rotor plane as function of radius and azimuth angle in normal operation. Isotropic (a) and extreme shear (b) conditions. The damping is normalised with the maximum value in the isotropic condition.

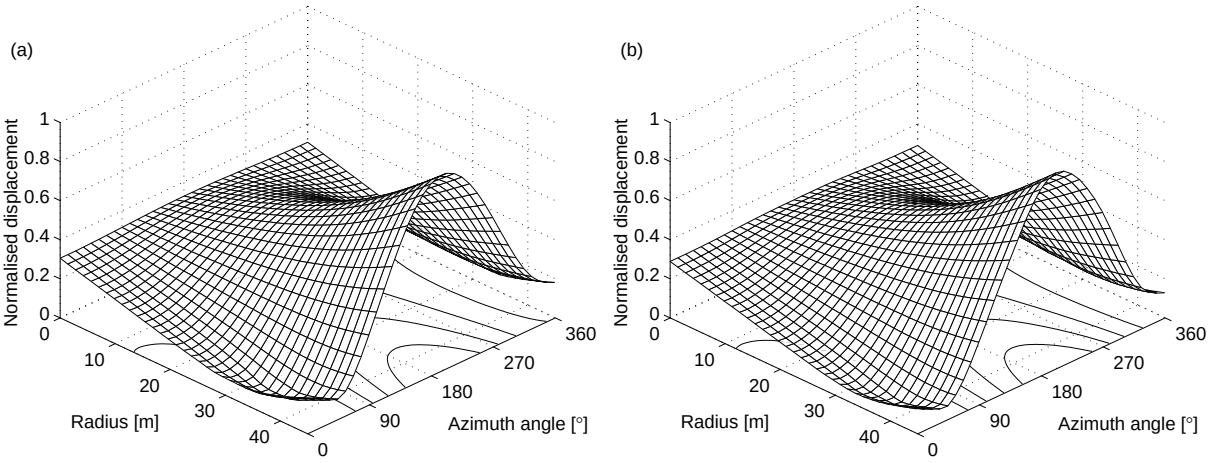

Figure 9: Amplitude of blade displacement perpendicular to the rotor plane in the first longitudinal tower mode as function of radius and azimuth angle in normal operation. Isotropic (a) and extreme shear (b) conditions.

which increases the lag in boundary layer, seen by a decrease of the proportionality factor in Equation (3). This effect of dynamic stall tends to increase the effective slope of the lift curve. Figure 7(b) shows the drag coefficient as function of angle of attack for the two operating conditions. The drag curves are approximately linear except for the inner part of the blade.

The influence of the angle of attack and the profile coefficients on the damping can be obtained from a linearised expression for the local quasi-steady viscous aerodynamic damping η of an airfoil section [19] given as

$$\eta = \tfrac{1}{2} c\rho W \big(C_D(3 + \cos(2\theta - 2\phi)) + C'_L(1 - \cos(2\theta - 2\phi)) + (C_L + C'_D)\sin(2\theta - 2\phi) \big) \tag{29}$$

where ρ is the air density, θ is the angle between the direction of motion and the rotor plane, $\phi = \alpha + \theta_\mathrm{p}$ is the inflow angle, θ_p is the sum of pitch and airfoil twist, and C_L, C'_L, C_D, C'_D, W, and ϕ are all evaluated at the steady state. This expression is only qualitative because the mode shape motion is not entirely unidirectional and because dynamic stall at large angles of attack with flow separation effectively increases the lift slope and thus increases the damping. Figure 8 shows the local damping for out-of-plane motion, $\theta = 90°$, which is the dominant direction of blade motion in the first longitudinal tower mode and the flapwise modes, which are the modes most affected by the wind shear. In this direction the damping is governed mainly by the slope of the lift curve. The local damping in the isotropic condition is constant during a rotor rotation while in the shear condition it increases when the blade is around the downward position (0°) and increases when the blade is

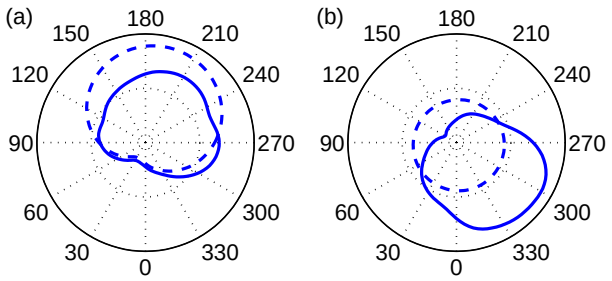

Figure 10: Local quasi-steady aerodynamic work as function of azimuth angle. Normal operation, first longitudinal tower mode (a) and first flapwise symmetric mode (b). Isotropic (- - -) and extreme shear (—) conditions.

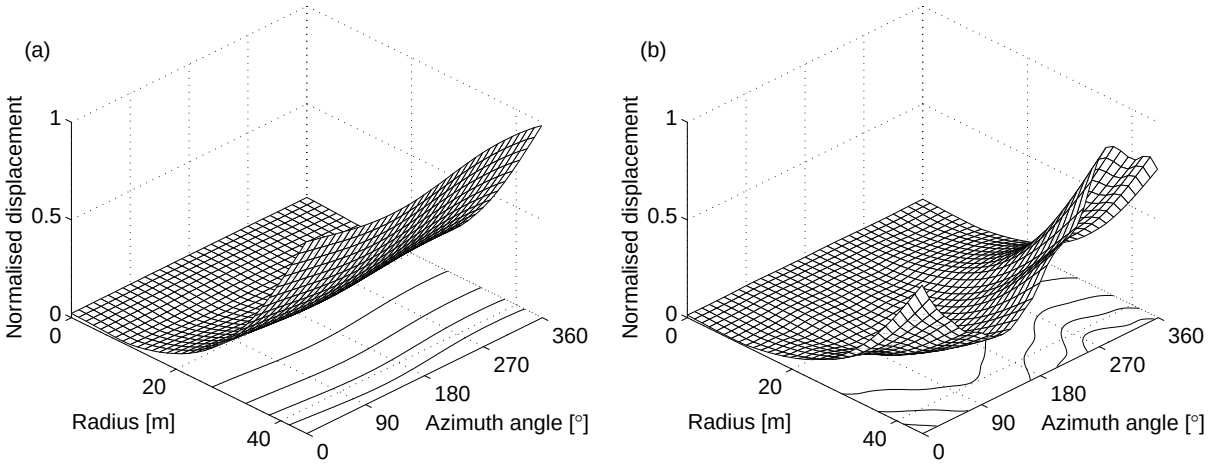

Figure 11: Amplitude of blade displacement perpendicular to the rotor plane in the first symmetric flapwise mode as function of radius and azimuth angle in normal operation. Isotropic (a) and extreme shear (b) conditions.

around the upward position (180°) due to the variation in angle of attack.

Figure 9 shows the amplitude of the out-of-plane motion of the blade in the mode shape of the first longitudinal tower mode during one rotor rotation. The largest amplitude is when the blade is pointing upwards, and it is smaller when the blade is pointing downwards. The displacement is mostly due to a rigid body tilt rotation of the nacelle, but there is also some elastic deformation, particularly when the blade is pointing upwards. The mode shapes of the isotropic and the shear conditions are almost identical. Because the mode shape amplitude is greater when the blade is pointing up, the decrease in damping outweighs the increase, resulting in lower modal damping for the first longitudinal tower mode in the shear condition. This argument is recapitulated in Figure 10(a) showing the azimuth-dependent local damping obtained as a qualitative estimate of the work of the aerodynamic forces. This work is approximated simply by multiplication of the local damping in Figure 8 with the mode shape amplitude in Figure 9 and integration over the length of the blade. The area enclosed by the curve represents the amount of total damping over one period, corresponding to the modal damping. Thus, the smaller area for the shear condition confirms the result of lower modal damping.

The amplitude of the out-of-plane blade displacement in the first symmetric flapwise mode is shown in Figure 11. In the isotropic condition the amplitude is largest at the tip and almost constant during a rotor rotation showing only a small 1P variation. By contrast, the mode shape in the shear condition has a multiple-P variation over azimuth, illustrating the difference between isotropic and anisotropic conditions. The mode shape for the shear condition is best understood as the mean amplitude over multiple periods of the steady state forced response to an ideal pure excitation of this mode. This response drops in amplitude with some delay after a period of high damping, and it increases in amplitude with some delay after a period of low damping. The amplitude in the shear condition is smallest around 120° when the blade is travelling upwards, which is caused by the high aerodynamic damping around 0° seen in Figure 8(b). Conversely, the amplitude is lowest around 280° when the blade is travelling downwards, caused by the low damping around 180°.

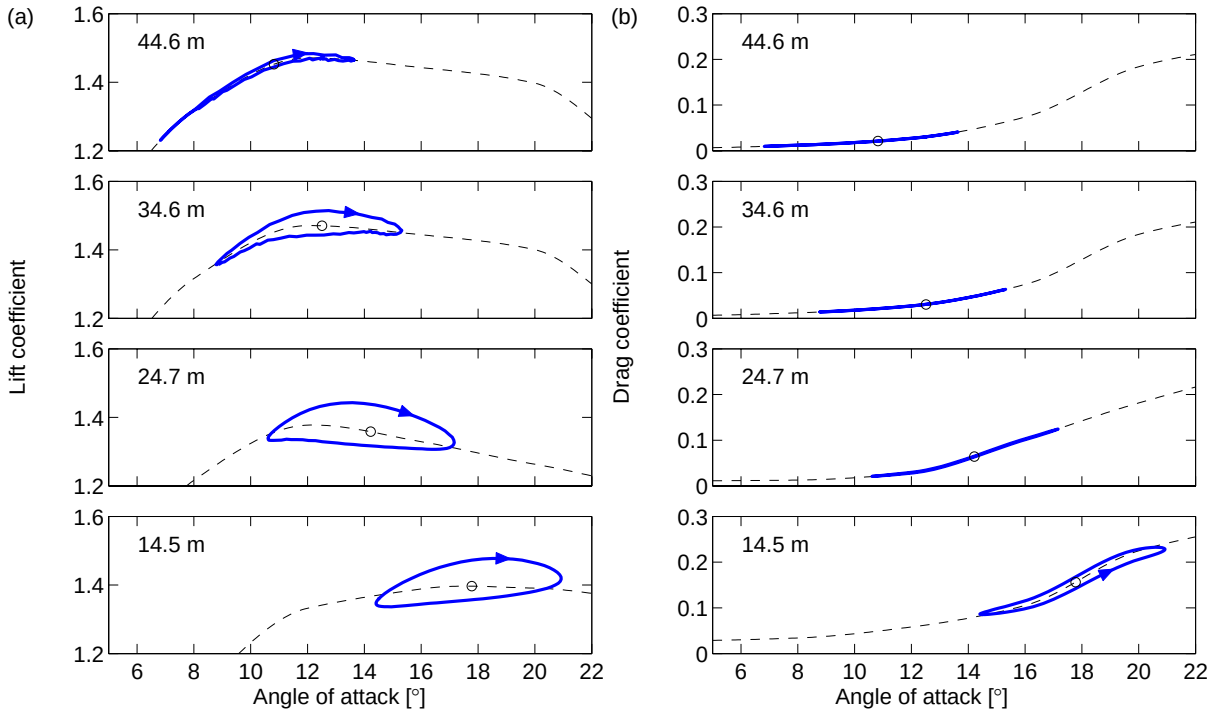

Figure 12: Lift coefficient (a) and drag coefficient (b) as function of angle of attack for different radial positions in stalled operation at 16 m/s. Profile data (- - -), working point in isotropic condition (○) and working points in extreme shear condition (——).

Figure 10(b) shows the estimate of the aerodynamic work as function of azimuth angle for both conditions caused by the interaction of the mode shape and the aerodynamic damping. The larger area of the curve in the shear condition explains the higher modal damping. The same effect is seen for the first flapwise backward whirling and the second flapwise symmetric modes.

The damping of the edgewise modes is caused mainly by drag. As shown in Figure 7(b) the drag coefficient in the shear condition varies approximately equally below and above the value in the isotropic condition, causing no significant change in the modal damping of the edgewise modes.

4.4 Stalled operation

To validate the conclusion that the curvature of the lift creates a large variation in the local damping and hence the observed changes in modal damping of the first longitudinal tower mode and first flapwise modes, the turbine is operated in developed stall outside its normal operating range, at 16 m/s wind with a rotor speed of 16 rpm and a pitch angle of 0°.

Figure 12(a) shows the lift coefficient as function of angle of attack at different blade radii. At most radial positions the turbine operates around the maximum lift coefficient, which gives a substantial curvature of the lift and more pronounced dynamic loops due to the lag in the boundary layer in the shear condition. Figure 12(b) shows the drag coefficient as function of angle of attack which is now considerably larger and has more curvature than in normal operation.

Figure 13 shows the modal frequencies and damping for isotropic and shear conditions. As in normal operation, the frequencies are approximately the same in the two conditions, and the damping of the flapwise modes increases due to the shear, while the damping of the first longitudinal tower mode decreases. These relative changes in modal damping are substantially larger than in normal operation, showing that the higher curvature of the lift and drag makes the azimuthal variation in damping more significant and therefore has a stronger effect on modes with blade motion perpendicular to the rotor plane.

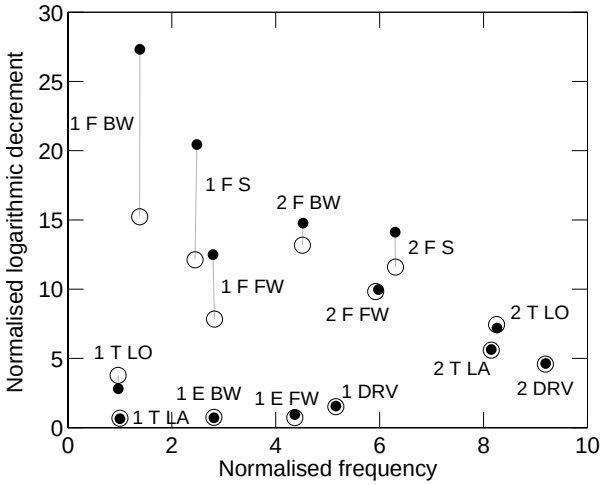

Figure 13: Logarithmic decrements and modal frequencies in stalled operation at 16 m/s normalised with the values for the first lateral tower mode in normal operation at 4 m/s (cf. Figure 3). Isotropic (○) and extreme shear (●) conditions.

5 Conclusions

A linear aeroelastic model is constructed from structural equations extracted directly from a nonlinear aeroelastic code and from numerically obtained aerodynamic equations. These system equations transformed into the inertial frame using the Coleman transformation yield the modal frequency and damping for isotropic systems. In the general case of anisotropic systems, the modal properties are obtained using implicit Floquet analysis.

A modal analysis of a three-bladed wind turbine is performed in extreme wind shear conditions. The wind shear leads to an azimuthal variation in the angle of attack, corresponding to a variation in local aerodynamic damping in stall, because of the varying lift slope. The modal damping of the first longitudinal tower mode decreases slightly for operation close to stall in the shear condition relative to the isotropic condition. On the other hand, the wind shear increases the damping of the the first flapwise backward whirling and symmetric modes close to stall. The phenomenon is validated by operating the turbine in developed stall, which increases the change in damping.

For the lowly damped modes, which are the ones observable from measurements on the turbine, the relative changes of the modal frequencies and damping values due to wind shear are small and assumed to be within the uncertainty of the predictions. Hence, the anisotropic effects of wind shear for similar turbines with similar operating conditions can be disregarded. The changes in modal damping may be more important for stall-regulated turbines or future pitch-regulated turbines with larger rotors, both because the variation in angle of attack due to wind shear would be larger, and because the increased flexibility of the longer blade could introduce couplings between the structure and the aerodynamics. The presented method can also be applied to turbines operating with cyclic pitch, which can be a way of handling the varying loading of an increased wind shear.

Acknowledgment

This work has been partially supported by the Danish Ministry of Science, Technology and Innovation through the Industrial PhD programme.

References

[1] F. Rasmussen, J.T. Petersen, and H.Aa. Madsen. Dynamic stall and aerodynamic damping. *Journal of Solar Energy Engineering*, 121:150–155, 1999.

[2] P.F. Skjoldan and M.H. Hansen. On the similarity of the Coleman and Lyapunov-Floquet transformations for modal analysis of bladed rotor structures. *Journal of Sound and Vibration*, 327:424–439, 2009.

[3] V.A. Riziotis, S.G. Voutsinas, E.S. Politis, and P.K. Chaviaropoulos. Aeroelastic stability of wind turbines: The problem, the methods and the issues. *Wind Energy*, 7(4):373–392, 2004.

[4] T.G. van Engelen and H. Braam. TURBU offshore, computer program for frequency domain analysis of horizontal axis offshore wind turbines. Technical Report ECN-C–04-079, Energy Research Centre of the Netherlands, 2004.

[5] M.H. Hansen. Aeroelastic stability analysis of wind turbines using an eigenvalue approach. *Wind Energy*, 7:133–143, 2004.

[6] G. Bir and J. Jonkman. Aeroelastic instabilities of large offshore and onshore wind turbines. *Journal of Physics: Conference Series*, 75(1), 2007.

[7] D. Lee, D.H. Hodges, and M.J. Patil. Multi-flexible-body dynamic analysis of horizontal axis wind turbines. *Wind Energy*, 5(4):281–300, 2002.

[8] K. Stol, M. Balas, and G. Bir. Floquet modal analysis of a teetered-rotor wind turbine. *Journal of Solar Energy Engineering*, 124:364–371, 2002.

[9] K.A. Stol, H.-G. Moll, G. Bir, and H. Namik. A comparison of multi-blade coordinate transformation and direct periodic techniques for wind turbine control design. In *Proceedings of 47th AIAA Aerospace Sciences Meeting*, Orlando FL, USA, 2009.

[10] D.A. Peters. Fast Floquet theory and trim for multi-bladed rotorcraft. *Journal of the American Helicopter Society*, 39(4):82–89, 1994.

[11] O.A. Bauchau and Y.G. Nikishkov. An implicit Floquet analysis for rotorcraft stability evaluation. *Journal of the American Helicopter Society*, 46(3):200–209, 2001.

[12] O.A. Bauchau and J. Wang. Efficient and robust approaches to the stability analysis of large multibody systems. *Journal of Computational and Nonlinear Dynamics*, 3:011001, 2008.

[13] P.F. Skjoldan and M.H. Hansen. Implicit Floquet analysis of wind turbines using tangent matrices of a nonlinear aeroelastic code. *Wind Energy*, 2010. Accepted for publication.

[14] R. Rubak and J.T. Petersen. Monopile as part of aeroelastic wind turbine simulation code. In *Proceedings of Copenhagen Offshore Wind*, Denmark, October 2005.

[15] J.T. Petersen, H.Aa. Madsen, A. Bjrck, P. Enevoldsen, S. ye, H. Ganander, and D. Winkelaar. Prediction of dynamic loads and induced vibrations in stall. Technical Report Ris-R-1045, Risø National Laboratory, 1998.

[16] S. ye. Dynamic stall simulated as time lag of separation. In *Proceedings of 4th IEA Symposium on Aerodynamics of Wind Turbines*, Rome, Italy, 1991.

[17] W. Johnson. *Helicopter Theory*. Dover Publications, 1980.

[18] L. Meirovitch. *Methods of Analytical Dynamics*. McGraw-Hill, New York, 1970.

[19] M.H. Hansen. Aeroelastic instability problems for wind turbines. *Wind Energy*, 10(6):551–577, 2007.

[20] M.H. Hansen and T. Buhl. Is the periodic loading of rotor blades important to the aeroelastic damping? (in Danish). In C. Bak, editor, *Forskning i aeroelasticitet EFP-2004*, chapter 6, pages 65–75. Ris National Laboratory, 2005. Ris-R-1509(DA).

[21] H.Aa. Madsen, R. Mikkelsen, N.N. Srensen, M.O.L. Hansen, S. ye, and J. Johansen. Influence of wind shear on rotor aerodynamics, power and loads. In C. Bak, editor, *Research in Aeroelasticity EFP-2006*, chapter 10, pages 101–116. Ris National Laboratory, 2007. Ris-R-1611(EN).

P5

Determination of Modal Parameters in Complex Nonlinear Systems

Journal of Nonlinear and Computational Dynamics, 6(3):031017, 2011.
doi:10.1115/1.4002975

Determination of Modal Parameters in Complex Nonlinear Systems

Peter F. Skjoldan
Development Engineer
Loads, Aerodynamics, and Control,
Siemens Wind Power A/S,
2630 Taastrup, Denmark
e-mail: peter.skjoldan@siemens.com

Olivier A. Bauchau
Professor
Fellow of ASME
Georgia Institute of Technology,
School of Aerospace Engineering,
Atlanta, GA 30332-0150
e-mail: olivier.bauchau@ae.gatech.edu

This paper describes a methodology for evaluating the modal parameters of complex nonlinear systems. It combines four different tools: the Coleman post-processing, the partial Floquet analysis, the moving window analysis, and the signal synthesis algorithm. The approach provides a robust estimation of the linearized modal parameters and qualitative information about the nonlinear behavior of the system. It operates on one or multiple discrete time signals and is able to deal with both time-invariant and periodic systems. The method is computationally inexpensive and can be used with multiphysics computational tools, and in principle, with experimental data. The proposed approach is validated using a simple, four degree of freedom model of a wind turbine. The predictions for the linear system are validated against an exact solution of the problem. For the nonlinear system, it is demonstrated that qualitative information concerning the nonlinear behavior of the system is obtained using the proposed method. Finally, the nonlinear behavior of a realistic, three-bladed horizontal axis wind turbine model is investigated. [DOI: 10.1115/1.4002975]

1 Introduction

An important aspect of the dynamic response of wind turbines and other flexible rotating systems is the potential presence of instabilities. For instance, ground and air resonance phenomena are well documented instabilities that occurs in rotorcraft, edgewise aeroelastic instabilities are observed in wind turbines, and flutter might become a problem for future wind turbines with longer, more flexible blades [1]. Even if the system is stable, the accurate evaluation of the decay rates for each mode of the system is a critical task. Indeed, in the presence of low decay rates, perturbations from steady equilibrium operation will damp out at a very slow rate, dramatically affecting the fatigue life of the turbine.

If the equations of motion of the system can be cast in the form of linear, ordinary differential equations with constant coefficients, classical stability analysis methodologies based on the characteristic exponents of the system can be used. For wind turbines, however, the equations of motion are in the form of linear, ordinary differential equations with periodic coefficients, assuming small amplitude response of the blades and tower. In this case, the Floquet theory [2] should be used. Under some restrictive assumptions, the equations of motion of periodic mechanical systems can be transformed into time-invariant equations using the Coleman transformation [3].

Stability analysis is typically performed on simplified models with the smallest number of degrees of freedom required to capture the physical phenomenon that causes the instability. The equations of motion are linearized and eigenvalue analysis then yields the system's modal parameters. This approach provides results that are easily interpreted, but ignores potential nonlinear behavior of the system. For instance, damping ratio could be a function of modal amplitude [4], or nonlinear modal coupling could affect modal parameters. Furthermore, as the number of degrees of freedom used to represent the system increases, the Floquet analysis becomes increasingly cumbersome, and quickly unmanageable.

Due to increased available computer power, the analysis of wind turbines and rotorcraft relies on increasingly complex, large scale models. Full finite element analysis codes are now routinely used for structural dynamics modeling [5–7] and aeroelastic phenomena are captured by coupling the structural dynamics model with simplified unsteady aerodynamics models, or sometimes with computational fluid dynamics code, to obtain accurate predictions of the airloads acting on the turbine. The size and complexity of these computational models makes it increasingly difficult to apply the classical tools used for stability analysis.

The only rigorous approach to nonlinear stability analysis is Lyapunov's function method, which cannot be applied to large dimensional numerical models, or to experimental data. This paper presents a procedure that extracts qualitative information about nonlinear stability and decay rates for such models through a careful combination of linearized methodologies. The desired procedure should be equally applicable to experimental measurements and to large scale simulation tools to allow a rational comparison of numerical predictions against experimental data.

Stability analysis methodologies that are applicable to experimental data typically deal with time signals that are processed to extract modal parameters. Clearly, manipulating or linearizing the equations of motion are not options when dealing with experimental data. The earliest such methods are probably Prony's [8] and moving block methods [9,10]. In view of the difficulty of applying the Floquet theory to experimental systems, the partial Floquet analysis (PFA) was developed by Peters and Wang [11] and Fuehne [12] and later refined by Bauchau and Wang [13–15], who also demonstrated the close relationship among Prony's, partial Floquet, and autoregressive methods. More recently, the wavelet [16,17] and Hilbert transform methods [18] have also been developed.

The work presented in this paper describes an approach to stability analysis that combines four different tools: the Coleman post-processing (CPP), the partial Floquet analysis, the moving window analysis (MWA), and the signal synthesis algorithm (SSA). The approach provides a robust estimation of the linearized modal parameters and qualitative information about the nonlinear behavior of the system. It operates on one or multiple discrete time signals and is able to deal with both time-invariant and

Contributed by the Design Engineering Division of ASME for publication in the JOURNAL OF COMPUTATIONAL AND NONLINEAR DYNAMICS. Manuscript received March 23, 2010; final manuscript received October 27, 2010; published online March 2, 2011. Assoc. Editor: Claude-Henri Lamarque.

periodic systems. Furthermore, the method is computationally inexpensive and can be used with multiphysics computational tools, and in principle, with experimental data.

2 Stability Analysis of Complex Systems

The present work focuses on flexible rotating systems such as wind turbines or rotorcraft, but is equally applicable to general flexible multibody systems. The system is assumed to be modeled by a set of nonlinear equations of the form $\dot{\underline{y}}=\underline{g}(t,\underline{y})$, where $\underline{y}$ is a vector containing the N state variables, t denotes time, and $(\dot{})$ is a derivative with respect to time.

The system is assumed to operate at a constant mean rotor speed, and small perturbations $\underline{x}=\underline{y}-\underline{y}_{ss}$ from a periodic steady state $\underline{y}_{ss}$ of the nonlinear system can be approximated by a linear system with periodic coefficients as

$$\dot{\underline{x}}=\underline{\underline{A}}(t)\underline{x}+\underline{f}(t) \tag{1}$$

where $\underline{\underline{A}}(t)=\underline{\underline{A}}(t+T)$ is the periodic system matrix of period $T=2\pi/\Omega$, Ω is the rotor speed, and $\underline{f}(t)$ is the external force vector.

2.1 Classical Floquet Analysis. For the purpose of stability analysis, it is convenient to assume that wind turbines are periodic systems. The theoretical basis for the analysis of periodic systems was developed by Floquet [19] who showed that the response of a linear system with periodic coefficients is the sum of modal contributions each consisting of a product of a periodic function by an exponential term of the form of $\exp(\lambda_k t)$, where the λ_k is called the characteristic exponents.

Typically, applications of the Floquet theory are based on the determination of the transition matrix $\underline{\underline{\mathbf{\Phi}}}$ which relates the states of the system at times t and $t+T$, where T is the period of the system. The eigenvalues of the transition matrix, denoted as ρ_k, are related to the characteristic exponents $\rho_k=\exp(\lambda_k T)$. The damping coefficient σ_k and principal frequency $\omega_{\mathrm{p},k}$ of mode k are determined from these eigenvalues as

$$\sigma_k=\frac{1}{T}\ln(|\rho_k|) \tag{2a}$$

$$\omega_{\mathrm{p},k}=\frac{1}{T}\arctan(\rho_k),\quad \omega_{\mathrm{p},k}\in\,]-\Omega/2,\Omega/2] \tag{2b}$$

Integer multiples of the rotor speed can be added to the principal frequencies as $\omega_k=\omega_{\mathrm{p},k}+j_k\Omega$ to obtain more physically meaningful frequencies. The damping ratio is then calculated as $\zeta_k=-\sigma_k/(\omega_k\sqrt{1+\sigma_k^2/\omega_k^2})$. The system is stable if $\zeta_k<0$ for all values of k.

2.2 Partial Floquet Analysis. For large multibody models, a formal linearization of the governing equations is difficult and costly to obtain for time-invariant systems, and even more arduous in the case of periodic systems. This is particularly true for the multiphysics models used to simulate wind turbines. Hence, the application of the Floquet theory to these systems is problematic.

To overcome these difficulties, Bauchau and Wang [13–15] developed several approaches to stability analysis and demonstrated their applicability to large scale multibody systems. They presented two classes of closely related robust algorithms based on partial Floquet and autoregressive approaches. Furthermore, they showed that a number of other methods, such as Prony's method or Poincaré mapping, are identical to those approaches.

A distinctive feature of these methods is that they operate on one or multiple discrete time signals characterizing the dynamic response of the system, and are able to deal with time-invariant or periodic systems. Consequently, these approaches are computationally inexpensive and consist of purely post-processing steps that can be used with any multiphysics computational tool or with experimental data, where the free response after an applied excitation has been measured. Unlike classical stability analysis methodologies, linearization of the system's equations of motion is not required. Singular value decomposition is used systematically as a means of dealing with the noisy, highly redundant data sets obtained from nonlinear systems. In this paper, this approach will be referred to as the PFA.

The PFA is based on a number of time signals, denoted as $h_s(t)$, which are components of the response vector $\underline{x}$. A total of N_h signals is used for the analysis. A typical signal is sampled at times $t=j\Delta t+\ell T$, where j denotes the time step number in period ℓ assuming that T is an integer multiple of Δt. An array storing m consecutive data points starting in period ℓ is set up as

$$\underline{h}_{s,\ell}=\{h_s(\Delta t+\ell T),\ldots,h_s(m\Delta t+\ell T)\}^T \tag{3}$$

Arrays $\underline{h}_{s,\ell}$ obtained over $n+1$ periods, $\ell=0,\ldots,n$, for all N_h signals are assembled into two Hankel-type matrices of size $N_h m\times n$, denoted as $\underline{\underline{H}}_0$ and $\underline{\underline{H}}_1$ [13–15], such that $\underline{\underline{H}}_1=\underline{\underline{Q}}\underline{\underline{H}}_0$, where $\underline{\underline{Q}}$ is an approximation of the transition matrix. For this relationship to allow the exact calculation of the transition matrix, all N state variables would have to be available over N periods, i.e., $N_h=N$ and $n=N$. If a single data point was then used, i.e., $m=1$, $\underline{\underline{H}}_0$ would be square and invertible, yielding the exact transition matrix as $\underline{\underline{Q}}=\underline{\underline{H}}_1\underline{\underline{H}}_0^{-1}$.

If the system is time-invariant, i.e., if $\underline{\underline{A}}(t)$ in Eq. (1) is constant, the period is arbitrary and may be selected $T=\Delta t$ to obtain the maximum amount of information from a given signal.

In practice, only a few signals are available and for much shorter times than required to calculate the full transition matrix. Therefore, an approximate transition matrix is evaluated as $\underline{\underline{Q}}=\underline{\underline{H}}_1\underline{\underline{H}}_0^{+}$, where superscripts $(\cdot)^+$ denote Moore–Penrose inverses [20]. Matrix $\underline{\underline{H}}_0$ is factorized using the singular value decomposition [20] to yield $\underline{\underline{H}}_0=\underline{\underline{\mathcal{U}}}\underline{\underline{\mathcal{S}}}\underline{\underline{\mathcal{V}}}^T$, where $\underline{\underline{\mathcal{U}}}$ contains the proper orthogonal modes of $\underline{\underline{H}}_0$, $\underline{\underline{\mathcal{S}}}$ is a diagonal matrix storing the singular values of $\underline{\underline{H}}_0$, and $\underline{\underline{\mathcal{V}}}$ is an orthogonal matrix.

The singular values can be interpreted as a measure of the energy associated with each proper orthogonal mode. To reduce noise, only the r largest singular values and the corresponding columns in $\underline{\underline{\mathcal{U}}}$ and $\underline{\underline{\mathcal{V}}}$ are retained. The number r can be interpreted as the rank of matrix $\underline{\underline{H}}_0$. The Moore–Penrose inverse of matrix $\underline{\underline{H}}_0$ then becomes $\underline{\underline{H}}_0^{+}=\underline{\underline{\mathcal{V}}}_r\underline{\underline{\mathcal{S}}}_r^{-1}\underline{\underline{\mathcal{U}}}_r^T$, and the estimated transition matrix of size $N_h m\times N_h m$ becomes $\underline{\underline{Q}}=\underline{\underline{H}}_1\underline{\underline{\mathcal{V}}}_r\underline{\underline{\mathcal{S}}}_r^{-1}\underline{\underline{\mathcal{U}}}_r^T$.

Matrix $\underline{\underline{H}}_0$ will store highly redundant data, and rank r is typically less than the number of rows $N_h m$. It follows that of the $N_h m$ eigenvalues of $\underline{\underline{Q}}$, only r are expected to be physically meaningful, whereas the remaining $N_h m-r$ eigenvalues are related to the noise in the data. Consequently, it makes sense to project the transition matrix $\underline{\underline{Q}}$ into the subspace defined by the r proper orthogonal modes of $\underline{\underline{H}}_0$, stored in $\underline{\underline{\mathcal{U}}}_r$, to find a transition matrix of size $r\times r$ as

$$\hat{\underline{\underline{Q}}}=\underline{\underline{\mathcal{U}}}_r^T\underline{\underline{Q}}\underline{\underline{\mathcal{U}}}_r=\underline{\underline{\mathcal{U}}}_r^T\underline{\underline{H}}_1\underline{\underline{\mathcal{V}}}_r\underline{\underline{\mathcal{S}}}_r^{-1} \tag{4}$$

The stability characteristics can then be extracted from the r eigenvalues, or characteristic multipliers, of $\hat{\underline{\underline{Q}}}$ by use of Eq. (2).

2.3 Signal Synthesis. Extracting the eigenvalues of the transition matrix defined by Eq. (4) yields the modal parameters of the system. To ascertain the accuracy of these predictions, it is important to reconstruct the signals based on these modal characteristics [15]. An estimation of signal $h_s(t)$ based on the r characteristic exponents is written as

$$\hat{h}_s(t)=\sum_{k=1}^{r}c_{s,k}(t)e^{\lambda_k t} \tag{5}$$

where $c_{s,k}(t)$ are the unknown periodic coefficients for mode k, which are determined by enforcing a least-squares fit between the actual signal $h_s(t)$ and its reconstructed counterpart $\hat{h}_s(t)$.

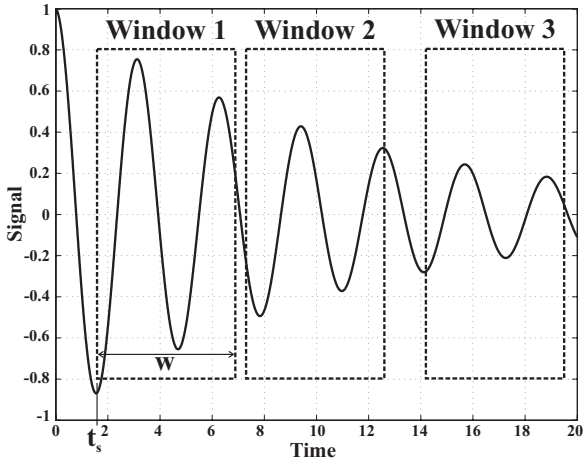

Fig. 1 Selecting various windows for a signal

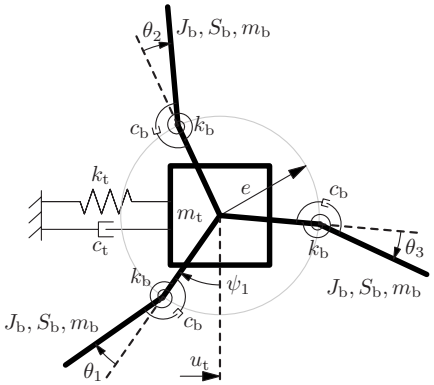

Fig. 2 Simplified model of a three-bladed wind turbine

2.4 Coleman Transformation. Lyapunov [21] showed that a linear system with periodic coefficients can be transformed into an equivalent, time-invariant system. A rotor is isotropic if it comprises three or more blades with identical properties and has symmetric interblade couplings. Coleman [3] proposed a change in coordinates that transforms the periodic system of linearized equations governing the dynamic response of isotropic helicopter rotors into a system of equations with constant coefficients, referred to as the *Coleman inertial system equations*.

Skjoldan and Hansen [22] generalized the notion of isotropy for wind turbines to include aerodynamic and control effects, thereby expanding the range of applicability of the Coleman transformation. While this transformation is a powerful and practical tool when applied to simple, low dimensional models, it is impractical when dealing with large scale multiphysics models coupled to computational fluid dynamics codes or experimental data.

When dealing with periodic systems, the discrete time signals selected for the PFA must be sampled once per rotor revolution. Consequently, the system must be simulated over many periods to obtain reliable estimates of the damping rates, leading to heavy computational burden. In this paper, the Coleman transformation is applied to the sole signals used for stability analysis rather than to the system's linearized equations of motion. The Coleman transformation then becomes part of the signal post-processing procedure, completely eliminating the difficulties associated with this approach. The efficiency and accuracy of this approach, called the CPP in this paper, will be demonstrated.

Consider a three-bladed rotor and three signals, h_1, h_2, and h_3, measuring the same quantity on the three blades, respectively. Application of the Coleman transformation to these three signals yields three transformed, multiblade coordinate signals, denoted as a_0, a_1, and b_1. Because they are measured in the rotating system, signals h_i characterize the dynamic response of the structure in the rotating system. On the other hand, a_0, a_1, and b_1 characterize the dynamic response of the structure in the inertial frame [1], which involve the backward and forward whirling harmonic components, denoted as BW and FW, respectively, and the symmetric component, denoted as S. The frequencies of the BW and FW components are the modal frequency ω_k in the inertial frame minus or plus the rotor speed, respectively.

2.5 Moving Window Analysis. The approaches to stability analysis discussed earlier are based on time signals describing the dynamic response of a complex wind turbine or rotorcraft. A typical signal is shown in Fig. 1. In practice, only a portion of the time series is used for stability analysis, corresponding to a window of size w, starting at time t_s.

If the signal corresponds to the response of a linear system with a single degree of freedom, it is associated with a single frequency and damping rate. Using any of the three windows presented in Fig. 1 should yield the same modal parameters. If the system is nonlinear, using the windows labeled *window 1*, *2*, and *3*, in Fig. 1 might lead to different parameters. For instance, if system damping is amplitude dependent, the damping ratios extracted from these three windows will be different because the average signal amplitude decreases from window 1 to window 3. This fact will be used to obtain qualitative information about the nonlinear behavior of the system.

Let a window of size w start at time t_s, as illustrated in Fig. 1. The PFA is then used to estimate modal parameters, denoted as $\omega_k(t_s)$ and $\zeta_k(t_s)$. Next, consider a window of identical size starting at time $t_s+\Delta t$, where Δt is the sampling rate. Application of the PFA to the signal in this new window yields $\omega_k(t_s+\Delta t)$ and $\zeta_k(t_s+\Delta t)$. Repeating the analysis for windows of identical size starting at times $t_s+i\Delta t$ leads to modal parameters $\omega_k(t_s+i\Delta t)$ and $\zeta_k(t_s+i\Delta t)$ that are discrete functions of the "moving window" starting time.

For each window, it is also possible to estimate the amplitude of excitation, $c_k(t_s+i\Delta t)$, of each mode using the SSA described above. Combining this amplitude information for each window with the corresponding modal parameters yields estimates of the modal parameters as functions of amplitude $\omega_k(c_k)$ and $\zeta_k(c_k)$. These functions provide qualitative information about the nonlinear dependency of the modal parameters on modal amplitudes. This procedure will be referred to in this paper as the MWA.

3 Numerical Examples

In this section, various stability analysis methods applicable to wind turbines are demonstrated. First, the methods are validated by using a simple structural model with four degrees of freedom. Next, the same approaches will be applied to a realistic, three-bladed horizontal axis wind turbine modeled using a finite element based simulation tool coupled with simplified aerodynamics models.

3.1 Simplified Wind Turbine Model. Figure 2 shows a simplified model of a three-bladed horizontal axis wind turbine with four degrees of freedom: the tip lateral deflection of the tower u_t and edgewise deflection of each of the three blades θ_1, θ_2, and θ_3. The tower is modeled as a concentrated mass m_t located at the center of the rotor hub of radius e and connected to the ground by means of a spring of stiffness constant k_t and viscous damper of constant c_t. The blades of mass m_b are modeled as rigid bodies connected to the hub by torsional springs of stiffness constant k_b and viscous dampers of constant c_b. The first and second edgewise moments of inertia of the blades with respect to their hinge point are denoted as S_b and J_b, respectively.

3.1.1 Equations of Motion. The equations of motion for the simplified wind turbine model depicted in Fig. 2 are derived using Lagrange's formulation, then linearized about the steady state equilibrium for a constant rotor speed Ω. The linearized equations are

$$\underline{\underline{M}}(\psi_1)\underline{\ddot{u}} + \underline{\underline{C}}(\psi_1)\underline{\dot{u}} + \underline{\underline{K}}(\psi_1)\underline{u} = \underline{f}(\psi_1) \tag{6}$$

where the generalized coordinate array is $\underline{u}^T=\{\theta_1,\theta_2,\theta_3,\bar{u}_t\}$, $\bar{u}_t=u_t/H$, H is a characteristic length of the system, such as the tower height, and $\underline{f}(\psi_1)$ is the external force vector. The angular position of the first blade $\psi_1=\Omega t$ is used as the nondimensional time variable and notation $(\cdot)$ is used to indicate a derivative with respect to ψ_1. The periodic, nondimensional mass, damping, and stiffness matrices are

$$\underline{\underline{M}} = \begin{bmatrix} 1 & 0 & 0 & \bar{S}_b\cos\psi_1 \\ 0 & 1 & 0 & \bar{S}_b\cos\psi_2 \\ 0 & 0 & 1 & \bar{S}_b\cos\psi_3 \\ \bar{S}_b\cos\psi_1 & \bar{S}_b\cos\psi_2 & \bar{S}_b\cos\psi_3 & \bar{J}_t \end{bmatrix}$$

$$\underline{\underline{C}} = \begin{bmatrix} \bar{c}_b & 0 & 0 & 0 \\ 0 & \bar{c}_b & 0 & 0 \\ 0 & 0 & \bar{c}_b & 0 \\ -2\bar{S}_b\sin\psi_1 & -2\bar{S}_b\sin\psi_2 & -2\bar{S}_b\sin\psi_3 & \bar{c}_t \end{bmatrix}$$

$$\underline{\underline{K}} = \begin{bmatrix} \bar{k}_b+\bar{e}\bar{S}_b & 0 & 0 & 0 \\ 0 & \bar{k}_b+\bar{e}\bar{S}_b & 0 & 0 \\ 0 & 0 & \bar{k}_b+\bar{e}\bar{S}_b & 0 \\ -\bar{S}_b\cos\psi_1 & -\bar{S}_b\cos\psi_2 & -\bar{S}_b\cos\psi_3 & \bar{k}_t \end{bmatrix}$$

respectively, and the nondimensional parameters are defined as $\bar{e}=e/H$, $\bar{J}_t=(3m_b+m_t)H^2/J_b$, $\bar{S}_b=HS_b/J_b$, $\bar{k}_t=k_tH^2/(J_b\Omega^2)$, $\bar{c}_t=c_tH^2/(J_b\Omega)$, $\bar{k}_b=k_b/(J_b\Omega^2)$, and $\bar{c}_b=c_b/(J_b\Omega)$. The azimuth angle for blade j is denoted as $\psi_j=\Omega t+2\pi(j-1)/3$. To investigate the dynamic behavior of this system in the presence of nonlinearities, the following nonlinear model will be considered:

$$\underline{\underline{M}}\underline{\ddot{u}} + \underline{\underline{C}}\underline{\dot{u}} + \underline{\underline{K}}\underline{u} + \underline{\underline{C}}_{nl}\underline{\dot{u}}_3 + \underline{\underline{K}}_{nl}\underline{u}_3 = \underline{f} \tag{7}$$

where the nonlinear coordinate vectors are $\underline{u}_3^T=\{\theta_1^3,\theta_2^3,\theta_3^3,\bar{u}_t^3\}$ and $\underline{\dot{u}}_3^T=\{\dot{\theta}_1^3,\dot{\theta}_2^3,\dot{\theta}_3^3,\dot{\bar{u}}_t^3\}$. For simplicity, the nonlinear damping matrix is selected to be diagonal, $\underline{\underline{C}}_{nl}=\mathrm{diag}(\bar{\gamma}_b\bar{c}_b,\bar{\gamma}_b\bar{c}_b,\bar{\gamma}_b\bar{c}_b,\bar{\gamma}_t\bar{c}_t)$, where the nondimensional coefficients $\bar{\gamma}_b$ and $\bar{\gamma}_t$ characterize the nonlinear damping of the blades and tower, respectively. Similarly, the nonlinear stiffness matrix is selected to be diagonal, $\underline{\underline{K}}_{nl}=\mathrm{diag}(\bar{\delta}_b\bar{k}_b,\bar{\delta}_b\bar{k}_b,\bar{\delta}_b\bar{k}_b,\bar{\delta}_t\bar{k}_t)$, where the nondimensional coefficients $\bar{\delta}_b$ and $\bar{\delta}_t$ characterize the nonlinear stiffness of the blades and tower, respectively.

3.2 Study of the Linearized System. The nondimensional parameters selected for this study are $\bar{e}=0.04$, $\bar{J}_t=400$, $\bar{S}_b=2$, $\bar{k}_t=600$, $\bar{c}_t=8$, $\bar{k}_b=15$, and $\bar{c}_b=0.1$. Because the system described above has an isotropic rotor, it can be transformed to a constant coefficient system using the Coleman transformation and the frequency and damping rates of the system are then readily obtained from the eigenvalues of this constant coefficient system. These values are used as a reference solution and will be shown as dashed lines in all figures pertaining to this problem.

Next, the response of the linearized simplified model was found by numerical integration of Eq. (7). An initial excitation lasting 16 rotor revs is applied as $\underline{f}=\underline{f}_0\cos(\Omega_f\psi_1)$, where $\Omega_f=3$ and $\underline{f}_0^T=\{4,-1,3,100\}$. For $\psi_1>32\pi$, the excitation vanished and signals θ_1, θ_2, θ_3, and $\underline{u}_t$ were then extracted during the subsequent free decay of the system.

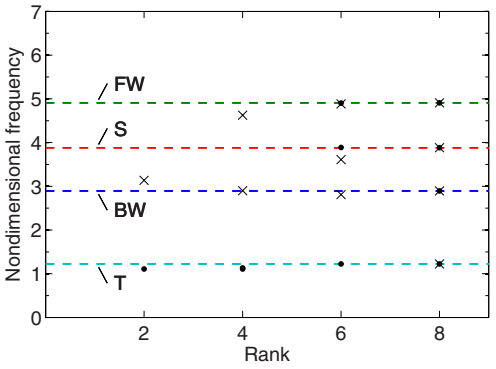

Fig. 3 Simplified model frequencies. Reference solution: dashed lines; PFA for periodic system: symbols "●;" and PFA with CPP: symbols "×."

First, the PFA is tested for this periodic problem. The four signals were sampled 64 times per rotor rev for the 16.25 rotor revs after the end of the external excitation. System frequencies were obtained from the eigenvalues of $\underline{\underline{\hat{Q}}}$ using $m=16$ consecutive data points in $\underline{h}_{s,\ell}$ and $n=16$ columns in $\underline{\underline{H}}_0$ and $\underline{\underline{H}}_1$ (see Eqs. (3) and (4)), and Fig. 3 shows the identified frequencies, with symbols "●" as a function of rank number together with the reference solution. For a rank number of 8, the four frequencies of the system are accurately identified. The four modes of the system are the tower mode (labeled "T"), which is the dominant contributor to the tower signal u_t, the backward and forward whirling modes (labeled "BW" and "FW," respectively), which are the major contributors to the multiblade signals a_1 and b_1, and the symmetric mode (labeled "S") corresponding to in-phase blade motions.

Next, the time-invariant version of the PFA was tested for this problem. Although the system is periodic, the four signals, sampled 64 times per rotor rev for 1.625 rotor revs, were processed as if the system were time-invariant using $m=32$ consecutive data points and $n=72$ columns in $\underline{\underline{H}}_0$ and $\underline{\underline{H}}_1$. Figure 4 shows the frequencies as a function of rank number together with the reference solution. This approach identifies the inertial system frequencies ω_k along with the rotating system frequencies $\omega_k\pm\Omega$. The signals contain three harmonics for each of the T, BW, and FW modes, and one harmonic for the S mode, thus requiring a rank number of 20 to resolve all modes accurately. A good approximation of the frequencies, however, is obtained at a rank lower than 20 because the amplitude corresponding to some of

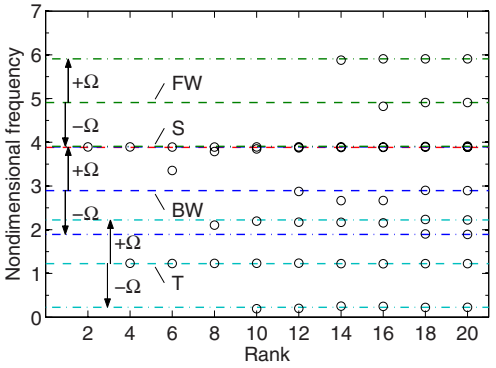

Fig. 4 Simplified model frequencies. Reference solution: dashed lines; and PFA for time-invariant system: symbols "○."

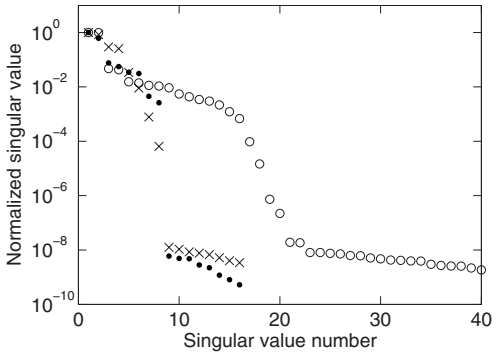

Fig. 5 Largest singular values in decreasing order for the three approaches. Periodic PFA: symbols "●;" time-invariant PFA: symbols "○;" and PFA with CPP: symbols "×."

these frequencies is very low.

Finally, the time-invariant version of the PFA was exercised using the tower signal and the multiblade signals θ_{a0}, θ_{a1}, and θ_{b1} obtained from the CPP of the blade signals. The signals were sampled 64 times per rotor rev over 0.5 rotor revs, and $m=16$ consecutive data points in $h_{s,\ell}$, and $n=16$ columns in $\underline{\underline{H}}_0$ and $\underline{\underline{H}}_1$ were used to obtain $\underline{\underline{Q}}$. The identified frequencies are shown in Fig. 3 with symbols "×." Because the CPP effectively transforms the signal to the inertial frame, a single harmonic of each mode is present and a rank number of 8 is sufficient to determine all frequencies.

The results presented thus far for this simple linear periodic system call for the following comments. First, processing the signals in the PFA "as if the system were time-invariant" (i.e., ignoring the periodic nature of the system) is not recommended. Although this approach correctly identifies system frequencies for this simple problem (see Fig. 4), it suffers two serious drawbacks. First, it fails to recognize the periodic nature of the signal, and hence, could yield erroneous answers. Second, the total energy of the signals is spread over a larger number of modes (ten instead of four in this simple case), complicating the identification process.

Second, processing the signals as periodic signals in the PFA yields the correct results. The energy contained in the signals is concentrated in a smaller number of modes (the four inertial system modes), easing the identification process. Unfortunately, this approach is burdened by a high computational cost; because the signals are treated as periodic, they must be sampled at once per rev, requiring longer simulation times to enable accurate identification.

Finally, the time-invariant version of the PFA can be safely used with CPP signals because they are those that would be generated by an equivalent, time-invariant system. Two advantages result; the energy contained in the signals is focused in a smaller number of modes and shorter simulation times are sufficient to gather the required information.

These findings concerning the three methods are reinforced by the data presented in Fig. 5, which show the singular values of the Hankel-type matrix $\underline{\underline{H}}_0$ for the three approaches. Singular values were normalized by the largest and presented in order of decreasing normalized value. The PFA with CPP results in eight high-energy singular values, all others are at the noise level. The periodic PFA performs well, also resulting in eight high-energy singular values. For the time-invariant version of the PFA, the energy is spread among 20 singular values.

3.3 Study of the Nonlinear System. Next, the behavior of the simplified wind turbine model will be investigated in the presence of nonlinearities. The system is now characterized by Eq. (7), and at first, nonlinear damping is introduced by selecting $\bar{\gamma}_t$

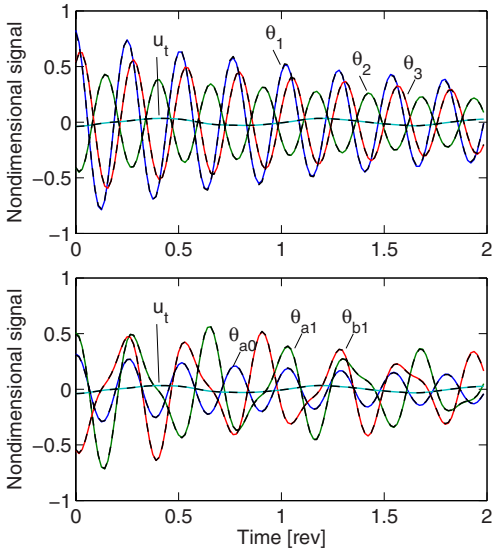

Fig. 6 Signals from the window starting at time 0. Original signals (top) and signals after applying CPP (bottom). Computed signals: solid line; and reconstructed signals: dashed line.

$=0.01$ and $\bar{\gamma}_b=0.04$. The signals were processed using the CPP followed by the MWA to assess the effects of the nonlinearities on the dynamic response of the system.

3.3.1 The Moving Window Analysis. The stability analysis is performed using a window size of two rotor revs, $m=42$ consecutive data points, and $n=85$ columns in $\underline{\underline{H}}_0$ and $\underline{\underline{H}}_1$. Figure 6 shows the signals of the window starting at time 0 before and after applying the CPP. In both cases, the signals reconstructed using Eq. (5) are also shown and found to be nearly indistinguishable from their original counterparts. Figure 7 shows the identified frequencies and damping ratios of the system as a function of the window starting time. Whereas the frequencies are nearly identical to their counterparts for the linear system, significant differences are observed for the damping ratios.

To understand this behavior, modal excitation amplitudes must be assessed first. The SSA was used to estimate the amplitudes of each of the modes contained in each signal. For instance, Fig. 8 shows the modal content of the θ_{a1} signal as a function of the window starting time. This signal contains contributions from the four modes of the system. The BW and FW modes dominate the response, whereas the T, and specially the S modal amplitudes are at the noise level. Plots of the modal content of the other signals reveal that the tower mode dominates the response of the tower signal u_t, the BW and FW modes are predominant in the θ_{a1} and θ_{b1} signals, and finally, the S mode dominates the multiblade mean signal θ_{a0}.

Because the scale on the vertical axis of Fig. 8 is logarithmic, the modal amplitude is expected to decay linearly for a linear system. Both BW and FW modes do not decay exactly linearly, indicating slightly higher damping ratios at high amplitude and lower damping ratios at lower amplitude. This observation is in agreement with the results presented in Fig. 7, which also predict higher damping ratios at high amplitude.

In the linear analysis, the θ_{a1} signal only contains contributions of the BW and FW modes. Figure 8 indicates that in the nonlinear regime, small contributions of the T and even S modes are present. Because the amplitudes are so small, no reliable frequency or damping ratio data can be extracted from these contributions. This explains the need to use multiple signals to extract the complete modal information for the system. Each mode must contribute a significant amount of energy to at least one of the

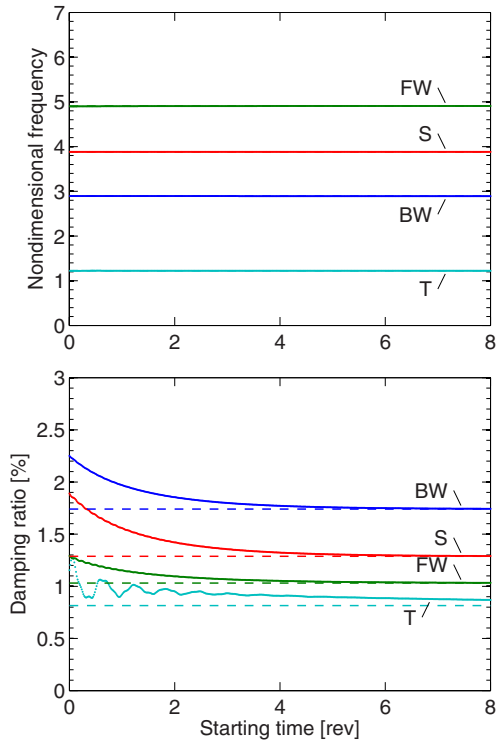

Fig. 7 System frequencies (top) and damping ratios (bottom) for the MWA

signals to extract reliable modal data.

Figure 8 provides a qualitative assessment of the effect of the damping nonlinearity of the system. The nearly constant slopes of the modal amplitudes of the BW and FW modes as a function of time imply nearly constant damping ratios as a function of amplitude. The extracted modal amplitudes of the T and especially S modes present oscillations that are an artifact of the numerical procedure because the contributions of these two modes to the θ_{a1} signal are very small.

Finally, Fig. 9 shows the system damping ratios as a function of modal amplitude, plotted on a logarithmic scale. The amplitude of each mode is calculated as the square root of the sum of the squares of that mode's amplitude in all signals. This plot confirms the trends discussed earlier in a more explicit manner.

3.3.2 Other Types of Nonlinearity. The results presented in the previous sections have focused on a system presenting nonlinear damping characterized by parameters $\bar{\gamma}_t$=0.01 and $\bar{\gamma}_b$=0.04.

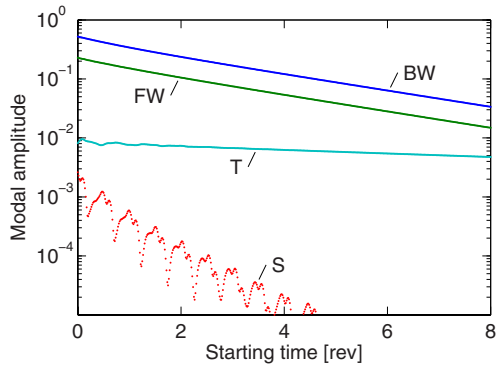

Fig. 8 Amplitudes of the modes contained in the θ_{a1} signal

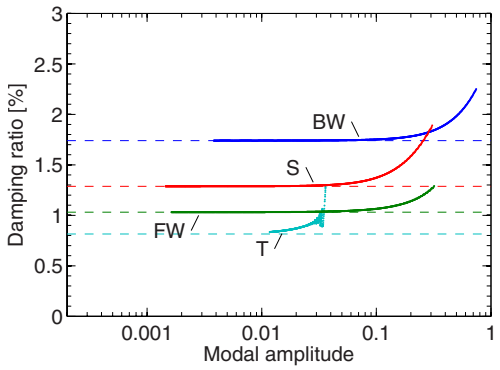

Fig. 9 Damping ratio versus modal amplitude

Other sets of parameter values will be investigated in this section. In all cases, the simulation was run for 16 rotor revs and a 2 rotor rev window was used for the MWA.

Final results will be presented in the form of damping ratio versus modal amplitude plots. Intermediate steps of the analysis, such as those presented in Figs. 7 and 8, will not be shown. While these intermediate steps are not shown here for brevity's sake, all data must be carefully examined to ensure that all relevant modes have been excited to a sufficient amplitude level.

First, Fig. 10 shows the case of a decrease in the damping nonlinearity with parameters $\bar{\gamma}_t$=−0.002 and $\bar{\gamma}_b$=−0.01. The proposed approach captures the expected qualitative trends for this system.

Finally, stiffness nonlinearities are examined. A softening stiffness nonlinearity is addressed by selecting $\bar{\delta}_t$=−0.01 and $\bar{\delta}_b$=−0.03. For the highest excitation amplitude, i.e., for a window starting time t_s=0, the frequencies of the T, BW, S, and FW modes decrease by 1.0%, 0.5%, 0.5%, and 0.3%, respectively, a very modest effect. A stiffening nonlinearity with parameters $\bar{\delta}_t$=0.01 and $\bar{\delta}_b$=0.04 yields an increase in the frequencies of the T, BW, S, and FW modes of 1.9%, 0.8%, 1.0%, and 0.8%, respectively.

3.3.3 Effect of Window Size. Additional simulations were performed using the MWA with window sizes of 1, 2, and 4 rotor revs. Frequency predictions were nearly unaffected by window size. Shorter window sizes result in more scattering of the data for damping ratio predictions, indicating that less reliable predictions are obtained. Longer window sizes reduce data scattering, but loss of resolution in time results, i.e., the changes in damping ratio become less pronounced because they are averaged over longer

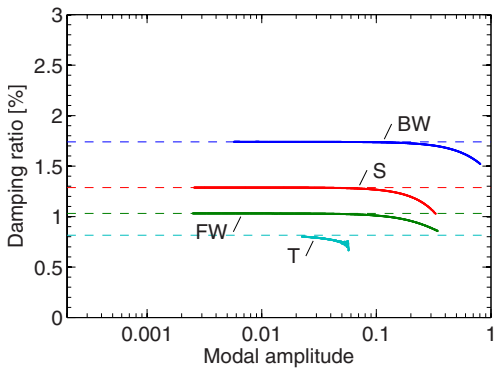

Fig. 10 Damping ratio versus modal amplitude. ($\bar{\gamma}_t$=−0.002, $\bar{\gamma}_b$=−0.01).

periods. This compromise between time resolution and modal parameter identification is also observed in wavelet analysis [16].

3.4 Complex Wind Turbine Model. The proposed stability analysis methods are now applied to a realistic, three-bladed horizontal axis wind turbine. The aeroelastic model is based on a fully nonlinear finite beam element structural model and aerodynamic forces are calculated using the blade element theory [23]. The turbine modeled with 381 structural degrees of freedom has a nominal power of 2.3 MW, a nominal speed of 16 rpm, a hub height of 80 m, and a blade length of 45 m. The wind field has a logarithmic shear profile excluding turbulence, and the effects of tower shadow and gravity forces are included. A variable speed controller regulating the blade pitch and generator moment is used in the simulations.

The rotor is balanced and thus isotropic. External loading, such as wind shear, tower shadow, and gravity forces are not isotropic, but their effects are assumed to remain small. The simulation code takes into account nonlinear effects, which again, are assumed to be small. Because these effects are assumed to be small, solutions are expected to be close to those of a system with periodic periodic coefficients and the CPP will be used for this problem although it is not strictly applicable.

The simulation is run until initial transients have damped out and a steady state is obtained, characterized by a constant mean rotor speed and a response of the turbine that is approximately periodic. Once that state is reached, excitation is applied. The duration of the excitation was kept short, one period of the first tower mode, to maintain the mean rotor speed as constant as possible. To ensure excitation of the four low damping modes of the turbine, periodic forces were applied. The tower first lateral mode (denoted as "T") was excited by the transverse force applied at the tower top. The first BW and FW edgewise modes (denoted as "BW" and "FW", respectively) were excited by applying forces with 120 deg phasing differences near the blade tips. Finally, the first drive train mode (denoted as "DRV") was excited by in-phase forces applied near the blade tips.

Once the excitation ceased, four signals were measured: the top lateral tower deflection and the three edgewise blade tip deflections resolved in the rotating frame. The steady state response of the system was then subtracted from these four signals, which were then normalized by the tower height and blade length, respectively. Finally, the CPP was applied to yield the multiblade signals u_{a0}, u_{a1}, and u_{b1} from the blade signals.

3.4.1 Stability Analysis Under Moderate Excitation. A stability analysis of the turbine with signals sampled 94 times per rotor rev over 5.3 rotor revs was performed using $m=66$ consecutive data points and $n=133$ columns in $\underline{\underline{H}}_0$ and $\underline{\underline{H}}_1$ when subjected to 12 m/s wind at hub height and a moderate excitation level resulting in initial edgewise blade tip deflection of about 0.3 m and tower top lateral deflection of about 0.2 m.

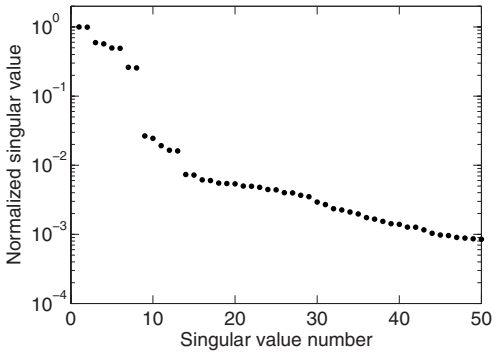

Fig. 11 Largest singular values in decreasing order for complex wind turbine model

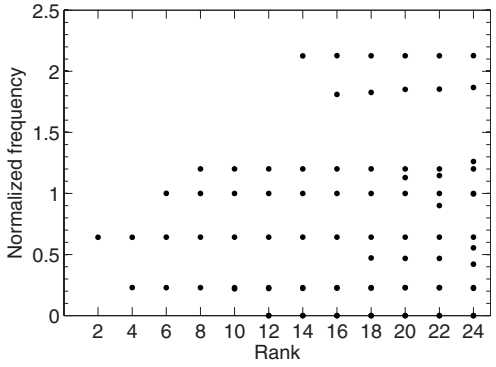

Fig. 12 Identified frequencies as function of rank number

Figure 11 shows the largest singular values of the Hankel-type matrix $\underline{\underline{H}}_0$, where the eight largest values correspond to the four excited modes. The next singular values have a much lower energy and are thus unlikely to yield reliable modal information.

Figure 12 shows the identified frequencies as a function of the rank number, where the frequencies are normalized by the average value of the FW mode frequency. The frequencies obtained at rank numbers up to 8 pertain to the four excited modes of the system. The additional frequencies obtained from higher rank numbers could be either additional physical modes or artifacts of the method. Because the associated modal amplitudes are very low, these estimates are unreliable. Higher excitation amplitudes at these frequencies would be required to ascertain the physical nature of these additional modes.

Next, a MWA of the data was performed with a window size of 2.1 rotor revs and Fig. 13 shows the frequency versus window starting time. The identified frequencies remain constant for all windows, which is an evidence of a reliable identification and validates the assumption that nonlinear effects remain small for this problem. As time increases, the excitation amplitude of the drive train mode becomes very small, and the identification of the corresponding frequency becomes unreliable, resulting in the observed scattering of the predictions.

Figure 14 shows the identified damping versus window starting time, where the damping ratios were normalized by the average value of the FW mode damping ratio. The damping ratios of the FW, BW, and DRV modes remain nearly constant for all windows. For longer window starting times, the amplitudes of the FW and DRV modes decrease significantly, leading to unreliable identification and scatter in the data. The damping ratio of mode T in-

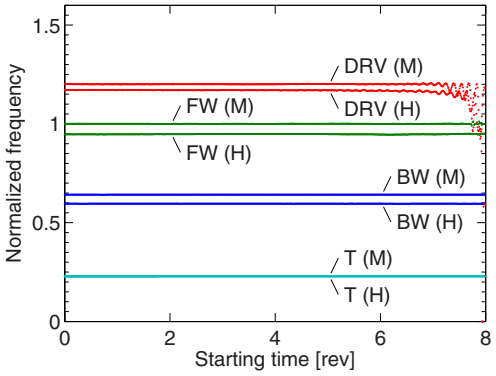

Fig. 13 Frequency identification using the MWA for the moderate (M) and high (H) excitation level

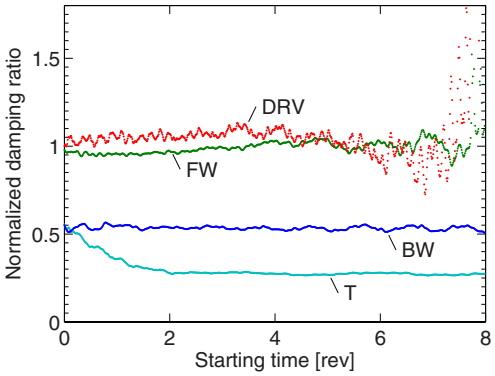

Fig. 14 Damping ratio identification using the MWA

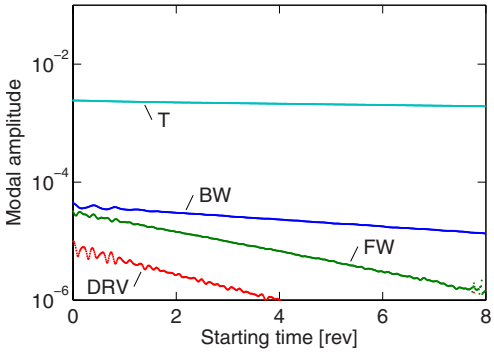

Fig. 17 Modal amplitudes from MWA for signal u_t

creases at higher amplitudes; this phenomenon is caused by the power-speed controller, which pitches the blades at the tower frequency, resulting in energy dissipation.

Figures 15–17 show the modal amplitudes as a function of time. The symmetric rotor signal u_{a0} in Fig. 15 consists mainly of the drive train mode, whose amplitude decays in a straight line, indicating a constant damping ratio. The BW and FW modes dominate the modal content of signals u_{a1}, as shown in Fig. 16, and u_{b1}. Finally, the T mode clearly dominates signal u_t (see Fig. 17). These figures show that low modal amplitudes cause poor modal parameter identification, resulting in data scattering, as observed earlier.

In this example, only four signals were used to estimate modal characteristics. Of course, many more signals could be used, at the expense of increasing the computational cost of the analysis. If a large number of computed degrees of freedom are used in the analysis, it becomes possible to also estimate mode shapes, increasing the amount of information that can be extracted from the data set.

3.4.2 Stability Analysis Under High Excitation. Next, a stability analysis of the turbine was performed as in the case of moderate excitation, but with 25 m/s wind at hub height and a high excitation level resulting in initial edgewise blade tip deflection of about 0.6 m and tower top lateral deflection of about 0.4 m.

The identified frequency of mode T is nearly identical to that obtained for the moderate excitation level, and the frequencies of the rotor modes differ because of different pitch angle settings in the two steady operating states; the results are compared in Fig. 13. Even at this higher excitation level, nonlinearities do not appear to be significant.

Figure 18 shows the identified damping ratios normalized by that of the FW for moderate excitation level. Comparing these results with those obtained for the moderate excitation presented in Fig. 14, it appears that all four normalized damping ratios are now slightly above one, whereas the BW and T damping ratios were below that level for the low amplitude excitation.

Figures 19–21 show the modal amplitudes as function of time. Mode T is lowly damped and its excitation remains high for the duration of the simulation. This explains the reduced scatter in the identified modal parameters as compared with those obtained for the low excitation case. The same observation holds for the BW mode. In contrast, the FW and DRV modes present higher damping ratios. Once their amplitudes become indistinguishable from noise, unreliable identifications result.

Comparison of the identified damping ratios for the moderate and high excitation levels, Figs. 15–17 and 19–21, respectively, calls for the following remarks. The increased excitation amplitude seems to yield poorer identification of the damping ratios. Because nonlinear behavior is not detected for modal parameters

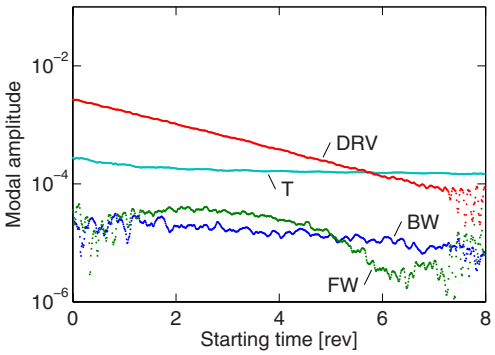

Fig. 15 Modal amplitudes from MWA for signal u_{a0}

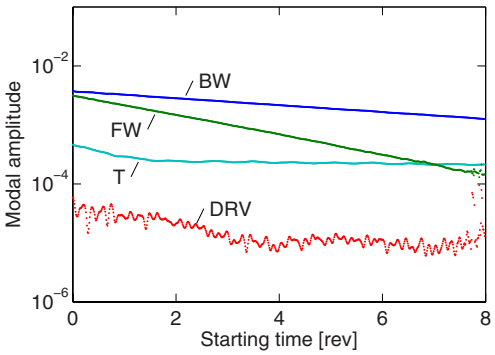

Fig. 16 Modal amplitudes from MWA for signal u_{a1}

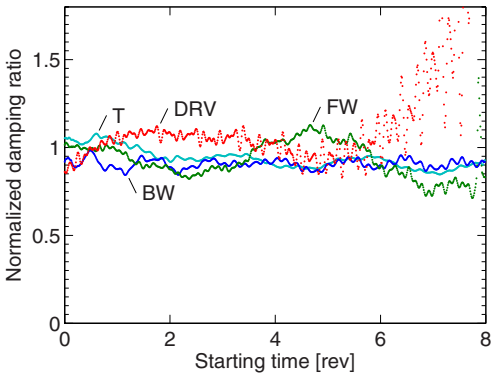

Fig. 18 Damping ratio identification using the MWA

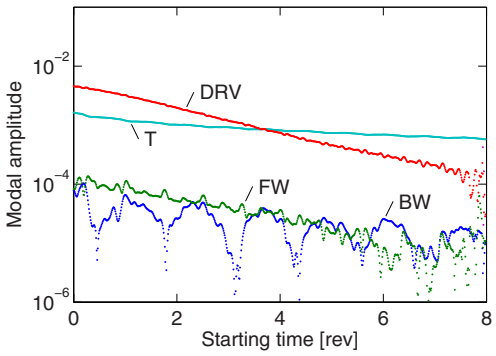

Fig. 19 Modal amplitudes from MWA for signal u_{a0}

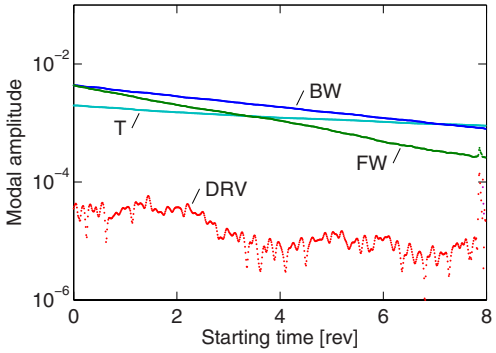

Fig. 20 Modal amplitudes from MWA for signal u_{a1}

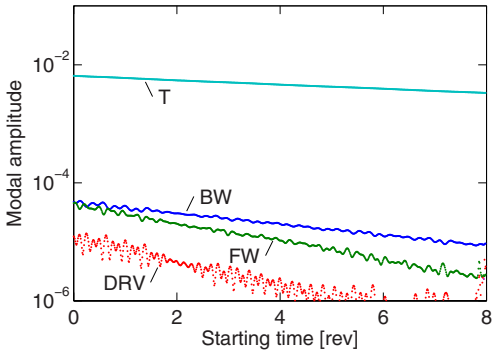

Fig. 21 Modal amplitudes from MWA for signal u_t

at the high excitation level, i.e., for small window starting times, geometric nonlinear effects do not seem to be the culprit. Rather, poorer damping ratio identification is more likely to be due to the fact that the larger excitation forces cause slight changes in angular speed of the rotor, thereby invalidating the periodic system assumption and the CPP.

4 Applicability to Measurements

Because they are based on signal processing, the methodologies described in this paper are applicable to both numerically computed and experimental data. Of course, noise levels will be higher with experimental data than with computed data. The proposed approach also requires the operation of the system at steady state, the application of a suitable excitation, and the measurement of the system free response.

In the case of operating wind turbines, setting up an experiment that satisfies these requirements might prove to be challenging. Excitation is conveniently applied through individual pitching of the blades and variation of the generator moment to excite the modes of interest. The system's dynamic response can be measured through accelerometers in the outer portions of the blades and tower or through strain gauges at the root of the blades and tower.

In the ideal case, the rotor would be driven at a nearly constant angular speed by a constant mean wind, resulting in a nearly periodic response. Successful field application of the proposed approach then depends on the ability to exert on the system well defined excitations of magnitudes larger than those associated with the uncontrollable wind turbulence and disturbance.

5 Conclusions

This paper has presented a method for evaluating the modal parameters of complex periodic systems. It combines four different tools: the Coleman post-processing, the partial Floquet analysis, the moving window analysis, and the signal synthesis algorithm. While these tools are not new, their combination leads to a robust estimation of the linearized modal parameters and provides qualitative information about the nonlinear behavior of the system. The proposed approach operates on one or multiple discrete time signals and is able to deal with both time-invariant and periodic systems. The method is computationally inexpensive and can be used with multiphysics computational tools, and in principle, with experimental data. The proposed approach was validated using a simple, four degree of freedom model of a wind turbine. Excellent correlation was observed when comparing the extracted linearized modal parameters with their exact counterparts. Qualitative information concerning the nonlinear behavior of the system was obtained with the proposed approach. Finally, the nonlinear behavior of a realistic, three-bladed horizontal axis wind turbine model was investigated. Nonlinear effects were found to be very mild for this specific wind turbine. For the larger wind turbines that are expected to be built in the near future, nonlinear effects could become more pronounced due to increased flexibility of the blades. Future work should investigate the ability of the proposed methodology to identify large changes in modal parameters that would be expected from such systems.

Acknowledgment

This work has been partially supported by the Danish Ministry of Science, Technology, and Innovation through the Industrial Ph.D. program.

References

[1] Hansen, M., 2007, "Aeroelastic Instability Problems for Wind Turbines," Wind Energy, **10**(6), pp. 551–577.
[2] Nayfeh, A., and Mook, D., 1979, *Nonlinear Oscillations*, Wiley, New York.
[3] Coleman, R., 1943, "Theory of Self-Excited Mechanical Oscillations of Hinged Rotor Blades," NACA Technical Report No. WR-L-308.
[4] Smith, C., and Wereley, N., 1996, "Transient Analysis for Damping Identification in Rotating Composite Beams With Integral Damping Layers," Smart Mater. Struct., **5**(5), pp. 540–550.
[5] Bauchau, O., Bottasso, C., and Nikishkov, Y., 2001, "Modeling Rotorcraft Dynamics With Finite Element Multibody Procedures," Math. Comput. Modell., **33**(10–11), pp. 1113–1137.
[6] Larsen, T., and Hansen, A., 2007, "How 2 HAWC2, The User's Manual," Risø Technical Report No. R-1597(EN).
[7] Riziotis, V., and Voutsinas, S., 2000, "Fatigue Loads on Wind Turbines of Different Control Strategies Operating in Complex Terrain," J. Wind. Eng. Ind. Aerodyn., **85**(3), pp. 211–240.
[8] Ewins, D., 1984, *Modal Testing: Theory and Practice*, Wiley, New York.
[9] Hammond, C., and Doggett, R. V., Jr., 1975, "Determination of Subcritical Damping by Moving-Block/Randomdec Applications," NASA Symposium on Flutter Testing Techniques, NASA Paper No. SP-415, pp. 59–76.
[10] Bousman, W., and Winkler, D., 1981, "Application of the Moving-Block Analysis," Proceedings of the 22nd Structures, Structural Dynamics, and Materials Conference, Dallas, TX, April 17–20.
[11] Peters, D., and Wang, X., 1998, "Generalized Floquet Theory for Analysis of Numerical or Experimental Rotor Response Data," Proceedings of the 24th European Rotorcraft Forum.
[12] Fuehne, C., 2000, "Application of Generalized Floquet Theory to Ground Resonance Data," Proceedings of the American Helicopter Society 56th Annual National Forum.

[13] Bauchau, O., and Wang, J., 2006, "Stability Analysis of Complex Multibody Systems," ASME J. Comput. Nonlinear Dyn., **1**(1), pp. 71–80.
[14] Bauchau, O., and Wang, J., 2008, "Efficient and Robust Approaches to the Stability Analysis of Large Multibody Systems," ASME J. Comput. Nonlinear Dyn., **3**(1), p. 011001.
[15] Bauchau, O., and Wang, J., 2010, "Efficient and Robust Approaches for Rotorcraft Stability Analysis," J. Am. Helicopter Soc., **55**, p. 032006.
[16] Le, T.-P., and Argoul, P., 2004, "Continuous Wavelet Transform for Modal Identification Using Free Decay Response," J. Sound Vib., **277**(1–2), pp. 73–100.
[17] Murtagh, P., and Basu, B., 2007, "Identification of Equivalent Modal Damping for a Wind Turbine at Standstill Using Fourier and Wavelet Analysis," Proc. Inst. Mech. Eng., Part K: J. Multi-body Dynamics, **221**(4), pp. 577–589.
[18] Simon, M., and Tomlinson, G., 1984, "Use of the Hilbert Transform in Modal Analysis of Linear and Non-Linear Structures," J. Sound Vib., **96**(4), pp. 421–436.
[19] Floquet, G., 1883, "Sur les équations différentielles linéaires à coefficients périodiques," Ann. Sci. Ec. Normale Super., **12**, pp. 47–88.
[20] Golub, G., and van Loan, C., 1989, *Matrix Computations*, 2nd ed., The Johns Hopkins University Press, Baltimore, MD.
[21] Lyapunov, A., 1992, *The General Problem of Stability of Motion*, Taylor & Francis, London.
[22] Skjoldan, P., and Hansen, M., 2009, "On the Similarity of the Coleman and Lyapunov–Floquet Transformations for Modal Analysis of Bladed Rotor Structures," J. Sound Vib., **327**, pp. 424–439.
[23] Rubak, R., and Petersen, J., 2005, "Monopile as Part of Aeroelastic Wind Turbine Simulation Code," Proceedings of Copenhagen Offshore Wind.

Risø DTU is the National Laboratory for Sustainable Energy. Our research focuses on development of energy technologies and systems with minimal effect on climate, and contributes to innovation, education and policy. Risø has large experimental facilities and interdisciplinary research environments, and includes the national centre for nuclear technologies.

Risø DTU
National Laboratory for Sustainable Energy
Technical University of Denmark

Frederiksborgvej 399
PO Box 49
DK-4000 Roskilde
Denmark
Phone +45 4677 4677
Fax +45 4677 5688

www.risoe.dtu.dk